"ADSORPTION MECHANISM OF CELLULOSE AND ITS DERIVATIVES ONTO VARIOUS SOLID SURFACES"

THESIS

SUBMITTED TO

BABASAHEB BHIMRAO AMBEDKAR UNIVERSITY
(A CENTRAL UNIVERSITY)
LUCKNOW

BABASAHEB BHIMRAO AMBEDKAR UNIVERSITY
LUCKNOW
प्रज्ञा शील करूणा
ESTABLISHED 1996

FOR THE DEGREE OF

Doctor of Philosophy
In
Applied Chemistry

Submitted by

ASHOK KUMAR

Ph.D. Research Scholar
Enrollment No. 548/14

Under the Supervision of

PROFESSOR KAMAN SINGH

DEPARTMENT OF APPLIED CHEMISTRY
SCHOOL FOR PHYSICAL SCIENCES
BABASAHEB BHIMRAO AMBEDKAR UNIVERSITY
(A Central University)
VIDYA VIHAR, RAEBARELLI ROAD, LUCKNOW-226025, UTTAR PRADESH (INDIA)

APRIL, 2021

बाबासाहेब भीमराव अम्बेडकर विश्वविद्यालय

BABASAHEB BHIMRAO AMBEDKAR UNIVERSITY

(A Central University)

Accredited 'A' Grade by NAAC 2015

ISO 14001:2015

DEPARTMENT OF APPLIED CHEMISTRY
SCHOOL FOR PHYSICAL SCIENCES
BABASAHEB BHIMRAO AMBEDKAR UNIVERSITY
(A Central University)
VIDYA VIHAR, RAEBARELLI ROAD, LUCKNOW-226025
UTTAR PRADESH (INDIA)


"Dedicated
to
My supervisor
and
My beloved family"

बाबासाहेब भीमराव अम्बेडकर विश्वविद्यालय
(केन्द्रीय विश्वविद्यालय)
विद्या विहार, रायबरेली रोड, लखनऊ–226025
BABASAHEB BHIMRAO AMBEDKAR UNIVERSITY
(A Central University)
Vidya Vihar, Raebareli Road, Lucknow-226025

Letter No.-....117.../COE/BBAU/2017 Dated: 06/07/17

Ph.D. Course Work Certificate

This is to certify that **Ashok Kumar**, Enrollment No. 548/14 Ph.D. Research Scholar, Department of Applied Chemistry of the University has successfully completed his Ph.D. Course work in the examination held during January, 2017.

(A.K. Maurya)
Deputy Registrar (Exam.)

BABASAHEB BHIMRAO AMBEDKAR UNIVERSITY
LUCKNOW
प्रज्ञा शील करुणा
ESTABLISHED 1996

बाबासाहेब भीमराव अम्बेडकर विश्वविद्यालय
विद्या विहार, रायबरेली रोड, लखनऊ–226025

BABASAHEB BHIMRAO AMBEDKAR UNIVERSITY
(A Central University)
Vidya Vihar, Raebareli Road, Lucknow-226025

Letter No. – 485/CC/DoC/BBAU/21
Date – 25.03.2021

Pre-Ph.D. Submission Seminar Completion Certificate

This is to certify that **Mr. Ashok Kumar**, a bonafide Ph.D. Research Scholar of this department, under the supervision of **Professor Kaman Singh**, has successfully completed the Pre-Ph.D. submission seminar (held on February 08, 2021) requirement, which is a part of his Ph.D. programme on his thesis entitled "**ADSORPTION MECHANISM OF CELLULOSE AND ITS DERIVATIVES ONTO VARIOUS SOLID SURFACES**".

25/03/21

Head
Department of Chemistry
आचार्य एवं विभागाध्यक्ष
रसायन विज्ञान विभाग
भौतिकीय एवं वर्णय विज्ञान विद्यापीठ
बाबासाहेब भीमराव अम्बेडकर विश्वविद्यालय
(केन्द्रीय विश्वविद्यालय)
लखनऊ-226025, उत्तर प्रदेश (भारत)

DECLARATION

I hereby declare that the thesis entitled **"ADSORPTION MECHANISM OF CELLULOSE AND ITS DERIVATIVES ONTO VARIOUS SOLID SURFACES"** submitted by me for the degree of Doctor of Philosophy, is the record out by me under the supervision of **Professor Kaman Singh**, Department of Applied Chemistry, School for Physical Sciences, Babasaheb Bhimrao Ambedkar University (A Central University) Lucknow. I further confirm that the aforesaid work has not submitted anywhere else for the award of any degree, diploma or fellowship, etc. either in this or any other university or other institution of higher learning. I, further declare that the material embodied in the present work is based on original research work and the indebtedness to others has been duly acknowledged at relevant places. I, Ashok Kumar, also declare that the thesis submitted by me essentially free from all kinds of plagiarism (checked by URKUND).

Kumar

Date: 16/04/2021

(ASHOK KUMAR)
Ph.D. Research Scholar
Enrollment No. 548/14
Department of Applied Chemistry
School for Physical Sciences
Babasaheb Bhimrao Ambedkar University
(A Central University)
Vidya Vihar, Raebareli Road, Lucknow-226025
Uttar Pradesh, India

CERTIFICATE

This is to certify that the thesis entitled **"ADSORPTION MECHANISM OF CELLULOSE AND ITS DERIVATIVES ONTO VARIOUS SOLID SURFACES"** submitted by **Mr. Ashok Kumar** is an original research work and has not been previously submitted in part or full for the award of any other degree or diploma to this or any other university.

The thesis submitted to Babasaheb Bhimrao Ambedkar University Lucknow satisfies all the requirements as stipulated in the *Doctor of Philosophy (Ph.D.) regulations-1999 as amended in 2008/2010/2013* and it is fit for submission and evaluation for the award of the degree of Doctor of Philosophy of the University.

Date: 16/04/2021

(Supervisor)

(Head of the Department)

Professor & Head
Department of Physics
School of Physical & Decision Sciences
Babasaheb Bhimrao Ambedkar University
(A Central University)
Lucknow-226025, Uttar Pradesh (INDIA)

PIONEERS OF THE SURFACE CHEMISTRY

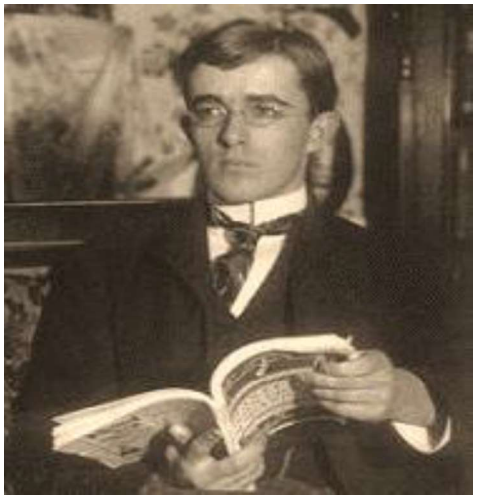

Irving Langmuir (1881–1957)
(N.L. 1932)

Erwin Finlay- Freundlich (1885-1964)

Rudolph Arthur Marcus (1923)
(N.L. 1992)

Gerhard Ertl (1936)
(N.L. 2007)

Prof. A.V. Kiselev (R) (1908–1984) and Sir Eric Rideal (L) (1890-1974)
Photo taken in N Wales in 1968 while attending a meeting at Portmeirion

ACKNOWLEDGEMENTS

I am indeed indebted to my distinguished Ph.D. supervisor **Professor Kaman Singh** for providing me with the scientific surroundings (technical and intellectual) and believing in me to do science with him to carry out the course of study. I will be forever grateful to him for introducing me to surface chemistry with special references. I also want to thank him for his inspirational way of teaching and brilliant scientific discussions for the secrets of physical chemistry theory to practice resulting in the re-evaluation of various century-old concepts. Certainly, I am short of words to convey my real feelings for his invaluable help and concern together with 'scholarly, insightful and critical' guidance. I do not hesitate to state that without his support it would not have been possible for me to complete the research work.

I am very much thankful to **Professor Gajanan Pandey**, Head, Department of Chemistry, Babasaheb Bhimrao Ambedkar University (A Central University) Lucknow, Uttar Pradesh, India and faculty members Dr. Anjani Kumar Tiwari, Dr. Jyoti Pandey, Dr. Shailesh Kumar, Dr. Preeti Gupta and Dr. Jawaharlal for providing moral support and valuable suggestions.

Words fail to express my appreciation to my father in law Mr. Ranveer Singh, mother in law Mrs. Guddi Devi, Mr. Anil Kumar Gautam, Miss Anjel Singh and Mr. Aryan Singh for providing moral support, encouragement, and consultation during the research work. I express my deep appreciation to Mrs. Nidhi Igral, Miss Tejal Singh and Mr. Ajeet Kumar Singh for their kind support.

I see myself privileged to have the opportunity to work with so many brilliant people. I would like to thank Dr. Shikha Awasthi for her expertise in SEM and XRD. I am ever so grateful to Dr. Sarvesh Kumar Pandey, Dr. Rayees Ahemad Bhatt and Dr. Anirudh Prashad Chaudhary for their outstanding input and work in the computational interpretation of experimental work.

I am also thankful to all seniors Dr. Satya Prakash Gupta, Dr. Ajay Kumar, Dr. Manisha Gautam, Dr. Gaurav Hitkari, Dr. Sandhya Singh, Dr. Azad Kumar and Dr. Deepak Kumar for providing moral support, encouragement, and consultation during the research work.

I am also thankful to all research scholars, especially Mr. Puneet Kumar, Mr. Manoj Dhemeja and Mr. Hariorm Kumar for their timely help and encouragement.

It is my immense pleasure to thank my dearest friends for bringing joy to my everyday life throughout this work. First of all, I want to express my fondest gratitude to Mr. Pankaj Singh. I also would like to thank my juniors and lab-mattes Mr. Prashant Mishra, Mrs. Madhu Lata, Miss. Auyshi Mishra, Mr. Utkarsh Dixit, and Mr. Presinjit for the laughter and also not just sharing a hard, skilful work in the lab, but also for sharing teaching thoughts and friendly atmosphere. I am most grateful to Mr. Sumit Kumar, Mr. Ajay Kumar Yadav, Mr. Gaurav Verma, Mr. Chandrabhan, Mr. Gulam Abbas, Miss Deepika Singh, Miss Priya Singh, Mr. Chandraprakash Gond and Mr. Vijy Kumar Singh for the fruitful, joyful and never-ending discussions and friendship.

I am extremely grateful to University Sophisticated Instrumentation Center (USIC) office staff especially Dr. Mukesh Kumar for providing SEM-EDS, and FTIR facility. I am thankful to IITR, Lucknow and IIT, Kanpur for permitting me and needed assistance for an experimental tryout and sample analysis/characterization. Thanks are due to the supporting staff of the Department of Applied Chemistry especially Pankaj Singh, Sarvesh Gupta and Anuj Saini, for all the assistance provided by them during the entire research work.

I find no way to express in word my deep gratitude and profound reverence to my Parents, **Mr. Naresh Pal** and **Mrs. Urmila Devi**. This undertaking would not have even been contemplated, let alone be completed, without their prayers, their blessings, their encouragement and the confidence they have shown in me. I recollect all the moments, they have shared with me all these years and waited patiently to see my research this destination in life.

A person who needs special mention here is my wife **Mrs. Anushka Singh.** She has boosted my moral at critical moments during this study. Her forbearance and loving care facilitated the completion of my research work. All the credit goes to her for what I am today and I am indebted to her.

Acknowledgement is heartily endless and incomplete and I wish indulgence from the many friendly and helpful people whom I do not name here. It has been a dream to have someone to share the science with.

"Straight from the heart''

Ashok Kumar
Ph.D. Research Scholar

CONTENTS

PREFACE

The industrial development of adsorbents and catalysts in the mid-twentieth century was closely associated with a renewed academic interest in adsorption science for various applications. The strong demand for fundamental research on adsorption by porous and non-porous solids attracted the attention of a number of researchers. Many applications of adsorption at the liquid–solid interface include flotation, pollution control, liquid chromatography and the refining of precious metals/mineral processing). Fundamental investigations of liquid/solid interfacial systems are therefore of great importance by analyzing the experimental data.

Cellulose and its derivatives (CDs) have been extensively used in various fields due to their valuable and remarkable chemical and physical properties. The applications of CDs have widely been recognized in various industries like textile & dyeing, papermaking, food, pharmaceutical, cosmetics, ceramic, leather, paint & lacquers, petroleum, building materials, mosquito-repellent, toothpaste, battery, detergent and tobacco industry. However, there was a lack of understanding of the interaction mechanism between the polysaccharides (CDs) and solid surfaces which has hindered their possible applications, hence, adsorption of polysaccharides onto solid-liquid interface has been a topic of long-standing debate. Several binding mechanisms have been developed, but as yet no common mechanism has received general acceptance. Thus, the associated problems have received adequate attention. Therefore, cellulose and its derivatives such as cellulose, carboxymethylcellulose, sodium carboxymethylcellulose, and hydroxyethylcellulose were chosen as representative selection of polysaccharides for the study of their binding mechanism with solid surfaces to enhance the understanding of the binding mechanism. The simple laboratory experimental observations that could allow macroscopic evaluation of adsorption behaviour of polysaccharides onto a solid surface and would provide a new idea for the binding mechanism aspects onto solid-liquid interfaces.

Furthermore, there is an urgent need for re-evaluation of century-old classical Langmuir adsorption especially for the calculation of the Gibbs free energy of adsorption (ΔG^o) and subsequent thermodynamic parameters of the adsorption process. We examined data carefully from the literature and found that the estimation of ΔG^o reported in these published references was seemingly incorrect. Based on the fact that this misapplication is now has become customary in the adsorption literature and it seems impossible to address this semantic confusion. We herein, however, attempted to correct the related literature and gave a descriptive comment and solution of this problem.

Chapter 1

Introduction and review of literature

Abstract

Cellulose ($C_6H_{10}O_5)_n$ is one of the most ubiquitous organic polymer on the earth. It is a significant structural component of the primary cell wall of green plants, various forms of algae and oomycetes. It is a polysaccharide consisting of a linear chain of several hundred to many thousands of β(1→4) linked D-glucose units. There are various extraction procedures for cellulose developed by using different processes like oxidation, etherification and esterification which convert the prepared celluloses into cellulose derivatives. Since it is a non-toxic, bio-degradable polymer with high tensile and compressive strength, it has widespread use in various fields such as mineral processing industry, nanotechnology, pharmaceutical industry, food industry, cosmetics, textile and paper industry, drug-delivery systems in treating cancer and other diseases. Micro-crystalline cellulose (MCC), in particular, is among the most frequently used cellulose derivatives in the food, cosmetics, pharma industry, etc. and is an important excipient due to its binding properties. Currently, about half of the waste produced in India contains about 50% cellulose which can be used productively. This chapter deals about basic information related to cellulose and its derivatives and basics about adsorption process onto various solid surfaces including objective, methodology and future aspects.

1. Introduction

Cellulose has been recognized as one of the most widely, abundant naturally occurring biopolymers in the world. Human beings had used cellulose as an extension of their hands for millions of years, even before the beginning of hominization due to its easy availability (cellulose is the primary constituent of plants) and low-cost. It has a component of at least a third of advanced plants: 40-60% (in weight) of dry wood, and more than 90% of raw cotton (99.9'%) of purified cotton and flax [1]. It is a homopolymer of anhydroglucose, with the glucose residues linked in a β -1, 4 fashion (Figure 1) [2]. Cell walls of plant cells attribute their mechanical strength to cellulose. Cellulose owes its cellulose structural properties to the fact that it can retain a semi-crystalline state of aggregation even in an aqueous environment, which is unusual for a polysaccharide [3, 4]. As far as cellulose-based products are concerned, paperboard are the most commonly used ones [5]. Smaller amounts of cellulose when processed under appropriate conditions can be converted to a wide variety of derivatives, these can be used in the manufacture of few commercial products like cellophane and rayon [6]. Since cellulose is a homo-polymer of a glucose derivative, it has a great source of fermentable sugar. It has been cultivated in the form of energy crops for the production of ethanol, ethers, acetic acid, etc. Besides energy requirements, the industrial demands of cellulose have been fulfilled by wood pulp and cotton crops [7]. Cellulose also fulfilled the dietary requirements of some animals, particularly ruminants and termite, they can digest cellulose with help of symbiotic microorganisms present in their gut, while some organisms secrete a group of enzymes called cellulases to aid the degradation of cellulose molecules [8]. Human beings are unable to digest cellulose due to a lack of cellulases, thus cellulose acts as a hydrophilic bulking agent for faeces and potentially aids in defecation [9]. Its abundance has attributed to the constant photosynthetic cycles taking place in higher plants, which can synthesize around 1011±12 tons of cellulose in a rather pure form. It has served mankind either as a construction material or as a versatile starting material for chemical reactions for the production of artificial cellulose-based threads and biofilms as well as for the production of a variety of stable cellulose and its derivatives which have been used for various industrial and domestic applications [10]. Cellulose was used for various biochemical conversions even before its polymeric nature was recognized and well understood. In the process of recognizing and understanding its polymeric structure, it

led to the discovery of nitrocellulose, synthesis of organo-soluble cellulose acetate and the preparation of Schweizer's reagent (first cellulose solvent). Another area of great interest has been recognized nanocellulose, the nanostructure of cellulose has proven to be advantageous because of its applications in a variety of fields [11, 12]. Due to such great economic significance of tree cellulose, the current scientific focus has more towards cellulose biosynthesis as it is still not well understood [13]. Most of the recent findings concerning the molecular mechanism of cellulose biosynthesis in higher plants resulted from research in model herbaceous plants and fibre crops and have been reviewed recently [13]. All these aspects trigger a researchers' curiosity and make them want to dig deeper and unveil other properties related to adsorption aspects.

In the 18^{th} century, the mechanization of spinning and weaving devices (inventions to improve productivity to meet market demand) for cotton fabrics formed a strong incentive to the industrial revolution, which brought about mass consumption of chemicals (in particular, inorganic compounds) for scouring, and finishing. In the second quarter of the 19^{th} century, cellulose became recognized as a chemical compound. It has a general formula $(C_6H_{10}O_5)n$ consisting of a linear chain of several hundred to many thousands of $\beta(1\rightarrow4)$ linked D-glucose units (Figure 1). The chemical structure of cellulose was extensively explained by several researchers [14]. The C4-OH group, the non-reducing end, while the terminating group is C1-OH, the reducing end with aldehyde structure. Some technical celluloses contain extra carbonyl and carboxyl groups, like the bleached wood pulp. The molecular structure is responsible for its significant properties: chirality, hydrophobicity, degradability and chemical variability due to high reactivity from the donor group -OH. The superior hydrogen bonds have been found responsible for crystalline fibre structures to cellulose [14]. It is established that cellulose has also been found in its purest form from the seed hairs of cotton. The wood cellulose, on the other hand, forms a composite with lignin and other polysaccharides, which was further separated by large scale chemical pulping and purification processes. Cellulose can be derived from algae, some specific bacteria, and fungi, apart from most plants. The supramolecular structures were used for research on cellulose structures, reactivity, and crystallinity with a further note on the development of biomaterials and new substances. Cyanobacteria are known to biosynthesize cellulose for nearly 3.5 billion years [15]. The first synthesis of cellulose *in vitro* was reported as the cellucellulase-cellulose formation by catalyzed cellobiosyl fluoride and

the chemosynthesis was processed in ring-opening polymerization of the d-glucose moieties [16].

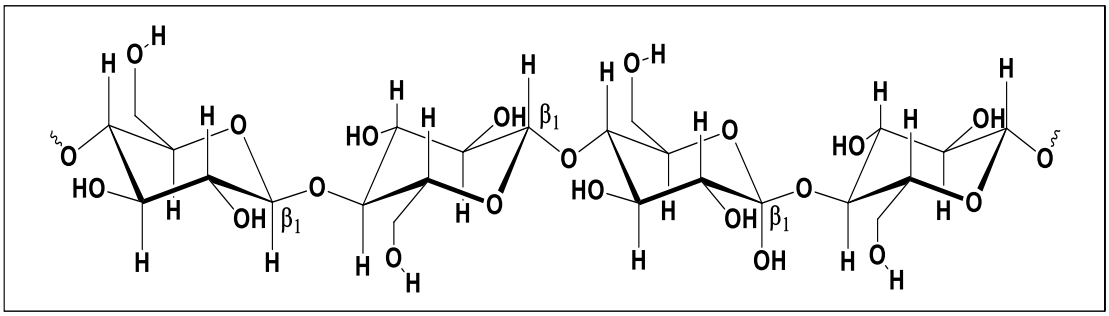

Figure 1. Structure of cellulose (repeating unit of glucose) shows the D-glucose units are linked through β-1, 4 bonds.

Cellulose has numerous applications in the field of pharmaceuticals and food technology. Modifying the structure of cellulose with other chemical group's results in the production of structures that have better biocompatibility, flexibility, stability, emulsifying effects. Further, cellulose being indigestible by human beings, tend to have a drastic increase in the population of the world coupled with an exponential increase in technological advancements and the need of the people, fossil fuels were being rapidly depleted. During this period, the term sustainable development comes into play. To develop sustainably, it has been important to switch to a fuel that is more clean, green and more cost-effective. One such alternative is cellulose derived biofuel [16-20]. There are numerous advantages of using biofuel, the first and foremost being cost-effective. Recent studies have shown that due to the increase in demand, the cost of biofuel is decreasing as ethanol costs lesser than petrol and diesel. Further, there is a significant reduction in carbon emission. The raw material used for biofuel is simply a substrate that has cellulose in it. Since cellulose is so widely abundant, the cost is significantly lower. The ethanol obtained from cellulose is used as an alternative substrate in the production of biofuel. It is considered a superior source due to its high energy efficiency and low cost as compared to other sources. This is a very good source of renewable energy as it is found most abundantly in stalks, leaves and stem of green plants [21-23]. Other sources for ethanol include feedstocks, including wheat straw, rice straw, sawdust, forest thinning and grasses perennial grasses and switchgrass. Cellulose can be broken down into fermentable sugars by using the fungus *Trichoderma reesei* or by using acid to convert them first into sugars and then into gas. The gut of termites also can be utilized for this purpose. Further, a group of bacteria collectively referred to as methanogens can digest cellulose and produce carbon dioxide and

methane, which is further processed [24-33]. One group of such bacteria called methane bacteria grow anaerobically on the cellulosic matter and degrade it to produce methane. They are also found in the rumen of cattle and the dung of cattle. It is quite easy to obtain a substrate for biogas production especially by using waste cellulosic material. Therefore, it is important to utilize even the apparent waste material to ensure a reduction in wastage and optimum usage of its potential [34, 35].

Cellulose, with its properties, as discussed in the above sections, were extensively used in the field of biomedicine and pharmaceuticals. The cost of several pharmaceutical products is extremely high due to production factors such as high cost, difficulty in procuring the material, complicated processing steps etc. These problems can be remedied by the use of cellulose, which is found abundantly in nature. The most productive use of cellulose would be the utilization of plant-based waste materials which are produced in bulk by many industries such as the sugar production industry as well as in minor quantities by households [36, 37]. The applications highlighted above could be brought to mainstream commercial use with the appropriate optimization techniques and novel modifications to the various steps of the production and processing of cellulosic material [37].

The solid dosage forms including pills, tablets, granules, pellets, microcapsules and spherules can be coated, usually to protect the drug from adverse environmental factors such as humidity, oxygen, enzymatic or acidic degradation. The coating may also be used to facilitate drug delivery systems with altered release mechanisms such as delayed-release, extended-release, step-by-step release, pulsatile release and sustained release [38]. Derivatives of cellulose such as esters and ethers are also extensively used as coating materials. In the process of solid dosage form manufacture by direct compression, a problem that frequently occurs is low compatibility of the drug, this is more seen more frequently when the amount of drug in the formulation exceeds 30%. Many attempts are being made to reduce the price of the final product by experimenting with various starting materials and test conditions [39].

From the advent of novel drug delivery systems, cellulose-based models seemed like strong candidates due to their projected benefits [40]. Since then various advances have been made to bring its use to common practice. There are still many hurdles to cross before this becomes a reality. Cellulose-based drug delivery is an important step in green and sustainable pharmacy which focuses on toxicity reduction, biodegradability

and less hazardous synthesis concerning drugs and drug delivery systems. Cellulose nanocrystals (CNCs) have the potential to acquire a negative charge during hydrolysis [41]. This coupled with their large surface area allow them to bind ionizable drugs such as tetracycline and doxorubicin permitting optimum dosing control. Sites for surface modification for multiple chemicals are provided by a multitude of surface hydroxyl groups. This is used in the case of non-ionized or hydrophobic drugs which do not generally bind to cellulose. The open-pore structure and high surface area of CNC based aerogels provide increased drug loading capacity and drug bioavailability. Extremely porous aerogel scaffolds were reported to attain sustained drug release [42]. Cellulose derivatives have also been researched in terms of drug delivery. For instance, cellulose acetate has been successfully used in several HIV drugs, five flavonoids, one pain reliever and two antibiotics among others. Hydroxypropyl methylcellulose has been used in oral drug delivery formulations [43].

The scaffolds are materials that have been engineered to cause desirable cellular interactions to contribute to the formation of new functional tissues for medical purposes by providing the microenvironment required by cells to proliferate, migrate and differentiate. It contributes the geometrical basis and building blocks to provide cell attachment. Gluconacetobacter xylinus sourced nanocellulose is an emerging biomaterial for this purpose. Bacterial nanocellulose has a very high affinity for water and therefore displays properties similar to those of hydrogels which provides an ideal environment to host cells. Studies have confirmed that human smooth muscle cells, bone-forming osteoblasts and fibroblasts and human embryonic kidney cells can grow in the presence of bacterial cellulose scaffolds. The main challenge in the production of these scaffolds seems to be biodegradability as cellulose, the enzyme required to breakdown cellulose is not present in humans. This property was reported to be enhanced by periodate oxidation [44, 45].

Bacterial cellulose has an important application in artificial blood vessels. Compared to the material generally used for vascular grafts, these materials show less thrombosis and occlusion. Heparin hybridized bacterial nanocellulose scaffolds with anticoagulant properties have potential use in vascular tissue engineering. The potential use of bacterial cellulose in the production of heart valve replacements has been explored [46, 47]. Nanocellulose are promising materials for the culture of various cells including osteoblasts and chondroblasts indicating that they have the potential for bone tissue regeneration and healing. A membrane of bacterial cellulose and hydroxyapatite was

developed as a biomaterial for potential bone regeneration, which delivered prone growth of osteoblast cells, a high level of alkaline phosphatase activity and greater bone nodule formation [48].

A lot of research is ongoing in the field of polymers and the study of cellulose over the past decade due to its broad range of applications. The structure and properties of cellulose including adsorption behaviour onto solid surfaces are quintessential to perform modifications processing of cellulose on the whole and its possible application areas.

2. Classification, structure and properties of cellulose

There are different classes of cellulose, namely cellulose nanocrystal [48], bacterial cellulose [49], nanofibrillated cellulose [50] ethyl cellulose and Payen [51] discovered the forms of cellulose. Cellulose and its derivatives are biodegradable polymers [52-55]. The properties of cellulose are associated with its structure. The structure of cellulose has been constantly a subject requiring intensive research as it was formed by the hydrogen bonds between the networks of hydroxy groups [56]. The progress was for more than a century years of intensive development on structure analysis methods like scanning electron microscopy (SEM), X-ray diffraction (XRD) and solid-state nuclear magnetic resonance (NMR) spectroscopy. A complete detailed analysis was required for the procedures of synthetic reactions and cellulose-based manmade products with extensive applications. The structure of cellulose as depicted in Figure 1 consists of hydroxyl groups of β-1, 4-glucan cellulose at C2, C3 and C6. The CH_2OH group is positioned relative to the C4 and C5 bonds along with shear relativity with O5–C5 bonds. The solid-state was equally likely to be represented in the crystalline (high order) and amorphous (low order). The crystal structure, in particular, is determined by the X-ray diffraction using a monoclinic unit cell which is made up of two cellulose chains in a parallel orientation and twofold screw axis [2, 57]. The investigations concerning the electron microbeam diffraction, combined X-ray and neutron diffraction have indicated that the cellulose crystalline structures have a triclinic and monoclinic unit cell.

The chemical and physical properties of cellulose can only be well understood by acquiring knowledge of the chemical nature of the cellulose molecule in addition to its structure [58]. A profound understanding of the structural properties of native cellulose was a requirement to understand the effects of different substituents on the chemical

and physical properties of cellulose and its derivatives (CDs) [59]. When considering CDs, three structural levels have been distinguished:-

i) The molecular level

This level has considered cellulose as a single macromolecule with the chemical constitution, molecular mass, molecular mass distribution, the presence of reactive sites and potential intermolecular interactions.

ii) The supramolecular level

This level has been assumed one step further up from the molecular level and considered cellulose molecules as interacting with other cellulose chains in the form of packing and mutual ordering of the macromolecules to form larger structures. This level had included important concepts like an aggregation of the molecular chains to form elementary crystals and fibrils, the degree of order within and around the fibrils and fibrillar orientation concerning the fibre axis.

ii) The morphological level

This level has covered structural entities formed by cellulose molecules. As the structures get larger, they may become very complex. On the morphological level, the existence of distinct cell wall layers in native cellulose fibres or skin-care structures in man-made cellulosic fibres, voids or interfibrillar interstices were investigated.

The molecular, supramolecular, morphological studies reported that because of the presence of several functional hydroxyl groups (-OH) in the polymeric chain of cellulose it has been well known polyhydroxy alcohol. These groups (hydroxyl groups) allowed numerous chemical modifications to obtained derivatives. Cellulose esters and cellulose ethers are most common chemically modified polysaccharides (sometimes referred to as classical cellulose derivatives) [58, 59].

3. Cellulose and its derivatives (CDs) and their applications

Generally, cellulose derivatives could be obtained by either mechanical or chemical processing or both. The hydroxyl groups of cellulose can be partially or fully reacted with the various reagent to afford derivatives with useful properties. Cellulose undergoes a variety of chemical reactions which have been used technological production level. The pure cellulose additional treatment using hydrogen chloride acid

produced various CDs [60]. Cellulose nitrate was the oldest known CDs and have been used for several applications including the separation of suspended particles. Methylcellulose, hydroxyethylcellulose and carboxymethylcellulose are the most active constituents of the cellulose ethers [61]. The hydroxyl groups (-OH) of cellulose treated with various reagents to afford derivatives with useful properties like mainly cellulose esters and cellulose ethers (-OR). In principle, although not always in current industrial practice, cellulosic polymers are renewable resources (Table 1). The CDs have been recognized versatile polymers for several industrial applications (Scheme 1). The cellulose acetate and cellulose triacetate are films- and fibre-forming materials that find a variety of uses [62]. The nitrocellulose was initially used as an explosive and was an early film-forming material. With camphor, nitrocellulose gives celluloid (Table 1).

Table 1 Some most common cellulose derivatives (CDs)

Cellulose ethers			
Category	**Reagents**	**Group R = H or**	**Derivatives**
Alkyl	Chloromethane	$-CH_3$	Methylcellulose (MC)
	Chloroethane	$-CH_2CH_3$	Ethylcellulose (EC)
	Chloromethane and chloroethane	$-CH_3$ or $-CH_2CH_3$	Ethylmethylcellulose (HMC)
Hydroxyalkyl	Ethylene oxide	$-CH_2CH_2OH$	Hydroxyethylcellulose (HEC)
	Propylene oxide	$-CH_2CH(OH)CH_3$	Hydroxypropylcellulose (HPC)
	Chloromethane and ethylene oxide	$-CH_3$ or $-CH_2CH_2OH$	Hydroxyethylmethyl cellulose (HEMC)
	Chloromethane and propylene oxide	$-CH_3$ or $-CH_2CH(OH)CH_3$	Hydroxypropylmethylcellulose (HPMC)
	Chloroethane and ethylene oxide	$-CH_2CH_3$ or $-CH_2CH_2OH$	Ethylhydroxyethylcellulose (EHC)
Carboxyalkyl	Chloroacetic acid	$-CH_2COOH$	Carboxymethylcellulose (CMC)
Cellulose ester			
Organic	Acetic acid and acetic anhydride	H or $-(C=O)CH_3$	Celluloseacetate
	Acetic acid and acetic anhydride	$-(C=O)CH_3$	Cellulosetriacetate
	Propionic acid	H or $-(C=O)CH_2CH_3$	Cellulosepropionate
	Acetic acid and propanoic acid	H or $-(C=O)CH_3$ or $-(C=O)CH_2CH_3$	Celluloseacetatepropionate (CAP)
	Acetic acid and butyric acid	H or $-(C=O)CH_3$ or $-(C=O)CH_2CH_2CH_3$	Celluloseacetatebutyrate (CAB)

Inorganic	Nitric acid or another powerful nitrating agent	H or $-NO_2$	Nitrocellulose (cellulose nitrate)
	Sulfuric acid or another powerful sulfuring agent	H or $-SO_3H$	Cellulose sulfate

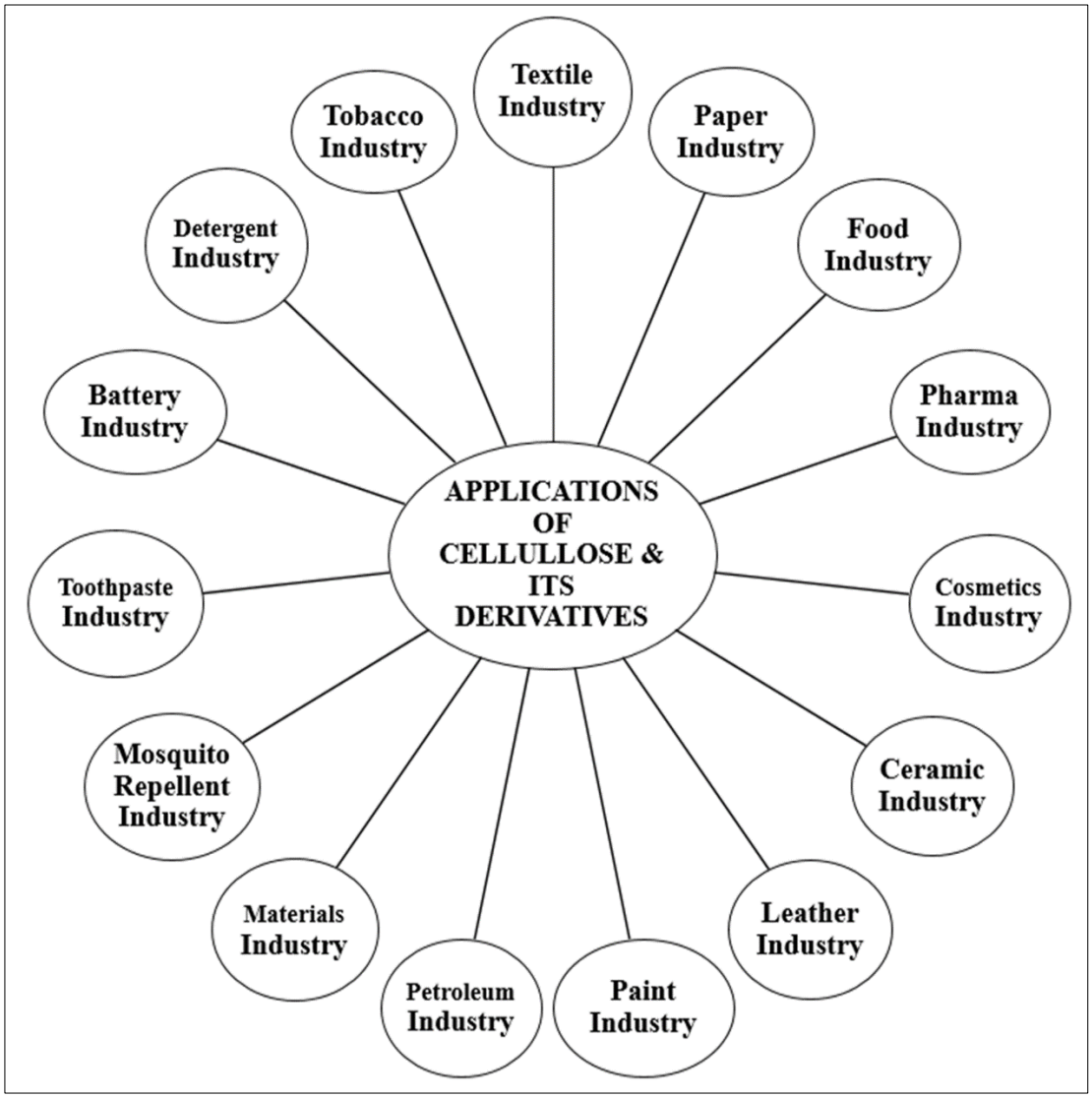

Scheme 1. Graphical representation of the importance of polymers (CDs) in broad range of applications

Some selected CDs have been discussed in details as follows-

(i) Microcrystallinecellulose (MCC)

The MCC is a valuable additive in pharmaceutical as a binder for tablets by direct compression and vitamin supplements, in food as an anticaking, thickener, texturizer, emulsifier and bulking agent as well as a fat substitute and in cosmetic as a filler [63, 64]). It is one of the most important tabletting excipients due to its superior dry binding

properties producing high-quality tablets by direct compression [65]. It is also used in plaque assays for counting viruses, as an alternative to carboxymethyl cellulose [66]. Other applications of the MCC such as paints, paper and nonwoven textiles, oils field services, medicine and composites because of its properties such as high strength, flexibility and aspect ratio (67, 68). Microcrystalline cellulose (MCC) is a purified, partially depolymerized cellulose having the formula $(C_6H_{10}O_5)_n$. It is prepared by treating alpha-cellulose with mineral acids. This polysaccharide polymer consists of a linear chain of several hundred to over ten thousand β(1 → 4) linked D-glucose units, consisting of linear chains of β-1,4-d anhydroglucopyranosyl units (Figure 2). The raw material used for MMC preparation is pulp from a fibrous plant such as conifer wood. Cotton is also a possible cellulose source for MCC [69, 70]. Pharmaceutical grade MCC, which needs a high-quality pulp, used wood as the most common source. From such a wooden source, cellulose chains are packed in layers and held together by strong hydrogen bonds from lignin, a cross-linking polymer. For that purpose, both softwoods (evergreen conifer) and hardwoods (deciduous broadleaf) can be used [71]. These woods differ not only in chemical composition including cellulose proportions, hemicelluloses, and lignin but also in structural organization, i.e., regions which are relatively more crystalline or amorphous. The amorphous regions are more prone to hydrolysis by acid resulting in shorter and more crystalline fragments.

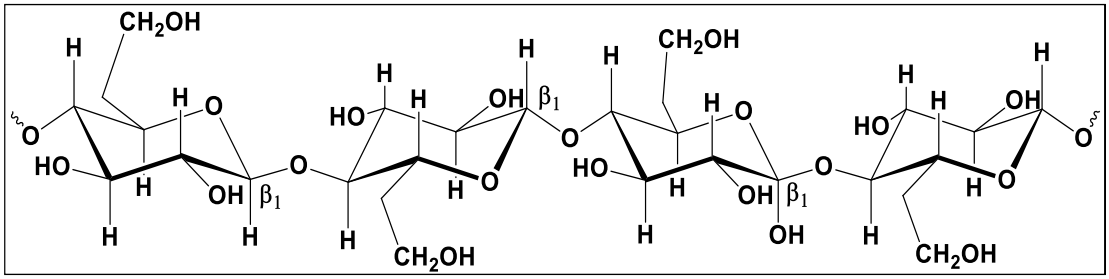

Figure 2. Structure of microcrystallinecellulose (MCC) (Repeating unit of glucose) shows the D-glucose units are linked through *β*-1, 4 bonds. O˜ represents the continuation of the polymeric chain

Non-woody lignocellulosic materials have also been developed as source of MCC such as cotton linters [72], cotton stalks [73], cotton rags [74], cotton fabric waste [75], cotton wool [76], soybean husk [77], corn cob [78], water hyacinth [79], coconut shells [80], oil palm biomass residue [81, 82], oil palm fronds [83], rice husk [84, 85], sugar cane bagasse [86-91], jute [92, 93], ramie [94], fibers and straw of flax [95], wheat straw [96], sorghum stalks [97], sisal fibers [98] and mangosteen [99], alfa grass fibers [100, 101], soybean hulls [102], orange mesocarp [103], Indian bamboo [104], roselle

fiber [105], and alfa fiber [106]. Seed flosses from milkweed pods (*Calotropis procera*), shrubs, and kapok (*Ceiba pentandra*) trees are also known as cellulosic resources. Due to its high purity of alpha-cellulose, most seed flosses must be treated to remove impurities including lignin, pectin, and wax [107]. Wooden sources contain cellulose chains which are packed as layers held by cross-linking hydrogen bonds [108]. Chemically it consists of a polymeric matrix of lignin, hemicelluloses, and pectin [109]. Different woods considerably possessed different chemical composition of cellulose (including allocations of cellulose, hemicelluloses, and lignin in the cell wall) and structural organization as well. Relatively different crystallinity in particular regions is observed as more amorphous according to softwoods (evergreen conifer) and hardwoods which are termed as deciduous broadleaf [110, 111]. The amorphous regions of cellulose provide a more susceptible property for depolymerization by acid hydrolysis. At optimum acid concentration, the process gave shorter and more crystalline fragments such as the MCC [112, 113].

(ii) Carboxymethylcellulose (CMC)

Carboxymethylcellulose (CMC) or cellulose gum (Figure 3) is an anionic cellulose ether derivatives [114, 115]. It has such abilities as thickening water, suspending solids in aqueous media and forming films it has proven to be of great commercial value.

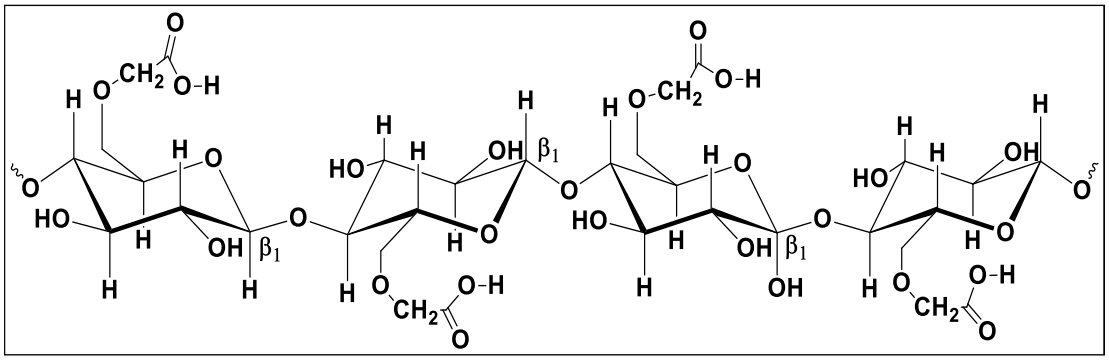

Figure 3. The structure of carboxymethylcellulose (Repeating unit of glucose) shows the d-glucose units are linked through β-1, 4 bonds. O^- represents the continuation of the polymeric chain

CMC is successfully applied as a thickener, as a soil-suspending agent, coating agent, thickener and suspending agent of several applications [116-120]. The average number of substitutes per glucose monomer known as degree of substitution is a significant

feature of CDs). The characteristics properties of CMC has already been recognized with degree of substitution [121] to enhance application in various areas.

Raw iron ore contains about 25-30% iron as mined. The iron content can be increased to 60-65% by magnetic separating drums [122]. Though the iron concentrate has an acceptable chemical quality for processing raw ore into iron, it must be agglomerated into a coarser form before it can be used in blast-furnaces. The most desirable size for blast-furnace feed ranges from 6 to 25 mm [123]. Methods of size enlargement have been known for many years ago. Of all methods available, sintering and pelletisation are the most important ones. In these process some most common inorganic binders such as CaO, CaCb and bentonite were used [124, 125]. The biggest drawback of such inorganic binders, however, is that the final product may be extremely contaminated. The pellet melting method combuses organic binders (polymers), thereby reducing the level of contamination significantly. Especially CMC has been successfully applied as an alternative for inorganic binders in the pelletisation process [126]. The success of this application depends critically on the structure of the interfacial CMC layer.

In paper industry, the most common pigments used in papermaking are China clay, calcium carbonate, aluminium trihydrate, and titanium dioxide. The main importance of CMC in papermaking relates to two applications. CMC is used alone, or in conjunction with starch, to increase dry strength properties and to improve surface characteristics [127-129]. CMC is also applied in combination with pigments. To achieve an optimal opacity with titanium dioxide, the pigments have to be of small particle size [129]. Therefore, to ensure optimal realisation the pigments must be sufficiently stabilised against flocculation by other coating ingredients. As CMC adsorbs on titanium dioxide it is frequently applied as a stabiliser. In addition, CMC associates the pigments to the paper surface due to its excellent binding ability, suggesting they can infiltrate the cellulose network. Thus, CMC acts as an adhesive as well. It used as an emulsion stabilizer in injections, adhesion and film-forming materials which have proved to be effective in controlling wound infections and can reduce postoperative oedema and wound stimulation phenomena. Animal experiments have shown that CMC is a safe and reliable carrier of anticancer drugs [130].

(iii) Hydroxyethylcellulose (HEC)

Hydroxyethylcellulose (Figure 4) in ice cream, frozen milk drinks, is added as a stabilizer to extend the storage life and improve the overflow property. It is also used as the stabilizer of beer foam. Food Due to its unique physical and chemical properties and its behaviour in water, it is today being increasingly used as a food additive to improve the bulk and the fibre content of foods without having a major impact on the flavour of the food. Since it is indigestible by humans, it has no caloric value and is thus used in excessive amounts in diet foods to create a sensation of fullness both physical and physiology without having consumed too many calories. It is also widely used as an emulsifier and a thickening agent in whipped cream, sauces and ice cream [131, 132].

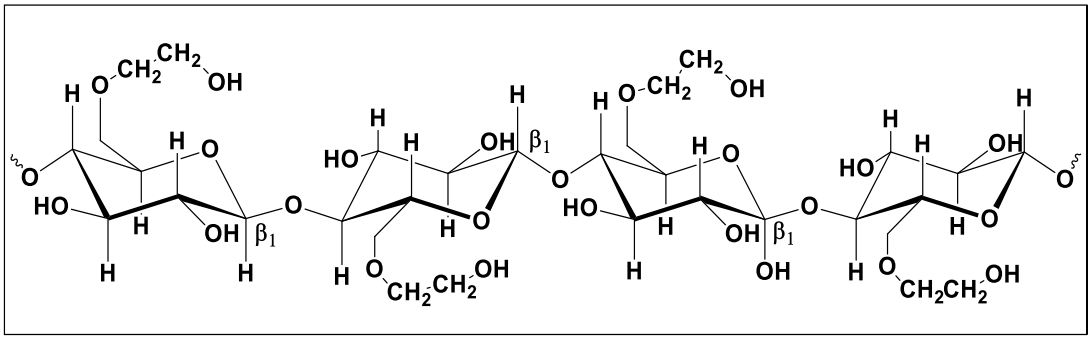

Figure 4. Structure Hydroxyethylcellulose (Repeating unit of glucose) shows the d-glucose units are linked through β -1, 4 bonds. O- represents the continuation of the polymeric chain

Hydroxyethylcellulose used as gel thickening, emulsifying, bubble-forming, water-retaining and stabilizing properties. It is used as a key ingredient in many household cleaning products, lubricants and cosmetics due to its non-ionic and water-soluble nature. HEC is widely utilized in the pharmaceutical industry not only because it is safe and non-toxic but also because it does not get engrossed orally and does not upsurge the energy of foods. It is utilized as a film-forming agent, thickener, blocker, sustained release agent, blending agent and suspending agent in many dosage forms, thus forming the numerous pharmaceutical preparation consistently discrete, tough short of being wrecked due to sustained release effects or steady emulsion without stratification. It is regularly used as a matrix, adhesives, frame ingredients, the film creating material or in the creation of sustained or controlled release microcapsules and pellets [133, 134].

Table 2 Applications cellulose and its derivatives (CDs) at the industrial level with their characteristics

Cellulose and its derivatives (CDs)	
Characteristics	**Applications at the industrial level**
Biodegradability, sustainable, high modulus, high surface area, surface functionality, high chemical resistance, renewable, excellent crystallinity, water stability, improve stability of the drug, good lubrication, rapid disintegration, good flowing properties and good binding properties	Mineral processing, petroleum, textile & dyeing, papermaking, food, pharmaceutical, cosmetics, ceramic, leather paints & lacquers, building materials, mosquito, repellent, toothpaste, battery, detergent and tobacco industry

The explanation of the diverse applications of CDs with their characteristics (Table 2) to promote more innovations that aim to bridge the gap between the amounts of cellulosic waste and its optimum utilization for industrial applications by understanding the adsorption aspects onto solid surfaces. Further, theoretical descriptions dealing with CDs adsorption has been performed based on density functional theory (DFT). The adsorption method was adopted to understand solid-liquid interphase analysis. The practical application of this technique was to analyze the feasibility of adsorbent-adsorbate system at the laboratory level due to very easy and cheap technique, hence, this aspect was also used for a small quantity of aqueous system having minimum adsorbate concentration; therefore, this operation could be feasible for the future prospectus.

4. Adsorption aspects

The term adsorption was first coined in 1881 by a German physicist named Heinrich Kayser [135]. Adsorption is often described as a surface phenomenon where particles are attached to the top layer of material. It normally involves the molecules, atoms or even ions of a gas, liquid or solid in a dissolved state that are attached to the surface. Adsorption is mainly a consequence of surface energy. Generally, the surface particles which can be exposed partially tend to attract other particles to their site. Interestingly, many physical, natural, bio- and chemical processes involve adsorption mechanism. Since adsorption is ecofriendly method which is also employed in many industrial applications [135].

The term adsorption implies the presence of an excess concentration of any particular component at the surface of a liquid or solid phase as compared to that present in the bulk of the material [136]. The adsorption phenomenon arises due to the presence of residual forces at the surface of the body. These residual forces, in solids, generates due to the presence of unsatisfied valence force of atoms and in liquid, arises because of the non-uniform distribution of molecules around the molecules at the surface. The substance that adsorbs is the adsorbate and the underlying material is the adsorbent or substrate (Figure 5). Adsorption is of great technological importance. Thus, some adsorbents are used on a large scale as desiccants, catalysts or catalyst supports; others are used for the separation of gases, the purification of liquids, pollution control or respiratory protection. Adsorption phenomena also played a vital role in many solid-state reactions and biological mechanisms [136].

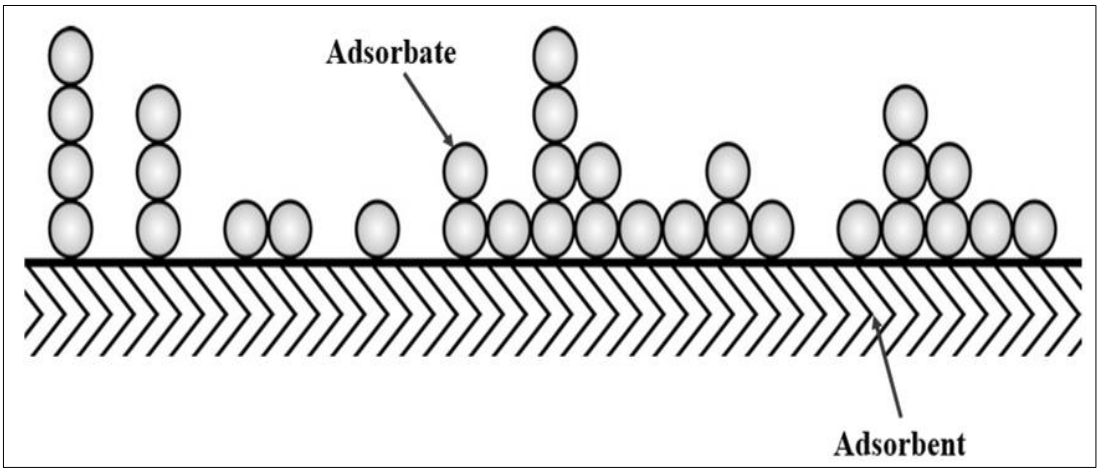

Figure 5. Adsorbate-adsorbent interaction during adsorption phenomenon

4.1. Types of adsorption

The adsorption can be categories into two types as shown in Figure 6.

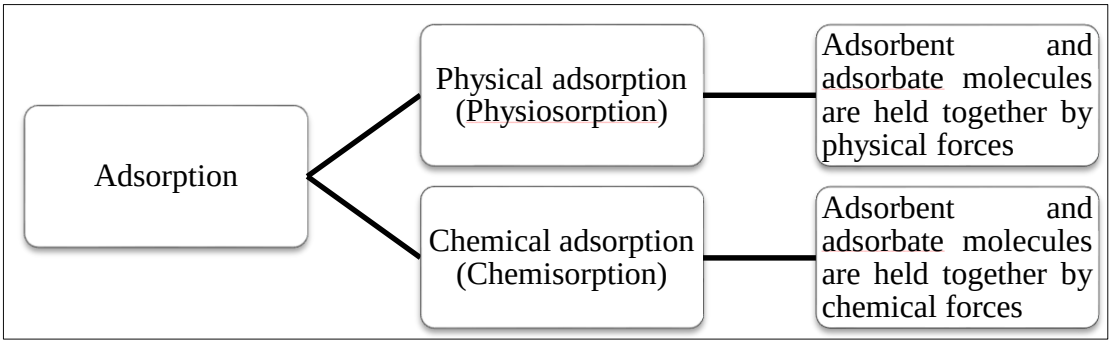

Figure 6. Types of adsorption

4.1.1 Physical adsorption (physisorption)

When adsorbate molecules do not form a strong chemical bond with the adsorbent molecule, this position is called physical adsorption or physisorption. It can be defined as 'intermolecular attractions between favourable energy sites takes place and are therefore independent of the electronic properties of the adsorbent and adsorbate concerned with no exchange of electrons is observed' (shown in Fig. 1.6). In this type of adsorption following common features are found [137-140]:-

Characteristics of physical adsorption:-

- This type of adsorption is caused by physical forces i.e. van der Waals interaction.
- Physisorption is a weak adsorption phenomenon.
- Multimolecular layers are formed at the surface of adsorbents.
- Physical adsorption is not specific and takes place all over the adsorbent.
- Surface area, temperature, pressure, nature of adsorbate effects physisorption.
- Low activation energy is required (20 – 40 kg/mol).
- Physisorption is favoured at low temperature and decrease with an increase in temperature.
- Small enthalpy change is not enough to lead to bond breaking and help to retain the identity of the physisorbed molecule.
- To initiate the process, external activation energy is not required.
- In this adsorption, the equilibrium condition is achieved very rapidly and is reversible.
- In this phenomenon without lowering the pressure, the adsorbate (contaminants) molecule can be removed.

1.4.1.2 Chemical adsorption (chemisorption)

The phenomenon where a chemical combination takes place between the adsorbent and the adsorbate the adsorption becomes very strong. This type of adsorption caused by forces similar to chemical bonds between the adsorbent and the adsorbate. In this type of adsorption, the following common features are found [141, 142]:-

Characteristics of chemical adsorption:-

- This type of adsorption is mainly caused by chemical forces (bonds).
- It is a very strong process.
- This type of adsorption is almost a single-layered phenomenon.
- Chemisorption is highly specific and takes place at reaction centres on the adsorbent.

- Surface area, temperature, nature of adsorbate effects chemisorption.
- A very high energy of activation is required (40 – 400 kJ/mol).
- The adsorbate-adsorbate forces are usually small compared to the adsorbate-adsorbent binding forces so that the adsorbate locations or sites are determined by the optimum adsorbate substrate bonding.
- The process occurs at high temperature and the heat of adsorption is 83 kJ /mol.
- External activation energy requires initiating the process.
- In this adsorption, the equilibrium condition is not very rapidly achieved and is irreversible.

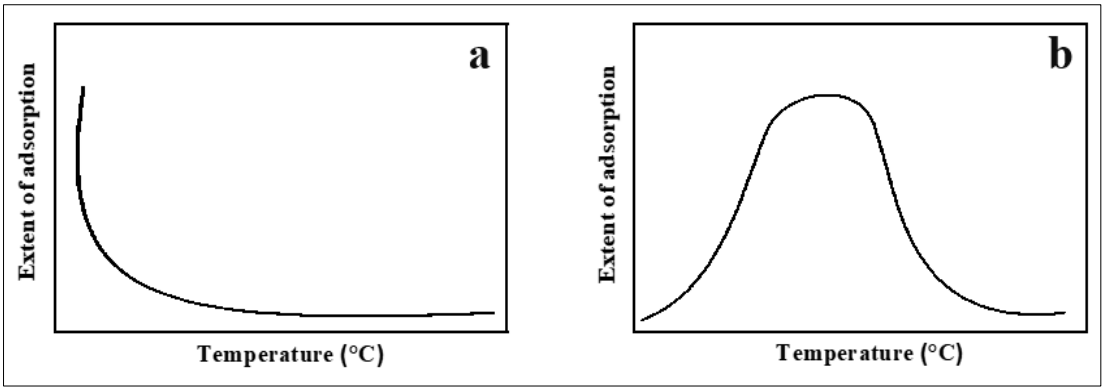

Figure 7. Graphical representation of (a). Physical adsorption, (b) Chemical adsorption

4.2. Definitions and terminology of adsorption

Some of the basic terms and properties associated with adsorption are listed in Table 3. These definitions are consistent with those proposed by the International Union of Pure and Applied Chemistry (IUPAC) [143-145] and by the British Standards Institution (146) and other Official Organizations [147].

Table 3 Some of the basic terms and their definition

S.No.	Term	Definition
1.	Adsorption	Accumulation of one or more components in an interfacial layer
2.	Adsorbate	Substance in the adsorbed state
3.	Adsorbent	Solid material on which adsorption occurs
4.	Chemisorption	Adsorption involving chemical bonding
5.	Physisorption	Adsorption without chemical bonding
6.	Desorption	The removal of the adsorbed substance from a surface is called desorption
7.	Sorption	The phenomenon in which adsorption and absorption occur simultaneously is called sorption

8.	Absorption	When the molecules of a substance are uniformly distributed throughout the body of a solid or liquid. This phenomenon is called absorption
9.	Occlusion	When adsorption of gases occur on the surface of metals this is called occlusion
10.	Adsorption complex	A molecular term used to denote the entity constituted by the adsorbate and that part of the adsorbent to which it is bound.
11.	Adsorption isotherm	The relation between the quantity adsorbed and the composition of the bulk phase (or the partial pressure in the gas phase) under equilibrium conditions at a constant temperature
12.	Capillary condensation	Occur when, in porous solids, multilayer adsorption from a vapour proceeds to the point at which pore spaces are filled with liquid separated from the gas phase by menisci
13.	Monolayer capacity	Either chemisorbed amount required to occupy all surface sites *or* physisorbed amount required to cover the surface
14.	Surface coverage	The ratio of the amount of adsorbed substance to monolayer capacity
15.	Powder	Dry material composed of discrete particles with maximum dimension < 1 mm
16.	Fine powder	Powder with particle size < 1 μm
17.	Surface area	The extent of the available surface area determined by a given method under stated conditions
18.	Specific surface area	The surface area of a unit mass of powder, as determined under stated conditions
19.	External surface	Area of the external surface of particles, as taking account of roughness (i.e. all cavities which are wider than they are deep), but not porosity
20.	Roughness factor	The ratio of external surface area to the area of smoothed envelope around particles
21.	Porous solid	Solid with cavities or channels which are deeper than they are wide
22.	Open-pore	Cavity or channel with access to the surface
23.	Interconnected pore	Pore which communicates with other pores
24.	Blind pore	Pore with a single connection to the surface
25.	Closed pore	Cavity not connected to the surface
26.	Void	Space between particles
27.	Micropore	The pore of internal width less than 2 nm
28.	Mesopore	The pore of internal width between 2 and 50 nm
29.	Macropore	The pore of internal width greater than 50 nm
30.	Pore size	Pore width (diameter of cylindrical pore or distance between opposite walls of the slit)
31.	Pore volume	The volume of pores determined by the stated method
32.	Porosity	The ratio of total pore volume to the apparent volume of particle or powder

33.	Total porosity	The ratio of the volume of voids and pores (open and closed) to the volume occupied by solid
34.	Open porosity	The ratio of the volume of voids and open pores to the volume occupied by solid
35.	Surface area	The extent of total surface area as determined by a given method under stated conditions
36.	External surface area	Area of the surface outside pores
37.	Internal surface area	Area of pore walls
38.	Interface	Any surface is a plane that separates any two phases in contact with each other. The plane which separates any two-phase is generally called an interface between the two phases.
39.	True density	The density of solid, excluding pores and voids
40.	Apparent density	The density of material including closed and inaccessible pores, as determined by the stated method

4.3 Adsorption process in aqueous solution

In general, adsorption of adsorbate (solutes) from solutions can occur on various adsorbents (solids) to different extents which are the same as for gases. It may in general be traced to two effects:-

1. Due to a decrease in the interfacial tension through adsorption of a solute, and
2. Due to solid surface acquiring electrostatic charge in a solvent.

This charged surface of the adsorbent then attaches oppositely charged ions from the solution. The adsorption process in an aqueous solution can be divided into three types [147-150].

4.3.1 Positive adsorption

When the concentration of adsorbate (solute) is more on the surface of the adsorbent as compared to its concentration in the aqueous phase means the only solute is adsorbed and the concentration of the solution gets decreased, this type of phenomenon is called 'Positive Adsorption'. When activated charcoal is kept in contact with the dilute solution of acetic acid, a part of the acid is absorbed by the charcoal and the concentration of the acid decreases is the typical example of 'Positive Adsorption' [151].

4.3.2 Negative adsorption

When the surface of the adsorbent have less concentration of the adsorbate than its concentration in the aqueous phase means when a solvent is adsorbed and the concentration of the solution is increased, this type of phenomenon is called 'Negative Adsorption'.When blood charcoal is added to a dilute solution of potassium chloride, the concentration of the solution gets increases is an interesting example of this phenomenon. This type of adsorption is very uncommon [152].

4.3.3 Electrostatic adsorption

Adsorbent surface (solids) when coming in contact with a water molecule (aqueous phase) acquire an electrostatic charge. The surface may be positively charged due to the attachment of H+ ions or negative charge due to the attached OH− ions. These acquired charges on the surface will tend to attract oppositely charged ions of adsorbate (solutes) from the solutions. This is termed electrostatic adsorption. An example of electrostatic adsorption is silica powder which acquires a negative charge when comes in contact with water. If this silica powder having a negative charge is shaken with positively charged $Fe(OH)_3$ sol and then filtered, the filtrate will be colourless, illustrating the phenomenon of electrostatic adsorption [153].

5. Method of activation of adsorbent

Adsorbents that are used for adsorption technology can be divided into two parts; one is commercial and the second is non-commercial. Commercial adsorbents are commonly derived from carbonaceous source materials like nutshells, wood and coal but their activation processes are much costly and sources are also limited. Non-commercial adsorbents (Table 4) are mostly synthesized by the low cost carbonaceous and non- carbonaceous materials, employing activation methods (chemical and physical) [154]. Activation is related to the loss of carbon. Weight loss of host carbon increases linearly with activation temperature and time. Activation at lower temperature predominates in the development of mesopores and macropores into carbon. Pore diameter decreases with increasing activation temperature to develop a micropore into carbon [155].

Activation of the carbonized materials with oxidizing atmosphere occurs by the following exothermic/ endothermic reactions. Activation with oxygen, following exothermic reactions, occurs predominantly:-

$$C + O_2 \rightarrow CO_2 \text{ (92.4 kcal)}$$

$$2C + O_2 \rightarrow 2CO \text{ (53.96 kcal)}$$

Activation with vapour and carbon dioxide following endothermic reactions may take place:-

$$C + H_2O \rightarrow CO + H_2 \text{ (29 kcal)}$$

$$C + CO_2 \rightarrow 2CO \text{ (39 kcal)}$$

$$CO + H_2O \rightarrow CO_2 + H_2 \text{ (10 kcal)}$$

It is reported that for calculations, impregnation and chemical dehydration of activated carbon, various types of activating agents have been used as phosphoric acid (H_3PO_4), zinc chloride ($ZnCl_2$), sulphuric acid (H_2SO_4), K_2S, alkali metal hydroxide like carbonate and chloride of Ca^{2+}, Mg^{2+} and Fe^{3+} [156].

Table 4 Adsorption of CDs onto various adsorbents [157]

Adsorbents	**Cellulose derivatives**
Biotite Mica	Guar gum
Amino-terminated surfaces	Carboxymethylcellulose
Talc	Carboxymethylcellulose
Pyrite	Guar gum, carboxymethylcellulose
Talc	Dextrin and guar gum
Talc	Guar gum
Leached Talc	Guar gum
Calcined Talc	Guar gum
Leached Calcined Talc	Guar gum
Talc	Carboxymethylcellulose
Polymeric surfaces	Carboxymethylcellulose
Mesoporous mustard carbon	Carboxymethylcellulose
Polymeric Surface	Carboxymethylcellulose
Mesoporous tea waste carbon	sodium carboxymethylcellulose

6. Selection of various sources of adsorbents

Several adsorbents had been employed for the adsorption of CDs from wastewater for the last few decades. The main categories of adsorbents, evaluated in the last few years are listed in table 4.

6.1 Commercial adsorbents

Several materials such as silica gel, activated alumina, zeolites and activated carbon, etc. have been extensively applied as commercial adsorbents for water contamination control that are main categories into four types-

6.1.1 Activated carbons

Among all the available adsorbent materials to date [158], activated carbon has become customary for the removal of pollutants from wastewater.

Dependence on its size and shape, activated carbon can be categorized into four types:

- Powder activated carbon (PAC)
- Granular activated carbon (GAC)
- Fibrous activated carbon (ACF)
- Cloth activated carbon (ACC)

CAC is prepared by a process consisting of raw material dehydration and carbonization followed by activation. Because of their large capacity to adsorb organic and inorganic contaminants, CAC is the most effective adsorbents. This capacity is mainly due to their structural characteristics with porous texture which gives them a large surface area (from 600 to 2000 m^2/g) and their chemical nature which can easily be modified by physical and chemical treatment to increase their properties [158].

6.1.2 Silica gel

Silica gel works as a good adsorbent due to it has a larger pore volume and mesoporosity. So it is used as a commercial adsorbent by several industries [159-160]. Based on their surface area regular, intermediate and low-density gels are the three main types of silica gels: Regular density silica gel is prepared in an acid medium and has a high surface area of 800 m^2/g. Intermediate and low-density silica gels have a low surface area of 300-350 and 100-200 m^2/g, respectively, in comparison to regular silica gel. Modified forms of silica gels have also been widely explored for the adsorption mechanism of CDs from their aqueous solutions [161].

6.1.3 Activated alumina

Activated alumina represents partially hydroxylated alumina oxide, Al_2O_3. They are porous solids made by the thermal treatment of alumina hydroxide precursors and find applications mainly as adsorbents, catalysts and catalyst supports. In general, a hydrous alumina precursor is heated; hydroxyl groups are driven off leaving a porous solid structure of activated alumina. Activated alumina having surface areas ranging from 200-300 m^2g^{-1} are versatile adsorbents and have been successfully utilized in the adsorption of CDs (Table 4) [162-163].

6.1.4 Clay and zeolites

Natural clay minerals are the strong participants as adsorbent, because of their abundance in nature, their low cost, high adsorption properties and potential for ion exchange.

Based on their layered structure, clays are mainly classified into several classes such as smectites (montmorillonite, saponite), mica (illite), kaolinite, serpentine, talc (pyrophyllite), vermiculite and sepiolite. Among minerals that possess sorbent properties, zeolites emerge as one of the most promising material as adsorbent [164-166]. Some disadvantages related to commercial adsorbents are given below:-

- Extensive
- Higher the quality, higher cost
- Performance is dependent on the type of carbon
- Requires the complexing agents to improve its removal performance
- Non-selective
- Problems with hydrophilic substances
- Ineffective for dispersing and vat dyes
- Reactivation results in a loss of carbon
- Limited sources

7. Adsorption aspects of CDs onto various solid surfaces

Many applications of cellulose (CDs) are a result of their adsorption process at a solid liquid interface, as discussed in the previous sections. Adsorption of polymer (cellulose and derivatives) molecules will take place if the interaction energy or adsorption energy of the adsorbate molecules is higher than the interaction between solvent molecules and the solid surfaces. In solution, the adsorbate molecules have many degrees of freedom which is reduced by adsorption. Thus, the energy of adsorption has to overcome the loss of conformational entropy [167]. When CDs adsorb, conformational entropy was maintained through sections of the polymeric chain which were not attached to the solid surface. The sequence of polymeric chain which were attached to the solid surface was called a tails. Loops were sections between two tails, tails consist of segments at the end of the chain dangling in the solution. Parameters that affect the conformation of the adsorbed polymer layer were the adsorption energy, the adsorbed amount of polymer, and the molar mass of the polymer, etc. In case the ratio of free surface sites and adsorbing segments was high (at low polymer concentration), the adsorption energy

contribution is the leading parameter [167]. The adsorbed amount is low, and most of the segments are situated in trails. At higher surface coverage, and if the adsorption energy is not high, loops and tails are also present. In general, for uncharged polymers, the size of the loops and tails increases with the length of the chain. Consequently, the adsorbed amount increases with molar mass. If CDs segments have high adsorption energy this quantity keeps dominating the adsorption. The conformation of the adsorbed layer was flat and the adsorbed amount does not depend on the chain length [167]. Polyelectrolytes (CDs) were charged polymers. One can distinguish polyelectrolytes with fixed charges (strong polyelectrolytes) and those with charges that depend on pH and salt concentration (weak polyelectrolytes). Electrostatic interactions play an important role in polyelectrolyte adsorption. Not only the charge of the CDs but also the charge of the substrate surface affects the adsorption. When polyelectrolyte and substrate have the same sign, electrostatics work against the adsorption. Adsorption can only take place if the non-electrostatic interaction was high enough to overcome the electrostatic repulsion between segments and substrate and the mutual repulsion between segments. As salt screens these electrostatic interactions, it can increase the adsorbed amount. Adsorption on an uncharged surface can also be enhanced by salt. If polyelectrolyte and substrate have opposite signs of charge, electrostatics favour the adsorption. Now salt can have either the effect of increasing or decreasing the adsorption. If the interaction is merely electrostatic (i.e. there is little non-electrostatic interaction) salts screens interactions between charged segments and the substrate, leading to less adsorption at the higher salt concentration (screening-reduced adsorption [168]). On the other hand, if the non-electrostatic interaction is high, the adsorption increases with salt concentration (screening-enhanced adsorption [168]). The interaction between segments and substrate with opposite charge is strong. As a consequence, at low salt concentration polyelectrolytes adapt a flat conformation when they adsorb; the adsorption does not depend on the chain length. If both the surface and CDs carry variable charges, electrostatics become a very complicated factor in the adsorption. When adsorption takes place, additional charges are introduced on the surface as well as on the CDs. The presence of charged segments near the surface affects the charge of the surface and *vice versa*. Both the surfaces used in this study (mineral and polymeric) and CMC has variable charges. At the inorganic surfaces, metal-OH groups are present, CMC has -COOH groups. Theoretical descriptions dealing with CDs adsorption were based on the assumption that the process of adsorption attains the lowest value of the free energy. When the lowest value of the free energy was reached

the process was said to be at equilibrium. So, by using thermodynamics we were able to calculate the adsorbed amount at equilibrium as a function of parameters such as polymer concentration, chain length or interaction energy. If a CDs chain has to overcome a barrier before it can adsorb, the adsorption process would be hampered. The existence of such a barrier was comparable to the activation energy of chemical reactions or the barrier for coagulation of colloidal particles. For neutral CDs, the barrier originates from loops and tails of adsorbed molecules, which obstruct the motion of chains to a surface (steric hindrance) [169-170]. In the case of CDs also long-range electrostatic interactions between a charged surface and chains approaching the surface were present. Hence, it was obvious that kinetic barriers in the adsorption process, especially for CDs, cannot be ignored. Experimental work (171-173) indicated that a barrier for CDs adsorption exists.

In many (industrial) processes CDs have found successful applications. For instance, they are well-known as an effective thickening agent in paints, preventing the settling of pigment. The rheological properties of CDs solutions also allow a uniform spreading of the paint. In papermaking, CDs has been used as additives to improve the retention of fibres and pigments or to increase the paper strength. Water-soluble CDs have practical importance in cosmetics, coatings, and wastewater purification [174-176]. Some applications were a consequence of the rheological properties of CDs solutions while others were due to adsorption at a solid-liquid interface reported by several researchers. Nowadays the relevance of understanding the adsorption behaviour of polymers at solid-liquid interfaces has been generally recognized. A detailed understanding of CDs was needed to develop new or to improve their current applications. Within the group of chemically modified natural polymers polysaccharides, in particular, CDs, have proven to be important components. Since, cellulose has been recognized as one of the world's most abundant polymers, non-toxic and biodegradable, whereby its derivatives were widely applied. An important representative of the cellulose derivatives was carboxymethyl cellulose (CMC). The CMC has been used as an additive in papermaking, in pharmaceuticals and cosmetics, and food products [174-176]. For the pelletisation of iron ore, the addition of an inorganic binder such as bentonite has proven to be very effective. However, inorganic binders have the disadvantage that they cause serious contamination in the final product. Organic binders (polymers) are combusted in the pellet melting process, thereby strongly reducing the amount of contamination. Especially, CMC has been successfully applied as an alternative for inorganic binders in the pelletisation process

[178]. This application was a consequence of its adsorption behaviour at a solid-liquid interface. Since CMC was a highly charged polyelectrolyte, its adsorption behaviour could be strongly affected by electrostatics. This clearly shown up in the adsorption dependence on pH and electrolyte concentration. For instance, for the adsorption of CMC with degree of substitution was DS=0.7 on barium sulphate [179]. Nag et al observed an increase in the adsorption of CMC with decreasing pH, at constant CMC concentration. At constant pH, an increase in adsorption of CMC with increasing salt concentration was also observed. The qualitative agreement with those experiments was found by Williams et al [180]. Besides, these authors investigated the influence of ds on adsorption. A slight difference was found between CMCs having degree of substitution 0.78 and 1.25, respectively. CMC having specific degree of substitution (0.45) showing a large amount of adsorption [181, 183]. The adsorption on hydroxylapatite slightly lower values for high molecular mass CMC (Mw=80 kg mol) than for CMC with Mw=10 kg mol. However, the adsorption of polymers has been less explored [184-190]. Our understanding of the binding mechanism of the CMC at the solid-liquid interface has been increasing year by year as significant work has been devoted to the adsorption of CMC onto the mineral surfaces. Several binding mechanisms have been developed, but as yet no common mechanism has received general acceptance. Thus, the associated problems have received adequate attention. Raju et al [191] reported the adsorption of polysaccharides (dextrin) onto graphite is apparently due to hydrophobic-hydrophobic interaction. Laskowski's investigation on adsorption of CMC on graphite has shown that while pure high-quality graphite (Ceylon) adsorbs CMC strongly. However, the same graphite purified by leaching practically does not adsorb CMC almost at all. According to Mackenzie and his co-workers [192], Pugh [193], Healy and Macromol [195] and Rath et al. [196] investigated adsorption of CMC onto mineral water surfaces is due to complex interplay of electrostatic, hydrophobic, hydrogen bonding and chemical interactions, although, the selective adsorption of CMC on minerals has not been demonstrated clearly. The binding mechanism of CMC on minerals was also proposed by Steenberg et al [197, 198] and Jenkins et al [199] and according to them, adsorption is primarily attributed to hydrophobic force onto basal planes. Contrary to this, Rath et al [200] and Jucker et al [201] reported that the binding mechanism of polysaccharides is attributed to hydrogen bonding on solids. Employing infrared spectroscopy, Bakinov et al [202] notices some changes in the carboxyl group upon adsorption and concluded that the carboxyl group interacts with metal ions on the surface of solid (talc). However, they

scanned infrared spectra (transmission mode) of dried samples causing any deduction on polymer binding mechanisms to be overshadowed by the substantial alteration to the polymer's environment during dehydration. Furthermore, no infrared spectra were presented in this work. Wang and Somasundaran [203] also used infrared spectroscopy to support their hypothesis of hydrogen bonding; however, their work also involved sample drying and analysis by infrared transmission. Cuba-Chiem et al [204] based on in situ films attenuated total reflection-Fourier transform infrared (ATR-FTIR) spectroscopy (in liquid form) has proposed that the polymer (CMC) most likely has two different interactions with the solid surface, with a stronger interaction with the talc edge through chemical complexation and a weaker interaction with the talk basal plane presumably through the hydrophobic interaction. Fujimoto and Petri [205] also studied the adsorption behaviour of CMC on amino-terminated surfaces and reported that CMC adsorbs onto amino-terminated surfaces driven by electrostatic interactions. The adsorbed amount decreases with ionic strength, in agreement with the screening-reduced adsorption regime. The charge on the amino-terminated substrate and molecules charge along the CMC chains is strongly influenced by the pH. However, adsorption behaviour is mainly controlled by the surface charge. On the other hand, advances in nanomedicine have promoted the development of nanomaterials, for many innovative applications regarding in vitro and *in vivo* diagnostics, imaging, immunolabeling, gene delivery, and cancer therapy because of their biometric features, high surface area to volume ratio, and the possibility of modulating their surface properties with biomolecules [206]. Nowadays, nanomaterial especially mesoporous material is broadly divided into two types, namely, inorganic and polymeric nanomaterials. A major area of polymer coatings uses CDs to modify surfaces and colloids, exploiting electrostatic attraction for their deposition.7,8 The adsorption of CDs onto oppositely charged curved and planar surfaces has attracted a great deal of interest and stimulated experimental,[207-210] theoretical,[211-214] and simulation [215-220] studies. These investigations have revealed that many parameters affect the adsorption of CDs onto oppositely charged colloidal surfaces. Generally, the strength of the electrostatic interaction has been found to depend on CDs characteristics such as the charge density of the hydroxyl groups, chain length, and chain flexibility as well as colloidal features such as the colloidal surface charge density, size, and shape. Besides, extensive system variables (i.e., temperature, pH, and ionic strength of the medium) can play important roles. It was usually observed that with increasing CDs concentration, adsorption increases until saturation occurs. In this process, the surface charge

decreases, changes sign, and continue to increase in value. Theoretical considerations16 suggested that the connectivity between the charges of the hydroxyl ions of CDs leads to an overcharge or charge inversion of the colloidal surface, which can adsorb a polyion chain with a total charge of up to 15/6 times its charge. In another theoretical approach, it was shown that the adsorption of polyions near an oppositely charged surface is mainly governed by the direct Coulomb attraction from the surface and the excluded volume effects. It was also demonstrated that charge inversion becomes more momentous when the surface charge density or polyion chain length increases. There was consensus about the view that electrostatic attraction plays an important role in polyion adsorption at an oppositely charged surface of a solid. The simplest theoretical approach was called the ion-exchange model [221] which was based on the idea that the adsorbed polyions successfully compete with small monovalent ions and neutralize the surface because of entropic effects. Although this model can qualitatively explain several properties, some phenomena such as charge overcompensation cannot be interpreted in the framework of the simple ion-exchange model. In this case, it was argued [222] that it was not the net surface charge that controls the polyion adsorption onto solid surfaces but rather the possibility of forming ion pairs between polymer chains and surface groups. Ion pairs were considered to be contacting molecular groups of opposite charge; the electrostatic binding energy is deemed to be weak. Therefore, the polyion sticks to the surface because there are many of these bonds, not because these bonds are strong. In many cases, the adsorbed polyion layer was thicker than the layer adsorbed by the corresponding uncharged polymer. Theoretical models for CDs adsorption to an oppositely charged surface suggested that at low surface charge densities the thickness of the adsorbed layer was determined by the balance between electrostatic attraction to the charged surface and chain entropy [223]. For higher surface charge densities, the thickness of adsorbed polyion chains was governed by the balance of the energy gain due to electrostatic attraction and the confinement entropy lost because of chain localization. The thickness of the adsorbed layer was expected to decrease with increasing surface charge density. The strong lateral repulsion that builds up when the polymer charge density increases frequently lead to a rather flat polyelectrolyte layer on an oppositely charged surface [224]. The adsorption of a hydrophobically modified polyelectrolyte may lead to a more intricate situation because in this case, molecular simulation studies show that the conformation of the polymer chains may change and this can lead to a redistribution of the number of trains, loops, and tails in the adsorbed layer. Besides, the enhanced hydrophobic interactions may

generate a multilayer of the adsorbed CDs. The addition of salt to a suspension of particles containing hydrophobically modified CDs may lead to an alteration of the adsorption process because of hydrophobic interactions between the surface and polyions. Earlier studies [225, 226] on the adsorption of CDs show that both the adsorbed amount and the conformation of the adsorbed polymers were sensitive to temperature changes and the hydrophobicity of the surface and the polymer. In previous work, [227-229] the study of the adsorption of uncharged CDs onto solid surfaces demonstrated that hydrophobic interactions between the polymer and the surface constitute the main driving force for adsorption. In this research work, we addressed how adsorption of polymers onto solid and polymeric surfaces occurred?

Cellulose-based polymers hydroxyethylcellulose (HEC) have numerous applications in the pharmaceutical industry. For example, as steric stabilizers of drug particles/nanoparticles in injectable and oral delivery [230, 231], as coatings for controlled release and taste masking of tablets [232, 233], as rheological modifiers in pharmaceutical formulations [234, 235], and for enhancing compaction and dissolution characteristics of drug powders [236, 237. It was generally the adsorption characteristics of the polymer at the pharmaceutical powder–liquid interface that controls performance in the above applications. In particular, it was the polymer conformation at a drug particle surface that plays a critical role in colloid stability, interfacial adhesion and dissolution behaviour. However, the crystal face-dependent surface chemistry, sensitivity to moisture, complex dissolution characteristics, and varied hydrophobicity of drug particles [238, 239] have conspired to make direct studies of adsorbed cellulose-based polymers on drug particles irreproducible [238, 239) and therefore rarely reported. Adsorption studies on model colloidal particles (240) and at solid-liquid interfaces (241) have therefore been employed to gain insight into the adsorption mechanisms of cellulose polymer excipients used during pharmaceutical processing. This study was primarily concerned with the adsorption characteristics of HEC, a water-soluble polymer with many pharmaceutical applications. Malmsten and co-workers have investigated HEC adsorption onto silica, hydrophobized silica, and mica surfaces using ellipsometry (242, 243), with complementary studies using the surface force apparatus (244, 245–247). The HEC was shown to adsorb more strongly onto the more hydrophobic surfaces. Adsorption also increased with increasing temperature and this effect was more pronounced on hydrophobic than hydrophilic substrates. Hydrophobic interactions were proposed to dominate the HEC adsorption mechanism [248]. Hoogendam et al. [249] have undertaken dynamic light scattering

studies of the layer thickness of hydroxyethyl cellulose (HEC) polymers on silica particles and reported extensively thick layers below pH 9.0 (up to 80 nm) in comparison with ~8 nm for HEC on mica [250]. These same authors also reported a strong influence of pH on adsorption and suggested that hydrogen bonding through the hydroxyethyl side group of HEC and the silanol groups of silica played a key role in the adsorption mechanism. It is clear that the adsorption mechanisms of cellulose polymers are subtly controlled through the solvent–segment and segment–surface interactions, and these were in turn strongly influenced by the temperature and surface chemistry of the adsorbent.

Further investigations are required to more fully understand the interplay between the specific surface interactions of cellulose-based polymers, their structure at the solid-liquid interface, and their steric stabilizing action [251]. This may then be used to optimize the performance of cellulose-based polymers during pharmaceutical processing. In the current investigation, HEC interaction with colloidal silica spheres was characterized in terms of equilibrium adsorption isotherms and thermodynamics of adsorption. The solution and surface interactions are probed through variation of the solution temperature and surface modification of the silica spheres by physical treatments [252]. The competition between electrostatic effects and hydrophobic interactions in the adsorption of these biopolymers onto solid surfaces can be scrutinized. Several studies have been included UV-visible spectroscopy, dynamic light scattering (DLS), and quartz crystal microbalance with dissipation monitoring (QCM-D) to monitor the adsorption of the different polymers onto solid surfaces [253-260]. However, this work aimed to elucidate hydrogen bonding rather than hydrophobic and electrostatic interactions on the adsorption of polymers onto solid surfaces. To the best of our knowledge, the combination of the varying various influencing parameters of a polysaccharide concerning adsorption onto various solid surfaces has not previously been addressed.

Herein, the CDs namely cellulose (CL), sodium carboxymethylcellulose (NaCMC) and hydroxyethylcellulose (HEC) and they were mainly used as flotation depressants. CL, Na-CMC and HEC are the main representatives of the cellulose ether group. The selected polymers exhibit the characteristics properties such as a water-soluble, hydrophilic, and macromolecular anionic polymer without any refinement in various sectors. HEC is prepared by treating alkali cellulose (cellulose in a hot aqueous solution containing about 50% sodium hydroxide (NaOH) with ethylene oxide (C_2H_4O). The

HEC usually has polyethylene oxide side chains. Since HEC has been recognized as a water-soluble polymer it was applied as a thickener and pigment-protective colloid in water-based paints. Further, it has also applications in cement, in pharmaceutical emulsions, as a binder in tablets, and in cosmetic products. The Na-CMC is prepared by the reaction of sodium monochloroacetic acid and alkali cellulose [254]. Though most applications concern the sodium salt of CMC, it is generally referred to Na-CMC. As Na-CMC has such abilities as thickening water, suspending solids in aqueous media and forming films it has proven to be of great commercial value as a thickener for textile printing pastes, as a soil-suspending agent in synthetic detergents, as a coating for powders and tablets, and as a thickener and suspending agent in water-based paints [255]. The applicability of polymers was associated with adsorption behaviour due to solid surfaces and makes them suitable for a wide range of applications in various sectors especially in mineral processing [256]. The adsorption behaviour of selected polymer could vary due to functional groups present on them (Scheme 2). Several studies were presented for the adsorption of natural polysaccharides (dextrin, starch) on mineral surfaces through chemical interaction with superficial metal hydroxides and it was suggested that their adsorption mechanism on mineral surfaces as chemical complex formations [257-260]. Even the chemical interaction was proposed as the main mechanism of polysaccharide adsorption on mineral surfaces the different mechanisms were observed by different researchers for the same mineral-polysaccharide system [261]. However, for the flotation system, it was crucial to understand how the adsorption of each reagent takes place on the minerals surfaces and what was the adsorption capacity of each one to have more information about the rate of overcoating of the minerals and which adsorption processes were involved [262]. The adsorption behaviour of cellulose and derivatives polysaccharides various solid surfaces have been reported including kaolinite surface and other oxide minerals at different pHs, background electrolyte, and ionic strength. The polymer adsorbed onto the mineral surface through various interaction were reported by several researchers [262].

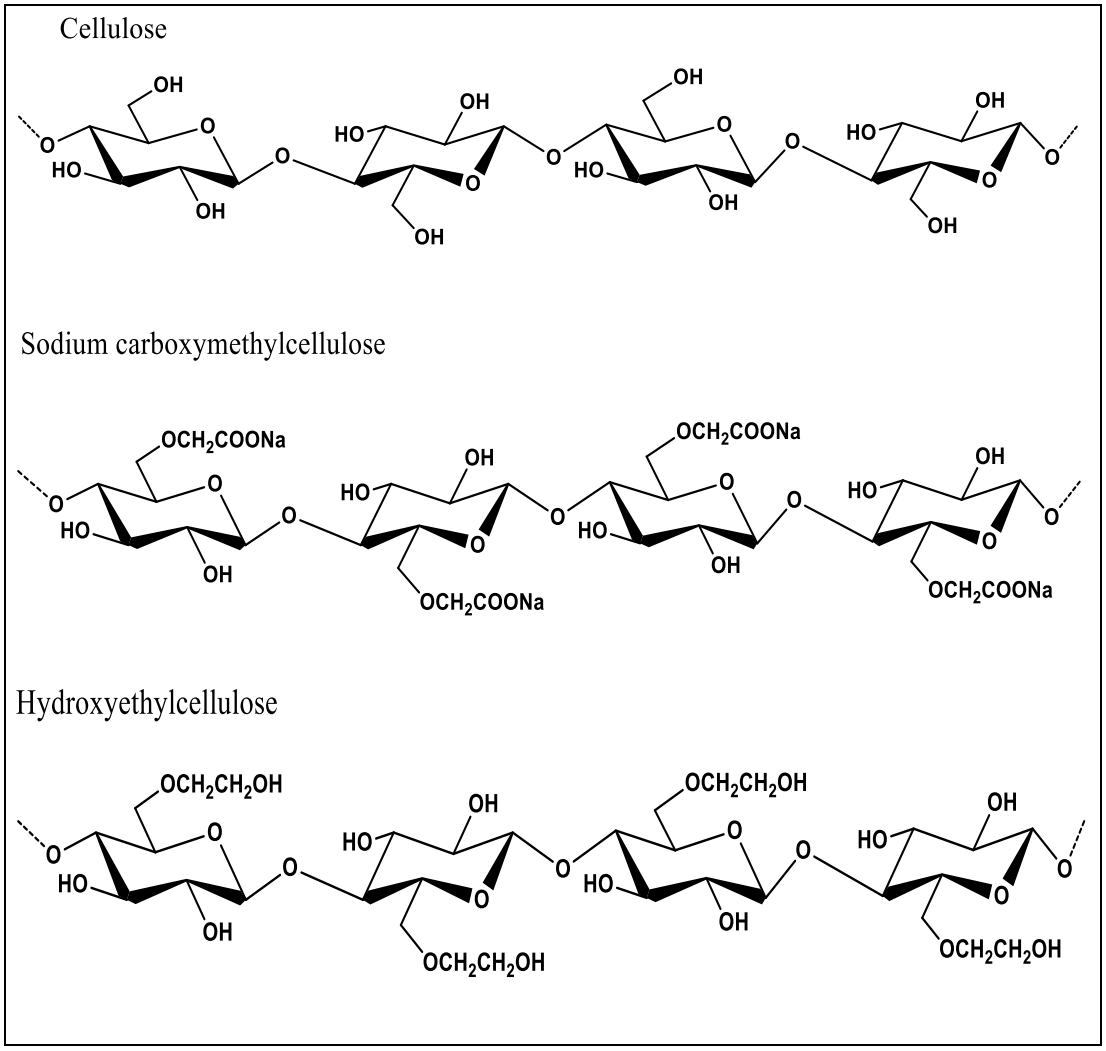

Scheme 2. Structure of CDs (Repeating unit of glucose) shows the d-glucose units are linked through β -1, 4 bonds. ----O represents the continuation of the polymeric chain (2D chain) respectively

The reported studies revealed that CDs have a natural affinity towards these mineral surfaces. The majority of these works were carried out to understand the application of polymers as a depressant in flotation, mineral processing and selective flocculation system. However, not many reports were available regarding the polymers for the adsorption behaviour mechanism. Therefore, new interest to observe the adsorption behaviours of polymers (CL, Na-CMC, and HEC) onto a solid surface was performed. However, several studies were conducted in the past but the mechanism of adsorption of polysaccharides on solid surfaces was not yet well understood. Several researchers proposed that the mechanisms governing the adsorption of polymers (polysaccharides) onto mineral surfaces include hydrophobic interaction, hydrogen bonding, chemical, and electrostatic interactions [263-270]. However, the reasons for the selectivity of the adsorption behaviour of depressants onto minerals have not been accounted for.

Therefore, the physiochemical aspect for the adsorption behaviour of CL, Na-CMC and HEC onto solid surfaces from its aqueous solutions was the topic of research interest and gave CL, Na-CMC and HEC's selective adsorption characteristics. The experimental data were treated and modelled according to adsorption theories because adsorption has been an effective separation process for a wide variety of applications and comparison of linear regression and nonlinear regression analysis of Langmuir and Freundlich have been applied to the experimental data.

The prime objective of this research was to establish an understanding of the adsorption behaviour of CL, CMC, Na-CMC and HEC onto solid surfaces and to determine the most desirable conditions to increase the applicability of selected polymers in various fields. The solid surfaces were evaluated with various physicochemical parameters such as zeta potential, specific surface area, pore diameter, pore-volume, particle size distribution, mesoporous nature employing various depth characterizations. Further, the validation of the adsorption data of aforesaid polymers two most common adsorption isotherm models namely Freundlich and Langmuir isotherms were considered. Based on the results, it was suggested that the physicochemical binding aspects of selected polymers onto solid surfaces were stabilized by H-bonding and other weak noncovalent interactions and such alteration could play a noteworthy role in the field of food, pharmaceutical, and industrial applications particularly in mineral processing by gaining a more developed understanding of the adsorption mechanism of cellulose and its derivatives onto various solid surfaces.

8. Objectives of the research work

Following were the main objectives of the present research work:-

- **Modified adsorbents were synthesized and characterized employing various analytical techniques.**
- **The adsorption of cellulose and its derivatives (CDs) such as carboxymethylcellulose, sodium carboxymethylcellulose, hydroxyethylcellulose as representative selection of polysaccharides onto these modified adsorbents.**
- **The effect of various process parameters such as effect of concentration of adsorbate, dose of adsorbent, pH, ionic strength, temperature, contact time, sonication and the presence of urea, etc. on adsorption.**
- **Observed data of studied adsorbent-adsorbate system were computed in terms of various adsorption models.**
- **Surface characterizations of adsorbents/adsorbates were done by photoelectron spectroscopy (XPS).**
- **Energetics of the studied adsorption system for evaluation of kinetic and thermodynamic parameters.**
- **Density functional theory (DFT) calculations were performed using Gaussian 16 program for some selected adsorbent-adsorbate systems.**

9. Proposed methodology

- **For the preparation of modified adsorbents chemicals such as H_2SO_4 and H_2O_2, etc. were used.**
- **Modified adsorbents were prepared employing physical and chemical activation methods.**
- **For the characterization of modified adsorbents FT-IR, UV-VIS, SEM, AFM, XRD, TGA, BET, BJH and, DFT, etc., techniques were used.**
- **Batch mode adsorption experiments were conducted.**
- **The residual concentration of cellulose and its derivatives was evaluated using UV-visible spectroscopy.**
- **Effect of various process parameters such as pH, ionic strength, temperature, the concentration of adsorbents, amounts of adsorbents, etc. on adsorption were investigated.**
- **Effect of sonication and presence of hydrogen bond breakers onto studied adsorption system were also investigated.**

10. Importance of the work

Adsorption is one of the effective methods to understand solid-liquid phase interaction analysis, which is used at the laboratory level. The importance of polysaccharides/polymers such as cellulose and its derivatives have been generally recognized. The use of CDs have been covered with a broad range of applications. Roughly speaking, it can classify these applications in terms of plastics, as thickening agents, or as coating materials, dispersant and depressant in mineral processing, etc. The work described in this thesis is related to CDs applied as adsorbate material for exploring the binding mechanism onto various slid surfaces. Often CDs are being used as an adsorbate for various industrial purpose, for instance, they provide the colloidal stability of the pigment in paints. The raw materials/polysaccharides are widely available from natural sources, they are non-toxic, and cause less harm to the environment than synthetic polymers. Since the interest in chemically modified CDs were still growing, more research concerning their behaviour at solid-liquid interfaces was needed. The use of new modified adsorbents was investigated as a replacement for existing non-economical methods for synthesis of adsorbent for understanding adsorption mechanism of CDs at solid-liquid interfaces. Nowadays, the relevance of understanding the adsorption behaviour of CDs at solid-liquid interfaces was an area of research interest. This detailed understanding of the adsorption behaviour was needed to develop new or to improve current applications of CDs. The simple laboratory experimental observations that could allow macroscopic evaluation of adsorption behaviour of polysaccharides onto a solid surface and would provide a new idea for the adsorption mechanism aspects onto solid-liquid interfaces during mineral processing and other allied applications. The applicability of CDs mainly depends on the adsorption mechanism during the solid/liquid interface. However, a satisfactory common adsorption mechanism of CDs onto solid surfaces was not established. Therefore, there was a need and area of research interest to explore the binding mechanism of CDs onto various solid surfaces. During the mineral processing like flotation of sulfide minerals highly toxic inorganic species were used as dispersant and depressant which ultimately cases environmental toxicity. Therefore, there was an urgent need for various alternative nontoxic dispersant and flocculants. This present study has provided clear understating related to the adsorption behaviour of CDs onto various solid surfaces. Thus, the use of studied potential adsorbates may contribute to the sustainability of the environment also.

11. Outline of this thesis

The main objective of the present research work was to explore the adsorption mechanisms that play an important role during the adsorption of cellulose and its derivatives namely carboxymethyl cellulose, sodium carboxymethyl cellulose and hydroxyethylcellulose (CMC, HEC, NaCMC) onto various solid surfaces. The effect of various process parameters like concentration of polymers, the dose of adsorbents, pH, salts concentration, the concentration of urea, DMSO, alcohols**,** contact time, temperature, and sonication during adsorption experiments were investigated. The theoretical aspects were also investigated employing density functional theory (DFT). The thesis consists of mainly seven chapters with some appendices as briefly described below:-

Chapter 1 describes basic information related to cellulose and its derivatives and basics about the adsorption process. The literature survey of adsorption of cellulose and its derivatives onto various adsorbents including conventional and non-conventional (low cost) adsorbents, their sources and their viability have also been illustrated in this chapter.

Chapter 2 presents the experimental methods and characterization techniques to characterize the synthesized adsorbent from various raw materials. It also deals with the details of methodology like physical and chemical methods for adsorbent preparation and solid-liquid interphase analysis for cellulose and its derivatives onto prepared solid surfaces (adsorbents). A brief discussion on Fourier-transform infrared spectrometer (FTIR), attenuated total reflection-Fourier transform infrared (ATR-FTIR) spectrometer, scanning electron microscope (SEM), energy dispersive X-Ray analysis (EDX), elemental mapping analysis (EMA), powder X-ray diffraction ($_P$XRD), Brunauer–Emmett–Teller (BET) surface area analyzer, X-ray photoelectron spectrometer (XPS), thermogravimetric analysis (TGA), advanced high-intensity ultrasonicator (AHIU), zeta-potential analysis and ultraviolet-visible (UV-Vis) spectrophotometer have been provided in this chapter.

In chapter 3, the adsorption mechanism of carboxymethylcellulose onto mesoporous mustard carbon has been described. Carboxymethylcellulose (CMC) is a versatile polymer for several industrial applications consisting of oil drilling, detergents, food and beverage, papers, ceramics, coatings, and other promising usages. The lack of

exploration of the CMC's binding mechanism on solid surfaces in the aqueous setting, indeed, retards its applications. An attempt has, therefore, been made here to enhance the understanding of the binding aspect of CMC on mesoporous mustard carbon (MMC). The MMC had a typical surface area (S_{BET}) of 16.576 m^2g^{-1}, primarily distributed by mesopores (average pore diameter and total pore volume of MMC were found to be 12.432nm and 0.051cm^3g^{-1}, respectively). The electrokinetic findings indicated that the MMC interface is negatively charged in basic medium, which favoured CMC adsorption acidic region. The adsorption free energy of CMC was found as -22.561 $kJmol^{-1}$ which was in close agreement with H-bond energy revealing hydrogen bonding to be a dominant force for CMC (L2 type) adsorption which was also confirmed by high-resolution X-ray photoelectron spectrophotometer, attenuated total reflection Fourier transformation infra-red and urea test. A simple description of the binding aspects of CMC on the MMC can therefore support CMC as a promising adsorbate for various industrial applications. The optimized titled model, adsorbent-adsorbate complex (MMC-CMC) considered in the theoretical study, is structured by mild to moderate noncovalent (intra- and intermolecular) interactions to assess the intermolecular interaction(s) between the adsorbent and adsorbate and is stabilized by these interactions. Based on binding energies (BEs), the FMO-based HOMO-LUMO gap, natural population analyses, the Bader's QTAIM-based parameters, and a recent measure reported recently as 'hydrogen bond strength based on interaction coordinate (HBSBIC)' with the deployment of computational B3LYP and M06-2X using 6-31+G basis set, the structural, stability, electronic, and charge transfer features were described.

In chapter 4, the adsorption mechanism of carboxymethylcellulose onto functionalized accurel was included. The functionalized accurel (FA) was derived from polypropylene-based (MP1001). The physiochemical parameters of FA such as specific surface area (S_{BET}) =34.472 m^2/g, pore volume (Vp) =0.07-0.121 cm^3/g, total pore volume (Vtp) = 0.115 cm^3/g, mean pore diameter = 13.692nm and pore diameter =39.402nm was determined by Burner Emmitt Teller (BET) analysis. The batch shaking adsorption experiments with various parameters were tested and the equilibrium isotherm data were fitted with Freundlich, Langmuir, Temkin and Jovanovic model of adsorption and compared by determination coefficient (R^2), and found to obey the order as Langmuir (R^2=0.9933)> Freundlich (R2=0.9830)>, Jovanovic (R^2= 0.9428)> Temkin (R^2 =0.8663). The infrared and X-ray photoelectron

spectral changes before and after adsorption were recorded which confirmed the hydrogen bonding between the carbonyl group of CMC and functional groups (-OH) present at the surface of FA in the region 288-280eV and 1772-1676cm^{-1}, respectively. To understand the type, nature, and strength of interaction(s) involved in the adsorbent-adsorbate complex (FA-CMC), a theoretical model is adopted herein this report. With the deployment of the DFT dispersion-corrected (DFT-D) and DFT approaches, the geometric, stability, and electronic feature analyses have been performed using the optimized structure, binding /interaction energy, HOMO-LUMO gap, natural population analyses, Bader's quantum theory of atoms in molecules (QTAIM) based parameters. The reactive sites of the aforementioned species have been detected by using the molecular electrostatic potential surface (MESP) map. The exhibition of different geometrical and electronic features including the binding aspects of the adsorbate CMC onto the polymeric surface was exercised *via* CMC accumulation stabilized by H-bonding and other weak noncovalent interactions.

In chapter 5, physiochemical aspects for the adsorption behaviour of sodium carboxymethylcellulose onto mesoporous granular fine quart surface from its aqueous solutions was mentioned. This chapter focused on adsorptive properties and the nature of the interaction between sodium carboxymethyl cellulose (NaCMC) and mesoporous granular fine quartz (MGFQ) applying various in-depth characterization techniques and adsorption isotherm models. The physiochemical parameters of MGFQ such as specific surface area (S_{BET}) =11.34 m^2/g, pore volume (Vp) =0.09 cm^3/g, total pore volume (Vtp) = 0.09 cm^3/g, mean pore diameter = 32.52 nm were determined. The thermal gravimetric analysis result revealed that NaCMC could be used at a specific temperature (251°C), which was suitable for its application. The equilibrium isotherm data were fitted with Langmuir, Freundlich, Temkin and Jovanovic model of adsorption and compared by linear determination coefficient (R^2), obeyed the order as Freundlich (R^2=0.9984)> Langmuir (R^2=0.9194)>Temkin (R^2 =0.8899)>Jovanovic (R^2= 0.8709). The infra-red spectral changes in the region 1104 cm^{-1} and 1076 cm^{-1} suggested that NaCMC accumulates onto MGFQ which was stabilized by H-bonding and some other weak noncovalent interactions depending on the solution optimized conditions.

.**Chapter 6** illustrates the adsorption behaviour of polymers onto activated kaoline derived by physical method. The systematic investigation of the adsorption behaviour of polymers such as cellulose (CL), sodium carboxymethylcellulose (Na-CMC) and hydroxyethylcellulose (HEC) onto activated kaolin was studied by measuring kinetics

and thermodynamic parameters. The specific surface area (S_{BET}) of activated kaolin was S_{BET} =18.57 m^2/g. The electrophoresis measurements at pH 7.0 revealed that activated kaolin possesses a positive surface. Moreover, the adsorption data were analyzed by the adjusted R^2 value of CL, Na-CMC and HEC. Adjusted R^2 suggested the results were in favour of the data collected from the experiment. The equilibrium data of activated kaolin was studied using Freundlich, Langmuir, Elvoich and Halsey and it was found to best fit the Langmuir one. Experimental data of the present work were excellently fitted to the Langmuir equation since the adjusted R^2 gave high correlation coefficients R^2>0.99 than HEC and CL. The values of Langmuir constants indicate that the mechanism that contributes most to the adsorption process in all experiments was hydrogen bonding. This exploration of the adsorption behaviour of polymers onto activated kaolin provides substantial evidence to prove beyond doubt that adsorption mainly occurs *via* hydrogen bonding followed by some electronic interactions.

Conclusions and prospects of the present work have been described in chapter 7. The overall aim of the work was to explore the adsorption behaviour of cellulose and its derivatives onto various solids. Last but not the least, the studied alternative adsorbents were found to be highly effective to explain solid-liquid phase integration analysis between polymers and various solid surfaces. In many (industrial) processes, cellulose and its derivatives have been found successful applications as an effective thickening agent in paints, preventing settling of pigment, additives to improve the retention of fibres, dispersants due to their characteristics properties. Nowadays, the relevance of understanding the adsorption behaviour of polysaccharides (cellulose and its derivatives) at solid-liquid interfaces is an area of research interest. This detailed understanding of the adsorption behaviour was needed to develop new or to improve current applications of cellulose and its derivatives. The simple laboratory experimental observations that could allow macroscopic evaluation, the adsorption behaviour of polysaccharides onto a solid surface and would provide a new idea for the adsorption mechanism aspects onto solid-liquid interfaces during mineral processing and other allied applications. The applicability of polysaccharides mainly depends on the adsorption mechanism. However, a satisfactory common adsorption mechanism of polysaccharides and their derivatives onto solid surfaces was not established. Therefore, there was a need to explore the binding/adsorption mechanism of polysaccharides and their derivatives) onto various solid surfaces. During the mineral

processing like flotation of sulfide minerals highly toxic inorganic species were used as dispersant and depressant which ultimately cases environmental toxicity. Therefore, there was an urgent need for various alternative nontoxic dispersant and flocculants. Thus, the use of studied potential adsorbates may contribute to the sustainability of the environment also. Undoubtedly, the present study could explore the insight related to the adsorption mechanism of polysaccharides onto solid surfaces and tested adsorbates seem to offer a lot of probable benefits for commercial purpose in future. Hence, the adsorption of cellulose and its derivatives onto various solid surfaces could also open new possibilities for various industries.

Reference

1. Yadav, P. Biomedical biopolymers, their origin and evolution in biomedical sciences: a systematic review.*J. Clin. Diagnostic Res*. **2015**, 9, 21-25.
2. Kumar, G. P.; Sai, R. S.; Venkatesh, P. D.; Venkat, P.; Shree, V.; Chithananthan, C.; Geetha, K. An update on overview of cellulose, its structure and applications. *Cellulose*. **2019**, 1, 1-21.
3. Aravamudhan, A.; Ramos, D. M.; Nada, A.; Kumar, S. Natural polymers: polysaccharides and their derivatives for biomedical applications. *Elsevier Science*. **2014**, 1, 67-89.
4. Zhang, Z.; Ortiz, O.; Goyal, R.; Kohn, J. Biodegradable polymer in principles of tissue engineering: 4th ed. Elsevier Inc. **2013**.
5. Rose, M.; Palkovits, R. Cellulose-based sustainable polymers: State of the art and future trends. *Macromol. Rapid Commun*. **2011**, 32, 1299-1311.
6. Kalia, S.; Dufresne, A.; Cherian, B.; Kaith, B.;Avérous, L.; Njuguna, J.; et al. Cellulose-based bio- and nanocomposites: A review. *Int. J. Poly. Sci*. **2011**, 1-35.
7. Aunina, Z.; Bazbauers, G.; Valters, K.; Feasibility of bioethanol production from Lignocellulosic biomass. *Scient. J. Riga Tech. Uni. Environ. Climate Tech*. **2010**, 4, 11-15
8. Niwińska, B. Digestion in ruminants. in: carbohydrates-comprehensive studies on glycobiology and glycotechnology. *IntechOpen*. **2012**.
9. Zhang, T.; Yang, Y.; Liang, Y.; Jiao, X.; Zhao, C. Beneficial effect of intestinal fermentation of natural polysaccharides. *Nutrients*. **2018**, 10, 1-55.
10. Serra, D.; Richter, A.; Hengge, R. Cellulose as an architectural element in spatially structured Escherichia coli biofilms. *J. Bacterio*. **2013**, 195, 5540-5554.
11. Fernandes, A.; Thomas, L.; Altaner, C.; Callow, P.; Forsyth, V.; Apperley, D, et al. Nanostructure of cellulose microfibrils in spruce wood. *Proceed. National Acad. Sci*. **2011**, 108,:E1195-E1203.
12. Chawla, S.; Kanatt, S.; Sharma, A. Chitosan, polysaccharides. *Springer, Cham*. 2015. pp. 219-246.
13. Li, S.; Bashline, L.; Lei, L.; Gu, Y. Cellulose synthesis and it's regulation. In: The Arabidopsis Book. Vol. 12. *BiOne Complete (Open Access)*. 2014. p. p0169.
14. Heise, K.; Delepierre, G.; King, A.; Kostiainen, M.; Zoppe, J.; Weder, C.; Kontturi, E. Chemical modification of cellulose nanocrystal reducing end-groups. *Angewandte Chemie International Edition*.**2020.**

15. Nakatsubo, F.; Kamitakahara, H.; Hori M. Cationic ring-opening polymerization of 3,6-di-O-benzyl-α-d-glucose 1,2,4-Orthopivalate and the first chemical synthesis of cellulose. J. American Chem. Soc.**1996**,118, 1677-1681.
16. Zugenmaier P. Conformation and packing of various crystalline cellulose fibers. *Progress Pol. Sci*. **2001**, 26, 1341-1417.
17. Nascimento, D. M.; Nunes, Y. L.; Figueirêdo, M. C. B..; de Azeredo, H. M. C.; Aouada, F. A.; Feitosa, J. P. A.; Dufresne, A. Nanocellulose nanocomposite hydrogels: technological and environmental issues. *Green Chem.*, **2011**, 20, 2428–2448.
18. Rosa S. M. L.; Rehman N.; de Miranda M.I.G.; Nachtigall S.M.B.; Bica, C. I. D. Chlorine-free extraction of cellulose from rice husk and whisker isolation. *Carbohydrate Polymers*. **2012**, 87, 1131-1138.
19. Mettler, M.; Paulsen, A.; Vlachos, D.; Dauenhauer, P. Pyrolytic conversion of cellulose to fuels: Levoglucosan deoxygenation via elimination and cyclization within molten biomass. *Ener.Environ. Sci*. **2012**, 5, 7864.
20. Ang T. N.; Ngoh, G.; Chua, A.; Gyu, L. M. Elucidation of the effect of ionic liquid pretreatment on rice husk via structural analyses. *Biotech. Biofuels*. **2012**, 5, 67.
21. Timilsina, G. R. Biofuels in the long-run global energy supply mix for transportation. *Philosophical Trans. Royal Soc. A: Math., Phy. Eng. Sci*. **2006**, 372, 20120323–20120323.
22. Rosales, C. O.; Arantes, V . A review on commercial-scale high-value products that can be produced alongside cellulosic ethanol. *Biotech. Biofuels*. **2019**, 12, 1529-1.
23. Somma, D.; Lobkowicz, H.; Deason, J. P. Growing America's fuel: an analysis of corn and cellulosic ethanol feasibility in the United States. *Clean Techno. Environ. Pol.* **2019**, 12, 373–380.
24. Bušić, A.; Marđetko, N.; Kundas, S.; Morzak, G.; Belskaya, H. Bioethanol production from renewable raw materials and its separation and purification: a review. *Food Technol. Biotechnol*. **2018**, 56.
25. Selim, K.; El-Ghwas. D.; Easa, S.; Abdelwahab H. M.Bioethanol a microbial biofuel metabolite; new insights of yeasts metabolic engineering. *Fermentation*. **2018**, 4, 1-6.
26. Hook, S. E.; Wright, A.-D. G.; McBride, B. W. Methanogens: methane producers of the rumen and mitigation strategies. *Archaea*.**2010**, 1, 1–11.

27. Kumar G. P.; Sai Raghunath, S.; Venkatesh Prasanna, D.;Venkat, P.; Shree, V.;Chithananthan, C.;Geetha, K. (2019). An update on overview of cellulose, its structure and applications. *Cellulose*.**2019**.
28. Aguilar, M. S. B., Betancur, M. C. L., Isaza, G. A., Mesa, H.; Jovel, J. Lower methane emissions were associated with a higher abundance of ruminal Prevotella in a cohort of Colombian buffalos. *BMC Microbiology*, **2020**, 20, 20-6.
29. Wood, D. E.; Lu, J.; Langmead, B. Improved metagenomic analysis with kraken 2. *Genome Biol*. **2019,** 20, 1-13.
30. Wallnöfer, P.; Baldwin, R. L. Pathway of propionate formation in Bacteroides ruminicola. *J. Bacteriol.* **1967**, 93, 504–505.
31. Difford, G. F.; Plichta, D. R.; Løvendahl, P.; Lassen, J.; Noel, S. J.; Højberg, O. et al. Host genetics and the rumen microbiome jointly associate with methane emissions in dairy cows. *PLoS Genet*. **2018**, 14, 1-22.
32. Lan, W.; Yang, C. Ruminal methane production: associated microorganisms and the potential of applying hydrogen-utilizing bacteria for mitigation. *Sci Total Environ*. **2019**, 654, 1270–83.
33. John, W. R.; Sasson, G.; Garnsworthy, P. C.; Tapio, I.; Gregson, E.; Bani, P. et al. A heritable subset of the core rumen microbiome dictates dairy cow productivity and emissions. *Sci Adv*. **2019**, 5, 1-13.
34. Ali, Shah, F.; Mahmood, Q.; Maroof, Shah, M.; Pervez, A.; Ahmad, Asad, S. Microbial ecology of anaerobic digesters: The key players of anaerobiosis. *Sci. World J.* **2014**, 1, 1–21.
35. Enzmann, F.; Mayer, F.; Rother, M.; Holtmann, D. Methanogens: biochemical background and biotechnological applications. *AMB Express*. **2018**, 8, 1-22.
36. Wróblewska, K. J.; Rydzkowski, T.; Michalska-Pożoga, I.; Thakur, V. K. Biopolymers for Biomedical and Pharmaceutical Applications: Recent Advances and Overview of Alginate Electrospinning. *Nanomaterial.* **2019**, 9, 1-23
37. Joseph, B.; Sagarika, V. K.; Sabu, C.; Kalarikkal, N.; Thomas, S. Cellulose nanocomposites: Fabrication and biomedical applications. *JB&B*. **2020**, 5, 223-237.
38. Singh, M.N.; Hemant, K.S.; Ram, M.; Shivakumar, H.G.; Microencapsulation: A promising technique for controlled drug delivery. *Res Pharm Sci*. **2010,** 5, 65-77.
39. Kamel, S.; Ali, N.; Jahangir, K.; Shah, S. M.; El-Gendy, A. A.; Pharmaceutical significance of cellulose: A review. *EXPRESS Polym. Lett.* **2008**, 2, 758–778.

40. Patra, J. K.; Das, G.; Fraceto, L. F.; Campos, E. V. R.; Rodriguez-Torres, M. del P.; Acosta-Torres, L. S.; Shin, H.-S. Nano based drug delivery systems: recent developments and future prospects. *Journal of Nanobiotechnology*. **2018**, 16, 1-33.
41. George, J.; Sabapathi, S. N. Cellulose nanocrystals: synthesis, functional properties, and applications. *Nanotechnology, Science and Applications.* **2015**, 8, 45-54.
42. Hanawa, T. A comprehensive review of techniques for biofunctionalization of titanium. *J. Periodontal Implant Sci.* **2011**, 41, 1-10
43. Li, B.; Konecke, S.; Harich, K.; Wegiel, L.; Taylor, L. S.; Edgar, K. J. Solid dispersion of quercetin in cellulose derivative matrices influences both solubility and stability. *Carbohydrate Polymers*, **2013**, 92, 2033–2040.
44. Chan, B. P.; Leong, K. W. Scaffolding in tissue engineering: general approaches and tissue-specific considerations. *European Spine Journal*, **2008**, 17, 467–479.
45. Chen, Y. M.; Xi, T.; Zheng, Y.; Guo, T.; Hou, J.; Wan, Y.; Gao, C. In vitro cytotoxicity of bacterial cellulose scaffolds used for tissue-engineered bone. *J. Bioact Compat Polym.* **2009**, 24, 137–145.
46. Lee, S. E.; Park, Y. S. The role of bacterial cellulose in artificial blood vessels. *Mol. Cell. Toxico.* **2017**, 13, 257–261.
47. Dasi, L. P.; Simon, H. A.; Sucosky, P.; Yoganathan, A. P. Fluid mechanics of artificial heart valves. *Clin. Exp. Pharma. Physio*. **2009**, 36, 225–237.
48. George, J.; Sabapathi, S. N. Cellulose nanocrystals: synthesis, functional properties, and applications. *Nanotechnology, Science and Applications.* **2015**, 8, 45-54.
49. Kadumudi, F. B.; Trifol, J.; Jahanshahi, M.; Zsurzsan, Tiberiu-Gabriel.; Mehrali, M.; Zeqiraj, E.; Shaki, H.; Alehosseini, M.; Gundlach, C.; Li, Q.; Dong, M.; Akbari, M.; Knott, A.; Almdal, K.; Dolatshahi-Pirouz, A. Flexible and green electronics manufactured by origami folding of nanosilicate-reinforced cellulose paper. *ACS Appl. Mater. Interfaces.* **2020**, 12, 48027- 48039.
50. Azeredo, H. M. C., Barud, H.; Farinas, C. S.; Vasconcellos, V. M.; Claro, A. M. Bacterial cellulose as a raw material for food and food packaging applications. *Front. Sust. Food Sys.* **2019**, 3, 1-14.
51. Abdul Khalil, H. P. S.; Davoudpour, Y.; Islam, M. N.; Mustapha, A.; Sudesh, K.; Dungani, R.; Jawaid, M. Production and modification of nanofibrillated cellulose using various mechanical processes: A review. *Carbohydrate Polymers*, **2014**, 99, 649–665.

52. Shaghaleh, H.; Xu, X.; Wang, S. Current progress in production of biopolymeric materials based on cellulose, cellulose nanofibers, and cellulose derivatives. *RSC Advances*, **2018**, 8, 825–842.
53. Fang, Z.; Zhang, H.; Qiu, S.; Kuang, Y.; Zhou, J.; Lan, Y.; Sun, C.; Li, G.; Gong, S.; Ma. Z.; Versatile wood cellulose for biodegradable electronics. *Adv. Mat. Tech.* **2021**, 4, 2000928.
54. Roopan, S.; Madhumitha, G. Biodegradable polymer-loaded nanoparticles: an overview of the synthesis and biomedical applications. *Nanomaterials*. **2016,** 625-683.
55. Orehek, J.; Dogsa, I.; Tomšič, M.; Jamnik, A.; Kočar, D.; Stopar. D.; Structural investigation of carboxymethyl cellulose biodeterioration by Bacillus subtilis subsp. subtilis NCIB 3610. *Int. Biodeterior. Biodegradation.* **2013**, 77, 10-17.
56. Kadla, J.; Gilbert, R.D.; Cellulose structure: A review, cellulose chemistry and technology. **2000**, 34,197-216
57. Peter, Z.; Order in cellulosics: Historical review of crystal structure research on cellulose. *Carbohydrate Polymers*. **2021**, 254, 117417.
58. Jedvert, K.; Heinze, T. Cellulose modification and shaping – a review. *J. Polym. Eng*. 2017, 37, 1-16.
59. Mischnick, P.; Momcilovic, D. Chemical structure analysis of starch and cellulose derivatives. *Adv. Carbohydr. Chem. Biochem*. **2010**, 117–210.
60. Teramoto, Y. Functional thermoplastic materials from derivatives of cellulose and related structural polysaccharides. *Molecules*. **2015**, 20, 5487–5527.
61. Nishiyama, Y., Langan, P.; Chanzy, H. Crystal structure and hydrogen-bonding system in cellulose Iβ from synchrotron X-ray and neutron fibre diffraction. *J. Am. Chem. Soc*. **2002**, 124, 9074–9082.
62. Volker, A. Encyclopedia of polymer science and technology (Wird aktualisiert. ed.). Hoboken, N.J.., Wiley-Interscience. **2005.**
63. Matrosovich, M.; Matrosovich, T.; Garten, W.; Klenk, H.-D. *Virology Journal*. **2006**, 3, 1-7.
64. Thoorens, G.; Krier, F.; Leclercq, B.; Carlin, B.; Evrard, B. Microcrystalline cellulose, a direct compression binder in a quality by design environment—A review. *Int. J. Pharm.* **2014**, 473, 64–72.
65. Baer, A.; Kehn-Hall, K. Viral concentration determination through plaque assays: using traditional and novel overlay systems. *J. Vis. Exp*. **2014**, 93, 1-2.

66. Sherif, S. Z. Hindi. Microcrystalline cellulose: The inexhaustible treasure for pharmaceutical industry. *J. Nanosci. Nanotechnol.* **2017**, 4, 17-24.
67. Ohwoavworhua, F. O.; Adelakun, T. A. Non-wood fibre production of microcrystalline cellulose from Sorghum caudatum: Characterisation and tableting properties. *Indian J. Pharm. Sci*. **2010**, 72, 295-301.
68. Turbak, A. F.; Snyder, F. W.; Sandberg, K. R.; Microfibrilated cellulose, a new cellulose product: properties, uses, and commercial potential. *J. Appl. Polym. Sci., Applied Polymer Symposium*. **1983**, 37, 815-827.
69. Herrick, F. W.; Casebier, R. L.; Hamilton, J. K.; Sandberg, K. R. Microfibrillated cellulose: morphology and accessibility. *J. Appl. Polym. Sci.* **1983**, 37, 797-813.
70. Schwartz, J. B.; Lachman, L.; Compressed tablets by wet granulation. In: Bandelin JF, editor. Pharmaceutical Dosage Forms: Tablets. New York, Basel, HongKong: Marcel Dekker Inc; **1990**, 1, p. 133
71. Kása, P.; Bajdik, J.; Zsigmond, Z.; Pintye, H. K. Study of the compaction behaviour and compressibility of binary mixtures of some pharmaceutical excipients during direct compression. *Chem. Eng. Process Chem. Eng. Process***. 2009**, 48, 859-863.
72. Chauhan, Y. P.; Sapkal, R. S.; Sapkal, V. S.; Zamre, G. S.; Microcrystalline cellulose from cotton rags (waste from garment and hosiery industries). *Int. J. Chem. Sci.* **2009**, 7, 681-688.
73. El-Sakhawy, M.; Hassan, M. L.; Physical and mechanical properties of microcrystalline cellulose prepared from agricultural residues. *Carbohydr. Polym*. **2007**, 67, 1-10.
74. Chauhan, Y. P.; Sapkal, R. S.; Sapkal, V. S.; Zamre, G. S.; Microcrystalline cellulose from cotton rags (waste from garment and hosiery industries). *Int. J. Chem. Sci.* **2009**, 7, 681-688.
75. Chuayjuljit, S.; Su-uthai, S.; Charuchinda, S.; Poly(vinyl chloride) film filled with microcrystalline cellulose prepared from cotton fabric waste: Properties and biodegradability study. *Waste Manag. Res*. 2010, 28, 109-117.
76. Rashid, M.; Gafur, M. A.; Sharafat, M. K.; Minami, H.; Miah, M. A. J.; Ahmad, H. Biocompatible microcrystalline cellulose particles from cotton wool and magnetization via a simple in situ co-precipitation method. *Carbohydr. Polym*. **2017**, 170, 72-79.
77. Uesu, N. Y.; Pineda, E. A.; Hechenleitner, A. A. Microcrystalline cellulose from soybean husk: Effects of solvent treatments on its properties as acetylsalicylic acid carrier. *Int. J. Pharm.* **2000**, 206, 85-96.

78. Suvachittanont, S.; Ratanapan, P. Optimization of microcrystalline cellulose production from corn cob for pharmaceutical industry investment. *IJCCE*. 2013, 7, 1136-1141.
79. Gaonkar, S. M.; Kulkarni, P. R. Improved method for the preparation of microcrystalline cellulose from water hyacinth. *Text. Dyer Print.* **1987**, 20, 19-22.
80. Gaonkar, S. M.; Kulkarni, P. R. Microcrystalline cellulose from coconut shells. *Acta Polym*. **1989**, 40, 292-293.
81. Fahma, F.; Iwamoto, S.; Hori, N. Iwata. T.; Takemura, A.; Isolation, preparation, and characterization of nanofibers from oil palm empty-fruit-bunch (OPEFB). *Cellulose*. **2010**, 17, 977-985.
82. Mohamad, Haafiz. M. K.; Eichhorn, S. J.; Hassan, A.; Jawaid, M. Isolation and characterization of microcrystalline cellulose from oil palm biomass residue. *Carbohydr. Polym*. **2013**, 93, 628-634.
83. Owolabia, A.; Haafiza, M.; Hossain, M.; Hussin, H.; Fazita, N. Influence of alkaline hydrogen peroxide pre-hydrolysis on the isolation of microcrystalline cellulose from oil palm fronds. *Int. J. Biolog. Macromol.*. **2017**, 95, 1228-1234.
84. Ilindra, A.; Dhake, J. D. Microcrystalline cellulose from bagasse and rice straw. *Indian J. Chem. Technol* .**2008**, 15,497-499.
85. Paralikar, K. M.; Bhatawdekar, S. P. Microcrystalline cellulose from bagasse pulp. *Biological Wastes*. **1988**, 24, 75-77.
86. Padmadisastra, Y.; Gonda, I.; Preliminary studies of the development of a direct compression cellulose excipient from bagasse. *J. Pharm. Sci.***1989**, 78, 508-521.
87. Shah, D. A.; Shah, Y. D.; Trivedi, B. M. Production of microcrystalline cellulose from sugar cane bagasse on pilot plant and its evaluation as pharmaceutical adjunct. *Res. Ind.*. **1993**, 38, 133-137.
88. Tang, L. G.; Hon, D. N. S.; Pan, S. H.; Zhu, Y. U.; Wang, Z.; Wang, Z. Z. Evaluation of microcrystalline cellulose. I. Changes in ultrastructural characteristics during preliminary acid hydrolysis. *J. Appl. Polym. Sci*. **1996**, 59, 483-488.
89. Abdullah, A. B. M. Production of jute microcrystalline cellulose. *J. Bangladesh Acad. Sci.* **1991**, 15, 85-87.
90. Jahan, M. S.; Saeed, A.; He, Z.; Ni, Y. Jute as raw material for the preparation of microcrystalline cellulose. *Cellulose*. **2011**, 18, 451-459.
91. Kuga, S.; Brown, R. M. Lattice imaging of ramie cellulose. *Polym. Communications Guildford*. **1987**, 28, 311-314.

92. Bochek, A. M.; Shevchuk, I. L.; Lavrentev, V. N. Fabrication of microcrystalline and powdered cellulose from short flax fiber and flax straw. *Russ. J. Appl. Chem.* **2003**, 76, 1679-1682.
93. Monschein, M.; Reisinger, C.; Nidetzky, B. Enzymatic hydrolysis of microcrystalline cellulose and pretreated wheat straw: A detailed comparison using convenient kinetic analysis. *Bioreso. Tech*. **2013**, 128, 679-687.
94. Ohwoavworhua, F. O.; Adelakun, T. A. Non-wood fibre production of microcrystalline cellulose from sorghum caudatum: Characterisation and tableting properties. *Indian J. Pharm. Sci.* **2010**, 72, 295-301.
95. Bhimte, N. A.; Tayade, P. T. Evaluation of microcrystalline cellulose prepared from sisal fibers as a tablet excipient: A technical note. Association of pharmaceutical scientists (AAPS). *Pharm. Sci. Technol*. **2007**, 8, 56-62.
96. Winuprasith, T.; Suphantharika, M. Microfibrillated cellulose from mangosteen (Garcinia mangostana L.) rind: Preparation, characterization, and evaluation as an emulsion stabilizer. *Food Hydrocolloids*. **2013**, 32, 383-394.
97. Trache, D.; Donnot, A.; Khimeche, K.; Benelmir, R.; Brosse, N. Physico-chemical properties and thermal stability of microcrystalline cellulose isolated from alfa fibres. *Carbohydr. Polym*. **2014**, 104, 223-230.
98. Trache, D.; Khimeche, K.; Mezroua, A.; Benziane, M. Physicochemical properties of microcrystalline nitrocellulose from alfa grass fibers and its thermal stability. *J. Therm. Anal. Calorim*. **2016**, 124, 1485-1496.
99. Merci, A.; Urbano, A.; Grossmann, M. V. E.; Tischer, C. A.; Mali, S. Properties of microcrystalline cellulose extracted from soybean hulls by reactive extrusion. *Food Res. Int*. **2015**, 73, 38-43.
100. Ejikeme, P. M. Investigation of the physicochemical properties of microcrystalline cellulose from agricultural wastes I: Orange mesocarp. *Cellulose*. **2008**, 15, 141-147.
101. Ngozi, U. O.; Chizoba, N. A.; Ifeanyichukwu, O. S. Physico-chemical properties of microcrystalline cellulose derived from Indian Bamboo (Bambusa vulgaris*). Int. J. Pharm. Sci. Rev. Res.* **2014**, 29, 5-9.
102. Kiana, L. K.; Jawaida, M.; Ariffina, H.; Alothmanb, O.Y. Isolation and characterization of microcrystalline cellulose from roselle fibers. *Int. J. Biol. Macromol*. **2017**, 103, 931-940.

103. Trachea, D.; Donnotb, A.; Khimechea, K.; Benelmirb, R.; Brosse, N. Physico-chemical properties and thermal stability of microcrystalline cellulose isolated from Alfa fibres. *Carbohydr. Polym*. **2014**, 104, 223-230.

104. Hindi, S. S. Z. Calotropis procera: The miracle shrub in the Arabian Peninsula. *IJSEI*. **2013**, 2, 48-57.

105. Thoorens, G.; Krier, F.; Leclercq, B.; Carlin, B.; Evrard, B. Microcrystalline cellulose, a direct compression binder in a quality by design environment: A review. *Int. J. Pharm*. **2014**, 473, 64-72.

106. Hindi, S. S. Z.; Abohassan, R. A. Cellulosic microfibril and its embedding matrix within plant cell wall. *Int. J. Innov. Res. in Sci, Eng. Techno.* **2016**, 5, 2727-2734.

107. Guy, A. Cellulose, microcrystalline. In: Rowe R. C.; Sheskey P. J.; Quinn M. E. Handbook of pharmaceutical excipients. UK: Pharmaceutical Press; **2009**. pp. 129-133.

108. Ohwoavworhua, F. O.; Kunle, O. O.; Ofoefule, S. I. Extraction and characterization of microcrystalline cellulose derived from Luffa cylindrica plant. *Afr. J. Pharma. Res. Develop*. **2004**, 1, 1-6

109. Albers, J.; Knop, K.; Kleinebudde, P. Brand-to-brand and batch-to-batch uniformity of microcrystalline cellulose in direct tableting with a pneumo-hydraulic tablet press. *La Pharmacie Industrielle*. **2006**, 68, 1420-1428.

110. Doelker, E. Comparative compaction properties of various microcrystalline cellulose types and generic products. *Drug Dev. Ind. Pharm.* **1993**, 19, 2399-2471.

111. Landín, M.; Martínez-Pacheco, R.; Gómez-Amoza, J. L.; Souto, C.; Concheiro, A.; Rowe, R.C. Influence of microcrystalline cellulose source and batch variation on the tabletting. **1993**

112. Williams, R. O.; Sriwongjanya, M.; Barron, M. K. Compaction properties of microcrystalline cellulose using tableting indices. *Drug Dev. Ind. Pharm*. **1997**, 23, 695-704.

113. Henny, W.; Yuliasmi, H.; Aisyah, S.; Riati. D. Characterization of synthesized sodium carboxymethyl cellulose with variation of solvent mixture and alkali concentration. *Maced. J. Med. Sci*. **2019**, 7, 3878–3881.

114. Nur'ain, N.; Nurhaeni, N.; Ridhay, A. optimization of reaction to the synthesis of carboxymethyl cellulose (cmc) from corn stalk (zea mays l.) *kovalen*. 2017, 3, 112.

115. Ott, E.; Spurlin, H. M.; Grafflin, M. W.; Cellulose Part II 2nd Ed., *Interscience Publishers*, New York. **1963**.

116. Britt K.W. Ed. Handbook of pulp and paper technology. 2nd Ed., *Van Nostrand Reinhold Company*, New York. **1970**.

117. Kirk, R. E.; Othmer D. F. Encyclopaedia of chemical technology. The Interscience Encyclopedia, Inc., New York. **1949**.

118. Whistler, R. L.; BeMiller, J. N. Industrial gums, polysaccharides and their derivatives, 2nd Ed, *Academic Press*, London. **1973**.

119. Sara, R.; GortonLo, G. Characterisation of the substituent distribution in starch and cellulose derivatives. *Analytica Chimica. Acta*. **2003**, 497, 27-65.

120. Grayson M. Encyclopaedia of chemical technology. *John Wiley & Sons*, New York.**1979**

121. Uwadiale, G. G. O. O. Upgrading Nigerian iron ores, minerals and metallurgical processing. **1989**. 6, 117–123,

122. Filippov L.O.; Severov V. V.; Filippova, I.V. An overview of the beneficiation of iron ores via reverse cationic flotation. *Int. J. Miner. Process*. **2014**, 127, 62–9.

123. Crabtree, E. H.; Vincent, J. D. Historical outline of major flotation developments. Froth flotation. 50th anniversary. *Rocky Mt. Fund Ser. AIME*. **1962**.

124. Meyer K. Pelletizing of iron ores. Heidelberg. *Springer-Verlag*. **1980**

125. Eisele, T. C.; Kawatra, S. K. A review of binders in iron ore pelletization. *Min. Process. Extract. Metall. Rev*. **2003**, 24, 1–90.

126. Laftah, W. A.; Wan, A.W.A. R. Pulping process and the potential of using non-wood pineapple leaves fiber for pulp and paper production: A review. *J. Nat. Fib.* **2016**, 13, 85-102.

127. Clark, J. A. Pulp technology and treatment for paper. *Miller Freeman Publications*. Inc., San Fransisco.**1978**

128. Howard, K.W.; Hodgson, K.T. Influence of pigment packing behavior on the adhesive requirements of aqueous paper coatings. *J. Coat Technol. Res.* **2015**, 12, 237–245.

129. Casey, J. P. Pulp and paper, chemistry and chemical technology. 2nd Ed. , *John Wiley & Sons*, New York.**1983.**

130. Kirk R. E.; Othmer, D. F. Encyclopaedia of chemical technology. *The Interscience Encyclopedia, Inc*., New York.**1949**.

131. Budtova, T.; Navard, P. Cellulose in NaOH–water based solvents: a review. *Cellulose*, Springer Verlag. **2016**.

132. Whistler, R. L.; BeMiller, J. N. Industrial gums, polysaccharides and their derivatives. 2nd Ed. *Academic Press*, London. **1973**.

133. Grayson, M. Encyclopaedia of chemical technology. *John Wiley & Sons*, New York.**1979**.

134. Kayser, H. Über die Verdichtung von Gasen an Oberflächen in ihrer Abhängigkeit von Druck und Temperatur. Annalen der Physik und Chemie. **1881**

135. Da˛browski, A. Adsorption from theory to practice. *Ad. Colloid Interface Sci*.**2001**, 93, 135-224.

136. Scott, K. N.; Green, J. F.; Do, H. D.; Mc Lean, S. J. Arsenic removal by coagulation. *J. Am. Water Works Assoc*. **1995**, 87, 114-126.

137. Atkins, P.; de Paula, J. Physical chemistry.7th Edition. *Oxford University* New York, **2003**.

138. Adamson, A. W. Physical chemistry of Surfaces. 2nd Ed. *Inter Science Publishers*, John Wiley & Sons, California. **1967**.

139. Edwards, M. Chemistry of arsenic: removal during coagulation and Fe-Mn oxidation. *J. Am. Water Works Assoc.* **1994**, 86, 64-78.

140. Oura, K.; Lifshits, V.G.; Saranin, A.A.; Zotov, A.V.; Katayama, M. Surface science, an introduction. *Springer*. **2003**.

141. Rettner, C.T.; Auerbach, D. J. Chemical dynamics at the gas-surface interface. *J. Phy.Chem.* **1996**, 100, 13021–33.

142. Somorjai, G.A. Introduction to surface chemistry and catalysis. *Johan Wiley and Sons, Enc.* New York. **1994**.

143. Sing, K. S. W.; Everett, D. H.; Haul, R. A. W.; Moscou, L.; . Pierotti, R. A.; Rouquerol, J.; Siemiemniewska, T. Physical and biophysical chemistry division commission on colloid and surface chemistry including catalysis. *Pure Appl. Chem.* **1985**, 57, 603-619.

144. Haber, J. Manual on catalyst characterization (recommendations 1991), *Pure App. Chem*. **1991**,63, 1227-1246.

145. Robens, E.; Krebs, K. F. Standardisation, reference materials and comparative measurements for surface area and pore characterisation. *Stu. Surf. Sci. Cataly*.**1991**, 62, 133-140.

146. EPA (Environmental protection agency), Mercury in medical laboratories, Centers for technology transfer and pollution prevention, Vol. 2, 1st Ed. In: Purdue University.**1998**.

147. Raj, G. Advanced physical chemistry.34th Ed. *Goel Publication House*, Meerut.**2008**.

148. Bansal, R.C.; Goyal, M. Activated carbon adsorption. *CRC Press, Taylor & Francis Group,* Boca Raton. **2005**.

149. Wasewar, K. L.; Prasad, B.; Gulipalli, S. Removal of Selenium by adsorption onto granular activated carbon (GAC) and powdered activated carbon (PAC). *Clean Soil Air Water*. **2009**, 37, 872-883.

150. Mohammed, S. J. Selective auxiliary function of zeolite molecular sieves and its uses in the manufacture of lead "free gasoline" *J. Scient. Comp*., Baghdad. **2004**

151. Stumm, W. Chemistry of the solid water interface. *John Willey & Sons*, New York. **1992**.

152. Mhammed, S.J. Surface chemistry and adjuvants. *College of Science Press* - University of Baghdad.**1980**.

153. Bandosz, T. J. Activated carbon surfaces in environmental remediation, *Interface Sci. Technol*. *Academic Press*, Elsevier Ltd. Oxford, UK.**2006**

154. Manocha, S. M. Porous carbons. *Sadhan*a **2003**, 28, 335-348.

155. Bansal, R.C. Active carbon. *Dekker*. New York.. **1988**.

156. Derbyshire, F.; Jagtoyen, M.; Thwaites, M. Porosity in carbons: characterization and applications. *Edward Arnold*, London.**1995**.

157. Singh, K.; Kumar, A. Physicochemical aspects for the binding mechanism of sodium carboxymethyl cellulose onto mesoporous tea waste carbon from its aqueous solutions. *J. Dispers. Sci. Tech.*1-20, 1, **2020**.

158. Dubey, A.; Shiwani, S. Adsorption of lead using a new green material obtained from Portulaca plant. *Int. J. Environ. Sci. Technol.* **2012**, 9, 15-20.

159. Rivera-Utrilla, J.; Bautista-Toledo, I.; Ferro-Garcia, M. A.; Moreno-Castilla, C. Bioadsorption of Pb(II) Cd(II) and Cd(VI) on activated carbon from aqueous solutions. *Carbon.***2003**, 41, 323-330.

160. Kannan, N.; Veemaraj, T. Batch adsorption dynamics and equilibrium studies for the of Cd(II) ions from aqueous solution using jack fruit seed and commercial activated carbons- a comparative study. *Electron J. Environ. Agric. Food Chem*. **2010**, 9, 327-336.

161. Sen, T. K.; Mohammod, M.; Maitra, S.; Dutta, B. K. Removal of cadmium from aqueous solution using castor seed hull: a kinetic and equilibrium study. *Clean -Soil Air Water*. **2010**, 38, 850-858.

162. Yang, R. T. Adsorbents: fundamental and applications. *John Wiley & Sons*. New Jersey. **2003**.

163. Naiya, T. K.; Bhattacharya, A. K.; Das, S. K. Adsorption of Cd(II) and Pb(II) from aqueous solutions on activated alumina. *J. Colloid Interface Sci*. **2009**, 333, 14-26.

164. Shichi, T.; Takagi, K. Clay minerals as photochemical reaction fields, *J. Photochem. Photobio. C: Photochem. Review*.**2000**, 1,113-130.

165. Keane, M. A. The removal of copper and nickel from aqueous solution using Y zeolite ion exchangers. *Colloid Surface A*.**1998**, 138, 11-20.

166. Hoogendam, C. W. Adsorption and desorption of cellulose derivatives. *Grafisch Service Centrum*, Wageningen. **1998.**

167. Fleer, G. J.; Stuart, C. M. A. Scheutjens, J. M. H. M.; Cosgrove, T.; Vincent, B. Polymers at Interfaces. *Chapman & Hall*, London.**1993**.

168. van de Steeg, H. G. M.; Stuart, C. M. A.; de Keizer, A.; Bijsterbosch, B. H. *Langmuir*.**1992**.

169. Dijt, J.C. Kinetics of polymer adsorption, desorption and exchange, Ph. D. thesis, *Wageningen Agricultural University*. **1993**.

170. Meadows, J.; Williams, P. A.; Garvey, M. J.; Harrop, R. A.; Phillips, G. O. *Colloids Surfaces.* **1988**.

171. Luckham P. F.; Klein, J. *J. Chem. Soc. Faraday Trans.* **1984**.

172. Semenov, A.N.; Joanny, J. F. *J. Phys. II (Paris).* **1995**.

173. Kramers, H. A.; Arancibia, C.; Lisboa, R. N.; Zuniga, R. N.; Matiacevich, S. Application of CMC as thickener on nanoemulsions based on olive oil: physical properties and stability. *Int. J. Poly. Sci*. **2106**, 2, 1-10.

174. Klemm, D.; Heublein, B.; Fink, H.; Bohn, A. Cellulose: fascinating biopolymer and sustainable raw material. *Angew. Chem. Int. Ed. Engl*. **2005**, 44 , 33583-93.

175. Hollabaugh, C. B.; Burt, L. H.; Walsh, A. P. Carboxymethylcellulose uses and applications. *Ind. Eng. Chem. Res.* **1945**, 37, 943-947.

176. Tian, Z.; Wu, Z.; Jones, M. J.; Gill, P. Mineral processing and extractive metallurgy. *The Institute of Mining and Metallurgy*, London, **1984**, 743-750.

177. Coffey, D. G.; Bell, D. A.; Henderson, A. Cellulose and cellulose derivatives. *Marcel Dekker Inc*. New York. **1995**.

178. Methocel Cellulose Ethers. Technical Handbook. Available online: www.dow.com/dowwolff/en/pdf/192-01062.pdf (accessed on 20 April 2015).

179. Ruta, B.; Czakkel, O.; Chusshkin, Y.; Pignon, F.; Zontone, F.; Rinaudo, M. Silica nanoparticlesas tracers of the gelation dynamics of a natural biopolymer physical gel. *Soft Matter*. **2014**, 10, 4547–4554.

180. Takahashi, M.; Shimazaki, M.; Yamamoto, J. Thermoreversible gelation and phase separation inaqueous methyl cellulose solutions. *J. Polym. Sci. B Polym. Phys*. **2001**, 39, 91–100.

181. Haque, A.; Morris, E. R. Thermogelation of methylcellulose. Part I: Molecular structures and processes. *Carbohydr. Polym*. **1993**, 22, 161–173.

182. Hirrien, M.; Chevillard, C.; Descrières, J.; Axelos, M.A.V.; Rinaudo, M. Thermogelation ofmethylcelluloses: New evidence for understanding the gelation mechanism. Polymer. **1998**, 39, 6251–6259.

183. Vigouret, M.; Rinaudo, M.; Desbrières, J. Thermogelation of methylcellulose in aqueous solutions. *J. Chim. Phys*. **1996**, 93, 858–869.

184. Hirrien, M.; Desbrières, J.; Rinaudo, M. Physical properties of methylcelluloses in relation withthe conditions for cellulose modification. *Carbohydr. Polym*. **1996**, 31, 243–253.

185. Kato, T.; Yokoyama, M.; Takahashi, A. Melting temperatures of thermally reversible gels. *Colloid Polym. Sci*. **1978**, 256, 15–21.

186. Sarkar, N. Kinetics of thermal gelation of methylcellulose and hydroxypropylmethylcellulose inaqueous solutions. *Carbohydr. Polym*. **1995**, 26, 195–203.

187. Nishinari, K. Rheological and DSC study of sol–gel transition in aqueous dispersion of industrially important polymers and colloids. *Colloid Polym. Sci*. **1997**, 275, 1093–1107.

188. Nasatto, P. L.; Pignon, F.; Silveira, J. L. M.; Duarte, M. E. R.; Noseda, M. D.; Rinaudo, M. Influence of molar mass and concentration on the thermogelation of methylcelluloses. *Int. J. Polym. Anal. Charact*. **2015**, 20, 1–9. 21.

189. Bodvik, R.; Karlson, L.; Edwards, K.; Eriksson, J.; Thormann, E.; Claesson, P.M. Aggregation of modified celluloses in aqueous solution: Transition from methylcellulose to hydroxypropylmethylcellulose solution properties induced by a low-molecular-weight oxyethylene additive. *Langmuir*.**2012**, 28, 13562–13569.

190. Raju, G. B.; Holmgren. A.; Forsling, W. J. Adsorption of dextrin at mineral/water interface. *J. Colloid Interface Sci*. **1997**,193, 215.

191. Laskowski, J. S.; Liu, Q. The role of metal hydroxides at mineral surfaces in dextrin adsorption. *Int. J. Min. Proc*. **1989**, 27, 297-316.

192. Solari, J. A.; de Araujo, A.C.; Laskowski, J. S. The effect of carboxymethyl cellulose on the flotation and surface properties of graphite. **1986**, 3, 15-31.

193. Mackenzie, M.; Malhotra, D.; Rigga W. F. Handbook of flotation reagents chemistry, theory and practice: flotation of sulfide ores. *Soc. Min. Eng*. **1986**, 165, 139-549.

194. Pugh, R. J. Macromolecular organic depressants in sulfide flotation-a review, 1. Principles, types and applications. *Int. J. Miner. Process*. 1989, 25, 101-130.

195. Healy, T. W. Principles of adsorptions of organics at solid-solution interfaces, *Sci. Chem. A*. 1974, 8, 603-619.

196. Rath, R. K.; Subramanian S. Studies on adsorption of guar gum onto biotite mica. *Miner. Eng*. **1997**, 12, 1405-1420.

197. Steenberg, E. Ph.D. Thesis, faculty of science, university of potchefstroom, Johannesburg. *South Africa*. **1982**, 28, 350-356.

198. Steenberg, E.; Harris, P. J. Adsorption of carboxymethyl cellulose, guar gum, and starch onto talc, sulfides, oxides and salt type minerals. *S. Afr. J. Chem*.**1984**, 36, 85–90.

199. Jenkins, P.; Ralston. The adsorption of a polysaccharide at the talc–aqueous solution interface. *Colloids Surf. A*. **1998**, 139, 27- 40.

200. Rath, R. K.; Subramanian, S.; Laskowski, J. S.; Poling G.W. Processing of hydrophobic minerals and fine coal. *Canadian Institute of Mining, Metallurgy and Petroleum, Montreal*, Canada.**1995**.

201. Jucker, B. A.; Harms, H.; Hug, S. J.; Zehnder A. J. B. Adsorption of bacterial surface polysaccharides on mineral oxides is mediated by hydrogen bonds.*Colloids Surf B: Biointerfaces*.**1997**, 9, 311-3643.

202. Bakinov K. G.; Vaneev, II.; Gorlovsky, S.I.; Eropkin, Y.; Zashikhin, N. V.; Konev, A. S. New methods of sulfide concentrate upgrading.*7th Int. Min. Process. Cong*. **1964**.

203. Wang, J.; Somasundaran P. Adsorption and conformation of carboxymethyl cellulose at solid-liquid interfaces using spectroscopic, AFM and allied techniques. *J. Colloid Interface Sci.* **2005**,29, 175-83.

204. Cuba-Chiem, L. T.; Huynh, L.; Ralston, J.; Beattie, D. A. In situ particle film ATR FTIR spectroscopy of carboxymethyl cellulose adsorption on talc: binding mechanism, ph effects, and adsorption kinetics. *Langmuir*. **2008**, 24, 8036-44.

205. Fujimoto, J.; Petri, D. F. S. Adsorption behavior of carboxymethyl cellulose on amino-terminated surfaces. *Langmuir*. **2001**, 17, 56-60.

206. Beaussart, A.; Mierczynska-Vasilev, A.; Beattie, D. A. Evolution of carboxymethyl cellulose layer morphology on hydrophobic mineral surfaces: variation of polymer concentration and ionic strength. *J. Colloid Interface Sci*. **2010**, 346, 303-10.

207. Cohen Stuart, M. A.; Fokkink, R. G.; Van Der Horst, P. M.; Lichtenbelt, J. W. T. Persistence length of carboxymethyl cellulose as evaluated from size exclusion chromatography and potentiometric titrations. *Colloid Poly. Sci*. **1998**, 276, 335-3.

208. Hoogendam, C. W.; de Keizer, A.; Cohen, M. A.; Stuart, M. A.; Bijsterbosch, B. H.; Batelaan, J. G.; Van, H. D. Adsorption mechanisms of carboxymethyl cellulose on mineral surfaces. *Langmuir*. **1998**, 14, 3825-3839.

209. Bacchin, P.; Bonino, J. P.; Martin, F.; Combacaum, M.; Barthes, P.; Petit, S.; Ferret, J. Surface pre-coating of talc particles by carboxyl methyl cellulose adsorption: study of adsorption and consequences on surface properties and settling rate. *Colloids and Surfaces A: Physicochem. Eng. Aspects*. **2006**, 272, 211-219.

210. Cuba-Chiem, L.; Huynh, L.; Ralston, J.; Beattie, D. A. In situ particle film ATR FTIR spectroscopy of carboxymethyl cellulose adsorption on talc: binding mechanism, pH effects, and adsorption kinetics. *Langmuir*. **2008**, 24, 8036-44.

211. Phenrat, T.; Saleh, N.; Sirk, K.; Kim, H. J.; Tilton, R. D.; Lowry, G. V. L. Comparative study of polymeric stabilizers for magnetite nanoparticles using ATRP. *J. Nanopart. Res*. **2008**, 10, 795-814.

212. Sedeva, G.; Fornasiero, D.; Ralston, J.; Beattie, D. A. Adsorption of modified dextrins on talc: effect of surface coverage and hydration water on hydrophobicity reduction. *Langmuir*. **2010**, 26, 15865-15874.

213. Duker, E.; Lindström, T. On the mechanisms behind the ability of CMC to enhance paper strength. *Nord. Pulp. Pap. Res. J.* **2008**, 23, 57-64.

214. Rakkolainen, M.; Kontturi, E.; Isogai, A.; Enomae, T.; Blomstedt, M.; Vuorinen, T. Carboxymethyl cellulose treatment as a method to inhibit vessel picking tendency in printing of eucalyptus pulp sheets. *Ind. Eng. Chem. Res.* **2009**, 48, 1887-1892.

215. Kumar, A.; Negi, Y. S.; Choudhary, V.; Bhardwaj, N. K. Microstructural and mechanical properties of porous biocomposite scaffolds based on polyvinyl alcohol, nano-hydroxyapatite and cellulose nanocrystals. *Cellulose*. **2014**, 21, 3409–3426.

216. Orelma, H.; Filpponen, I.; Johansson, L.; Laine, J.; Rojas, O. J. Affibody conjugation onto bacterial cellulose tubes and bioseparation of human serum albumin. *Biomacromolecules*. **2011**, 12, 4311-4318.

217. Filpponen, I.; Kontturi, E.; Nummelin, S.; Rosilo, H.; Kolehmainen, E.; Ikkala, O.; Laine, J. Generic method for modular surface modification of cellulosic materials in aqueous medium by sequential "click" reaction and adsorption. *Biomacromolecules*. **2012**, 13, 736-42.

218. Orelma, H.; Teerinen, T.; Johansson, L.; Holappa, S.; Laine, J. CMC-modified cellulose biointerface for antibody conjugation. *Biomacromolecules*. **2012**, 13, 1051-1058.

219. Mohan, T.; Kargl, R.; Kö Stler, S.; Doliska, A. G.; Findenig, G.; Ribitsch, V.; Stana-Kleinschek, K. Functional polysaccharide conjugates for the preparation of microarrays. *ACS A ppl. Mater. Interfaces*. **2012**, 2743-2751.

220. Kulterer, M. R.; Reichel, V. E.; Kargl, R.; Kö Stler, S.; Sarbova, T.; Heinze, K.; Kleinschek, S. Ribitsc, V. Functional polysaccharide composite nanoparticles from cellulose acetate and potential applications. *Adv. Funct. Mater*. **2012**, 22, 1749-1758.

221. Laine, J.; Lindström, T.; Nordmark, G. G.; Risinge, G. Studies on topochemical modification of cellulosic fibres. part 2. the effect of carboxymethyl cellulose attachment on fibre swelling and paper strength. *Part 1 Nord.Pulp. Pap. Res. J.* **2000**, 17, 50-56.

222. Mohan, T.; Kargl, R.; Doliška, A.; Ehmann, H. M. A.; Ribitsch, V.;. Stana-Kleinschek, K. functional polysaccharide conjugates for the preparation of microarrays. *Carbohydr. Polym*. **2012**, 93, 191-198.

223. Mohan, T.; Kargl, R.; Kö Stler, S.; Doliska, A. G.; Findenig, G.; Ribitsch, V.; Stana, K. K. Enzymatic digestion of partially and fully regenerated cellulose model films from trimethylsilyl cellulose. *J. Colloid Interface Sci*. **2011**, 358, 604-10.

224. Liu, Z.; Choi, H.; Gatenholm, P.; Esker, A. R. Quartz crystal microbalance with dissipation monitoring and surface plasmon resonance studies of carboxymethyl cellulose adsorption onto regenerated cellulose surfaces. *Langmuir*. **2011**, 27, 8718-28.

225. Amim, J.; Kosaka, P.; Petri, D. Characteristics of thin cellulose ester films spin-coated from acetone and ethyl acetate solutions. *Cellulose*. **2008**, 15, 527–535.

226. Karg, R.; Mohan, T.; Bracič, M.; Kulterer, M.; Doliska, A.; Kleinschek, K. S.; Ribitsch. V. Functional polysaccharide conjugates for the preparation of microarrays. *Langmuir*. **2012**, 28, 11440-11447.

227. Chanzy, H.; Henrissat, B.; Vincendon, M.; Tanner, S.; Belton, P. S. Solid-state 13C-N.M.R. and electron microscopy study on the reversible cellulose I→Cellulose III Transformation in Valonia. *Carbohydrate Res*. **1987**, 160, 1-11.

228. Kondo, T.; Sawatari, C.; Manley, R.; St, J.; Gray, D. G. Characterization of hydrogen bonding in cellulose-synthetic polymer blend systems with regioselectively substituted methylcellulose. *Macromolecules*. **1994**, 27, 210-215.

229. Ozaki, K.; Ito, S. Purification and Properties of an Acid Endo- 1, 4-P-Glucanase from Bacillus SP. KSM-330. *J. Gen. Microbio*. **1991**, 137, 41-48.

230. Wu, G.; Dai, R.Y.; Li, W. G.; Yin Chen, P. P.; Wang, M. Solution-processed organic uv photodetectors based on polyfluorene and naphthalene diimide. *Current App. Phy*. **2011**, 11, 750-754.

231. Singh, K.; Bharose, R.; Singh, V. K.; Verma. S. K. Sugar decolorization through selective adsorption onto functionalized accurel hydrophobic polymeric support. *Ind. Eng. Chem Res*. **2011**, 50, 10074-10082.

232. Gunning, A. P.; Kirby, A. R.; Ridout, M. J.; Brownsey, G. J.; Morris, V. J. Atomic force microscopy as a tool for interpreting the rheology of food biopolymers at the molecular leve. *Macromolecules.***1996**, 29, 6791-6796.

233. Wilkinson, K .J.; Balnois, E.; Leppard, G. G.; Buffle, J. Characteristic features of the major components of freshwater colloidal organic matter revealed by transmission electron and atomic force microscopy. *J. Colloids Surf. A.* **1999**, 155, 287-310.

234. Rath, R. K.; Subramanian, S.; Laskowski, J. S. Adsorption of dextrin and guar gum onto talc. a comparative study. *Langmuir*. **1997**, 13, 6260-6266.

235. C. Chen, Y.; Yanwei, X.; Hu, X.; i2, M.3.; Yan, L.; Mai3, P.; Hu, Shan, B.; Huang, Y. Na(+) intercalation pseudocapacitance in graphene-coupled titanium oxide enabling ultra-fast sodium storage and long-term cycling. *Nat. Commun*. **2015**, 2, 1-8.

236. Brunauer, S.; Emmett, P. H.; Teller, E. Adsorption of gases in multimolecular layers. *J. Am. Chem. Soc*. 1**938**, 60, 309-319.

237. Barrett, E. P.; Joyner, L. G.; Halenda, P. P. The Determination of pore volume and area distributions in porous substances. i. computations from nitrogen isotherms. *J. Am. Chem. Soc.* **1954** 73, 373-380.

238. McIntire, T. M.; Penner, R.; Brant, D. A. Observation of circular, triple helical polysaccharides using nanocontact atomic force microscopy. *Macromolecules*.**1995**, 28, 6375-6377.

239. Langmuir, I. The adsorption of gases on plane surfaces of glass, mica and platinum. *J. Am. Chem. Soc.* **1918**, 40, 1361–1403.

240. Singh, K.; Gautam, M. Development of inexpensive biosorbents from de-oiled mustard cake for effective removal of As(V) and Pb(II) ions from their aqueous solutions. *J. Sci. Ind. Res*. **2016**, 75, 444-451.

241. Slobodan, K. M. Consideration of the correct calculation of thermodynamic parameters of adsorption. *J. Serb. Chem. Soc.* **2004**, 72, 1363–1367.

242. Zhou, X. The unit problem in the thermodynamic calculation of adsorption using the Langmuir equation. *Chem. Eng. Commun*. **2014**, 201, 1459–1467.

243. Salvestrini, S.; Leone, V.; Iovino, P.; Canzano, S.; Capasso, S. Considerations about the correct evaluation of sorption thermodynamic parameters from equilibrium isotherms. *S. J. Chem. Thermo*. **2014**, 68, 310–316.

244. Frisch, M. J.; Trucks, G. W.; Schlegel, H. B.; Scuseria, G. E.; Robb, M. A.; Cheeseman, J. R.; Scalmani, G.; Barone, V.; Petersson, G. A.; Nakatsuji, H.; Li, X.; Caricato, M.; Marenich, A.V.; Bloino, J.; Janesko, B. G.; Gomperts, R.; Mennucci, B.; Hratchian, H. P.; Ortiz, J.V.; Izmaylov, A. F.; Sonnenberg, J. L.; Williams-Young, D.; Ding, F.; Lipparini, F.; Egidi, F.; Goings, J.; Peng, B.; Petrone, A.; Henderson, T.; Ranasinghe, D.; Zakrzewski, V. G.; Gao, J.; Rega, N.; Zheng, G.; Liang, W.; Hada, M.; Ehara, M.; Toyota, K.; Fukuda, R.; Hasegawa, J.; Ishida, M.; Nakajima, T.; Honda, Y.; Kitao, O.; Nakai, H.; Vreven, T.; Throssell, K.; Montgomery, J. A.; Jr., J. E.; Peralta, F.; Ogliaro, M. J.; Bearpark, J. J.; Heyd, E. N.; Brothers, K.N.; Kudin, V.N.; Staroverov, T. A.; Keith, R. ;Kobayashi, J.; Normand, K.; Raghavachari, A.P.; Rendell, J.C.; Burant, S.S.; Iyengar, J.; Tomasi, M.; Cossi, J. M.; Millam, M.; Klene, C.; Adamo, R.; Cammi, J. W.; Ochterski, R. L.; Martin, K.; Morokuma, O.; Farkas, J. B.; Foresman, D.J. Fox, Gaussian 16, Revision B.01, Gaussian, Inc., Wallingford CT, **2016**.

245. Lee, C.; Yang, W.; Parr, R. G. Development of the Colle-Salvetti correlation-energy formula into a functional of the electron density. *Phys. Rev. B.* **1988**, 37, 785-789.

246. Miehlich, B.; Savin, A.; Stoll, H.; Preuss, H. Results obtained with the correlation energy density functionals of becke. *Chem. Phys. Lett*. **1989**, 157, 200-206.

247. Dennington, R.; Keith, T.; Millam, J. Gauss View Version 5.0, *Semichem Inc.* KS, **2005**.

248. Bader, R. F. W. Atoms in molecules: a quantum theory.2nd Ed. *Oxford University Press*. New York. **1990**.

249. Espinosa, E.; Molins, E.; Lecomte, C. Hydrogen bond strengths revealed by topological analyses of experimentally observed electron densities. *Chem. Phys. Lett*. **1998**, 285, 170–173.

250. Ermolaev, V.; Miluykov, V.; Rizvanov, I.; Krivolapov, D.; Zvereva, E.; Katsyuba, S.; Sinyashin, O.; Schmutzler, R. Phosphonium ionic liquids based on bulky phosphines: synthesis, structure and properties. *Dalton Trans*. **2010**, 39, 5564–5571.

251. Pandey, S. K.; Manogaran, D.; Manogaran, S.; Schaefer III, H. F. Quantification of hydrogen bond strength based o interaction coordinate: A new approach. *J. Phys. Chem. A.* **2017**, 121, 6090-6103.

252. Fukui, K. Role of frontier orbitals in chemical reactions. *Science*. **1982**, 218, 747-754.

253. Fukui, K.; Yonezawa, Shingu, T. H. A molecular orbital theory of reactivity in aromatic hydrocarbons**.** *J. Phys. Chem.* **1952**, 20, 722-725.

254. Sinha, N.; Prasad, O.; Narayan, V.; Shukla, S. R. Raman, FT-IR spectroscopic analysis and first-order hyperpolarisability of 3-benzoyl-5-chlorouracil by first principles. *Mol. Simul*. **2011**, 37, 153-163.

255. Scrocco, E.; Tomasi, J. Electronic molecular structure, reactivity and intermolecular forces: an euristic interpretation by means of electrostatic molecular potentials. *Adv. Quantum Chem*. **1978**, 11, 115-193.

256. Scrocco, E.; Tomasi, J. The electrostatic molecular potential as a tool for the interpretation of molecular properties. *Top. Curr. Chem.* **1973**, 42, 95-170.

257. Kapsabelis, S.; Prestidge, C. A. Adsorption of ethyl(hydroxyethyl)cellulose onto silica particles: the role of surface chemistry and temperature. *J. Colloid and Interface Sci.* 2000, 228, 297–305.

258. Eraghi, K. A.; Fatehi, P. Interaction of synthetic and lignin-based sulfonated polymers with hydrophilic, hydrophobic, and charged self-assembled monolayers. *RSC Advances*. **2020**, 10, 36778–36793.

259. Klemm, D.; Heinze, T.; Philipp, B.; Wagenknecht, W. New approaches to advanced polymers byselective cellulose functionalization. *Acta Polym*. **1997**, 48, 277-297.

260. Liu, Q.; Zhang, Y.; Laskowski, J. S. The adsorption of polysaccharides onto mineral surfaces: an acid/base interaction. *Int. J. Min.l Process*. **2000**, 60, 229–245.

261. Balajee, S.R., Iwasaki, I. Adsorption mechanism of starches in flotation and flocculation of iron ores.*Trans. AIME.***1969**, 244, 401–406.

262. Balajee, S. R.; Iwasaki, I. Interaction of British gum and dodecylammonium chloride at quartz and hematite surfaces. *Trans. AIME*. **1969**, 244, 407–411.

263. Barker, C. A.; Storey, M. J. Development of flotation practice at Trojan nickel mine. *Trans. IMM, Section* C. **1982**, 91, C135–C141.

264. Bogusz, E.; Brienne, S.R.; Butler, I.; Rao, S.R.; Finch, J.A. Metal ions and dextrin adsorption on pyrite. *Miner. Eng*. **1997**, 10, 441–445.

265. Bolger, J. C. Acid base interactions between oxide surfaces and polar organic compounds. In: Mittal, L. Ž . Ed. *Adhesion Aspects of Polymeric Coatings*. Plenum, New York, NY. **1983**.

266. Bolger, J. C.; Michaels, A.S. Molecular structure and electrostatic interactions at polymer–solid interfaces. In: Weiss, P., Cheever, G.D. Eds. *Interface Conver. Poly. Coatings. Elsevier*, New Ž . York, NY. **1968**.

267. Bolin, N. J.; Laskowski, J. S. Polysaccharides in flotation of sulphides. Part II: Copperrlead separation with dextrin and sodium hydroxide. *Int. J. Miner. Process*. **1991**, 33, 235–241.

268. Brien, F.B.; Kar, G. An electrophoresis study of the flotation properties of talc minerals. *Trend Eng.* **1968**, 20, 8–12.

269. Chang, C.S.; Cooke, S. R. B.; Huch, R.O., Starches and starch products as depressants in amine flotation of iron ore. *Trans. AIME*, **1953**, 196, 1282–1286.

270. Cooke, S.R.B.; Schulz, N.F.; Lindroos, E.W. The effect of certain starches on quartz and hematite suspensions. *Trans. AIME*. **1952**, 193, 697–698.

Chapter 2

Experimental methods and characterization techniques

Abstract

This chapter describes as to working principles and specifications of the each equipment employed for in-depth characterizations of the adsorbents, adsorbates and adsorbent-adsorbate systems during this research work. A brief discussion of method used for preparation of various adsorbents and their physicochemical parameters employing Fourier-transform infrared spectrometer (FTIR), attenuated total reflection-Fourier transform infrared (ATR-FTIR) spectrometer, scanning electron microscope (SEM), energy dispersive X-Ray analysis (EDX), elemental mapping analysis (EMA), powder X-ray diffraction (PXRD), Brunauer–Emmett–Teller (BET) surface area analyzer, X-ray photoelectron spectrometer (XPS), zeta potential analyzer (ZPA) thermogravimetric analysis (TGA), advanced high-intensity ultrasonicator (AHIU) and ultraviolet-visible (UV-Vis) spectrophotometer has been mentioned in this chapter. It also deals the methodology of adsorption process applied for cellulose and its derivatives (CDs) onto various solid surfaces.

1. Introduction

Characterization, when used in materials (CDs and adsorbents) analysis, refers to the broad and general process by which a material's structure and properties were probed and measured. It could be a fundamental process in the field of materials cauterizations, without which no scientific understanding of analysis of materials could be ascertained. Analysis of materials characterization is the basis for understanding the composition and determination of various parameters when the materials are put into use. We have tried to give a brief description of some of the most common techniques available for determination of physiochemical parameters of CDs and various adsorbents [1]. The aim of this section was to facilitate the comprehension of the work in term of structural characterization and, in some way, to include a general description of a group of basic structural characterization techniques in a clear way. For that, the principles in which the different techniques were depends were presented. Additionally, the instrumentation used in each case is basically described, without entering in any case in detail. For a reader interested in more details, a group of additional readings have been included. The adsorption of CDs were carried out onto various solid surfaces. The solid surfaces were successfully prepared from various sources using important agricultural wastes, after only one simple modification step, and utilized for adsorption for CDs from their aqueous solutions. The physicochemical characterizations and experiments were confirmed by several depth characterization techniques.

2. Experimental

2.1. Chemicals and reagents

All the reagents used for synthesis and experimental studies were of analytical and laboratory grade. The mustard cake (MC) was purchased from a local mill, M/s Shyam Enterprises, Lucknow, India. The accurel product (MP 1001) having average pore diameter 0.014μm was a generous gift by Accrual System, Membrana GmbH, (Obernberg, Germany). Its trade name is Accrual. The tea waste was collected from local tea stalls and houses. The granular fine quartz (99.9%), Kaoline (99.9%), extra pure sodium carboxymethylcellulose (99.5%), sodium hydroxide (98%), hydrochloric acid (35.5%), potassium chloride (99.5%), methanol and isopropyl alcohol (99.9%),

sodium sulphate (99.9%), sulfuric acid (98%), cetrimide (96%) and dimethyl sulfoxide (99%) used were purchased by Loba Chemie Pvt. (Maharashtra, India). Urea (99%) was supplied by Fisher Scientific: Lab Equipment and Lab Supplies (Massachusetts, United States). Reference activated carbon 20-40 mesh (99.97%) purchased from Sigma Aldrich Chemie Gmb H. (Steinheim, Germany) was used for iodine and molasses test. Iodine resublimed (99.8%) was purchased by Sisco Research Laboratories Pvt. Ltd. (Maharashtra, India).Organic sugar, brown (100%) was supplied by Pro Nature (Maharashtra, India). High-purity grade of nitrogen gas (99.999%) and helium gas (99.9999%) were used for physiochemical characterization of the sample supplied by Krishna Gas Agencies (Lucknow, India). The double distilled water (DDW) was prepared using double distillation unit (GLDD15AQ, Glassco Laboratory Equipment Pvt. Ltd, Ambala Cantt., India) and used for the preparation of modified adsorbent, batch adsorption experiments and other required purpose throughout of this study.

2.2. Methods

2.2.1. Preparation of adsorbents

2.2.1.1. Carbonization method

The raw materials were crushed and washed with distilled water followed by drying in sunlight. This material was treated with 20 wt% H_2O_2 /H_2SO_4 at 60 °C for 24 h to oxidize the adhering organic matter and it was washed multiple times using double distilled water [2]. This powder was burned in the presence of N_2 gas at 715 °C for 25 min using Atmosphere-Controlled Muffle Furnace (ACMF, Thermo WW-33900-40) (Photograph 1). The material, powdered mustard carbon was grounded and sieved in to obtain the desired particle sizes for further analysis.

Photograph 1. ACMF (Thermo WW-33900-40**)**
Source. CSIR-IITR, Lucknow

ACMF is a critical component for high-temperature laboratory heating, enabling samples to be heat-treated at temperatures exceeding 1000°C with low risk of cross-contamination equipped with N_2 gas flow digital controller panels. The defining

characteristic of ACMF is that it separates the object to be heated from all byproducts of combustion from the heat source. With modern electrical furnaces, this means heat is applied to a chamber through induction or convection by a high-temperature heating coil inside an insulated material [3]. The experimental facility was provided by CSIR-IITR (Indian Institute of Toxicology Research), Lucknow (CSIR-IITR, Lucknow).

2.2.1.2. Calcination method

The samples were crushed and washed with distilled water followed by drying in sunlight. This material was treated with 20 wt% H_2O_2 /H_2SO_4 at 60°C for 24 h to oxidize the adhering organic matter [4] and it was washed multiple times using double distilled water. This powder was burned in the presence of O_2 gas at 715 °C for 25 min using Muffle Furnace (UTS AF-777). The material, powdered mustard carbon was grounded and sieved in to obtain the desired particle sizes for further analysis.

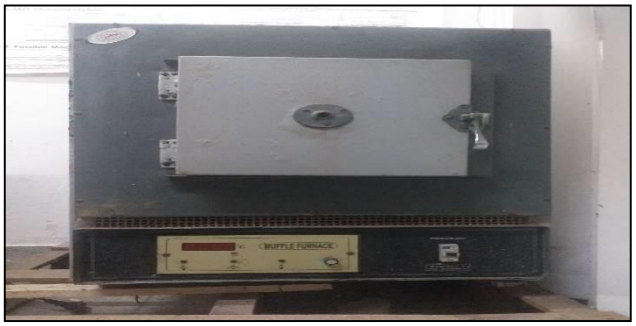

Photograph 2. MF (UTS AF-777). Source. LPC, DOC, BBAU, Lucknow

In the present study, Muffle Furnace (Agilent 5500) (Photograph 2) was used to for calcination purpose of the samples from Laboratory of Physical Chemistry, Department of Chemistry, Babasaheb Bhimaro Ambedkar University (A Central University) Lucknow (LPC, DOC, BBAU, Lucknow).

2.2.1.3. Oxidation method

The polypropylene, an inactive material was dried for 24 hrs under vacuum. To get modified polymeric surface the dried polypropylene was treated with an oxidizing solution containing a 1:1:2 (by weight) mixture of H_2SO_4, CrO_3, and double-distilled water; in the 500 ml volumetric flask with a thermometer [5]. After the treatment for 5 min, the new modified polypropylene was obtained from the slurry under stirring (30 ppm) at atmospheric pressure and 70°C, on a thermostat heating plate. The sample was washed first with double distilled water and then with acetone and finally, the modified polypropylene was ground and passed through a 100 mesh sieve and stored in a desiccator for further use.

2.2.1.4. Physical method

The supplied materials was washed with double distilled water in order to avoid possible interference during the determination of physicochemical and absorbance properties. It was then sun dried and grounded using pestle mortar. After proper crushing the material was kept in a hot air oven (JSGW/1210D/6, Jain Scientific Glass Works, Ambala Cantt., India) equipped with microprocessor based PID electric digital temperature controller at 110±1°C for 3-4 h (Photograph 3). This facility was availed from Laboratory of Organic Synthesis, Department of Chemistry, Babasaheb Bhimaro Ambedkar University (A Central University) Lucknow (LOS, DOC, BBAU, Lucknow). After the cooling the sample at room temperature, it was sieved using standard test sieves (BSS240, Continental Scientific Emporium, Lucknow, India) to remove all the debris and was stored in desired sample tubes [6]. Finally, the derived material from physical method was obtained. These tubes containing desired adsorbents were kept in a desiccator (159PC/PP, Kasablanka Corporation, Mumbai, India) and further identities of the adsorbents were confirmed using stored samples by depth characterization techniques/experiments.

Photograph 3. Hot Air Oven (SDO-4554). Source. LOS, DOC, BBAU, Lucknow

2.2.2. Computational details

Computational science is a discipline concerned with the design, implementation and use of mathematical models to analyse and solve scientific problems. Typically, the term refers to the use of computers to perform simulations or numerical analysis of a scientific system or process. DFT studies have been performed using Gaussian 16 program with B3LYP representing Becke's three parameter hybrid exchange functional (B3LYP) and Lee-Yang-Parr correlation functional, 6-31+G (d,

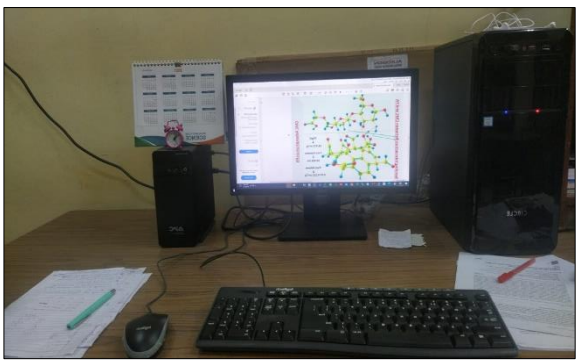

Photograph 4. CS. Source. IPC, IISc, Bengaluru

p) as the basis set. In order to probe the noncovalent interactions (NCIs) engaged in the adsorbate-adsorbent system, the Bader's QTAIM tool was performed. Computational models are mathematical models used to numerically study the behaviour of complex systems by means of a computer simulation [7, 8]. The computationals studies was performed using high advance computer (Photograph 4) to help in interpretation the experimental data. This computational studies were availed using computer system (CS) from Inorganic and Physical Chemistry - Indian Institute of Science, Bengaluru (IPC, IISc, Bengaluru).

2.2.3. Adsorption study

A stock solution (desired concentration) was prepared by dissolving appropriate amounts of CDs followed by vigorously stirred double distilled water and further stirring for 30 min. This solution was refrigerated for 24h then after it was used for further experiments (desired concentrations). After agitating the conical flasks for optimized time samples were withdrawn from the conical flasks. The adsorbent was separated from the polymer solution by centrifugation. The absorbance of the supernatant solution and residual concentration of polymers was determined by the earlier reported method [9] by spectrophotometrically at specific wavelength. The adsorption amount of CDs onto adsorbent was calculated using the following equation:

$$\Gamma = \frac{C_o - C_e}{m} \times V \qquad (1)$$

Where Γ= Amount of the CDs adsorbed (mg/g), C_o =Initial concentration of the CDs (mg/L), C_e=equilibrium concentration of the solution (mg/L), V=Volume (L) and W= Weight of adsorbent (g).

Batch adsorption experiments were also carried out to investigate the effect of various factors like the initial concentration of CDs, adsorbent dose, pH, ionic strength (0.1mol/L), temperature (°C) and urea (0.1mol/L) and sonication, etc.

2.3.4. Characterization of samples

2.3.4.1. Point of zero charge (pH_{ZPC})

The pH_{ZPC} is a very important surface parameter to characterize the acid-base nature of the solid material, therefore, the acidic-basic nature of adsorbents was determined by the salts addition method [10-14]. The ZPC values for adsorbent were evaluated using 0.1M $NaNO_3$/KCl solution at room temperature. In this process, the 40 ml of 0.1M $NaNO_3$ solution were taken in six different Stoppard bottles (100ml) namely 1, 2, 3, 4, 5, 6, 7, 8 and then an initial pH value of 2.0, 4.0, 6.0, 8.0, 10.0, 12.0, and 14.0 were adjusted respectively by either 0.1 M HNO_3 or 0.1 M NaOH solutions using digital pH meter. The adsorbent (0.1 g) was added to each bottle. Each flask then was stirred at 500rpm on a magnetic stirrer (MS-M-S10, DLAB Scientific Pvt Ltd. Hyderabad, India) for 24 h (Photograph 5**)**. After stirring the samples these were kept for equilibrium, and then was filtered using Millipore filter paper (0.45µm), the final pH of each bottle (filtrate) was recorded very carefully. The difference between the final and initial pH (ΔpH) values were calculated and then plotted against the initial pH values. The initial pH at which ΔpH was zero was taken as the pH_{PZC} of the adsorbent.

Photograph 5. Digital pH Meter (CL54+).
Source. DOC, BBAU, Lucknow

2.3.4.2. Iodine test

The physio-chemical and adsorption characteristic of adsorbent was evaluated by percentage iodine removal (PIR) analysis. The following formula [15] was applied to calculate the PIR value for adsorbent:-

$$PIR_{MTWC} = \frac{\text{ml thiosulphate used for blank} - \text{ml thiosulphate used for sample}}{\text{ml thiosulphate used for blank}} \times 100 \qquad (2)$$

The $PIR_{adsorbent}$ was evaluated which suggested that it follow a similar trend as reference activated carbon (RAC). This experimental study supports that adsorbent has sufficient adsorptive potential for present work.

2.3.4.3. Molasses test

The adsorptive characteristic of adsorbent was determined by percent molasses colour removed (PMCR) analysis. The $PMCR_{adsorbent}$ was determined using the following formula [15]:-

$$PMCR_{adorbent} = \frac{\text{Absorbance of blank} - \text{Absorbance of adorbent treated samples}}{\text{Absorbance of blank}} \times 100 \qquad (3)$$

The $PMCR_{adsorbent}$ was evaluated which was similar trend indicator with refrence activated carbon. The obtained data suggest that adsorbent has potential adsorption application for interpretation of the adsorption behaviour of CDs.

2.3.4.4. Fourier transform infrared (FT-IR) spectroscopy

Fourier transform infrared spectroscopy, also known as FTIR spectroscopy (Photograph 6), is an analytical technique used to identify organic, polymeric, and, in some cases, inorganic materials by scanning test samples and observe chemical properties [16]. It is a very powerful method for the identification of functional groups (CDs in the present study as an example Table 1). In general, the working principle of FTRI is to measure how well a sample absorbs or transmits light at each different wavelength [17]. FT-IR is used with the basic goal of determining changes in the intensity of infrared light as it interacts with a material as a function of wavelength. Therefore, infrared spectroscopy can applied as a very powerful tool for qualitative identification of different functional group and chemical bonds in different environment [18].

Photograph 6. FTIR (Nicole 6700) Source. DOC, BBAU, Lucknow

Working principle: A muffle furnace is a piece of oven-type equipment with O_2 flow rate control that can reach high temperatures. It usually works by putting a high-temperature heating coil in an insulated material. The insulating material effectively acts as a muffle, preventing heat from escaping [19]. Furnace is usually heated to desired temperatures. In FT-IR analysis there are three commonly examined pieces of

data known as peak position, the peak width and the peak intensity. The peak position is probably the most commonly used for the identification of materials. These peaks are unique since, at characteristic frequencies, certain functional groups will display their own set of peaks [20]. This is because infrared techniques measure the vibrational energies of the molecules. In order for a molecule or functional group to be IR active, the dipole moment of the molecule must change. When the desired sample for testing is opaque, transmission experiments are not practical [21]. To overcome this problem, reflection experiments in the FT-IR become more appropriate.

When the infra-red beams enter in the sample it can be reflected, transmitted or absorbed. The infra-red energy reflecting off the surface is typically lost. The infra-red beam that passes through a particle can either reflect off the next particle or to be transmitted through the next particle. Scattered infra-red energy is collected by a spherical mirror that is focused onto a detector. These are the basics of how the diffuse reflectance mode of the FT-IR works [22].

Sample analysis process

i. **The source**: Infrared energy is emitted from a glowing black-body source. This beam passes through an aperture which controls the amount of energy presented to the sample (and, ultimately, to the detector).

ii. **The interferometer**: The beam enters the interferometer where the "spectral encoding" takes place. The resulting interferogram signal then exits the interferometer.

iii. **The sample:** The beam enters the sample compartment where it is transmitted through or reflected off of the surface of the sample, depending on the type of analysis being accomplished. This is where specific frequencies of energy, which are uniquely characteristic of the sample, are absorbed.

iv. **The detector:** The beam finally passes to the detector for final measurement. The detectors used are specially designed to measure the special interferogram signal.

v. **The computer:** The measured signal is digitized and sent to the computer where the Fourier transformation takes place. The final infrared spectrum is then presented to the user for interpretation and any further manipulation

With the help of FTIR spectra, the study of different adsorbents and CDs were carried out. Some selected wavenumbers for CDs has been shown in the following table.

Table 1 General assignments of the most important IR absorption frequencies for CDs adapted from [17]

Wavenumber (cm^{-1})	**Assignment**
3450–3570	-OH stretch, intramolecular H-bridge between the -OH groups
3200–3400	-OH stretch, intermolecular H-bridge between the -OH groups
2933–2981	-CH_2 antisymmetric stretch
2850–2904	-CH_2 symmetric stretch
2247	-CN
1725–1730	-C=O stretch from acetyl or -COOH groups
1635	Adsorption of water
1591	-COO^- in CMC
1455–1470	CH_2 symmetric ring stretch at pyrane ring; OH in-plane deformation
1416–1430	-CH_2 scissors vibration
1374–1375	-CH deformation
1335–1336	-OH in-plane deformation
1315–1317	-CH_2 tip vibration
1370, 1176–1162	-O–SO_2–R (tosylates, mesylates)
1277–1282	-CH deformation
1225–1235	-OH in-plane deformation, also in -COOH groups
1200–1205	-OH in-plane deformation
1125–1162	-C–O–C antisymmetric stretch
1107–1110	Ring antisymmetric stretch
1015–1060	-C–O stretch
985–996	-C–O stretch
925–930	Pyran ring stretch
892–895	-C-anomeric groups stretch, -C1–H– deformation; ring stretch
826–800	-C–O–S (tosylates, mesylates)
800	Pyran ring stretch

2.3.4.5. Attenuated total reflectance-Fourier transform infrared (ATR-FTIR) spectroscopy

ATR stands for attenuated total reflection and is developed in order to enhance the surface sensitivity since IR spectroscopy is a bulk method. The ATR-FTIR is a useful technique for measuring the infrared spectra of solids and liquids as well as probing adsorption on particle surfaces without sample preparations [23]. Attenuated total reflectance (ATR) is a special accessory unit which can be used with Fourier transform infrared (FTIR) spectrometer (Photograph 7) hence the working principle of ATR-FTIR is similar to FTIR. The ATR technique is based on a special reflectance setup where the sample is pressed directly onto various crystals with high refractive indices [24]. It enables you to measure directly onto a solid state sample surface by pressing the sample towards an ATR crystal (e.g. diamond), including liquid and gas samples, thus avoiding the need to prepare pellets (small concentration of sample in e.g. KBr, mechanically and/or chemically dissolved) for use in the normal transmittance mode. Hence, the extensive, time-consuming and often cumbersome sample preparation by pressing thin KBr pellets as in traditional FTIR transmittance spectroscopy is avoided [25]. The traditional technique might even change the sample material in question. The ATR technique is based on a special reflectance setup where the sample is pressed directly onto various crystals with high refractive indices, e.g. diamond. When interpreting ATR-FTIR spectra where quantitative results are important, note that non-corrected ATR spectra have much stronger absorbance bands at longer wavelengths (smaller wave numbers) than at shorter wavelengths (larger wave numbers) compared to normal FTIR transmittance spectra [26, 27]. Qualitative measurements (location of absorbance peaks at wave numbers) do not represent a problem as long as the contact area is large enough to ensure a sufficient strong measurement signal [28].

Photograph 7. ATR-FTIR (Bruker-Tensor 27). Source. DOC, IIT, Knapur

2.3.4.6. X-ray diffraction (XRD)

X-ray diffraction (XRD) is one of the powerful characterization tools used in solid state chemistry and material science (Photograph 8, 9). The atomic planes of a crystal cause an incident beam of X-rays to interfere with one another as they leave the crystal. The phenomenon is called X-ray diffraction [29]. It is a material characterization technique that can be useful for analyzing the lattice structure of a material. The sample is irradiated with non-chromatic X-ray light and the stray radiation recorded. An important field of application is the identification of crystalline fractions in powders [30]. The X-ray radiation most commonly used is emitted by copper having characteristic wavelength of the K radiation is 1.5418 Å. When the incident beam strikes sample diffraction occurs in every possible orientation of 2θ. The diffracted beam may be detected by using a moveable detector such as Geiger counter, which is connected to a chart recorder. In normal use, the counter is set to scan over a range of 2θ values at a constant angular velocity. Routinely a 2θ range of 10° to 80° is sufficient to cover the most useful part of the powder pattern. The scanning speed of the counter is usually 2θ of 2 °/min and therefore about 30 minutes are needed to obtain a trace [31].

Photograph 8. X-ray diffraction (Panalytical) Source. ACMS, IIT, Kanpur

Photograph 9. X-ray Diffraction (Bruker ECOD8 ADVANCE), Source. USIC, BBAU, Lucknow

Basic principle of XRD: XRD analysis uses the property of crystal lattices to diffract monochromatic X-ray light. This involves the occurrence of interference of the waves scattered at the successive planes which are described by Braggs equation [32 -33].

$$n\lambda = 2d \sin\theta \ (n = 1, 2, 3) \qquad (4)$$

Where λ is the wavelength, n is the order of diffraction, d is the lattice plane distance and θ is the half the diffraction angle. This relation is used for the structure analysis of crystals.

2.3.4.7. Atomic force microscopy (AFM)

AFM is a type of scanning probe microscopy (SPM) (Photograph 10), with demonstrated resolution on the order of fractions of a nanometer, more than 1000 times better than the optical diffraction limit. The information is gathered by "feeling" or "touching" the surface with a mechanical probe one of the most important tools for imaging on the nanometer scale, AFM uses a cantilever with a sharp probe that scans the surface of the specimen [34]. AFM was developed when people tried to extend STM technique to investigate the electrically non-conductive materials, like proteins. In 1986, Binnig and Quate demonstrated for the first time the ideas of AFM, which used an ultra- small probe tip at the end of a cantilever [35]. AFM provides a 3D profile of the surface on a nanoscale, by measuring forces between a sharp probe and the surface. The AFM has three major abilities: force measurement, imaging, and manipulation. It is powerful because an AFM can generate images at atomic resolution with angstrom scale resolution height information, with minimum sample preparation [36].

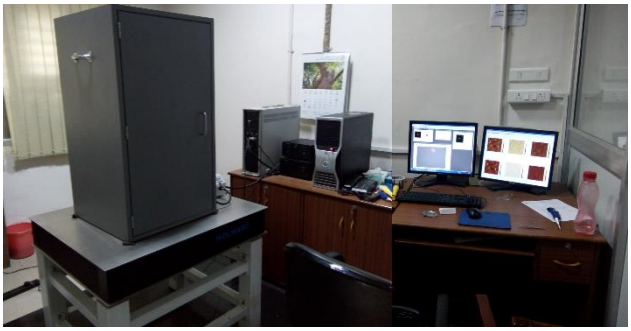

Photograph 10. AFM (Agilent 5500). Source. DOC, IIT, Kanpur

Principle of AFM: Surface sensing an AFM uses a cantilever with a very sharp tip to scan over a sample surface. As the tip approaches the surface, the close-range, attractive force between the surface and the tip cause the cantilever to deflect towards the surface. However, as the cantilever is brought even closer to the surface, such that the tip makes contact with it, increasingly repulsive force takes over and causes the cantilever to deflect away from the surface [37].

Detection method: A laser beam is used to detect cantilever deflections towards or away from the surface. By reflecting an incident beam off the flat top of the cantilever, any cantilever deflection will cause slight changes in the direction of the reflected beam. A position-sensitive photo diode (PSPD) can be used to track these changes. Thus, if an AFM tip passes over a raised surface feature, the resulting

cantilever deflection (and the subsequent change in direction of reflected beam) is recorded by the PSPD [38].

Imaging: An AFM images the topography of a sample surface by scanning the cantilever over a region of interest. The raised and lowered features on the sample surface influence the deflection of the cantilever, which is monitored by the PSPD. The AFM can generate an accurate topographic map of the surface features [39].

How are force measured? The probe is placed on the end of a cantilever (which one can think of as a spring). The amount of force between the probe and surface is dependant on the spring constant (stiffness of the cantilever and the distance between th probe and the sample surface. This force can be described using Hooke's Law:

$$F= -k \cdot x \quad (5)$$

F = Force k = spring constant x = cantilever deflection

If the spring constant of cantilever (typically ~ 0.1-1 N/m) is less than surface, the cantilever bends and the deflection is monitored. •This typically results in forces ranging from nN (10) to µN (10-6) in the open air [40].

Applications: The AFM has been applied to problems in a wide range of disciplines of the natural sciences, including solid-state physics, semiconductor science and technology, molecular engineering, polymer chemistry and physics, surface chemistry, molecular biology, cell biology, and medicine. It gives information about the toughness, roughness and smoothness value of surface. Applications in the field of solid state physics include (a) the identification of atoms at a surface, (b) the evaluation of interactions between a specific atom and its neighboring atoms. In molecular biology, AFM can be used to study the structure and mechanical properties of protein complexes and assemblies. For example, AFM has been used to image microtubules and measure their stiffness [41].

In present study, AFM (Agilent 5500) (Photograph 10) was used to analysis the surface roughness of the samples and their surface morphology in 3D view from Department of Chemistry, Indian Institute of Technology, Kanpur (DOC, IIT, Kanpur).

2.3.4.8. Zeta potential analyzer (ZPA)

Zeta potential is a scientific term for electrokinetic potential in colloidal dispersions. It is usually denoted using the Greek letter zeta (ζ), hence ζ-potential. The electric potential at the boundary of the double layer is known as the Zeta potential of the particles and has values that typically range from +100 mV to -100 mV [42]. It is the potential observed at the shear plane. Zeta potential or electrokinetic potential is defined as the difference in the potential between shear plane and electroneutral region of the solution. Zeta potential is more important than Nernst potential because the electrical double layer also moves, when the particle is under motion [43].

Photograph 11. ZPA (NanoPlus Common), Source. DPS, BBAU, Lucknow

Zeta potential measurement: Zeta potential is not directly measurable, it can be calculated using theoretical models like electrokinetic phenomena and electroacoustic phenomena.

Working principle: Zeta potential measurement principle (Laser Doppler Electrophoresis) many nanoparticles or colloidal particles have a surface charge when they are suspension. When an electric field is applied, the particles move due to the interaction between the charged particle and applied field [44].

Applications: ZP (ζ) measurement is a very useful but often under-utilized technique that can provide information about the material surface-solution interface. Knowledge of ZP can be used to predict and control the stability of suspensions and emulsions; measurement of ZP is often the key to understanding dispersion and aggregation processes. The presence, or absence of charged groups/moieties on the surface of materials, as revealed by their ZP, can directly affect their performance and processing characteristics in suspension. The sign and magnitude of ZP affects process control, quality control, product specification; at the simplest level, it can help maintain a more consistent product and at a complex level it can improve product quality and performance. The zeta potential (ZP) can be used to evaluate the charge stability of a disperse system, such as liposomes; it is used to quantify the magnitude

of the electrical charge of the lipid bilayer. A measurement is taken by applying an electric charge across the sample in a folded capillary flow cell [45].

In present study, ZPA (NanoPlus Common) (Photograph 11) was used to analysis the zeta potential and their colloidal stability in aqueous solutions of the samples from Department of Pharmaceutical Sciences, Babasaheb Bhimrao Ambedkar University (A Central University) Lucknow (DPS, BBAU, Lucknow).

2.3.4.9. Ultrasonication

Sonication is a process in which sound waves are used to agitate particles in solution. Such disruptions can be used to mix solutions, speed the dissolution of a solid into a liquid (like CDs into water), and remove dissolved gas from liquids. The CDs solution was irradiated with ultrasonic waves (20 kHz, 750 W) for optimized time with help of ultrasonicater (Sonics, vibra-cell 20 kHz±50Hz, 750 W) [46].

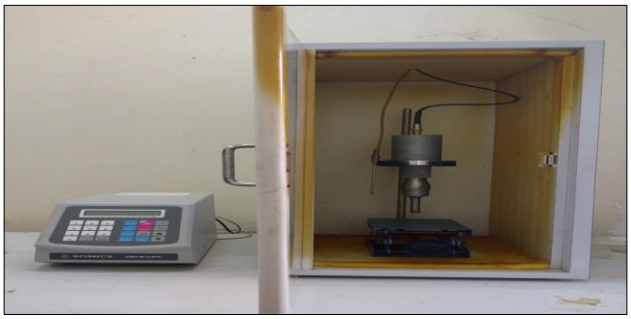

Photograph 12. AHIU (Sonics, vibra-cell 500)
Source. LPC, DOC, BBAU, Lucknow

Working principle: Sonication uses sound waves to agitate particles in a solution. It converts an electrical signal into a physical vibration to break substances apart. These disruptions can mix solutions, accelerate the dissolution of a solid into a liquid, such as sugar into water, and remove dissolved gas from liquids [47].

Applications : Sonication can be used for the production of nanoparticles, such as nanoemulsions, nanocrystals, liposomes and wax emulsions, as well as for wastewater purification, degassing, extraction of seaweed polysaccharides and plant oil, extraction of anthocyanins and antioxidants, production of biofuels, crude oil desulphurization, cell disruption, polymer and epoxy processing, adhesive thinning, and many other processes. It is applied in pharmaceutical, cosmetic, water, food, ink, paint, coating, wood treatment, metalworking, nanocomposite, pesticide, fuel, wood product and many other industries [48].

In current study, sonication using AHIU (Photograph 12) was applied to homogenize the samples in aqueous mediums and to observe the influence of sonication during the

adsorption of CDs onto various solid surfaces. This facility was available at Laboratory of Physical Chemistry, Department of Chemistry, Babasaheb Bhimrao Ambedkar University (A Central University) Lucknow (LPC, DOC, BBAU, Lucknow).

2.3.4.10. Ultraviolet–visible spectrophotometry (UV–Vis or UV/Vis)

UV-Vis spectrophotometer uses visible light and ultraviolet to analyze the chemical structure of substance. A spectrophotometer is a special type of spectrometer, which is used to measure the intensity of light. When ultraviolet light project to various substance**,** they will absorb it. Therefore, we can use UV-Vis spectrophotometer to measure the absorption of light by compound and can we determine molecular structure, as well as the related information [49].

Photograph 13: UV (Carry 100). Source: SIL, DOC, BBAU, Lucknow

Principle: UV-Vis is often called a general technique, as most molecules absorb light in the UV-visible wavelength range. The UV range extends from 100–400 nm, and the visible spectrum ranges from 400–700 nm. The spectrophotometer is a much more refined version of a colorimeter [50]. In a colorimeter, filters are used which allow a broad range of wavelengths to pass through, whereas in the spectrophotometer a prism (or) grating is used to split the incident beam into different wavelengths. By suitable mechanisms, waves of specific wavelengths can be manipulated to fall on the test solution. The range of the wavelengths of the incident light can be as low as 1 to 2 nm. The spectrophotometer is useful for measuring the absorption spectrum of a compound, that is, the absorption of light by a solution at each wavelength [51]. Molecules containing bonding and non-bonding electrons (n-electrons) can absorb

Photograph 14: of UV (Spectronic 20D+). Source: LPC, BBAU, Lucknow

energy in the form of ultraviolet or visible light to excite these electrons to higher anti-bonding molecular orbitals.

Quantitative relationships for optical spectroscopy:

Beer and Lambert laws

$$A = \varepsilon bc \tag{6}$$

$$A = -log\, T = log \frac{I_0}{I} = \varepsilon bc$$

$$T = \frac{I}{I_0}$$

(Where A= Absorbance, I_0= intensity of incident light, I= Intensity of emitted light = molar absorptivity coefficient , T= Transmittance, b= path length of sample, c =molar concentration of solute)

From the Beer-Lambert law it is clear that greater the number of molecules capable of absorbing light of a given wavelength, the greater the extent of light absorption [52].

Instrumentation and working of UV-visible spectrophotometer: Instrumentation and working of the UV spectrometers can be studied simultaneously. Most of the modern UV spectrometers consist of the following parts-

Light Source: Tungsten filament lamps and Hydrogen-Deuterium lamps are most widely used and suitable light source as they cover the whole UV region. Tungsten filament lamps are rich in red radiations; more specifically they emit the radiations of 375 nm, while the intensity of Hydrogen-Deuterium lamps falls below 375 nm [53].

Monochromator: Monochromators generally composed of prisms and slits. The most of the spectrophotometers are double beam spectrophotometers. The radiation emitted from the primary source is dispersed with the help of rotating prisms. The various wavelengths of the light source which are separated by the prism are then selected by the slits such the rotation of the prism results in a series of continuously increasing wavelength to pass through the slits for recording purpose. The beam selected by the slit is monochromatic and further divided into two beams with the help of another prism [54].

Sample and reference cells: One of the two divided beams is passed through the sample solution and second beam is passé through the reference solution. Both sample and reference solution are contained in the cells. These cells are made of either silica or quartz. Glass can't be used for the cells as it also absorbs light in the UV region.

Detector: Generally two photocells serve the purpose of detector in UV spectroscopy. One of the photocell receives the beam from sample cell and second detector receives the beam from the reference. The intensity of the radiation from the reference cell is stronger than the beam of sample cell. This results in the generation of pulsating or alternating currents in the photocells.

Amplifier: The alternating current generated in the photocells is transferred to the amplifier. The amplifier is coupled to a small servometer. Generally current generated in the photocells is of very low intensity, the main purpose of amplifier is to amplify the signals many times so we can get clear and recordable signals.

Recording devices: Most of the time amplifier is coupled to a pen recorder which is connected to the computer. Computer stores all the data generated and produces the spectrum of the desired compound [55].

In current study, the absorbance of the supernatant and residual concentration of CDs from aqueous solutions onto various solid surfaces were determined by the earlier reported method by spectrophotometrically (Photograph 13, 14) at specific wavelengths. This facility was available at Laboratory of Physical Chemistry and Department of Chemistry, Babasaheb Bhimrao Ambedkar University (A Central University) Lucknow (LPC & DOC, BBAU, Lucknow).

3. Conclusions

This chapter describes the role of several techniques for the characterization of CDs and various adsorbents during this research work. Through this comprehensive summary of characterization methods and instrumental techniques we described how they can complement each other and utilized for various studies. By presenting the role of each technique in a comparative way, it may act as a robust platform, helping the scientific community to understand better the titled topic. In this way, researchers will be benefited for the choice of the most suitable techniques for their characterization for CDs and adsorbents including allied materials, together with the ability to assess their use in a more precise manner.

References

1. Croy, R.; Mostafa, S.; Hickman, L.; Heinrich, H.; Cuenya, B. R. Bimetallic Pt-metalcatalysts for the decomposition of methanol: effect of secondary metal on the oxidationstate, activity, and selectivity of Pt. *Appl. Catal. A Gen.* **2008**, 350, 207–216.
2. De Gisi, S.; Lofrano, G.; Grassi, M.; Notarnicola, M. Characteristics and adsorption capacities of low-cost sorbents for wastewater treatment: A review. *Sust. Mat. Tech*. **2016**, 9, 10–40.
3. Agbaba, J.; Jazić, J. M.; Tubić, A.; Watson, M.;vMaletić, S.; Isakovski, M. K.; Dalmacija, B. Oxidation of natural organic matter with processes involving O_3, H_2O_2 and UV light: formation of oxidation and disinfection by-products. *R.S.C. Advances*. **2016**, 6, 86212-86219.
4. Al-Azzawi, M. S. M.; Kefer, S.; Weißer, J.; Reichel, J.; Schwaller, C.; Glas, K.; Drewes, J. E. Validation of sample preparation methods for microplastic analysis in wastewater matrices—reproducibility and standardization. *Water*, **2020**, 12, 2445.
5. Tao, G.; Gong, A.; Lu, J.; Sue, H.-J.; Bergbreiter, D. E. Surface functionalized polypropylene: synthesis, characterization, and adhesion properties. *Macromolecules*, **2001**, 34, 7672-7679.
6. Khedr, S.; Shouman, M.; Fathy, N.; Attia, A. . Effect of physical and chemical activation on the removal of hexavalent chromium ions using palm tree branches. *ISRN Env. Chem.* **2014**, 1, 1–10.
7. Frisch, M. J.; Trucks, G. W.; Schlegel, H. B.; Scuseria, G. E.; Robb, M. A.;. Cheeseman, J. R.; Scalmani, G.; Barone, V.; Petersson, G. A.; Nakatsuji, H.; Li, X.; Caricato, M.; Marenich, A. V.; Bloino, J.; Janesko, B. G.; Gomperts, R.; Mennucci, B.; Hratchian, H. P.; Ortiz, J. V.; Izmaylov, A. F.; Sonnenberg, J. L.; Williams-Young, D.; Ding, F.; Lipparini, F.; Egidi, F.; Goings, J.; Peng, B. A.; Petrone, T.; Henderson, D.; Ranasinghe, V. G.; Zakrzewski, J.; Gao, N.; Rega, G.; Zheng, W.; Liang, M.; Hada, M.; Ehara, K.; Toyota, R.; Fukuda, J.; Hasegawa, M.; Ishida, T.; Nakajima, Y.; Honda, O.; Kitao, H.; Nakai, T.; Vreven, K.; Throssell, J. A.; Montgomery Jr., J. E.; Peralta, F.; Ogliaro, M. J.; Bearpark, J. J.; Heyd, E. N.; Brothers, K. N.; Kudin, V. N.; Staroverov, T. A.; Keith, R.; Kobayashi, J.; Normand, K.; Raghavachari, A. P.; Rendell, J. C.; Burant, S. S.; Iyengar, J.; Tomasi, M.; Cossi, J. M.; Millam, M.; Klene, C.;

Adamo, R.; Cammi, J. W.; Ochterski, R. L.; Martin, K; Morokuma, O.; Farkas, J. B.; Foresman, D. J.; Fox, Gaussian 16, RevisionB.01, Gaussian, Inc., Wallingford CT. **201**6.

8. Lee, C.; Yang, W.; Parr, R. G. Development of the Colle-Salvetti correlation-energyformula into a functional of the electron density. *Phys, Rev. B.* **1988**, 37, , 785–789.
9. DuBois, M.; Gilles, K. A.; Hamilton, J. K.; Rebers, P. A.; Smith, F. Colorimetric method for determination of sugars and related substances. *Anal. Chem.* **1965**, 28, 350–356.
10. Chiban, M.; Carja, G.; Lehutu, G.; Sinan, F. Equilibrium and thermodynamic studies for the removal of as(v) ions fromaqueous solution using dried plants as adsorbents. *Arabian J.Chem*. **2016**, 9, S988–S999.
11. Chowdhury, Z. Z.; Zain, S. M.; Khan, R. A.; Rafique, R. F.;Khalidc, K. Batch and fixed bed adsorption studies of lead(Ii) cations from aqueous solutions onto granular activatedcarbon derived from mangostana garcinia shell. *Bio Res*. **2012**, 7, 2895–2915.
12. Singh, K.; Gautam, M. Development of Inexpensive biosorbents from de-oiled mustard cake for effectiveremoval of as(v) and pb(ii) ions from their aqueous solutions. *J. Sci. Ind. Res*. **2016**, 75, 444.
13. Mahmood, T.; Saddique, M. T.; Naeem, A.; Westerhoff, P.;Mustafa, S.; Alum, A. Comparison of different methods forthe point of zero charge determination of NiO. .*Ind. Eng.Chem. Res*. **2011**, 50, 10017–10023.
14. Fiol, N.; Villaescusa, I. Determination of sorbent point zerocharge: usefulness in sorption studies. *Environ. Chem. Lett*. **2009**, 7, 79–84.
15. Singh, K.; Chandra, B. Synthesis, characterization of new adsorbent material from agriculture waste and its use for removal of phenols. *Frontiers Env. Res*. **2014**, 1, 11–21
16. Baker, M. J.; Trevisan, J.; Bassan, P.; Bhargava, R.; Butler, H. J.; Dorling, K. M.; Martin, F. L. Using Fourier transform IR spectroscopy to analyze biological materials. *Nature Protocols*. **2014**, 9, 1771-1791.
17. Fengel D.; Ludwig M. Possibilities and limits of FTIR spectroscopy for thecharacterization of cellulose. Part 1. Comparison of various cellulose fibers and bacterial-cellulose. *Papier*. **1991**, 45, 45–51
18. Smith, B.C. Fundamentals of Fourier transform infrared spectroscopy. CRC Press, Boca Raton, 2nd Edition, **2011**

19. Gouthama, T. R.; Harisha, G.; Manjunatha, Y. R.; Kumara, S. M. M.; Srinath, M. S.; Lingappa, M. S.. Melting of tin using muffle furnace and microwave energy and its characterization. IOP Conference Series: *Mat. Sci. Eng.* **2016**, 149, 1-10.
20. Clark D. E.; Sutton W.H. Microwave processing of materials. *Annual Review Mat. Sci.*, **1996**, 26, 299-331.
21. Tran, C. D. Principles, instrumentation, and applications of infrared multispectral imaging, an overview. *Analyt. Letters*. **2005**, 38, 735–752.
22. Alexander, T.; Gao, G. H.; Tran, C. D. Development of a novel fluorimeter based on superluminescent light emitting diodes and an acousto-optic tunable filter and its application in the determination of chlorophyll a and b. *Appl. Spectrosc*.**1997**, 51, 1603– 1606.
23. Alexander, T.; Tran, C. D. Near-infrared multispectral imaging technique for visualizing sequences of di- and tripeptides synthesized by solid phase combinatorial method. *Appl. Spectrosc*. **2001**, 55: 939– 945.
24. Baptista, M. S.; Tran, C. D.; Gao, G. H. Near infrared detection of flow injection analysis by acousto-optic tunable filter based spectrophotometry. *Anal. Chem.* **1996**, 68, 971– 976.
25. Barton, J. G.; Cannata, R. F.; Petronio, S. M. InGaAs NIR focal plane arrays for imaging and DWDM applications. *Proc. SPIE*. **2002**, 4721: 37 – 47.
26. Bhargava, R.; Levin, I. W. Fourier transform infrared imaging: Theory and practice. *Anal. Chem*. **2001**, 73, 5157-5167.
27. Cabelli, S.A., Pan, J., Bernd, S.G., Tennant, W.E., Blackwell, J.D., Bhargava, S.,
28. Pasko, J. G.; Piquette, E. C.; Edwall, D. D. High resolution extended NIR camera. Proc. SPIE. **2003**, 5074: 343– 352.
29. Fischer, M.; Tran, C. D. Evidence for kinetic inhomogeneity in the curing of epoxy using the near-infrared multispectral imaging technique. *Anal. Chem*.**1999,** 71, 953– 959.
30. Jelle, B. P.; Nilsen, T.-N.; Hovde P. J.; Gustavsen, A. Accelerated climate aging of building materials and their characterization by fourier transform infrared radiation analysis. *J. Build. Phy*. **2012**, 36, 99-112, 2012.
31. Bunaciu, A. A.; Udriştioiu, E.; Gabriela, Aboul-Enein, H. Y. X-ray diffraction: instrumentation and applications. *Crit. Rev. Analyt. Chem.* **2015**, 45, 289–299.
32. Aaltonen, J.; Alleso, M.; Mirza, S.; Koradia, V.; Gordon, K. C.; Rantanen, J. Solid Form Screening—A Review. *Eur. J. Pharm. Biopharm*. **2009**, 71, 23–37.

33. Andreeva, P.; Stoilov, V.; Petrov, O. Application of X-ray diffraction analysis for sedimentological investigation of middle devonian dolomites from northeastern bulgaria. *Geol. Balcanica.* **2011**, 40, 31–38.
34. Shinato, Kebede W.; Huang, Feifei, Jin, Ying. Principle and application of atomic force microscopy (AFM) for nanoscale investigation of metal corrosion. *Corrosion Reviews*. **2020**, 38, 423-432.
35. Lapshin, R. V. Feature-oriented scanning methodology for probe microscopy and nanotechnology. *Nanotech*. **2004**, 15, 1135–1151.
36. Giessibl, Franz J. High-speed force sensor for force microscopy and profilometry utilizing a quartz tuning fork. *App.Phy. Lett.*. **1998**, 73, 3956
37. Carpick, R. W.; Salmeron, M. Scratching the surface: fundamental investigations of tribology with atomic force microscopy. *Chemical Reviews*. **1997**, 97, 1163–1194.
38. Giessibl, Franz J. Advances in atomic-force microscopy. *Rev. Mod. Phy.* **2003**, 75, 949–983
39. Nagy, A.; Neuman, K. C. Single-molecule force spectroscopy: optical tweezers, magnetic tweezers and atomic force microscopy. *Nature Methods*. **2008**, 5, 491 – 505.
40. Frank, O. True atomic resolution by atomic force microscopy through repulsive and attractive forces. *Science*. **2013**, 260, 1451–6.
41. Hunter, R. J. Zeta potential in colloid science: principles and applications. *Academic Press,* UK.**1998**
42. Verway, E. J. W.; Overbeek, J. Th. G. Theory of the stability of lyophobic colloids. *Elsevier*. Amsterdam. **1948**
43. Ostolska, I.; Wiśniewska, M. Application of the zeta potential measurements to explanation of colloidal Cr_2O_3 stability mechanism in the presence of the ionic polyamino acids. *Colloid and Poly. Sci*. **2014**, 292, 2453–2464.
44. Wiśniewska M. A review of temperature influence on adsorption mechanism and conformation of water soluble polymers on the solid surface. *J. Dispers. Sci. Technol.* **2011**, 32, 1605–1623.
45. Semenov, A. N. Theory of colloid stabilization in semidilute polymer solutions. *Macromolecules*. **2008**, 41, 2243–2249.
46. Chemat, F., Zill-e-Huma, Khan, M. K. Applications of ultrasound in food technology: Processing, preservation and extraction. *Ultrason. Sonochem*. **2011**, 18, 813–835.A

47. Gallo, M.; Ferrara L.; Naviglio, D. Application of ultrasound in food science and technology: a perspective. *Food*s. 2018, 7, 164.
48. Cook, K. L. K.; Hartel, R.W. Mechanisms of ice crystallization in ice cream production. *Compr*. *Rev. Food Sci. Food Saf.* **2010**, 9, 213–222.
49. Bürgi, Thomas. Combined in situ attenuated total reflection infrared and UV–vis spectroscopic study of alcohol oxidation over Pd/Al_2O_3. *J. Cataly.* **2005**, 229, 55-63.
50. Bentrup, Ursula, et al. Linking simultaneous in situ WAXS/SAXS/Raman with Raman/ATR/UV–vis spectroscopy: comprehensive insight into the synthesis of molybdate catalyst precursors. *Topics in Cataly*. **2009**, 52, 1350-1359
51. Sharma, K.; Agrawal, S. S.; Gupta, M. Development and validation of uv spectrophotometric method for the estimation of curcumin in bulk drug and pharmaceutical dosage forms. *Int. J. Drug Dev. Res*. **2012**, 4, 375-380
52. Skoog, Douglas A.; Holler, F. James; Crouch, Stanley R. Principles of instrumental analysis (6th ed.). *Belmont, CA: Thomson Brooks/Cole*. **2007**, pp. 169–173.
53. Sooväli, L.; Rõõm, E.-I.; Kütt, A.; et al. Uncertainty sources in UV–Vis spectrophotometric measurement". *Accred. Qual. Assur*. **2006**, 11, 246–255.
54. Sharma B. K. Instrumental methods of chemical analysis. 25th ed. Meerut (India): Krishna Prakashan Media. **2005**.
55. Stein, S. E. An integrated method for spectrum extraction and compound identification from gas chromatography/mass spectrometry data. *J. Am. Soc. Mass. Spectrom*. **1999**, 10, 770–781.

Chapter 3

Adsorption behaviour of carboxymethylcellulose onto mesoporous carbon derived from mustard cake

Abstract

Carboxymethylcellulose (CMC) is a versatile polymer for several industrial applications such as oil drilling, detergents, food and beverage, papers, ceramics, coatings, and other promising usages. The lack of exploration of the binding mechanism of CMC on solid surfaces in the aqueous system, indeed, retards its applications. An attempt has, therefore, been made here to enhance the binding aspect of CMC on mesoporous mustard carbon (MMC). The typical BET surface area (S_{BET}) =16.576 m^2g^{-1} was primarily distributed by mesopores (average pore diameter and total pore volume was 12.432nm and 0.051cm^3g^{-1}, respectively). The electrokinetic findings indicated that the MMC interface is negatively charged with point of zero charge value of 9.8, which favoured CMC adsorption at a specific pH value (pH=3.0). The adsorption free energy of CMC was found as -22.561 $kJmol^{-1}$ which was in close agreement with H-bond energy revealing hydrogen bonding to be a dominant force for CMC (L2 type) adsorption and was also confirmed by high-resolution X-ray photoelectron spectrophotometer, attenuated total reflection Fourier transformation infra-red and urea test. A simple description of the binding elements of CMC on the MMC can therefore supports CMC as a promising adsorbate for various industrial applications. The optimized titled model, adsorbent-adsorbate complex (MMC-CMC) considered in the theoretical study, is modeled by mild to moderate noncovalent (intra- and intermolecular) interactions to assess the intermolecular interaction(s) between the adsorbent and adsorbate and is stabilized by these interactions. Based on binding energies (BEs), the FMO-based HOMO-LUMO gap, natural population analyses, the Bader's QTAIM-based parameters, and a recent measure reported recently as 'Hydrogen Bond Strength Based on Interaction Coordinate (HBSBIC)' with the deployment of computational B3LYP and M06-2X using 6-31+G basis set, the structural, stability, electronic, and charge transfer features were described.

1. Introduction

Carboxymethylcellulose (CMC) is a water-soluble natural polymer with carboxymethyl groups covalently linked to glucopyranose hydroxyl groups on the cellulose chains. It is a found naturally anionic monosaccharides with characteristics such as non-harmful, high biocompatibility, and biodegradability [1]. It's been used as a viscosity control, thickening agent, sizing agent, coating agent, emulsion stabilizer, and electrode binder in a wide range of industries [2-4]. It is widely used as a depressant, dispersant, and flocculant in mineral processing, especially in the flotation of sulphide ores [5]. The polymeric structure of the CMC contains multiple repeating units, each with three -OH groups which are often accountable for H-bonding [9]. Since so much effort has done into studying CMC adsorption on clay minerals, our understanding and knowledge of the binding interaction of CMC on metallic surfaces are growing steadily. As a result, the related problems received serious attention. According to Raju, the adsorption of polymers (dextrin) to graphite was mainly due to hydrophobic-hydrophobic interactions [10]. CMC adsorption on graphite was investigated by Laskowski, who reported that pure high-quality graphite (Ceylon) adsorbs CMC well enough [11]. Graphite that has been laboratory experiments purified using leaching techniques, on the other hand, demonstrates no enough CMC adsorption. Pugh, Healy, and Rath claimed that CMC adsorption on mineral water surfaces is controlled by several interrelationships of electrostatic, hydrophobic, hydrogen bonding, and chemical interactions, even though there was no evidence of CMC adsorption on minerals that was selective [12-16]. Jenkins suggested another binding mechanism for CMC onto minerals, claiming that adsorption occurred on the basal planes due to the hydrophobic influence [17-19]. Rath and Jucker, on the other hand, implemented that the hydrogen bond was extremely important in the binding of polysaccharides to solids [20, 21]. Bakinov confirmed substantial changes in the carboxyl group after solid surface adsorption employing spectroscopic techniques and established that these spectral changes were caused by an interaction between the carboxyl group and metal ions present on the adsorbent (talc) surface [22]. Furthermore, when infrared spectra were obtained using a transmission with dried samples, the certain deduction from polymer binding mechanisms was typically overshadowed by the substantial change in the polymer environment during dehydration. Furthermore, no infrared spectra have been simply indicated in this work. Wang likewise utilized infrared spectroscopy on a dry

sample to support the hydrogen bonding phenomenon [23]. The adsorption of polymer on solid materials, as observed by Cuba primarily through *in vitro* studies film ATR FTIR spectroscopy (in liquid form), is accomplished through various separate interactions, specifically chemical complexation and hydrophobic interaction[24]. Fujimoto also investigated further into adsorption processes of CMC on amino-terminated surfaces, revealed that CMC adsorbs on these selected applications to electrostatic interaction [25].

The above results were all meant to show how CMC interacts with talc solid surfaces (hydrophobic and hydrophilic minerals), metal particles, and hydrophobic self-assembled monolayers [26-32]. With the exception of adsorption on inorganic materials, the binding mechanism of CMC with cellulose-based surfaces were studied in depth to optimize paper strength, inhibit vessel picking in papermaking, alter textile fibres, or irreversibly connect functional molecules [33-40]. Many of these CMC surface modification methods were based on the assumption that there was a particular interaction between CMC and cellulose that arises from structural similarities between the polyelectrolyte and biopolymer surfaces. Other interaction studies of CMC on cellulosic fibers or spin-coated regenerated cellulose model films from trimethylsilyl cellulose using a quartz crystal microbalance (QCM-D) and surface plasmon resonance (SPR) model Pure cellulose (CE), cellulose acetate (CA), partially deacetylated cellulose acetate (DCA), polyethene terephthalate (PET), and cycloolefin polymer (COP) [41-47]. Chanzy, Kondo, and Ozaki [48-50] have also described the hydrogen bonding structure in cellulose in an experimental environment. On contrary to crystalline cellulose, Wu investigated the structure of carboxymethyl cellulose sodium salt (NaCMC) [51].

The literature shows notable adsorption phenomenon of CMC on different adsorbent but substantial mechanistic aspects of the interactions between CMC and solid surface is not well established. Therefore, the present work illustrates in-depth study of binding aspect of CMC onto mesoporous mustard carbon (MMC) using various characterization techniques.

2.2. Experimental

2.2.1. Materials and methods

The mustard cake (MC) was purchased from a local mill M/s Shyam Enterprises Lucknow, India). Analytical and laboratory-grade reagents were used for the synthesis purpose and experimental studies. Extra pure sodium carboxymethylcellulose (99.5%), sodium hydroxide (98%), hydrochloric acid (35.5%), potassium chloride (99.5%), sulfuric acid (98%), cetrimide (96%), urea (99 %) and dimethyl sulfoxide (99%), were purchased from Loba Chemie Pvt. Ltd. (Maharashtra, India).

The mustard cake (MC) sample was crushed and washed with distilled water and then sun-dried. This material was treated with H_2O_2 (20 wt%) at 60^oC for 24 h to oxidize the adhering organic matter and it was washed several times using double distilled water. This powder was burned in the presence of N_2 gas at 715^oC for 25 min. The material, mesoporous mustard carbon (MMC) was grounded and sieved to desired particle sizes.

2.2. Characterization of materials

2.2.1. Electrokinetics measurements

Using cetrimide solutions (0.002 M), the surface potential/point of zero charges (PZC) of MMC was calculated using the solid addition method. In a 100.0 mL stoppered conical flask, 40.0 mL of HCl and cetrimide solution were added. By adding either 0.1 N HCl or 0.1 N NaOH, the pH of the solution was precisely adjusted between 2.0 and 12.0. By adding the 0.1N KCl and cetrimide solution, the total volume of the solution in each flask was measured to exactly 50.0 ml. The solution's initial pH was then accurately measured. Each flask received 0.2 g of MMC. The suspension was shaken and allowed to remain for two days while being shaken intermittently. The pH of the supernatant liquid was measured at the end. The difference between the initial and final pH values was plotted against the initial value. The PZC was its point of intersection of the resulting curve where the pH value was zero.

2.2.2 Microstructural and phase characterizations

At a voltage of 10 kV, the microstructure of the MMC was examined using a field emission scanning electron microscope (W-SEM, JSM6010LA; JEOL 200). AFM (Agilent 5500) measurements in tapping mode with a V-shaped cantilever were used to

determine the topography and surface roughness of the samples (Si_3N_4). For laser beam reflection, the back of this cantilever was coated in gold. The NP-20 AFM probe was used in both air and water. X-ray diffraction (Rigaku Miniflex II desktop) was used to determine the crystallographic parameters of the MMC at copper K radiation (λ=1.5405). The 2-scan was performed at a scan rate of 2°/min between 20° and 80°. The copper goal had a voltage and current of 40 kV and 40 mA, respectively. The phase identification and indexing of peaks were done using a JCPDS card.

2.2.3 Characteristics of functional groups

The characterization of functional groups present in MMC was carried out using the attenuated total reflection Fourier transformation infrared (ATR-FTIR) (Bruker Tensor, 27). The XPS experiments were carried out in an ultrahigh vacuum (UHV) with a high-resolution X-ray photoelectron spectrophotometer (HR-XPS), a PHI 5000 Versa Prob II from FEI Inc. (1,486.6 eV; 100W; spot size, 10mm to 200 mm). Before the XPS study, all samples were vacuumed and dehydrated. The samples on the stub were then moved into the HR-analysis XPS's chamber, which had a background pressure of 1.5 10-9 Torr. The pressed samples' surfaces were scraped in place to reveal new powder surfaces. At 187.85 eV, both survey and narrow area scans were performed. All data were background-subtracted, smoothed with a five-point quadratic Savitzky–Golay algorithm, and charge corrected to achieve binding energy of 285.0 eV for the carbon-carbon bond. Casa XPS Version 2.3.17PRI.I and Origin Pro 8 SRO v8.0724 (B724) software were used to map and match the data.

2.2.4 BET surface area measurements

A high precision gas/vapour adsorption surface area analyzer **(**BELSORP-mini II**)** was used to measure the surface physical parameters of MMC (N_2 isotherm, specific surface area, average pore diameter, and total pore volume, among others). A specific amount of MMC (0.24 g) was taken for pretreatment in the presence of N_2 gas at 400°C under vacuum for approximately 5-6 hours before conducting BET analysis of MMC to exclude undesirable adsorbed entities. The BET analysis was carried out using a surface area analyzer after the MMC had been pretreated. BELMaster Version 2.3.1 software was used to collect all of the data.

.

2.2.5 Adsorption measurements

By dissolving sufficient amounts of CMC in distilled water, stirring vigorously for 30 minutes, a stock solution of CMC (1000 ppm) was developed. The solution was then refrigerated overnight to completely hydrate CMC until filtration **(**Millipore 0.45μm**)** was used to eliminate any undissolved impurities.

Standard solutions were made by diluting stock solutions further. Adsorption experiments in the batch mode were carried out. An accurately weighed quantity of MMC (0.2g) was mixed with a known volume (25ml) of CMC solutions of known concentration in a series of stoppered bottles and shaken until equilibrium adsorption was achieved. The adsorbent was filtered off using Millipore 0.45μm filter paper after a specified period (3-4 hours). The residual concentration of CMC was determined by clear solutions employing UV spectroscopy (UV-Visible spectrophotometer, Cary 100) at λ_{max} = 265nm. The adsorption density of CMC onto MMC was calculated using the following equation [52]:

$$q_e = \frac{(Co-Ce)V}{m} \quad (1)$$

Where C_o and C_e are initial and equilibrium concentrations (mg l^{-1}) of CMC in the solution, V the volume (l), m the weight MMC and q_e is the amount of CMC adsorbed by the MMC (mg g^{-1}).

Adsorption equilibrium data were obtained at different initial concentrations of CMC ranging from 100-700 ppm utilizing the stock solution, 45 mg of MMC, and 180 min contact time with 50mL CMC solution at room temperature for the Adsorption isotherm models analysis.

2.2.7 Kinetic study

The kinetic mechanism is critical in the adsorption process because it determines how CMC binds to MMC and regulates the entire adsorption process in terms of time. As a result, the kinetics experiments were carried out at room temperature with 100 ppm of CMC and 45 mg of MMC. The period of interaction between CMC and MMC was varied from 10 - 180 minutes to determine the kinetics data.

3. Results and discussion

3.1 Charge measurement of MMC

Figure 1 shows the results of the electrokinetic analysis, which illustrates that the MMC's surface was negatively charged. Since the PZC of the adsorbent is 9.8, the surface was positively charged at any pH below pH_{ZPC} and negatively charged at any pH above pH_{ZPC}. When the pH of the solution was lower than pHZPC, the repeat units of polysaccharides are more easily attracted to the positively charged surface of MMC, supporting CMC adsorption on MMC and thus increasing adsorption. When the pH was higher than pH_{ZPC}, the negatively charged surface repulsed the repeating units of CMC, resulting in decreased adsorption.

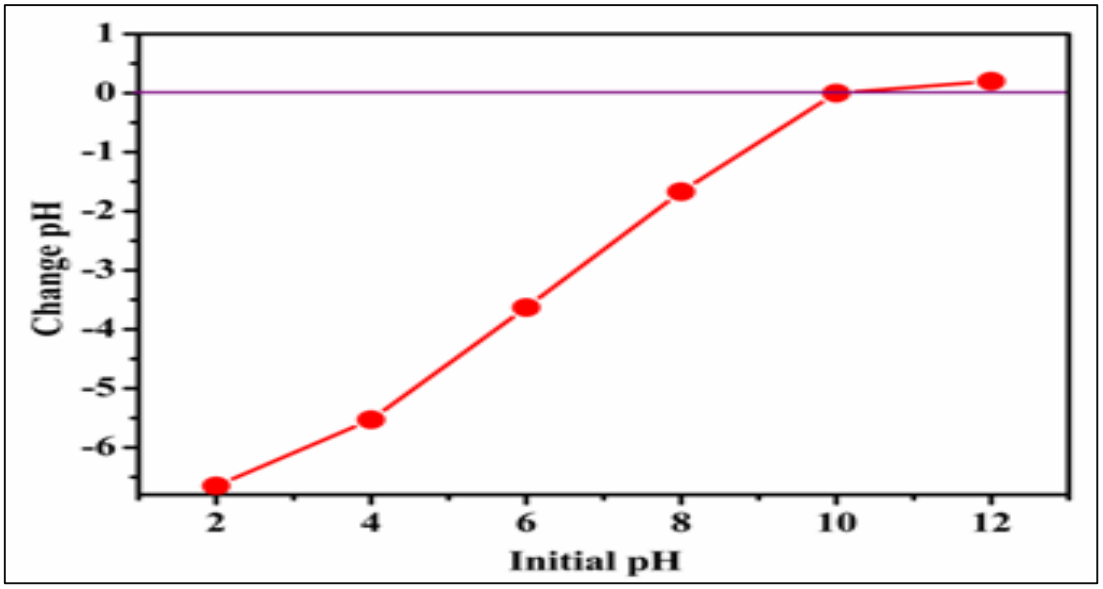

Figure 1**.** Point of zero charges (PZC) of MMC by solid addition method

3.2 Microstructural and phase analysis

The average roughness parameter (Ra) of MMC (3.81nm) provides more active sites for CMC adsorption, as shown in the topographical image (Figure 2a). Figures (2b) and (2c) display SEM images of MMC and MMC adsorbed CMC, which clearly show the porosity and texture of a spongy aspect, fibrous surface with irregular and heterogeneous structure, and many pits and fissures through the surface, likely due to the strong oxidising agent H_2O_2, which caused some changes in the surface of the adsorbent. On the other hand, AFM was used to investigate the distribution of CMC at different pH levels, and it was observed that CMC was more widely distributed in an acidic medium than in a basic medium. At the same concentration (200 ppm), CMC

was more adsorbed on the adsorbent surface acidic region than basic medium (Figure 3a, b). Several researchers [53-56] published similar findings for CMC in its aqueous environment. Keeping these two pHs and the ZPC value of MMC (pH_{ZPC} = 9.8), the adsorption was carried out at both pHs and obtained result suggested that electrostatic interactions do affect the adsorption of CMC on MMC surface. Further, the average thickness of the adsorbed cluster is around 1 nm, it shows that a flat confirmation of this CMC on the MMC surface.

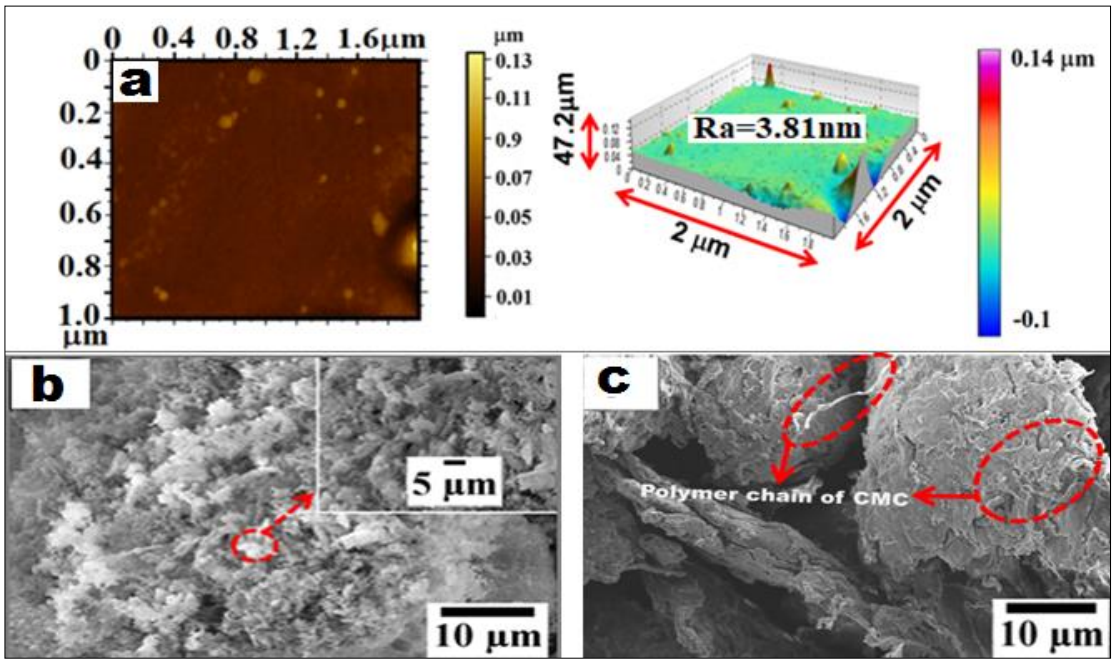

Figure 2. (a) AFM images and SEM images of MMC (b) before adsorption (inset at high magnification) and (c) after adsorption of CMC.

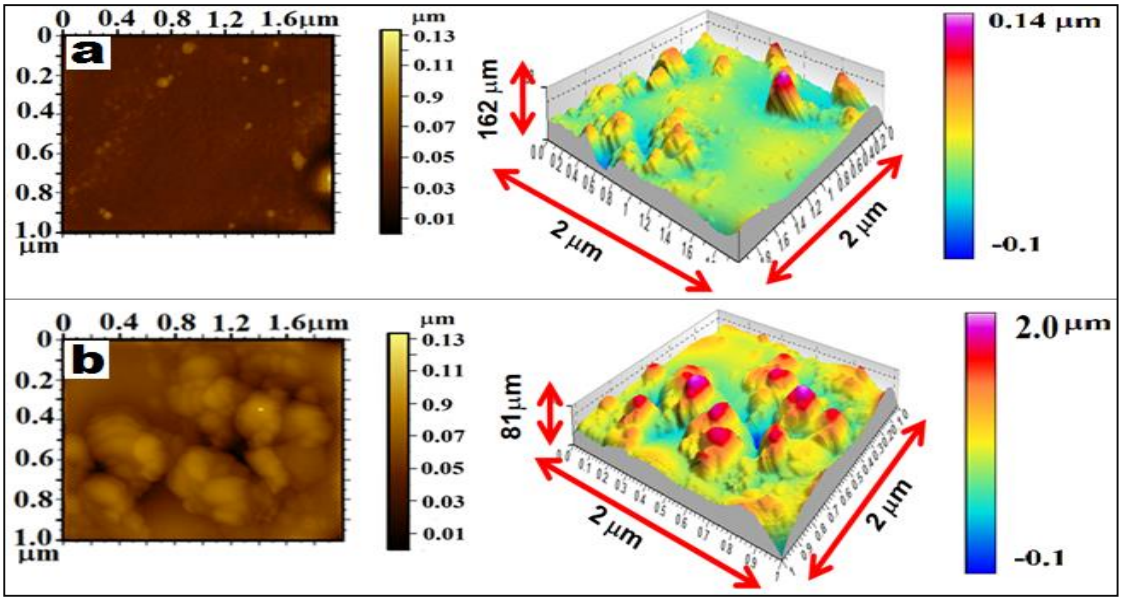

Figure 3. AFM images of CMC adsorbed on MMC at (a) pH 9.8, (b) pH 3.0.

The XRD spectrum shown in Figure 4 illustrates that the treated carbon from de-oiled mustered cake under optimum preparation condition is crystalline in structure**.** There are seven broad peaks centred on 2θ value of 25º, 30º, 37º, 47º, 52º, 54º and 63º.

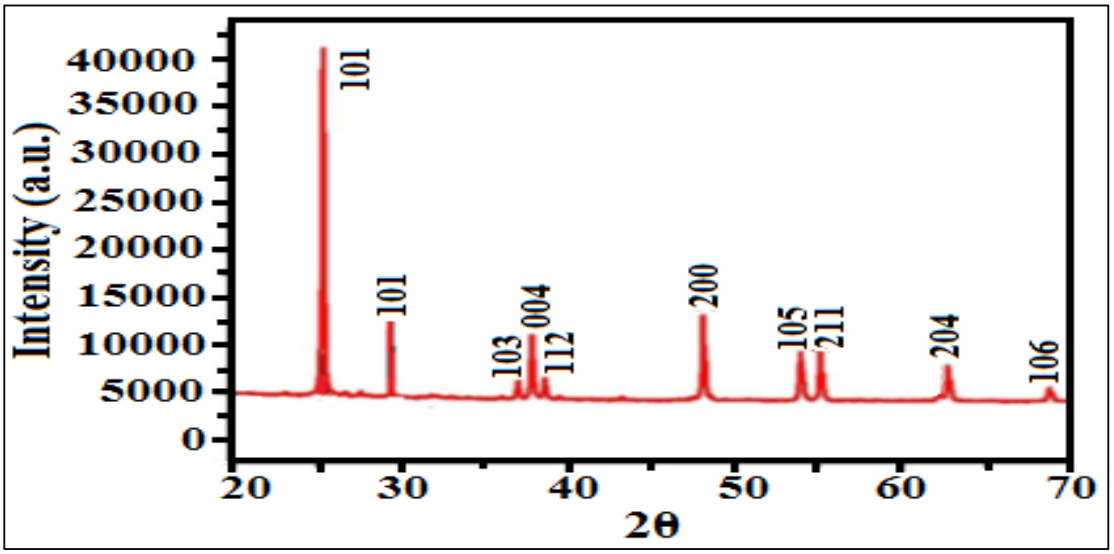

Figure 4. XRD spectrum of MMC

3.3 Functional groups analysis

The ATR-FTIR spectrum of synthesized MMC and CMC adsorbed on MMC are shown in Figure 5. The –OH stretching band at 3454 cm^{-1} was due to chemisorbed water and a surface hydroxyl group. The band near 876 cm^{-1} is due to -C-OH bond stretching which reveals that the condensation of C-OH groups was not complete on thermal treatment. The typical bands at 1040 cm^{-1} and 876 cm^{-1} for -C-O-C network vibrations were observed. The ATR-FTIR spectrum of CMC illustrates a band at 2920.8 cm^{-1} which is attributed to C–H stretching of the $–CH_2$ groups. The band at 1610.32 cm^{-1} is attributed to ring stretching of glucose. Additionally, there are bands in 1350–1450 cm^{-1} due to symmetrical deformations of $-CH_2$ and -COH groups. The appearance of peaks at 1060 and 1010 cm^{-1} is due to primary alcoholic $–CH_2OH$ and CH_2 twisting vibrations, respectively. The ring stretching and deformation of α-D-(1–4) and α-D-(1–6) linkages appears at around 714-610.70 cm^{-1}. The ATR-FTIR spectrum of CMC adsorbed onto MMC/ water interface clearly shows the characteristics band at 1632.23 cm^{-1} due to COO^- of the carboxyl groups of CMC appeared to be less sharp and shifted to 1650 cm^{-1} after adsorption. The difference in ATR-FTIR spectrum is attributed to the hydrogen bond formation between carboxylate (COO^-) ions of the CMC and surface

hydroxyls of MMC. Since, adsorption experiments were conducted at pH 3.0, under such condition the CMC gets ionized (pKa =3.3) and provides -COO^- ions. The appearance of the XPS peak at 286.7 eV (Figure 5) attributes the presence of hydroxyls as evidenced by high-resolution XPS of MMC. Therefore, the possibility of hydrogen bonding between carboxylate ions and –OH surface hydroxyls cannot be ruled out. This observation was further confirmed by the fact that in the presence of urea amount of adsorption reduced significantly.

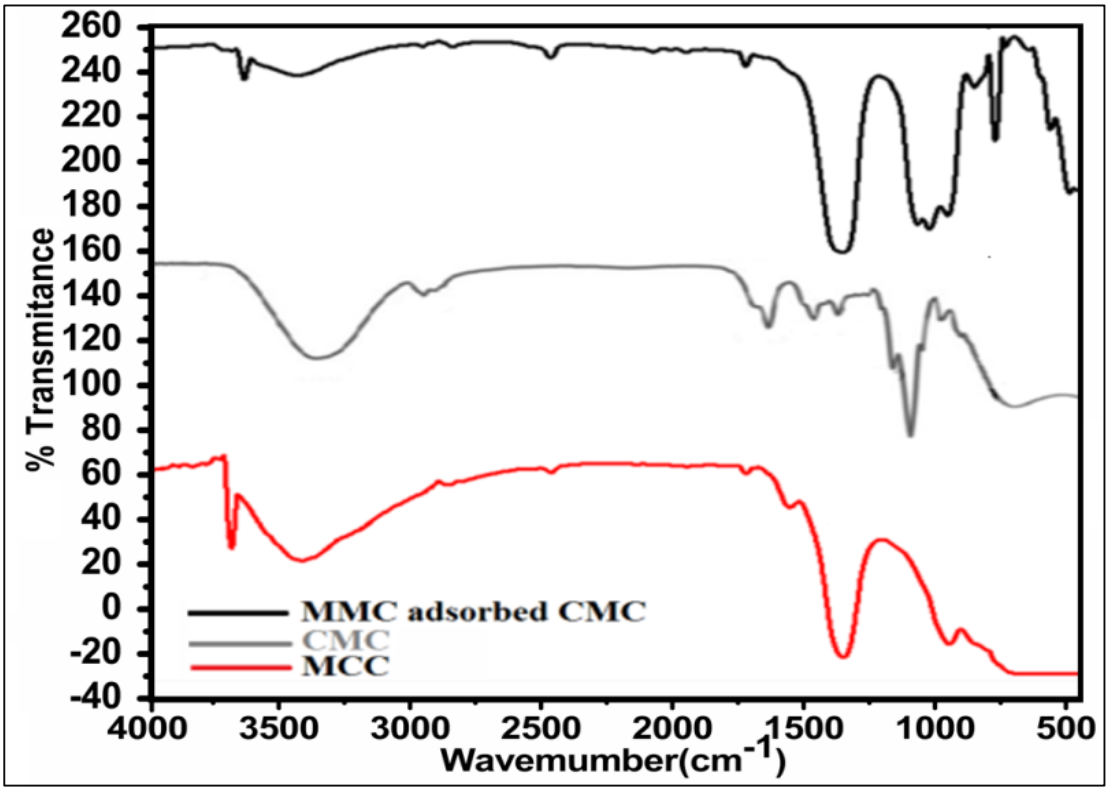

Figure 5. ATR-FTIR spectra of MMC, CMC and adsorbed CMC.

To determine the chemical composition of the MMC, and MMC adsorbed CMC XPS analysis was performed. The surveys scan of MMC in (Figure 6a) demonstrates that its oxygen content is around 17.4 %, suggesting abundant surface oxygenic functional groups. In the C 1s XPS spectra of MMC (Fig.6a), the peaks at 284.8, 286.7, and 288.9 eV are ascribed to the sp2 hybridized (C–C), alcoholic (C–OH) and carbonyl (C=O) carbon atoms, respectively. The XPS survey scan of CMC was also performed as shown in Figure 6b, as well as high-resolution C 1s XPS spectra of CMC, was taken. The CIs XPS spectrum of CMC is deconvoluted into 3 peaks C-C, CC-H (283.60), O-C (284.34 and O-C=O (287.01). The approach involves the subtraction of a shirley background followed by a charge correction referenced to C1s of adventitious carbon at 285.0 eV. After the adsorption of CMC onto the surface of MMC both XPS survey scan (Figure

6c.) and high-resolution C is XPS spectra were taken in which binding energy is different because the chemical shifts are related to electron density changes. This is due to available hydroxyl groups on MCC much interacts with carboxylate ion of CMC increasing in carbon-oxygen functional groups (C-O and C = O) of MMC.

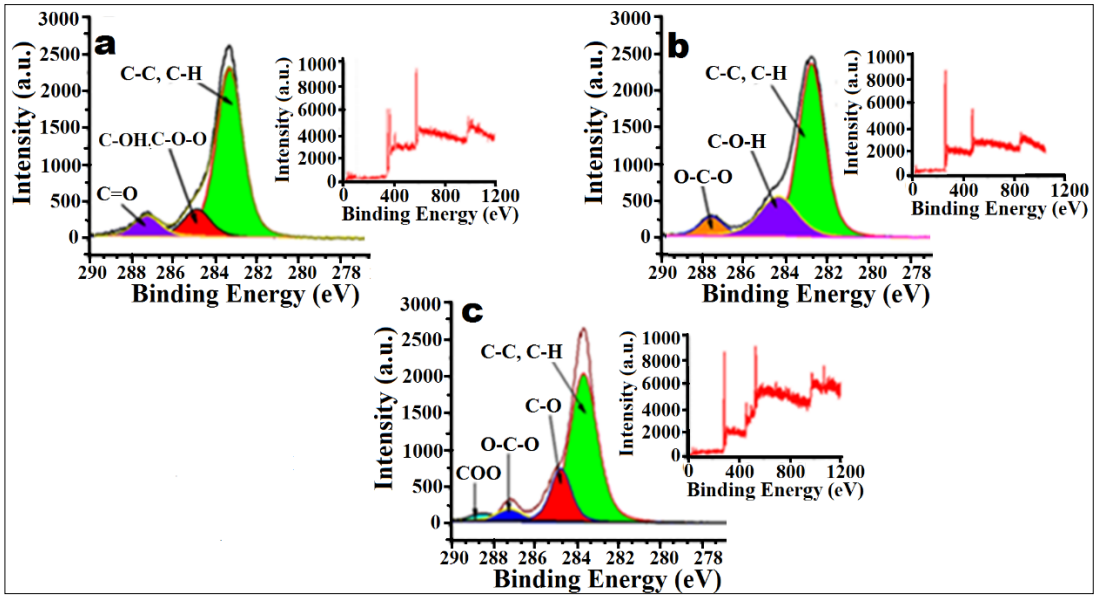

Figure 6. XPS spectra of (a) High-resolution C1s XPS spectra of MMC (inset XPS survey AlKα PES), (b) High-resolution C1s XPS spectra of CMC (inset XPS survey AlKα PES), (c) High-resolution C1s XPS spectra of MCC after adsorption of CMC (inset XPS survey AlKα PES).

3.4 Specific surface area and pore size distribution analysis

In N_2 adsorption-desorption process (Figure 7a) of MMC, the Brunauer–Emmett–Teller (BET) surface area (Figure 7b) was measured employing the standard BET equation [57]. The pore size distribution (Figure 7c) was calculated employing Barrett-Joyner – Halenda (BJH) [58]. The BET analysis reveals that MMC had a surface area (S_{BET}) = 16.576 $m^2\ g^{-1}$, (Figure 7b) which was primarily distributed by mesopores. The average pore diameter and total pore volume of MMC were found to be 12.432 nm and 0.051cm^3g^{-1} respectively. These obtained results confirm that the MMC is a mesoporous material having good adsorption capacity due to capillary condensation of CMC.

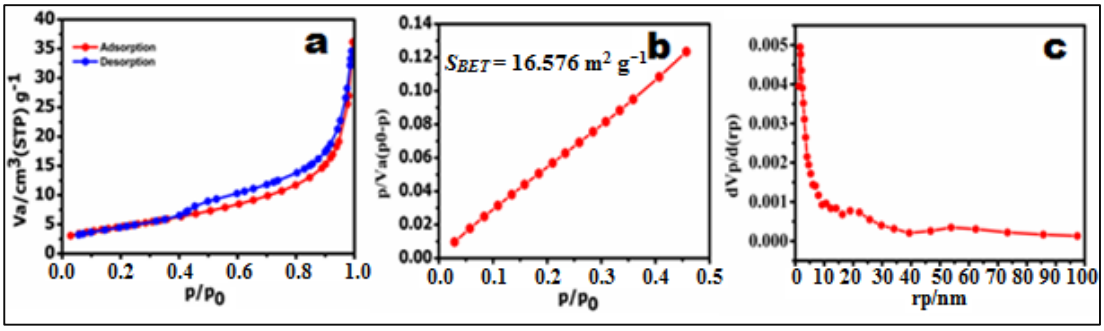

Figure 7. (a) N_2 adsorption-desorption isotherm (b) S_{BET} plot and (b) BJH plot of MMC by N_2 adsorption data.

3.5 Adsorption studies

3.5.1 Effect of concentration and pH

The effect of increasing concentrations of CMC solutions on adsorption onto MPP has been investigated by varying it in the range of 100 to 700 ppm. The results illustrate that the amount of adsorption increases with increasing the concentration of CMC (Figure 8a) and finally becomes constant. This is because with increasing concentration of CMC, the availability of CMC molecules at the interface increases, which in turn enhances the adsorption: Finally, when all the available sites on MMP surface are occupied, it becomes difficult for CMC to infract with the MMP surface, resulting in saturated adsorption.

Adsorption isotherm of CMC onto MMC at different pHs was recorded (Figure 8b). It was found that the adsorption of CMC onto MMP surface at pH 3.0 was more in comparison at pH 9.8. Since it was observed that the adsorption density of CMC was reduced significantly with an increase in pH value from acidic to basic medium. Thus, it can be concluded that electrostatic repulsion plays an important role in this system.

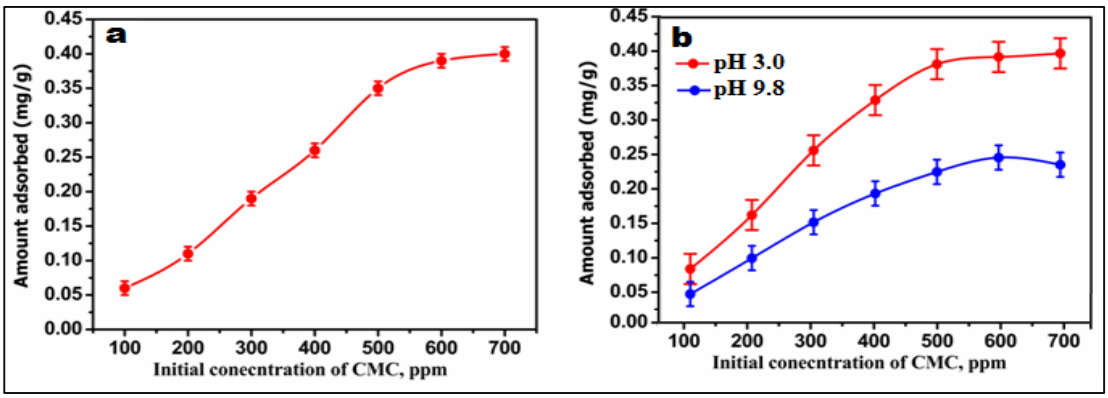

Figure 8. (a) Plots illustrating the effect of concentration and (b) Adsorption isotherms at different pH values of CMC adsorption onto MMC surface.

3.5.2 Effect of ionic strength, temperature and time

Adsorption of CMC on MMC was studied by using solutions of different ionic strengths (Figure 9a). The amount of adsorption increases with the increase of ionic strength; this is because of the screening effect of KCl. Therefore, at pH 9.8, the CMC and MMC are negatively charged, the addition of salt will reduce the electrostatic repulsion between them and thus increasing CMC adsorption density.

The effect of temperature on adsorption of CMC has been studied in the temperature range of 30, 50, 70 and 90°C and the result shown in Figure 9b clearly illustrate the exothermic nature of adsorption. The amount of adsorption decreases with the rising of temperature which may be due to the enhanced escaping tendency of the CMC (adsorbate) from the surface of the MMC. With increasing temperature, the binding forces between the CMC and the surface are weakened and thus adsorption decreases.

The findings clearly show that the saturation of the surface increases over time. Of course, more CMC molecules were interacting with the binding site on the MMC surface as time increases, resulting in increased amount of adsorption.

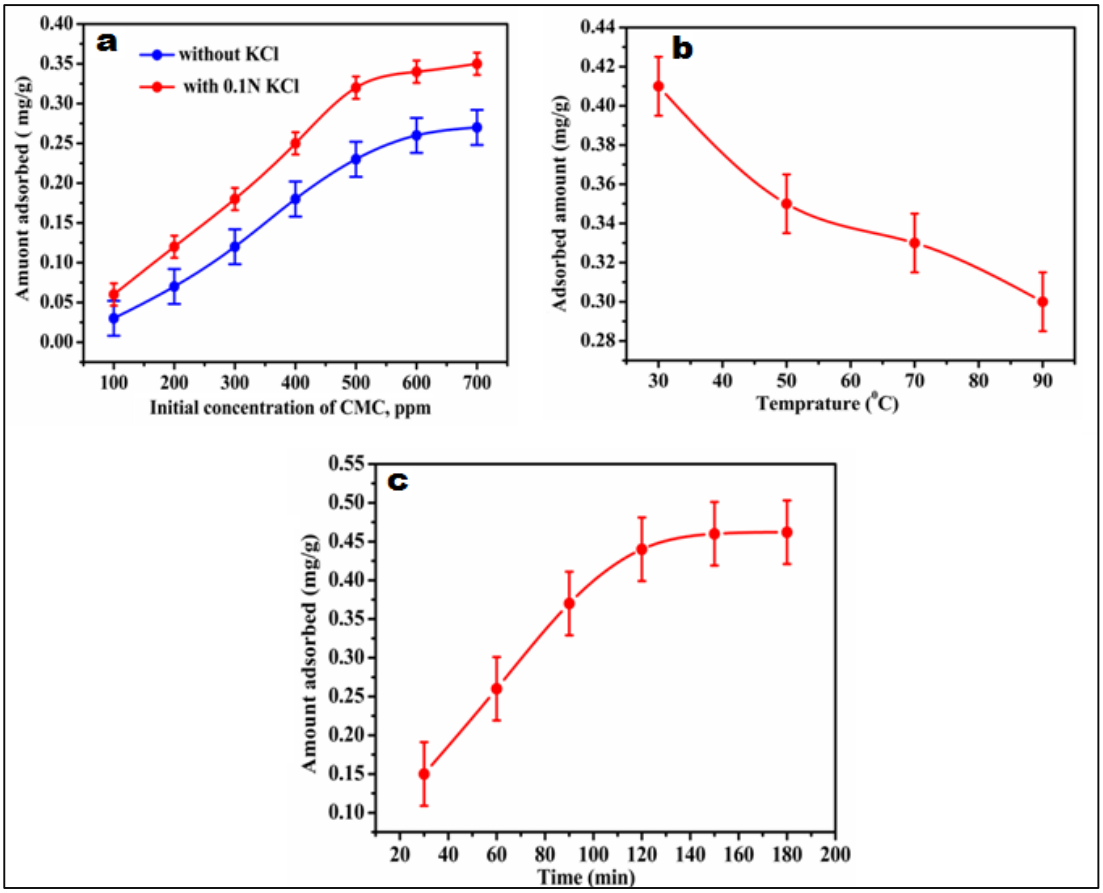

Figure 9. (a) Plots illustrating the effect of ionic strength, (b) temperature and (c) time on adsorption of CMC onto MMC.

3.5.3 Adsorption of CMC onto MMC (with and without urea)

To provide experimental proof to show that hydrogen bonding plays a vital role in the adsorption process in the present case, experiments were conducted by adding urea in the adsorbate solution. In the presence of urea, since urea is a hydrogen bond breaker, the amount of adsorption decrease significantly (Figure10). These results consist with this statement clearly illustrate that in the presence of urea, the amount of adsorption decreased significantly. Therefore, it is beyond doubt that hydrogen bonding plays an important role during adsorption.

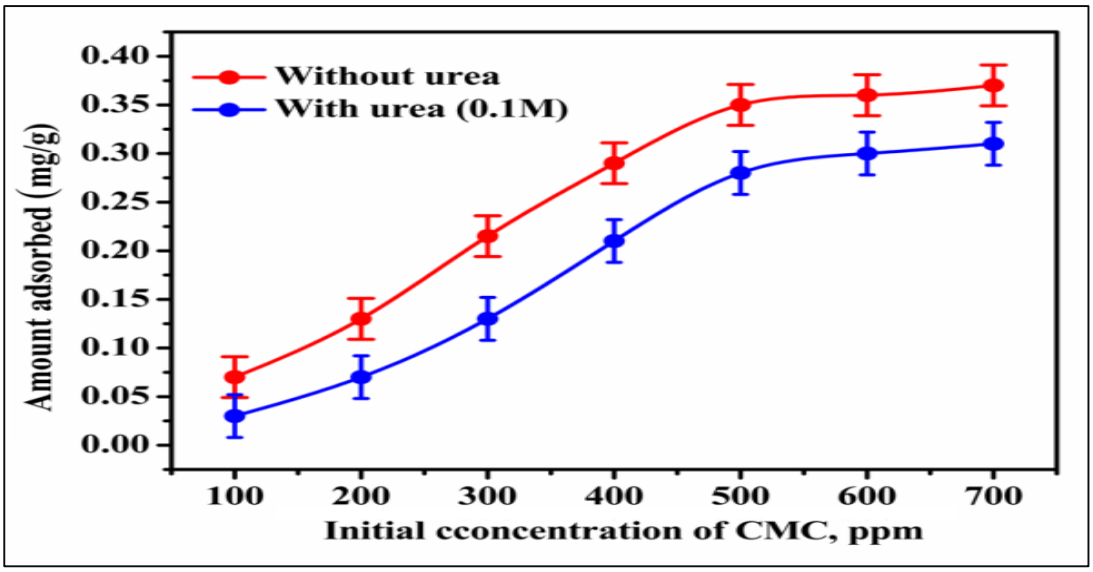

Figure 10. Plot showing the effect of urea on adsorption of CMC onto MMC

3.5.4 Langmuir adsorption isotherm

To obtain a better understanding of the binding mechanism of CMC on solids, the standard free energy of adsorption (G^0_{ads}), was calculated. The adsorption isotherm of CMC on MMC shows a pseudo-Langmuir adsorption isotherm. The Langmuir equilibrium isotherm is based on the fact that the adsorption occurs at a specific homogenous site within the surface of adsorbent and monolayer sorption onto a surface with a finite number of identical sites assuming that there are no interactions between adsorbed molecules on the surface. Hence, the covered surface by the polymer (CMC) is given by the linearized equation as [59],

$$\frac{C_e}{q_e} = \frac{1}{K_L C_e} + \frac{C_e}{q_m} \qquad (2)$$

Where q_e(mg/g) is the amount of solute adsorbed per unit weight of adsorbent, C_e(ppm) is the equilibrium concentration of solute, q_m is the monolayer adsorption capacity (mg/g) and is a constant, and K_L is a constant related to the free energy of sorption (K_L α $e^{-\Delta G/RT}$). It is the reciprocal of the concentration at which the adsorbent is half-saturated. Values of the constants were evaluated using a plot of C_e/q_e vs. C_e (Figure 11).

Calculation of ΔG^0_{ads} of adsorption using Langmuir equilibrium constant (K_L),

The standard free energy of adsorption, ΔG^0_{ads} , related to the Langmuir equilibrium constant, $K_{L,}$ can be calculated using the flowing expression.

$$\Delta G^0_{ad} = -RTlnK_L \quad (3)$$

Where R is the general gas constant (8.314J/(mol K) and T is the absolute temperature. Several authors employed K_L for the calculation of ΔG without its qualification (expressed instead of dimensionless in some concentration units (for example l mol^{-1}, l g^{-1}, ml mg^{-1}, etc.) [60-63]. Therefore, before calculation of ΔG^0_{ads} we first expressed the value of K_L dimensionless. From Eq. (ii) ΔG^0_{ads} was found as -22.561kJ/mol which demonstrates that adsorption of CMC on MPP is highly favoured ($\Delta G^0_{ads} < 0$). Since the free energy of hydrogen bond formation is about $-25kJmol^{-1}$, which is very close to the ΔG^0_{ads} of the CMC in the present case. These results further confirm the major role of hydrogen bonding rather than hydrophobic force in binding at the polymeric interface.

3.5.5 Freundlich adsorption isotherm

Freundlich adsorption isotherm was modeled to understand heterogeneous surface energy through monolayer adsorption of CMC onto MMC in an aqueous system employing Freundlich adsorption equation given below:

$$\ln q_e = \ln K_f + n \ln Ce \quad (4)$$

Where, K_f = Adsorption capacity of the adsorbent

By plotting the graph between $\ln q_e$ vs $\ln Ce$ slope gave the value of n and intercept K_f. The Value of Freundlich parameters (K_f=0.0158), adsorption coefficient (n=0.0019) and correlation constant (R^2=0.9972) was evaluated by Freundlich isotherm (Figure 11

b). The obtained equilibrium data gave close agreement to Langmuir (R^2 = 0.9972) model than the Freundlich model (R^2 = 0.9878) suggesting the surface homogeneity of the MMC and monolayer adsorption of CMC.

3.5.6 Temkin isotherm

Temkin isotherm model assumes that the adsorption heat of all adsorbate molecules decreases linearly with the increase in coverage of the solid surface, and adsorption is characterized by a uniform distribution of binding energies, up to a maximum binding. The linearized form of the Temkin isotherm equation given as:

$$q_e = B_1 ln K_T + B_1 C_e \quad (5)$$

Where, B_1 is the Temkin energy constant ($Jmol^{-1}$). K_T is Temkin isotherm constant (Lmg^{-1}). After plotting a graph between q_e *vs* C_e the isotherm constants b, (B_1 = 0.1305) and (K_T = 50.394) were obtained from slope and intercept, respectively (Figure 11C).

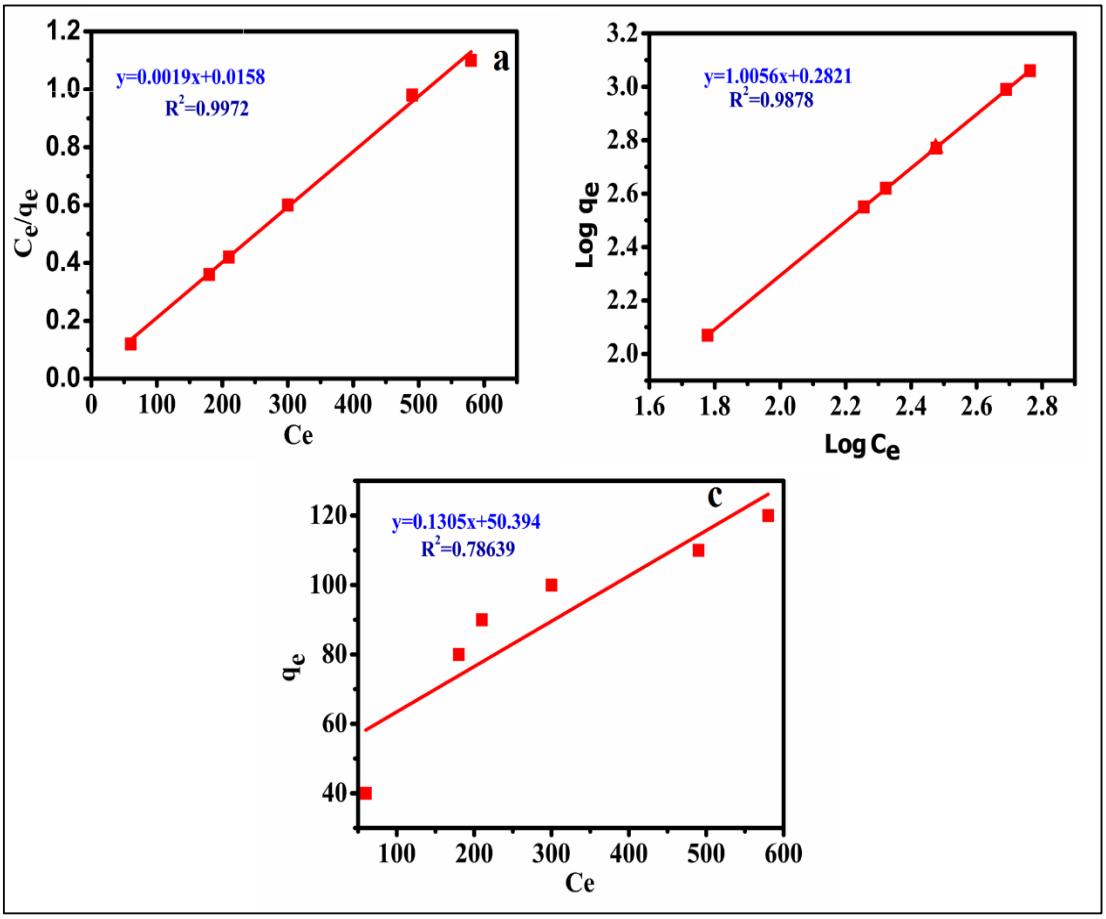

Figure 11. (a) Langmuir (b) Freundlich and (c) Temkin adsorption isotherm of CMC onto MPP at 30^0C

4. Kinetic studies

The understanding of the dynamics of the CMC adsorption onto MMC was evaluated by kinetic models. Some of the important widely used kinetic models such as first order, second order, pseudo-first-order, and pseudo-second-order were applied to the adsorption kinetic data to observe the behaviour of CMC adsorption onto MMC. It was found that initially, the amount of adsorption of CMC occurs fast and at equilibrium time, becomes slow because in initial time large numbers of unoccupied surface sites of MMC were available for CMC adsorption.

4.1 First-order kinetics equation

For the evaluation of the first-order kinetic the linear form of the first-order kinetics equation were applied as given below:

$$ln\frac{C_o}{C_t} = k_1 t \quad (6)$$

Where C_o (ppm) and C_t (ppm) are concentration at the time zero (initial) and a given time't' concentration of CMC in solution respectively. k_1 (min^{-1}) is the first-order rate constant. The k_1=0.00084 min^{-1} and regression (R^2= 0.9985) were determined by plotting the graph between ln (C_o/C_t) vs t. For CMC, the obtained value of R^2 =0.9985 was more than 0.9, which shows a close agreement with a good fit of the kinetic experimental data **(**Figure 12a).

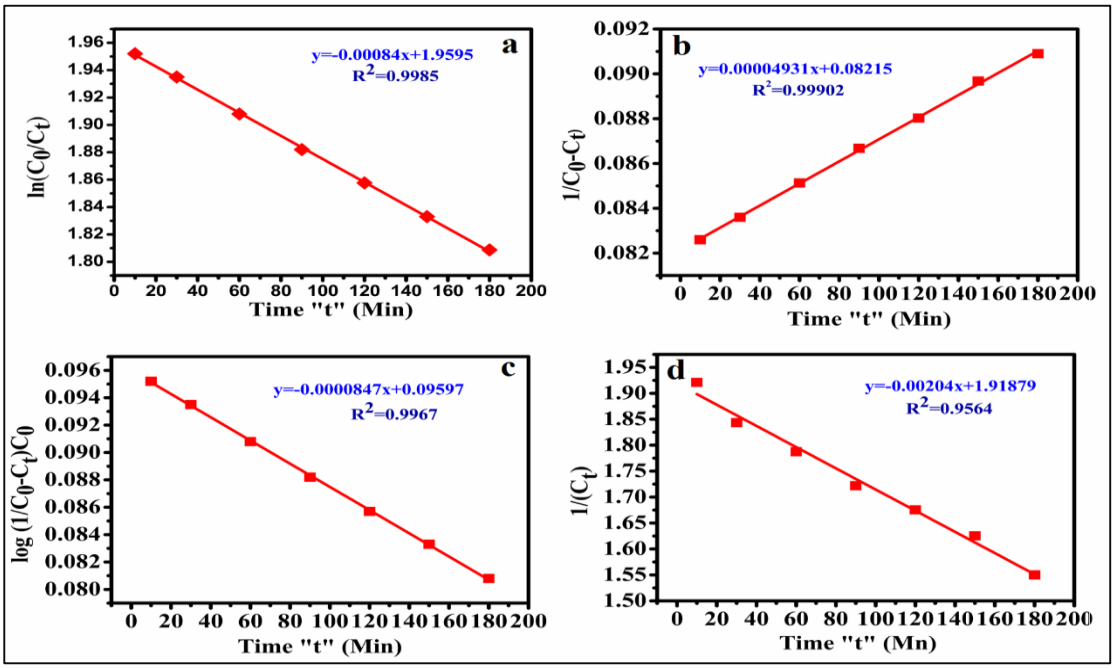

Figure 12. Kinetic study for the adsorption of CMC onto MMC (a) first order (b) second order (c) pseudo-first order (d) pseudo-second-order

4.2 Second order rate equation

The second-order kinetic mechanism was performed employing the linear form second-order of kinetics equation as given in the equation below:

$$\frac{1}{(C_o - C_t)} = k_2 t \quad (7)$$

Where C_o (ppm) and C_t (ppm) are concentration at the time zero (initial) and a given time‘t’ concentration of CMC in solution respectively. Where k_2 is the second-order rate constant for the sorption process of CMC. By linear plot of $(1/Q_t - 1/Q_o)$ against t, the $k_2 = 4.9X10^{-5}$ min^{-1} and regression R^2 =0.99902 were calculated (Figure 12b).

4.3 Pseudo-first-order kinetic equation

To define the effect on increasing or decreasing concentration of CMC on the rate of first-order kinetic the assumption of pseudo-first-order kinetic was also performed. Therefore, there is no doubt that first-order reaction occurs by nature while the order of reaction was made by altering certain conditions. The pseudo-first-order kinetic was evaluated employing, the following linear form of pseudo-first-order equation:

$$log \frac{(C_o - C_t)}{C_o} = log\ C_o - \frac{k_1 t}{2.303} \quad (8)$$

Where, C_0, C_t, and k_1 are adsorption ability at equilibrium, adsorbate at time t and rate constant respectively. A plot of $log\ ((Co - Ct))/Co\ vs$ t parameter from sloe and intercept rate constant (k_1=1.1135X10^{-5} min^{-1}) and regression constant (R^2=0.9967) (Figure 12c).

4.5 Pseudo second order kinetics equation

The pseudo-second-order kinetic rate was studied employing the following equation:-

$$\frac{t}{C_t} = \frac{t}{k_2 Q_e{}^2} + \frac{t}{Q_e} \quad (9)$$

Where k_2, C_t and Q_e represent rate constant, the concentration at a given time‘t’ and amount adsorbed at equilibrium, respectively. By plotting the graph between $t/Qt\ Vs\ \ t$, the value of K_2=4.16X 10^{-5} min^{-1} Q_e=490.00 g mg^{-1} min^{-1} and R^2=0.9564 were calculated (Figure 12 d). The obtained kinetic adsorption data confirmed that the CMC adsorption onto MMC water interfaces was in close agreement with an overall

rate of CMC adsorption by MMC appeared to be highly controlled by the physicochemical process [63].

Figure 13 inferences that MMC derived from the mustard cake have BET surface area 16.576 m^2 g^{-1} and mesoporous nature. The adsorption of CMC on MMC revealed H-bonding interaction which was confirmed by the adsorption free energy of CMC (-22.561kJ/mol). FTIR, XPS and urea testing further established the H-bonding as a dominant factor for the interaction between CMC and MMC. The variation in adsorption behaviour of CMC was explored with different concentration, pHs temperature and time, which provided ideal conditions of CMC adsorption (600ppm CMC concentration, 3.0 pH, 30º C temperature increased).

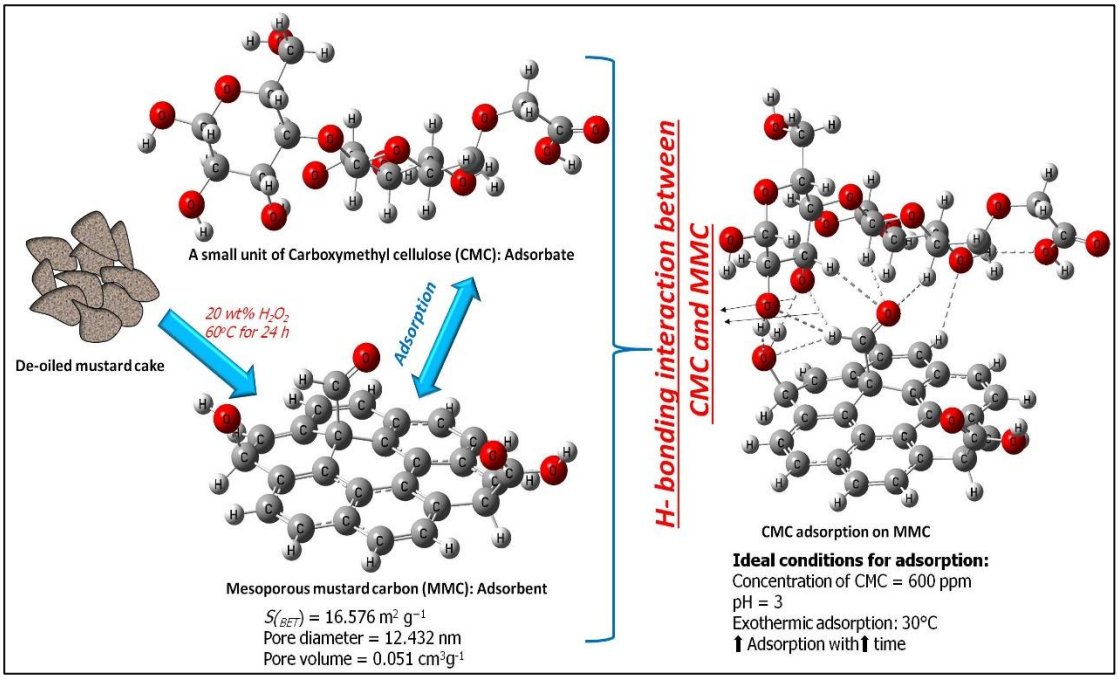

Figure 13. Schematic representation an overall summary of the adsorption mechanism of CMC on MMC

5. Computational details

Computational experiments rooted in the density functional theory (DFT) play an important role in understanding the detailed atomistic features governing the performance of interface study of two interacting species. To fill this void, here we present a quantum chemical study about the intermolecular interaction(s) between adsorbent (functionalized coronene acquired from MMC) and adsorbate [dimer unit (α-D glucose) of the carboxymethyl cellulose (CMC)] nanostructure by choosing a model system. We pay particular attention to the geometries, molecular orbital analyses, charge transfer phenomenon, and the adsorption *via* the interaction phenomenon such

as BE, interaction energy obtained from the QTAIM tool. The role of the charge transfer from the adsorbate to the adsorbent surface is also tested. Moreover, we study the effect of interaction on the electronic properties of the adsorbate-adsorbent complex.

In the present work, the DFT calculations were performed using Gaussian 16 program [64] with a hybrid functional B3LYP representing Becke's three-parameter hybrid exchange functional [65] (B3LYP) and Lee-Yang-Parr correlation functional [66,67] and 6-31+G (d, p) as the basis set. In the optimized geometry of the AAC, no imaginary frequency was obtained. To probe the noncovalent interactions (NCIs) involved in the MMC-CMC, Bader's QTAIM tool was performed [68].

The quantum chemical calculations suggest that the considered dimer unit (α-D glucose) of the carboxymethyl cellulose (CMC) (adsorbate) aggregates at the functionalized coronene (adsorbent) taken from the mesoporous mustered carbon (MMC) surface can be stabilized by the H-bonding and the other weak NCIs. The CMC aggregation model proposed in this study constructs a three-dimensional MMC/CMC interfacial structure and facilitates a better understanding of the CMC coverage and CMC adsorption energy (i.e. BE) with the MMC surface, theoretically. Particularly, a dimer complex forms by HBs and other weak conventional and nonconventional NCIs between two species (adsorbent as MMC and adsorbate as CMC) where CMC chemisorbs on the MMC surface.

To the best of our knowledge, the reliability of the theoretical approach in producing the structural, stability, and electronic feature analyses of the MMC-CMC complex has not been evaluated yet and a detailed discussion of this is carried out here. To model the interaction(s) between the adsorbent and adsorbate (see Figure 14), we consider that the adsorbate as the monomer unit (α-D glucose) of the carboxymethyl cellulose (CMC) sitting on the adsorbent as functionalized coronene consisting of several weak to strong intra- and intermolecular interactions.

5.1 Geometrical feature analyses and energetics

The optimized structures of the adsorbate (CMC) (see the top in Figure 13), adsorbent (MMC) (see the bottom in Figure 13), and the complex (see Figure 14) with proper atomic labelling. Some useful geometrical parameters related to the three-atom H-

bonded fragment of the adsorbate, adsorbent, and AAC model employed throughout this work, can be seen from Table 1.

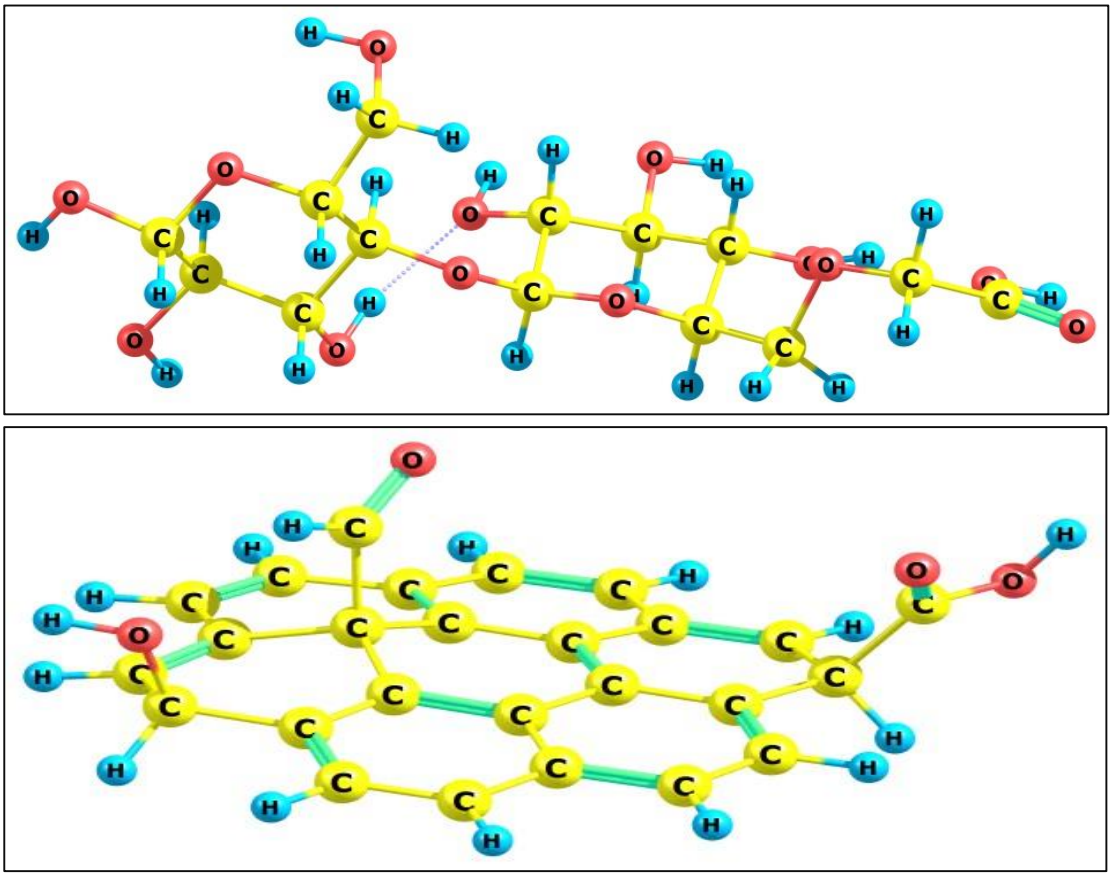

Figure 14. Optimized geometrical structures of the (a) Sucrose (Adsorbate, top) and (b) Coronene (Adsorbent, bottom) models considered in this work at M06-2X/6-31+G (d, p) level of theory.

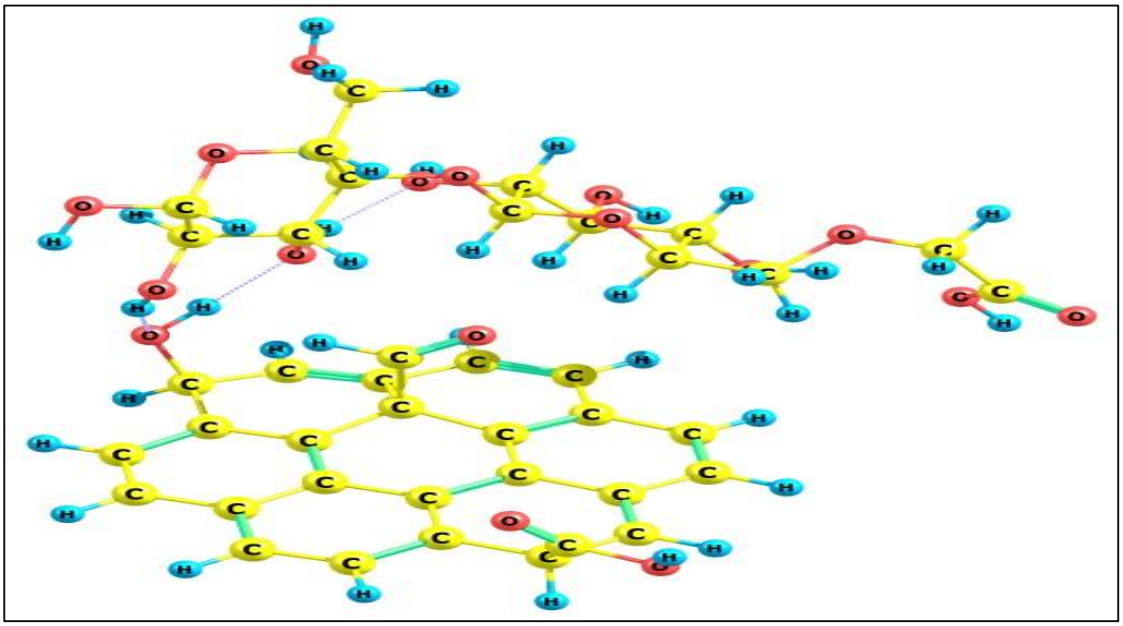

Figure 15. Optimized (Equilibrium) geometrical structures of the adsorbent-adsorbate Complex Model Considered in This Work at M06-2X/6-31+G (d, p) Level of Theory

Table 1 Covalent bonds associated with the intra- and intermolecular H-bonds and some selected covalent bonds of functionalized coronene at B3LYP and M06-2X level of theories with 6-31+G (d, p) Basis Set.

System	B3LYP/6-31+G (d, p)	M06-2X/6-31+G (d, p)
Sucrose	O27-H44 (0.969) Intramolecular H-bond Case: O24-H43 (0.975), O6-H38 (0.970)	O27-H44 (0.968) Intramolecular H-bond Case: O24-H43 (0.972), O6-H38 (0.969)
Coronene	O92-H93 (0.968) C-H (1.108) of CHO, C=O (1.204) of CHO	O92-H93 (0.965) C-H (1.110) of CHO, C=O (1.198) of CHO
Complex	Intermolecular H-bonds Case: O27-H44 (0.978), O92-H93 (0.980)	Intermolecular H-bonds Case: O27-H44 (0.972), O92-H93 (0.978)
	Intramolecular H-bonds in Sucrose: O24-H43 (0.977), O6-H38 (0.970)	Intramolecular H-bonds in Sucrose: O24-H43 (0.974), O6-H38 (0.969)
	Coronene: C-H (1.108) of CHO, C=O (1.206) of CHO	Coronene: C-H (1.108) of CHO, C=O (1.202) of CHO

In these model systems, one CHO group connected to a C atom of the central benzene ring, one COOH group linked to a C atom of the outer benzene ring, and an OH group attached to a C atom of the other outer benzene ring, are contained by the functionalized coronene system (MMC) (adsorbent). The original geometries of the adsorbent-adsorbate complex were constructed by adjusting the adsorbates in orientation, which could maximize the number of NCIs between the adsorbent and adsorbate units. Moreover, in this theoretical model approach, the interaction(s) between the adsorbent and adsorbate unit is (are) considered from one side of the adsorbent surface to get the favourable BE. Some selected and important geometrical parameters of the covalent bond associated with the inter and intramolecular HBs of the equilibrium structure of the model interface in the gas phase are shown in Table 1.

The HBs have been perceived as the strongest and the most directional of the intra-/intermolecular interactions and hence these are the key components in the construction of supramolecular structures. The HB donors and acceptors are capable to come together in diverse ways with the proton donors approaching to interact with the proton acceptors. The O92 of the OH group of CMC and O24 of the OH group of the MMC unit are playing their role as proton acceptors to O27 and O92 atoms *via* H44 and H93 bridging atoms, respectively, and form moderate intermolecular HBs. Similarly, O24 and O6 are acting as a proton donor to O11 and O37 *via* H43 and H38 connecting atoms,

correspondingly and forming the moderate intramolecular HBs. Weak conventional (C-H···O) and nonconventional (C-H···C and C-H···H) HBs joins the molecules and thus appears to be responsible for the formation of the stabilizing AAC structure. The results presented in Table 2 reveal that the energetic compounds considered in the present investigation form a favourable and stable complex. The complex is strongly stabilized by the presence of two strong intermolecular HBs formed between HB accepting and donating sites of adsorbates to the complementary sites of the adsorbents. Two strong intramolecular HBs have been probed in the CMC (adsorbate). Furthermore, it fairly appears that eleven weak NCIs are also responsible for the formation of the stable complex. Further, small contributions from stacking interactions for complexes containing ring systems will also help towards the stability of the system.

Table 2 The electronic parameters HOMO (in eV), LUMO (in eV), HOMO-LUMO gap (in eV), dipole moment (in Debye), and binding energy (BE) (kcal/mol) at B3LYP and M06-2X level of theories Using 6-31+G (d, p) Basis Set.

Adsorbent (MMC)	B3LYP/6-31+G (d, p)	M06-2X/6-31+G (d, p)
HOMO	-4.881	-5.758
LUMO	-1.894	-0.996
HLEG	2.917	4.762
Dipole Moment	3.753	3.406
Adsorbate (CMC)		
HOMO	-7.178	-8.846
LUMO	-1.059	-0.199
HLEG	6.119	8.647
Dipole Moment	5.538	5.474
Adsorbent-Adsorbate (MMC-CMC) Complex		
HOMO	-4.991	-5.940
LUMO	-2.046	-1.154
HLEG	2.945	4.796
BE	-9.07	-14.15
Dipole Moment	7.193	7.462

To get a better understanding of the stability of the AAC, an analysis of the binding energy (BE) was carried out using two computational approaches. The BE engaged in the formation of a complex system (XY), for instance, is the difference of the energy of the particular species E(XY) and the energy associated with its monomer units [nE(X) and nE(Y); where 'n' is the no. of individual monomers units present in the compound and E is the total electronic energy of an individual species with the inclusion of a zero-point correction] as shown in the equation 9. Since the related BE can be formulated as:

$$BE = E(XY) - nE(X) - nE(Y) \quad (9)$$

The BE has been analyzed at the two levels of theories (B3LYP and M06-2X) in vacuo. Using the B3LYP functional, the BE value was -9.07 kcal/mol. To look into the change in BE value by varying the methods, the M06-2X functional was used and the computed BE (-14.15 kcal/mol) was found to be increased by -5.08 kcal/mol from -9.07 kcal/mol which may be due to the involvement of the dispersion correction in the dispersion-corrected DFT (M06-2X) functional.

4.2 Quantum theory of atoms in molecules (QTAIM) analyses

Nowadays, the Atoms in Molecules (AIM) based on Bader's "quantum theory of atoms in the molecule (QTAIM)"[69] is broadly used in probing the structure and reactivity of polyatomic molecules based on NCIs (weak to strong) present in a system. The special points in space which portrays the maxima, minima or saddle point of ED are well known as the critical points (CPs). As shown in Figure 15, among four kinds of the CPs [(3, −3), (3, −1), (3, +1) and (3, +3)] affirmed by Bader, the (3, −1) CP is frequently used and the related atomic interaction line highlights that electronic charge density is accumulated between the nuclei that are bonded, is represented by the presence of (3, −1) CP. Since it is known as a bond path (BP) and the (3, −1) CP is referred to as bond critical point (BCP) which is a descriptor (a necessary and sufficient condition) for the NCIs (holding a BP) between two atoms. Indeed, the BCP plays an important role in describing the molecular structure as it forms it possible to make the presence of binding between the atoms *via* valence bonds and NCIs. The value of the delocalization index (DI) can be directly interpreted as the bond order.

The QTAIM tool has facilitated details of the important parameters of the NCIs for instance, bond path length (BPL), ED $\rho(r)$, potential energy density [$V(r)$], Laplacian, $\nabla^2\rho(r)$, and delocalization index (DI), that are displayed in Table **3**. The QTAIM technique can be used to probe the energy of intra/intermolecular (stabilizing) primary (covalent) or secondary (noncovalent) interactions[70]:

$$E = 1/2V(r) \sim E = 313.754\ V(r) \quad (10)$$

where E (au or kcal/mol) is the energy of intra-/intermolecular (stabilizing) primary or non-covalent interactions).

Table 3 Some selected and important QTAIM based parameters and HBSBIC values for the conventional and nonconventional noncovalent interactions (NCIs) of the adsorbent-adsorbate complex at M06-2X/6-31+G (d, p) level of theory.

NCI	BL(Å)	BPL(Å)	ρ (au)	$\nabla^2\rho$ (au)	*V(r)* (kcal/mol) (HBSBIC)	DI (au)
Conventional H-bond (Moderate)						
O27-H44···O92	1.930	3.731	0.0250	+0.0799	-6.40 (0.101)	0.0639
O92-H93···O24	1.836	3.543	0.0310	+0.1028	-7.91 (0.192)	0.0746
O24-H43···O11	1.885	3.637	0.0275	+0.0904	-7.03 (0.143)	0.0663
O6-H38···O37	2.066	3.978	0.0177	+0.0574	-4.58 (0.150)	0.0432
Conventional H-bond (Weak)						
C2-H10···O24	2.292	4.399	0.0164	+0.0599	-4.08	0.0456
C4-H12···O95	2.435	4.648	0.0098	+0.0348	-2.20	0.0333
C2-H10···O95	2.326	4.447	0.0127	+0.0421	-2.95	0.0404
C32-H23···O95	2.504	4.778	0.0097	+0.0349	-2.26	0.03
C20-H22···O11	2.595	5.255	0.0097	+0.0380	-2.20	0.0243
C73-H76···O6	2.629	5.032	0.0076	+0.0267	-1.57	0.0303
C94-H96···O92	2.726	5.210	0.0074	+0.0245	-1.44	0.0187
C94-H96···O27	2.642	5.038	0.0075	+0.0240	-1.51	0.0260
C94-H96···O24	2.488	4.928	0.0113	+0.0427	-2.57	0.0246
Nonconventional H-Bond						
C4-H12···C73	2.796	5.332	0.0062	+0.0192	-0.09	0.0187
C13-H42···C52	3.378	6.573	0.0022	+0.0063	-0.31	0.0081
C16-H7···C74	2.675	5.111	0.0083	+0.0252	-1.32	0.0274
C94-H96···H23/ C32-H23···H96	2.189	4.422	0.0092	+0.0411	-1.82	0.0110

The sign of the Laplacian operator at a BCP, $\nabla^2\rho(r)$, exposes the possibility of the gathering of charge at a point surface. In a primary interaction such as "shared" covalent

bonds the value $\nabla^2\rho(r) < 0$ and $\rho(r) > \sim 0.1$ au whereas in the case of the depleted or "closed shell" as in case the of NCIs, the value of $\nabla^2\rho(r) > 0$ and with the usually small magnitude of $\rho(r)$ i.e. the order of $\sim 10^{-2}$ au for the H-bonding and $\sim 10^{-3}$ au for *van der* Waals' type NCI. According to this theory, the values of some topological parameters at BCP decide the nature of chemical interaction. The values of topological parameters are shown in Table **3** (all quantities are measured in au except the interaction energy). The intermolecular HBs and other weak NCIs can be responsible for the geometry and the stability of a predominant adsorbate-adsorbaent complex.

Keeping all this in mind, the QTAIM based analyses facilitate an excellent overview of the involved moderate (intra- and intermolecular) HBs and other weak NCIs involved in the titled system and the related QTAIM based structures are shown in Figure 15. The analysis of the aforementioned Figure, a total of *seventeen* NCIs in which 4 are the conventional moderate HBs; 2 intermolecular HBs {BE: -6.40 kcal/mol for O27-H44···O92 HB and -7.91 kcal/mol for O92-H93···O24 HB) and 2 intramolecular HBs {BE: -7.03 kcal/mol for O24-H43···O11 HB and -4.58 kcal/mol for O6-H38···O37 HB}] connected *via* the BP is detected in the AAC model system considered in this report. Generally, a decrease in the *ρ(r),* and *V(r)* (magnitude) values correspond to an increase in the length of the corresponding bond and, thus, it can be used to probe more essential insights regarding the structural features of any system. The ED values decrease as the BLs and BPLs increase for all the four moderate HBs [O92-H93···O24 (BL: 1.836 Å, BPL: 3.543 Å, ED: 0.0310 au, and IE: -7.91 kcal/mol) > O24-H43···O11 (BL: 1.885 Å, BPL: 3.637 Å, ED: 0.0275 au, and IE:-7.03 kcal/mol) > O27-H44···O92 (BL: 1.930 Å, BPL: 3.731 Å, ED: 0.0250 au, and IE: -6.40 kcal/mol) > O6-H38···O37 (BL: 2.066 Å, BPL: 3.978 Å, ED: 0.0177 au, and IE: -4.58 kcal/mol)], respectively. It should be noted that the above order is shown concerning the ED and the IE values. To further validate the nature and order of the intra- and intermolecular H-bonding interactions, another useful index, very recently, given by Pandey et al. was performed as the "hydrogen bond strength based on interaction coordinates (HBSBIC)" [71]. Using the HBSBIC approach, the hydrogen bond strengths for O92-H93···O24, O24-H43···O11, O27-H44···O92, and O6-H38···O37 HBs were found to be 0.192, 0.143, 0.101, and 0.150, respectively which shows that the first one has the strongest hydrogen bond strength.

Moreover, a total of *nine* NCIs fall under the weak conventional H-bond category showing C-H···O type interactions which also give a big favour for making an equilibrium and stabilized structure of AAC. In addition to this, four more but nonconventional HBs (three C-H···C and one C-H···H) were detected by performing the QTAIM tool which may also stabilize the systems.

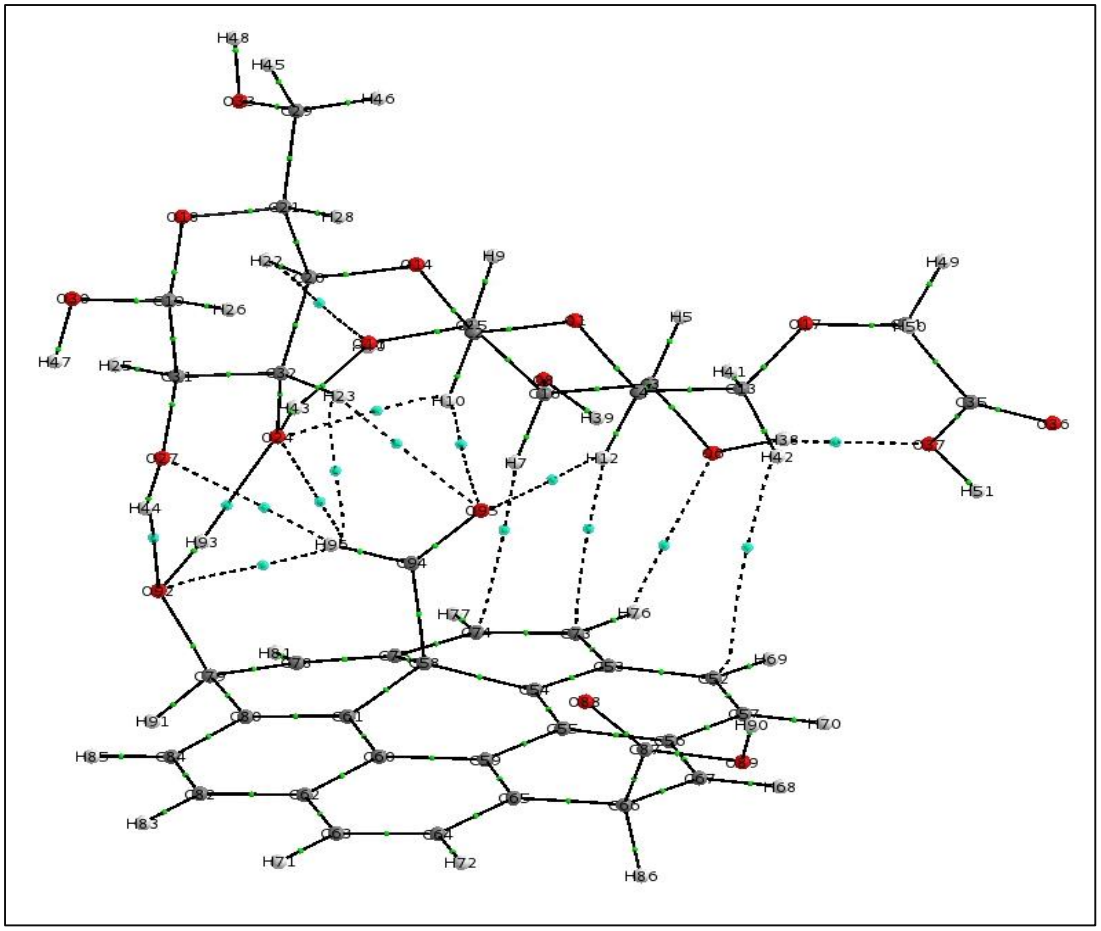

Figure 16. QTAIM molecular graph showing the different BCPs of the MMC-CMC calculated at B3LYP/6-31+G (d, p) level. The BCPs are denoted as light greenish-blue small points

4.3 Chemical reactivity

The highest occupied molecular orbitals (HOMOs), lowest unoccupied molecular orbitals (LUMOs), and their HOMO-LUMO energy gaps (HLEGs) are useful quantum chemical descriptors in the field of quantum chemistry to identify the electrical transport properties in the molecules [72] and are found to be particularly useful in the study of conjugated P electron systems [73]. A molecular system's HOMO and LUMO are involved in chemical reactions and interactions with other systems. The HOMO represents the system's ground state, while the LUMO represents its first excited state,

and any electrical change from the HOMO to the LUMO causes charge conversion from one region to another within the same system. The HLEG parameter also quantifies a system's proclivity for interacting with other entities. The FMO distance is used to determine a molecule's molecular function and the ability to absorb light. The electronic transport characteristics are determined by the smaller HLEG between HOMO and LUMO, which allows for improved tunnelling of photo/thermally excited electrons. A small HLEG-based molecular species exhibits more polarizable behaviour and is associated with high chemical reactivity (low kinetic stability) [74]. Two separate functionals (B3LYP and M06-2X) were used to analyses the difference in HLEG values, and the optimized structure's HLEG (Table 2) was found to be 2.944 eV using the B3LYP functional, which is lower than the HLEG of the same (4.786 eV) using the M06-2X level of theory.

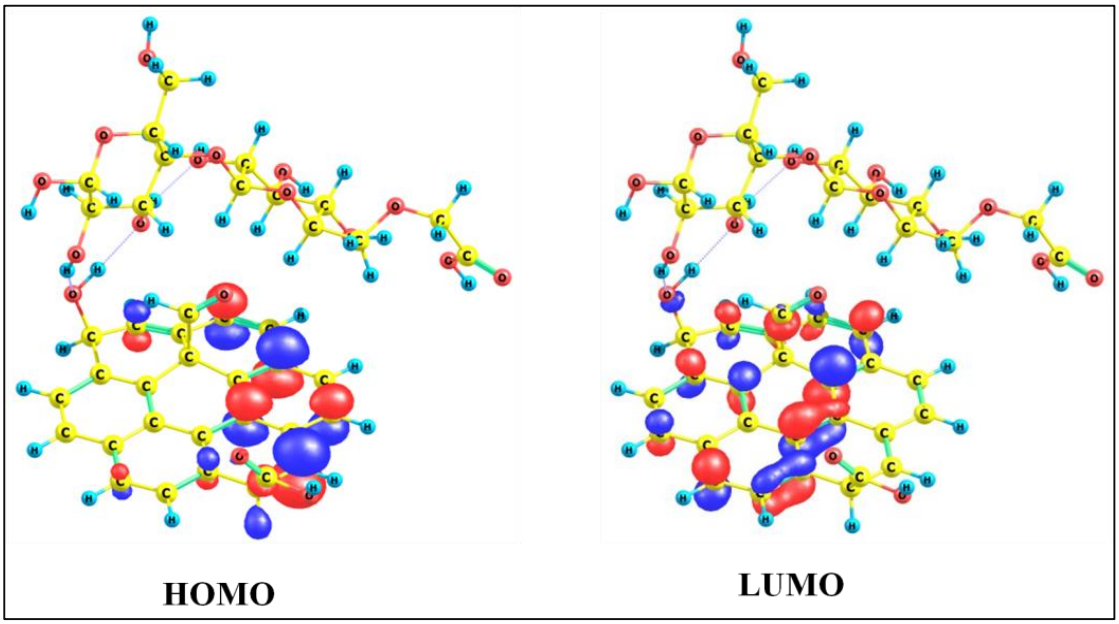

Figure 17. HOMO-LUMO plots of the AAC system

Figure 17 illustrates the HOMO and LUMO surfaces determined by the M06-2X/6-31+G (d, p) for an integrated model framework. The HOMOs are primarily contained by the opposite side (i.e. left side) of the carbon frameworks of the three benzene rings and a minor contribution of a C atom from two benzenes of the functionalized coronene unit, while the LUMOs are primarily contained by the opposite side (i.e. left side) of the carbon frameworks of the three benzene rings and a marginal contribution of the central benzene unit of the functionalized coronene unit. As a result, the electron density exchange between a few benzene rings and other benzene rings in the same structure corresponds to the transformation from HOMO to LUMO.

4.4 Molecular electrostatic potential (MEP) surface

The electron density (ED) is related to the molecular electrostatic potential (MEP), which is used to consider relative polarity. The MEP is critical for understanding electrophilic and nucleophilic attack sites, as well as NCIs. [75]. The MEP is also well suited to studying processes dependent on a molecule's "recognition" by another molecule [76]. With the aid of a three-dimensional MEP surface, the reactivity nature of the molecule can be visualised. The charge distribution in the molecule is depicted by the MEP map. Figure 18 depicts the MEP map for the adsorbent-adsorbate pair. It shows the molecular structure, size, and charge distribution all at once. The electron-rich (absolute negative charge) region's reactive sites are shown in red, and they are vulnerable to electrophilic attack. The colour blue denotes a strong positive area that is prone to nucleophilic attack. The green colour scheme represents a possible middle ground between the two extremes of red and blue. Figure 18 demonstrates that the title compound's more electronegative region (electrophilic region) was found over the electronegative O atoms, while the more electropositive region (nucleophilic region) was found in some of the OH group's H atoms.

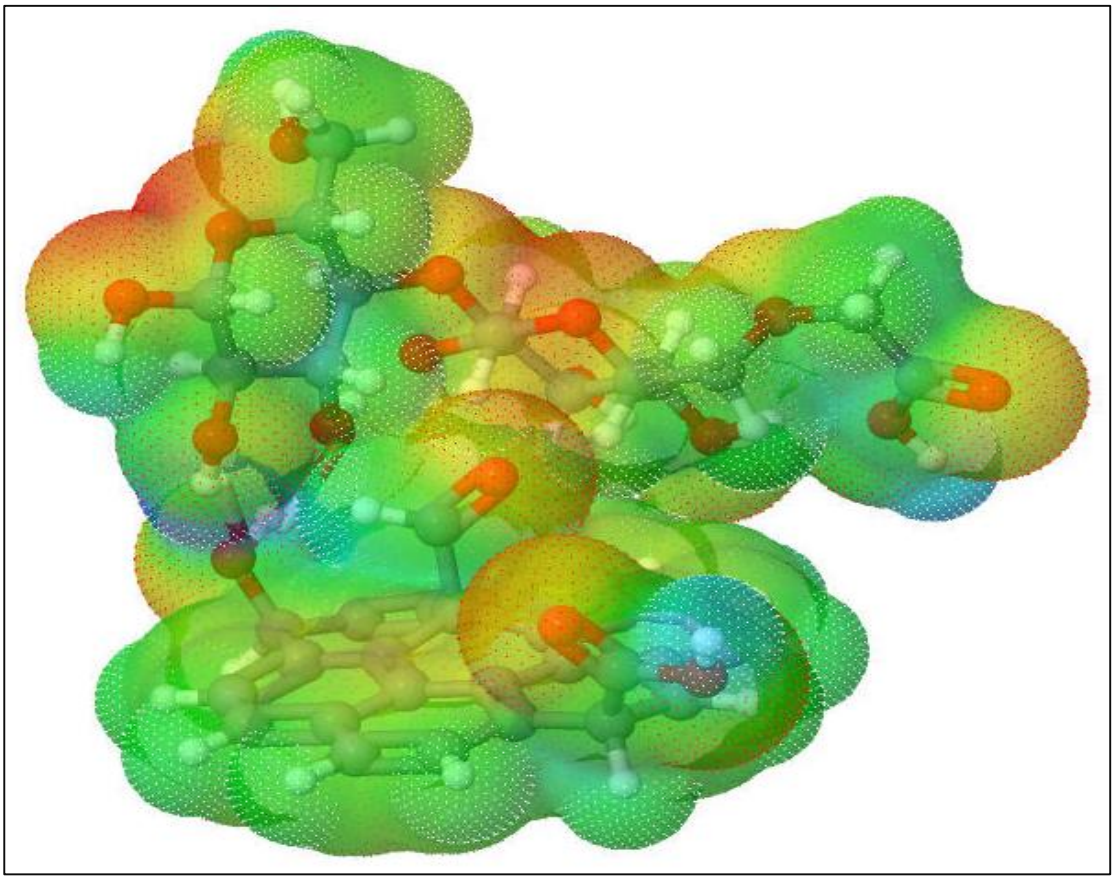

Figure 18. MESP plot of the CMC-MMC system

4.5 Natural charge analyses (NPA)

The application of quantum mechanical equations to molecular structures highly depends on the determination of atomic charges. A statistical approach to partitioning the charge density into charges on the nuclei, bond orders, and other significant details was known as population analysis. Natural Population Analysis (NPA) is a well-known and widely used statistical technique. The electron population of each atom, as defined by the basis function, is used to quantify natural charges. Normal population analysis (NPA) is used to determine the atomic charges on various atoms. It is worthy to mention that the carbon C87 of the -COOH group of coronene has the most positive natural charges (0.43329) and the oxygen O24 atom of the OH group of glucose exhibits the most negative charge (-0.41690) at the B3LYP level of theory whereas in the case of M06-2X level of study, the carbon C87 of the COOH group of coronene contains the most positive natural charges (0.44197) and the oxygen O24 atom of the OH group of glucose consisting of the most negative charge (-0.42458) with the marginal increment. Many of the O atoms in the system, on the other hand, have a negative charge, and all of the H atoms have a net positive charge. Negative charges on the C and O atoms, as well as a net positive charge on the H atom, can indicate the development of intermolecular interaction. To probe the charge distribution on the corresponding monomer units (adsorbent and adsorbate), the NPA shows that the adsorbent (functionalized coronene unit) contains a total natural atomic positive charges as 0.49884 and 0.49445 at B3LYP and M06-2X level of theories while the adsorbate having total natural atomic charges as 0.00115 and 0.00557 at the same level of studies, fairly revealing that the coronene unit acts as an electron donor.

5. Conclusions

The present study revealed that MMC had a surface area (S_{BET}) = 16.576 m^2 g^{-1}, which was largely distributed by mesopores. The average pore diameter and total pore volume of MMC were found to be 12.432 nm and 0.051 cm^3g^{-1}, respectively which confirmed the mesoporous nature of the MMC as per the IUPAC classification of materials. The adsorption of CMC on MMC was found to be affected by changes in pH and ionic strength. These findings indicated that the electrostatic force plays an important role in CMC binding at MMC/water interfaces. The findings of the ATR-FTIR study helped **to** detect spectral differences associated with hydrogen bonding between adsorbate (CMC) and adsorbent (MMC). The differences in the ATR-FTIR bands in the 1000–

1080 cm^{-1} region were important, owing to the -C–O stretch coupled to the -C–C stretch and -O–H disability, confirming strong bond formation due to hydrogen bonding at MMC/water interface. Since urea functions as a hydrogen bond breaker, the presence of urea during adsorption greatly reduced the amount of CMC adsorption on MMC. This finding further favoured a hydrogen bonding-based system rather than a hydrophobic one. Since the adsorption free energy (-22.561 $kJmol^{-1}$) of CMC is similar to that of hydrogen bond formation, Langmuir adsorption isotherm studies endorses hydrogen bonding as the dominant force for CMC adsorption. The kinetic adsorption data revealed that CMC adsorption onto MMC water interfaces was in near alignment with the overall rate of CMC adsorption by MMC, indicating that the physicochemical process was closely controlled. The average roughness parameter was revealed CMC was adsorbed in a very smooth confirmation on the MMC surface per polymer chain, according to AFM evaluation. The survey scan and high resolution of C1S XPS spectra confirmed that the -OH groups on the MMC surface associate with the CMC carboxylate ion. Thus, the current research provided significant evidence to show that CMC adsorption on the MMC/water interface was governed by electrostatic interaction and hydrogen bonding but was influenced by experimental conditions. This adsorbent-adsorbate model was supposed to pave a new path towards a deeper understanding of molecular aggregation mechanisms in food and industrial applications, based on theoretical investigations.

References

1. Abdul, K. H. P. S.; Tye, Y. Y.; Saurabh, C. K.; Leh, C.P.; Lai, T. K.; Chong, E.W.N.; Fazita, M.R.N.; Hafiidz, J.M.; Banerjee, A.; Syakir, M.I. Biodegradable polymer films from seaweed polysaccharides: A review on cellulose as a reinforcement material. *eXPRESS Poly. Lett*. **2017**, *11*, *244*-265.
2. Arancibia, C.; Lisboa, R. N.; Zuniga, R. N.; Matiacevich, S. Application of CMC as thickener on nanoemulsions based on olive oil: physical properties and stability. *Int. J. Poly. Sci*. **2016**, 2, 1-10.
3. Klemm, D.; Heublein, B.; Fink, H.; Bohn, A. Cellulose: fascinating biopolymer and sustainable raw material. *Angew. Chem. Int. Ed. Engl*. **2005**, 44, 33583-93.
4. Hollabaugh, C. B.; Burt, L. H.; Walsh, A. P. Carboxymethylcellulose uses and applications. *Ind. Eng. Chem. Res*. **1945**, 37, 943-947.
5. Tian, Z.; Wu, Z.; Jones, M.J.; Gill, P. Mineral processing and extractive metallurgy. *The Institute of Mining and Metallurgy, London*. **1984**, 743-750.
6. Rhodes, M. K.; Mineral processing. proc. 13th International mineral processing congress. *Warsaw*. **1979**, 139, 346-366**.**
7. Boruvkova, K.; Wiener, J. Water absorption in carboxymethyl cellulose. *AUTEX Res. J.* **2011**, 11, 1-4.
8. Hamad, A. M. A.; Ates, S.; Durmaz, E. Evaluation possibilities of cellulose derivatives in food products. *J. Forest. Facult*, **2016**, 16, 383-400.
9. Mackenzie, M.; Malhotra, D.; Riggs, W.F. Chemical reagents in the mineral processing industry. *Society of Mineral Engineerings, Colorado, USA*, **1986**, pp. 139–145.
10. Raju, G.B.; Holmgren, A.; Forsling, W.J. Adsorption of dextrin at mineral/water interface. *J. Colloid Interface Sci*. **1997**, 193, 215-222.
11. Laskowski, J.S.; Liu, Q. The role of metal hydroxides at mineral surfaces in dextrin adsorption. *Int. J. Min.* Proc. **1989,** 27, *297*-316.
12. Solari, J.A.; de Araujo, A.C.; Laskowski, J.S. The effect of carboxymethyl cellulose on the flotation and surface properties of graphite. **1986**, 3, 15-31.
13. Mackenzie, M.; Malhotra, D.;. Rigga W. F. Handbook of flotation reagents chemistry, theory and practice: flotation of sulfide ores. *Soc. Min. Eng*. **1986**, 165,139-549.
14. Pugh, R. J. Macromolecular organic depressants in sulfide flotation-a review, 1. Principles, types and applications. *Int. J. Miner. Process*. **1998**, 25, 101-130.

15. Healy, T.W. Principles of adsorptions of organics at solid-solution interfaces. *Sci Chem A.* **1974**, 8, 603-619.
16. Rath, R. K.; Subramanian S. Studies on adsorption of guar gum onto biotite mica. Miner. Eng. **1997**, 12, 1405-1420.
17. Steenberg, E. Ph.D. Thesis, faculty of science, university of potchefstroom, *Johannesburg*, South Africa, **1982**, 28, 350-356.
18. Steenberg, E.; Harris, P. J. Adsorption of carboxymethyl cellulose, guar gum, and starch onto talc, sulfides, oxides and salt type minerals. *S. Afr. J. Chem.* **1984**, 36, 85–90.
19. Jenkins, P.; Ralston. The adsorption of a polysaccharide at the talc–aqueous solution interface. Colloids Surf. A. **1998**, 139, 27- 40.
20. Rath, R. K.; Subramanian, S.; Laskowski, J. S.; Poling, G. WProcessing of hydrophobic minerals and fine coal, *Canadian Institute of Mining, Metallurgy and Petroleum. (Eds.), Montreal, Canada*, **1995**, p.p.105.
21. Jucker, B. A.; Harms, H.; Hug, S. J.; Zehnder A. J. B.; Adsorption of bacterial surface polysaccharides on mineral oxides is mediated by hydrogen bonds. *Colloids Surf B: Biointerfaces.* **1997**, 9, 311-3643.
22. Bakinov, K. G.; Vaneev, II, Gorlovsky, S. I.; Eropkin, Y; Zashikhin, N. V.; Konev, A. S. New Methods of sulfide concentrate upgrading.*7th International Mineral **Processing Congress***. 1964.
23. Wang, J. P. Somasundaran Adsorption and conformation of carboxymethyl cellulose at solid-liquid interfaces using spectroscopic, AFM and allied techniques, *J. Colloid Interface Sci*. **2005**, 29, 175-83.
24. Cuba-Chiem, L.T.; Huynh, L.; Ralston, J.; Beattie, D. A. In situ particle film ATR FTIR spectroscopy of carboxymethyl cellulose adsorption on talc: binding mechanism, ph effects, and adsorption kinetics. *Langmuir*. **2008**, *24*, 8036-44.
25. Fujimoto, J.; Petri, D. F. S. Adsorption behavior of carboxymethyl cellulose on amino-terminated surfaces. *Langmuir*. **2001**, 17, 56-60.
26. Beaussart, A.; Mierczynska-Vasilev, A.; Beattie, D. A. Evolution of carboxymethyl cellulose layer morphology on hydrophobic mineral surfaces: variation of polymer concentration and ionic strength. *J Colloid Interface Sci*. **2010**, *346, 303*-10.
27. Cohen Stuart, M. A.; Fokkink, R. G.; Van Der Horst, P. M.; Lichtenbelt, J. W. T. *Persistence length of carboxymethyl cellulose as evaluated from size* exclusion chromatography and potentiometric titrations. *Colloid Poly. Sci*. **1998**, 276, 335-3.

28. Hoogendam, C. W.; de Keizer, A.; Cohen, M. A.; Stuart, M. A.; Bijsterbosch, B. H.; Batelaan, J.G.; Van, H. D. Adsorption mechanisms of carboxymethyl cellulose on mineral surfaces. *Langmuir*. **1998**, *14*, *3825*-3839.
29. Bacchin, P.; Bonino, J. P. Martin, F.; Combacaum, M.; Barthes, P.; Petit, S.; Ferret, J. Surface pre-coating of talc particles by carboxyl methyl cellulose adsorption: study of adsorption and consequences on surface properties and settling rate. *Colloids and Surfaces A: Physicochem. Eng. Aspects*. **2006**, 272, 211-219.
30. Cuba-Chiem, L.; Huynh, L.; Ralston, J.; Beattie, D. A. In situ particle film ATR FTIR spectroscopy of carboxymethyl cellulose adsorption on talc: binding mechanism, pH effects, and adsorption kinetics. *Langmuir*. **2008**, *24, 8036*-44.
31. Phenrat, T.; Saleh, N.; Sirk, K.; Kim, H. J.; Tilton, R. D.; Lowry, G. V. L.; comparative study of polymeric stabilizers for magnetite nanoparticles using ATRP. *J. Nanopart. Res*. **2008**, 10, 795-814.
32. Sedeva, G.; Fornasiero, D.; Ralston, J.; Beattie, D. A. Adsorption of modified dextrins on talc: effect of surface coverage and hydration water on hydrophobicity reduction. *Langmuir*. **2010**, 26, 15865-15874.
33. Duker, E.; Lindström, T. On the mechanisms behind the ability of CMC to enhance paper strength. *Nord. Pulp. Pap. Res. J*. **2008**, 23, 57-64.
34. Rakkolainen, M.; Kontturi, E.; Isogai, A.; Enomae, T.; Blomstedt, M.; Vuorinen, T.; Carboxymethyl cellulose treatment as a method to inhibit vessel picking tendency in printing of eucalyptus pulp sheets. *Ind. Eng. Chem. Res*. **2009**, 48, 1887-1892.
35. Kumar, A.; Negi, Y. S.; Choudhary, V.; Bhardwaj, N. K. Microstructural and mechanical properties of porous biocomposite scaffolds based on polyvinyl alcohol, nano-hydroxyapatite and cellulose nanocrystals. *Cellulose*. **2014**, 21, 3409–3426.
36. Orelma, H.; Filpponen, I.; Johansson, L.; Laine, J. Rojas, O.J. Affibody conjugation onto bacterial cellulose tubes and bioseparation of human serum albumin. *Biomacromolecules*. **2011**, 12, 4311-4318.
37. Filpponen, I.; Kontturi, E.; Nummelin, S.; Rosilo, H.; Kolehmainen, E.; Ikkala, O. Laine, J. Generic method for modular surface modification of cellulosic materials in aqueous medium by sequential "click" reaction and adsorption. *Biomacromolecules*. **2012**, *13, 736*-42.
38. Orelma, H.; Teerinen, T.; Johansson, L.; Holappa, S.; Laine, J. CMC-modified cellulose biointerface for antibody conjugation. *Biomacromolecules*. **2012,** 13, 1051-1058.

39. Mohan, T.; Kargl, R.; Kö, S.; Stler, A.G.; Doliska, G.; Findenig, V; Ribitsch, Stana-Kleinschek, K., Functional polysaccharide conjugates for the preparation of microarrays. *ACS Appl. Mater. Interfaces*. **2012**, 2743-2751.
40. Kulterer, M. R.; Reichel, V. E.; Kargl, R.; Kö, S.; Stler, T.; Sarbova, K.; Heinze, Stana-Kleinschek, Ribitsc, V. Functional polysaccharide composite nanoparticles from cellulose acetate and potential applications. *Adv. Funct. M*ater. **2012,** 22, 1749-1758.
41. *Laine, J.; Lindström, T.; Nordmark,* G. G.; *Risinge.* G. Studies on topochemical modification of cellulosic fibres. part 2. the effect of carboxymethyl cellulose attachment on fibre swelling and paper strength. *Part 1 Nord.Pulp. Pap. Res. J.* **2000**, 17, 50-56.
42. Mohan, T.; Kargl, R.; Doliška, A.; Ehmann, H. M. A. Ribitsch, V.; Stana-Kleinschek, K. Functional polysaccharide conjugates for the preparation of microarrays. *Carbohydr. Polym*. **2012**, 93, 191-198.
43. Mohan, T.; Kargl, R.; Kö, S.; Stler, A.G.; Doliska, G.; Findenig, V.; Ribitsch, K.; Stana-Kleinschek, K. Enzymatic digestion of partially and fully regenerated cellulose model films from trimethylsilyl cellulose *J. Colloid Interface Sci*. **2011**, 358, 604-10.
44. Liu, Z.; Choi, H.; Gatenholm, P.; Esker, A. R.; Quartz crystal microbalance with dissipation monitoring and surface plasmon resonance studies of carboxymethyl cellulose adsorption onto regenerated cellulose surfaces. *Langmuir*. **2011**, *27, 8718-28*.
45. Amim, J.; Kosaka, P.; Petri, D. Characteristics of thin cellulose ester films spin-coated from acetone and ethyl acetate solutions. *Cellulose*. **2008**, 15, 527–535.
46. Karg, R.; Mohan, T.; Bračič, M.; Kulterer, Doliska, M. A.; Kleinschek, K. S.; Ribitsch, V. Functional polysaccharide conjugates for the preparation of microarrays. *Langmuir*. **2012**, 28, 11440-11447.
47. *Chanzy, H.*; *Henrissat, B.; Vincendon,* M.; Tanner, S.; Belton, P. S.; Solid-state ^{13}C-N.M.R. and electron microscopy study on the reversible cellulose I→Cellulose III Transformation in *Valonia. Carbohydrate Res. **1987***, 160, 1-11.
48. Kondo, T.; Sawatari, C.; Manley, R.; St, J.; Gray, D. G. Characterization of hydrogen bonding in cellulose-synthetic polymer blend systems with regioselectively substituted methylcellulose. *Macromolecules*. **1994,** 27, 210-215.
49. Ozaki, K.; Ito, S. Purification and properties of an acid endo- 1, 4-P-glucanase from Bacillus SP. KSM-330. *J. Gen. Microbio*. **1991**, 137, 41-48.

50. Wu, G.; Dai, R.Y.; Li, W. G.; Yin Chen, P. P.; Wang, M. Solution-processed organic uv photodetectors based on polyfluorene and naphthalene diimide. *Current App. Phy*. **2011**, 11, 750-754.
51. Singh, K.; Bharose, R.; Singh, V. K.; Verma, S.K. Sugar decolorization through selective adsorption onto functionalized accurel hydrophobic polymeric support. *Ind. Eng. Chem Re*s. **2011**, 50, 10074-10082.
52. Gunning, A.P.; Kirby, A. R.; Ridout, M. J.; Brownsey, G. J.; Morris, V. J. Atomic force microscopy as a tool for interpreting the rheology of food biopolymers at the molecular leve. *Macromolecule*s. **1996**, 29, 6791-6796.
53. Wilkinson, K . J.; Balnois, E.; Leppard, G. G.; Buffle, J. Characteristic features of the major components of freshwater colloidal organic matter revealed by transmission electron and atomic force microscopy . *J. Colloids Surf. A.* **1999**, 155**,** 287-310.
54. Rath, R. K.; Subramanian, S.; Laskowski, J. S. Adsorption of dextrin and guar gum onto talc. a comparative study. *Langmuir.* 13, **1997**, 6260-6266.
55. C. Chen, Y.; Yanwei, X.; Hu, X.; i2, M.; Yan, L.; Mai3, P.; Hu, B.; Shan, Y. Huang, Y. Na(+) intercalation pseudocapacitance in graphene-coupled titanium oxide enabling ultra-fast sodium storage and long-term cycling. *Nat. Commun*., 2, **2015**, 1-8.
56. Brunauer, S.; Emmett, P. H.; Teller, E. Adsorption of gases in multimolecular layers. *J. Am. Chem. Soc.* **1938,** 60, 309-319.
57. Barrett, E. P.; Joyner, L. G.; Halenda, P. P. The Determination of pore volume and area distributions in porous substances. i. computations from nitrogen isotherms. *J. Am. Chem. Soc.* 1**954** 73, 373-380.
58. McIntire, T. M.; Penner, R.; Brant, D. A. Observation of circular, triple helical polysaccharides using nanocontact atomic force microscopy. *Macromolecules*. **1995**, 28, 6375-6377.
59. Langmuir, I. The adsorption of gases on plane surfaces of glass, mica and platinum. *J. Am. Chem. Soc.* **1918**, 40, 1361–1403.
60. Singh, K.; Gautam, M. Development of inexpensive biosorbents from de-oiled mustard cake for effective removal of As(V) and Pb(II) ions from their aqueous solutions. *J. Sci. Ind. Res.* **2016**, 75, 444-451.
61. Slobodan, K. M. Consideration of the correct calculation of thermodynamic parameters of adsorption. *J. Serb. Chem. Soc.* **2004,** 72, 1363–1367.

62. Zhou, X. The unit problem in the thermodynamic calculation of adsorption using the Langmuir equation, *Chem. Eng. Commun*. **2014**, 201, 1459–1467.
63. Salvestrini, S.; Leone, V.; Iovino, P.; Canzano, S.; Capasso, S. Considerations about the correct evaluation of sorption thermodynamic parameters from equilibrium isotherms. *S. J. Chem. Thermo*. **2014,** 68, 310–316.
64. Frisch, M. J.; Trucks, G. W.; Schlegel, H. B.; Scuseria, G. E.; Robb, M. A.; Cheeseman, J. R.; Scalmani, G.; Barone, V.; Petersson, G. A.; Nakatsuji, H.; Li, X.; Caricato, M.; Marenich, A.V.; Bloino, J.; Janesko, B. G.; Gomperts, R.; Mennucci, B.; Hratchian, H. P.; Ortiz, J. V.; Izmaylov, A. F.; Sonnenberg, J. L.; Williams-Young, D.; Ding, F.; Lipparini, F.; Egidi, F.; Goings, J.; Peng, B.; Petrone, A.; Henderson, T.; Ranasinghe, D.; Zakrzewski, V.G.; Gao, J.; Rega, N.; Zheng, G. ; Liang, W. ; Hada, M. ; Ehara, M. ; Toyota, K. ; Fukuda, R. ; Hasegawa, M. Ishida, T. Nakajima, Y. Honda, O. Kitao, H. Nakai, T. Vreven, K. Throssell, J. ; Montgomery, J.A. ; Jr. J. Peralta, E. ; Ogliaro, F. ; Bearpark, M. J. ; Heyd, J. J.; Brothers, E. N.; Kudin, K. N.; Staroverov, V. N. ; Keith, T. A.; Kobayashi, R.; Normand, J.; Raghavachari, K.; Rendell, A. P. ; Burant, J. C.; Iyengar, S.S. ; Tomasi, J.; Cossi, M. ; Millam, J. M.; Klene, M.; Adamo, C.; Cammi, R.; Ochterski, J. W.; Martin, R. L.; Morokuma, K.; Farkas, O.; Foresman, J. B.; Fox, D.J. *Gaussian 16, Revision B.01, Gaussian, Inc., Wallingford CT*, **2016**.
65. Lee, C.; Yang, W.; Parr, R.G. Development of the Colle-Salvetti correlation-energy formula into a functional of the electron density *Phys. Rev. B.* **1988**, 37, 785-789.
66. Miehlich, B.; Savin, A.; Stoll, H.; Preuss, H. Results obtained with the correlation energy density functionals of becke and Lee, Yang and Parr *Chem. Phys. Lett.* **1989**, 157, 200-206.
67. Dennington, R.; Keith, T.; Millam, J. *Gauss View Version 5.0, Semichem Inc.,* KS, **2005.**
68. Bader, R. F. W.; Atoms in Molecules: A Quantum Theory, Second Ed., Oxford University Press, New York, **1990.**
69. Espinosa, E.; Molins, E.; Lecomte, C.; Hydrogen bond strengths revealed by topological analyses of experimentally observed electron densities *Chem. Phys. Lett.* **1998**, 285, 170–173.
70. Ermolaev, V.; Miluykov, V.; Rizvanov, I.; Krivolapov, D.; Zvereva, E.; Katsyuba, S.; Sinyashin, O.; Schmutzler, R. Phosphonium ionic liquids based on bulky phosphines: synthesis, structure and properties. *Dalton Trans.* **2010**, 39, 5564–5571.

71. Pandey, S. K.; Manogaran, D.; Manogaran, S.; Schaefer III, H. F. Quantification of hydrogen bond strength based o interaction coordinate: A new approach. *J. Phys. Chem. A* **2017**, 121, 6090-6103.
72. Fukui, K. Role of frontier orbitals in chemical reactions, *Science* **1982**, 218, 747-754.
73. Fukui, K.; Yonezawa, T. H.; Shingu, A molecular orbital theory of reactivity in aromatic hydrocarbons. *J. Phys. Chem.* **1952**, 20, 722-725.
74. Sinha, N.; Prasad, O.; Narayan, V.; Shukla, S. R. Raman, FT-IR spectroscopic analysis and first-order hyperpolarisability of 3-benzoyl-5-chlorouracil by first principles. *Mol. Simul.* 2011, 37, 153-163.
75. Scrocco, E.; Tomasi, J. Electronic molecular structure, reactivity and intermolecular forces: a euristic interpretation by means of electrostatic molecular potentials. *Adv. Quantum Chem.* **1978**, 11, 115-193.
76. Scrocco, E.; Tomasi, J. The electrostatic molecular potential as a tool for the interpretation of molecular properties. *Top. Curr. Chem.* **1973**, 42, 95-170.

Chapter 4

Interpretation of adsorption behaviour of carboxymethyl cellulose onto functionalized accurel polymeric surface

Abstract

Carboxymethylcellulose (CMC) is a highly flexible cellulose derivative with a broad variety of industrial uses, including mineral refining, palletization, oil drilling, surface modification, surface functionalization, and other promising applications. However, due to a lack of understanding of the CMC's adsorption behaviour onto solid surfaces in its aqueous medium, its applications are limited. As a result, an attempt has, therefore, been to investigate binding aspects of CMC on functionalized accurel (FA) chemically modified from polypropylene-based Accurel (MP1001). Burner Emmitt Teller (BET) study was used to evaluate the physiochemical parameters of FA, such as specific surface area (S_{BET}) =34.472 m^2/g, pore volume (Vp) =0.07-0.121 cm^3/g, total pore volume (Vtp) = 0.115 cm^3/g, mean pore diameter = 13.692nm, and pore diameter =39.402nm. The equilibrium isotherm data were fitted with Freundlich, Langmuir, Temkin, and Jovanovic models of adsorption and compared by determination coefficient (R^2) and found to follow the sequence Langmuir (R^2=0.9933)> Freundlich (R^2=0.9830)>, Jovanovic (R^2= 0.9428)> Temkin (R^2 =0.8663). The hydrogen bonding between the carbonyl group of CMC and functional groups (-OH) of FA in the regions 288-280 eV and 1772-1676 cm^{-1} was verified by infrared and X-ray photoelectron spectral changes before and after adsorption, respectively. A theoretical model was used in this report to explain the type, nature, and intensity of interaction(s) involved in the adsorbent-adsorbate complex (FA-CMC). The geometric, stability, and electronic feature studies have been conducted using the optimised structure, binding /interaction energy, HOMO-LUMO gap, natural population analyses, and Bader's quantum theory of atoms in molecules (QTAIM) related parameters with the deployment of the DFT dispersion-corrected (DFT-D) and DFT approaches. The molecular electrostatic potential surface (MESP) map was used to find the reactive sites of the above entities. The binding aspects of the adsorbate (CMC) onto the polymeric surface of the adsorbent (FA) were exercised through CMC aggregation stabilized by H-bonding and other weak noncovalent interactions, and since such modification could play a noteworthy role in the field of food, pharmaceutical, and industrial applications.

1. Introduction

Carboxymethylcellulose (CMC) is a commercially available cellulose derivative with a number of desirable characteristics, including anionic water solubility, non-toxicity, biocompatibility, biodegradability, and natural polysaccharide. CMC's characteristic properties are related to the presence of hydroxyl groups in its composition. CMC has been commonly used in various industrial applications, including biopolymeric and nanopolymeric materials [1–8] . The majority of understanding of interfacial binding aspects (adsorption) into polymeric/solid/mineral surfaces was needed for CMC to be useful in various areas. Many researchers used the adsorption consequences not only to better explain CMC adsorption on different materials, but also in environmental and pharmaceutical studies. The authors [9-12] of these studies used linearly plotted diagrams to explain the distribution of various adsorbate species between liquid and multiple adsorbents, based on a series of hypotheses about the heterogeneity or homogeneity of various adsorbents, surface coverage, and the different binding behaviour between the various adsorbates. Therefore, various adsorptions models were adopted to describe and understand the present work [9-12]. CMC's binding properties have been linked to a variety of commercial uses, including thickening agents, oil drilling agents, viscosity modifiers, water retaining agents, suspending agents, stabilisers, and bio-adhesive agents. The readily available hydroxyl groups present on each unit of CMC structure are primarily responsible for the interfacial/adsorption aspects of CMC [13]. Adsorption of cellulose derivatives on different solid surfaces/mineral surfaces, such as graphite [14], pure high-quality graphite-ceylon [15,16] mineral solid surfaces, has been publicised [17 – 21] The findings attempted to prove that CMC adsorption at solid-liquid interfaces is driven by electrostatic, hydrophobic, hydrogen bonding, chemical interactions [22-27], chemical complexation and hydrophobic-hydrophobic interaction [28], electrostatic interactions [29], hydrophobic-hydrophilic, or hydrophobic self-assembled monolayers [29 -51]. The CMC's interaction behaviour on cellulose fibres or spin-coated regenerated cellulose model films from trimethylsilyl cellulose by adding a quartz crystal, as well as various model films, has also been reported [54-52].

According to the results, there's also no proof of peculiar selectivity for CMC adsorption on the polymeric surface. As a result, the adsorption of CMC onto functionalized accurel (FA) was investigated in order to find evidence of CMC's

specific interaction with FA. Table 1 compares some other adsorbents mentioned in the literature with those of polymeric surfaces, which we previously functionalized using a physical method [55]. The adsorption potential of FA (250 mg/g) is comparable to the highest recorded values, as shown in table 1. However, in this research, the FA was produced using accurel MP1001 as a precursor and a chemical method (simple oxidation process). FA is low-cost and does not require a complex functionalization process. Because of its physiochemical properties, such as zero point charge, mesoporous nature, and specific surface area, the FA was used as a possible adsorbent (functionalized polymeric surface).

Table 1 Comparison of polypropylene based accurel adsorbents

Adsorbents	Adsorption characteristics	Method	Results	References
Accurel MP 1001	Specific surface area (S_{BET}) (m^2 /g) = 35, Average pore diameter (nm) 1.4	Physical process	Successfully loaded surfactants onto Accurel MP 1001 surface	55
Modified polypropylene powder accurel MP1002)	Specific surface area (S_{BET}) (m^2 /g) = 27, Average pore diameter (nm) 2.8nm	Physical process	Successfully modified polypropylene powder	56
Polypropylene (PP)	Not reported by the author	Oxidation process	There was no detectable carbonyl group in the IR spectrum onto PP	57
Funcalized accurel (FA) from polypropylene (PP)	See Table 3	Simple oxidation process	Successfully introduced carbonyl group onto PP chromic acid and used as a potential adsorbent for CMC adsorption behaviour interpretation	Present study

The purpose of this study is to confirm the current literature concerning the binding behaviour of CMC onto functionalized polymeric surfaces from its aqueous solutions. It's also been stated that a simple oxidation process can be used to modify the surface properties of polymeric materials and add new functionalities. A theoretical model was used to explain the type, nature, and strength of interaction(s) involved in the adsorbate-

adsorbent complex (FA-CMC). Such laboratory experiments could have a major impact on the performance of CMC on a functionalized surface for a range of industrial applications, primarily in pharmaceutical and industrial products.

2. Experimental

2.1 Materials

Accrual System, Membrana GmbH (Obernberg, Germany), generously provided the Accurel MP product 1001 with an average pore diameter of 0.014m [55]. Accrual is its brand name. CMC was purchased from M/s Akshar Exim Company Private Limited (Kolkata**)**. In the synthesis and experimental tests, analytical and laboratory-grade reagents were used. Bionic Enterprises, India, supplied sulphuric acid (98%), chromium trioxide (99.5%), cetrimide (96%), sodium chloride (9905%), sodium hydroxide (98%), potassium chloride (99.5%), and urea (99%). For the synthesis and adsorption analysis, double distilled water was used.

The chemical structures of newly synthesized FA were investigated using a Fourier transform infrared (FTIR) spectrophotometer (Nicole-6700) with a wavenumber range of 4000 to 500 cm^{-1} in which the FA was mixed with 200 mg of KBr and then pelletized. The microstructural analysis was carried out on a scanning electron microscope (SEM) (JEOL JSM 6490LV) before scanning, the samples were well dried on critical point dryer (CPD, Emitech K 850) and gold spin-coated by an ion sputter coater (JFC 1600, auto fine coater). Energy-dispersive X-ray spectroscopy (EDX) was used to analyze the elemental composition and elemental mapping using SEM (JSM 6490LV) by EV dry detector (INCAx-act). A surface area analyzer (BELSORP-max) was used to determine the FA's specific surface area, pore diameter, and pose size distribution. For 5-6 hours, a certain amount of FA materials (0.20 g) were heated under vacuum at 120°C for pre-treatment. This pre-treated sample was scanned with nitrogen (as adsorbate) and helium (as carrier) gas, and all measurements were monitored in real time using the BELSORP data analysis software (BDAP). After complete scanning of the sample, the results (data) were analysed by Version info of the analysis software (VAS). X-ray diffraction powder X-ray diffraction (PXRD) (RigakuMiniflex II desktop) in the 2-theta angle range 10°-60° at 30kV using CuK radiation was used to investigate the crystallographic nature of FA. The surface potential of FA was measured by the point of zero charge (ZPC) by solid addition method [90-92] using ZPC Analyzer (TIPLH) at 25°C. The XPS experiments were carried out in an ultrahigh vacuum (UHV) with a high-

resolution X-ray photoelectron spectrophotometer (HR-XPS) (PHI 5000 Versa Prob II, FEI Inc) at a specific energy and resolution. All samples were dehydrated under vacuum before XPS analysis. All data of XPS analysis were plotted using Casa XPS Version 2.3.17PRI. I and Origin Pro 8 SRO v8.0724 (B724) software. The pH of the solution was measured using a digital pH meter (TIPLH). The ultrasonicator with (Sonics Vibra-cell VCX750) high-intensity liquid processor was used for sonication to examine the effect of power ultrasound on adsorption of CMC onto FA. The ultrasonicator used here case was an amplifier power (automated) probe with stepped tip 1/8″-630-0422 (Coupler solid, Part No.630-0421). Adsorption studies were carried in a temperature-controlled orbital shaker (REMI brand) at 35°C at a constant speed of 125 rpm. The FA was separated from the CMC solution by centrifugation (Sprout make) at 6000 rpm for 15 minutes. The absorbance of the supernatant and residual concentration of CMC was determined by reported method [58] by spectrophotometrically at λ_{max}=265nm (UV-Visible spectrophotometer, Cary 100).

2.2. Functionalization of Accurel MP 1001 (functionalized accurel)

The published protocol was used to produce the functionalized acccurel (FA) [57]. In a 500 ml volumetric flask with a thermometer, the dried accurel MP 1001 was treated with an oxidizing solution containing a 1:1:2 (by weight) mixture of H_2SO_4: CrO_3: H_2O. At 70°C and ambient pressure, the entire material was stirred (30 rpm) on a thermostat heating plate. The slurry-like material (FA) was collected after 5.0 minutes. This material was washed with double distilled water, then acetone, and finally the FA was powdered and placed in a desiccator for further experiments.

2.3. Adsorption measurements

A stock solution (1000 mg/L) was prepared by dissolving appropriate amount of CMC in double distilled water and stirring vigorously for 30 minutes. This solution was refrigerated for 24 hours before being used in further experiments (desired concentrations). Adsorption experiments were carried out using conical flasks (100mL) containing 0.1g of FA with 50 mL of CMC solutions. After agitating the conical flasks for a fixed amount of time, samples were withdrawn from the flasks. Centrifugation at 6000 rpm for 15 minutes separated the FA from the CMC solution. The absorbance of the supernatant solution and residual concentration of CMC was determined by the

reported method [58] by spectrophotometrically at λ_{max}=265nm. The adsorption amount of CMC onto FA was calculated using the following equation [55, 58]:-

$$Qe = \frac{(Co - Ce)}{W} \times V \quad (1)$$

Where Q_e= Amount of the CMC adsorbed (mg/g) onto the FA, Co =Initial concentration of the CMC (mg/L), Ce=equilibrium concentration of the solution (mg/L), V=Volume (L) and W= Weight of FA (g).

Batch adsorption experiments were also carried out to investigate the effect of various factors like the initial concentration of CMC, FA dose, pH, ionic strength (0.1mol/L), temperature (℃), sonication and presence of urea (0.1mol/L). All the experiments (except the study of pH effect) were carried out at a pH of 3.0. The effect of pH on CMC adsorption was investigated at different pH by adjusting pH with HCl(0.1 mol/L) or NaOH (0.1mol/L) [91-92].

2.4. Optimization of various adsorption parameters

The adsorption analysis was carried out by varying only one parameter at a time, with the other parameters remaining constant. Various adsorption parameters were investigated such as the effect of concentration, pH, ionic strength (0.1mol/L), the temperature (°C), and effect of urea (0.1mol/L).

Adsorption equilibrium data was accomplished at various initial concentrations of CMC ranging from 100 mg/L to 600 mg/L using 1 mg of FA, pH 3.0, 60min contact time with 50 mL CMC solution.

2.5. Computational studies

Computational experiments, especially density functional theory, play a vital role in understanding the extensive atomistic characteristics governing the performance of interface studies of two interacting entities (DFT). To look into such type of features, the structural (geometries), stability [binding energy (BE) and intermolecular noncovalent interaction (NCI)], electronic feature analyses (molecular orbital, electrostatic potential, and charge transfer analyses), the quantum chemical calculations (QCCs) have been performed by choosing two systems constructing the adsorbent - adsorbate interface as a model consisting of intermolecular NCIs. The current work extensively explores the adsorption process in terms of the effect of interactions such

as BE and interaction energy obtained using the quantum theory of atoms in molecules (QTAIM) technique. The charge transfer phenomenon occurring between the adsorbent and the adsorbate interface has been described using the frontier molecular orbital (FMO) and molecular electrostatic potential (MESP) surface plots.

3. Results and discussion

3.1 Characterizations

3.1. 1 Functional group analysis

FTIR spectra of FA were scanned in the 400-4500 cm^{-1} range before and after adsorption **of** CMC (Figure 1). Earlier attempts [91] to alter polypropylene with the same reagent failed to modify polypropylene products (Accurel MP1001), as demonstrated by FTIR spectroscopy [55, 56]. However, the Accurel MP1001 was successfully oxidised in the present study, resulting in the addition of the carbonyl group at 1712.2cm^{-1} (Figure 1a). The band at 3020.8cm^{-1} is induced by -C–H stretching of the CMC's $–CH_2$ groups. The ring stretching of glucose appears at 1610.32 $cm^{–1}$. Furthermore, the bands at 1350–1450 cm^{-1} are induced by symmetrical deformations of the $-CH_2$ and -COH groups. At 1060 and 1010 cm^{-1}, the bands due to primary alcoholic $–CH_2OH$ stretching mode and $-CH_2$ twisting vibrations, respectively, appear. The mid-frequency bands at 714-610.70 cm1 were supposed to allow by ring stretching and ring deformation of -D-(1–4) and -D-(1–6) linkages (Figure 1b). The adsorbed CMC had a broad –OH band at 3399.3 cm^{-1} within the spectrum. In comparison to the non-adsorbed CMC onto FA, the position of this band increased slightly and the bandwidth decreased significantly. The CMC adsorbed onto FA shows carbonyl band at 1712.2 cm^{-1} which changes after adsorption confirms the inter-hydrogen bonding between the carbonyl group of CMC and functional groups(-OH) of FA surfaces (Figure 1c). The adsorption seems to occurs as evident from the changes in the IR frequencies of some main functional groups -OH, -C=O, -C-O, -C-H, and –COOH and their corresponding frequencies as shown in Table 2 [59-66].

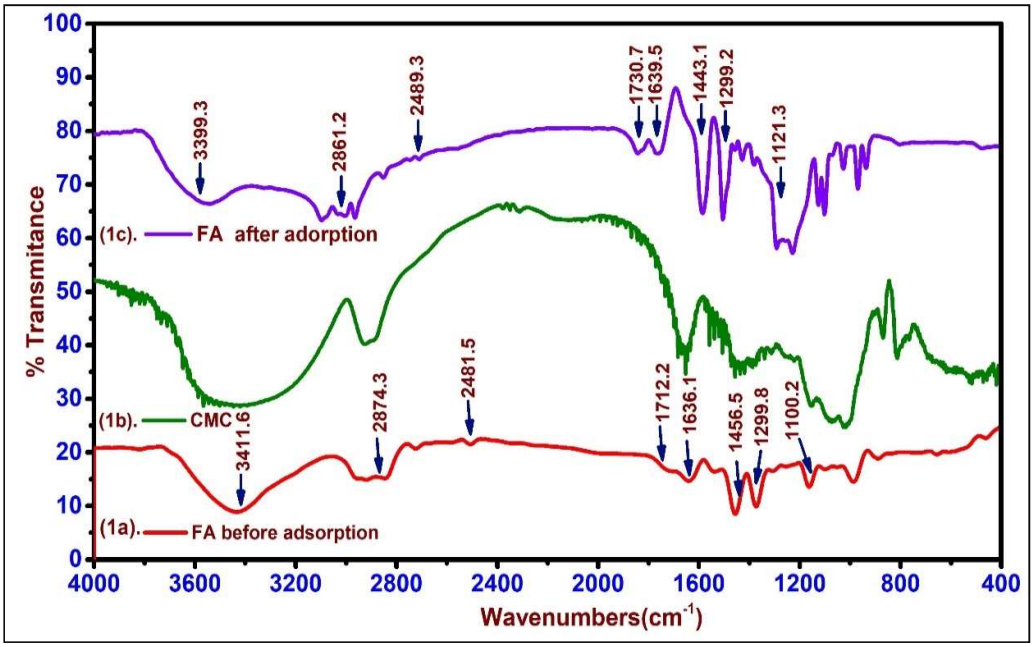

Figure 1. FT-IR spectra of (1a). FA before adsorption, (1b). CMC, (FA After adsorption of CMC

Table 2 FT-IR spectral characteristics of FA before and after adsorption of CMC

Wavelength range (cm^{-1})	**Frequencies (cm^{-1})**		**Difference**	**Assignment**
	Before adsorption	**After adsorption**		
3500-3000	3411.6	3399.3	-12.3	Bonded—OH
2900-2800	2874.3	2861.2	-13.1	-C-H stretching
2500-2300	2481.5	2489.3	-7.8	-O-H carboxylic acid
1740-1680	1712.2	1730.7	-18.5	>C=O carbonyl
1620-1680	1636.1	1639.5	-3.4	>C=C stretching
1500-1400	1456.5	1443.1	-13.4	>C–O stretching
1080-1,360	1299.8	1299.2	+0.6	-C–N stretching
1070-1150	1100.2	1121.3	-21.1	-C–OH stretching

The difference in frequencies >12 cm^{-1} given in the above table clearly demonstrates a band shift.

3.1. 2 Microstructural analysis

The scanning the samples with a scanning electron microscope revealed microscopic properties regarding surface morphology of FA (Figure 2). The micrographs in Figure 2 show a spongy, irregular, and heterogeneous surface with several pits spreading through it, likely due to the oxidising agent used during the simple oxidation method that produced some changes in the surface of Accurel MP1001. As expected, these morphological properties were advantageous to the adsorption process.

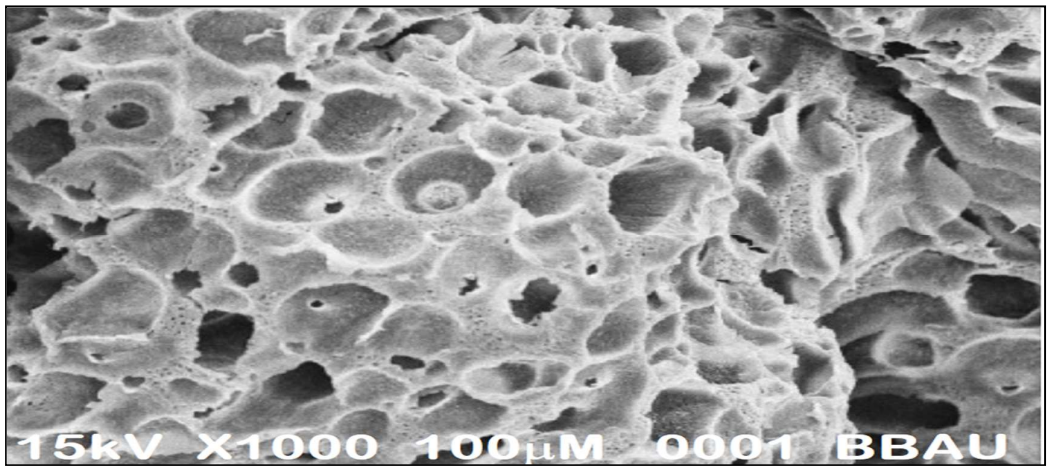

Figure 2. SEM micrograph of FA at 1000X magnification

3.1.3 Elemental mapping of microstructures by scanning electron microscopy-energy dispersive X-ray spectrometry (SEM-EDS)

Since, SEM-EDS has been commonly used to identify the elemental microanalysis of materials in a wide range of physical and biological sciences, engineering, technology, and forensic investigations [66]. As a result, elemental measures are computed using SEM and EDS microanalysis to determine the elemental composition and spatial distribution of elements present in FA. The element images were used to describe the spatial distribution of elements in the FA, and they were extremely effective for illustrating element distributions in the material's textural context. Figure 3 illustrates the scanned elemental maps (Left). The elemental identification and spatial elemental distribution are confirmed by the microanalysis study. The presence of carbon (88.12 %), oxygen (11.32 %), and sulphur (11.32 %) in FA modified from the precursor (MP1001) is attributed to the adsorption characteristics of FA modified from the precursor (MP1001) (0.49 %).

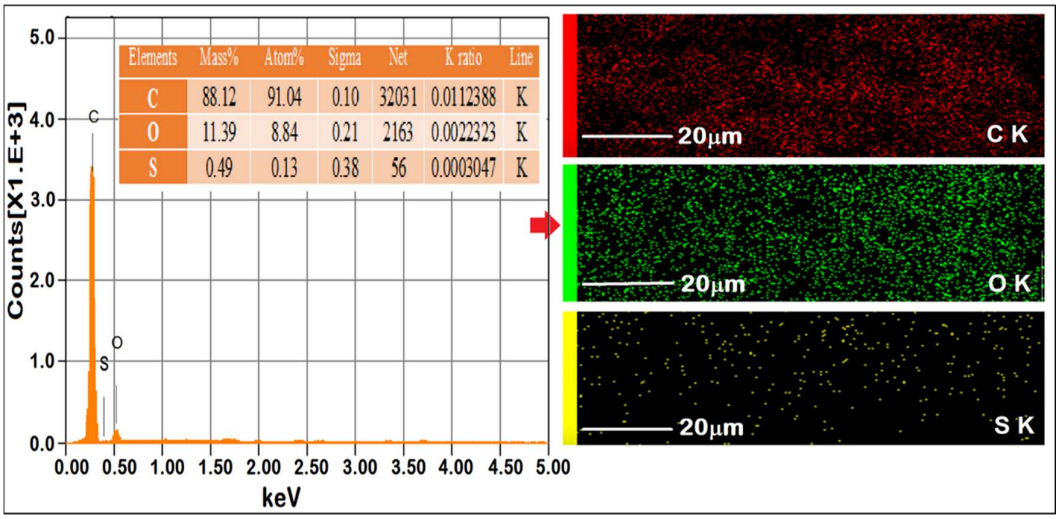

Figure 3. EDX spectrum, elemental composition and elemental maps (left) of FA

3.1. 4 BET analysis

BET analysis [67] was used to determine the textural properties of FA (Figure 4), such as specific surface area, surface nature, particle size distribution, and total pore volume. The $\mathbf{N_2}$ adsorption isotherm, which is a type IV isotherm (Giles' classification) [67] resulting from a capillary phenomenon in the low-pressure area, was measured (Figure 4a). The capillary condensation phenomenon is the characteristic properties of mesoporous material, therefore, it was interpreted that FA was mesoporous material. The BET analysis [67] (Table 3) reveals that FA had a typical specific surface area (S_{BET} =34.74m^2g^{-1}) (Figure 4b). For the determination of pore size distribution, Barrett-Joyner-Halenda (BJH) model [68, 69] was applied (Figure 4c). The pore diameter of FA was found 39.402 nm using T-method [70] (Figure 4d) which confirm the mesoporous nature of FA as defined by IUPAC nomenclature [71-73]. These physicochemical properties [55] of FA makes it suitable and potential adsorbent for the adsorption of CMC.

Table 3 Physiochemical parameters obtained from the BET analysis presented in figure 4

BET Analysis				
Methods	**Surface parameters of FA**			
N_2Adsorption-desorption	Sample weight (g)	Saturated pressure (kPa)	Degassing Time (hr)	
BET	1.00	98.963	2.50	
	Specific surface area (S_{BET}) (m^2 /g)	Monolayer volume (V_{mono}) (cm^3 /g)	Total pore volume (Vp) (cm^3/g)	Mean pore diameter (nm)
	34.742	7.691	0.115	13.692
BJH	Pore volume (Vp) (cm^3 /g)	Pore specific surface area (a_p) (m^2/g)	Micropore radius (cylindrical shape (r_p) (nm)	
	0.121	45.495	6.852	
T	Total specific surface area (a_1) (m^2/g)	External surface area (a_2) (m^2/g)	Pore volume (V_1 &V_2) (cm^3/g)	Pore diameter (2t) (nm)
	24.704	20.943	0.07	39.402

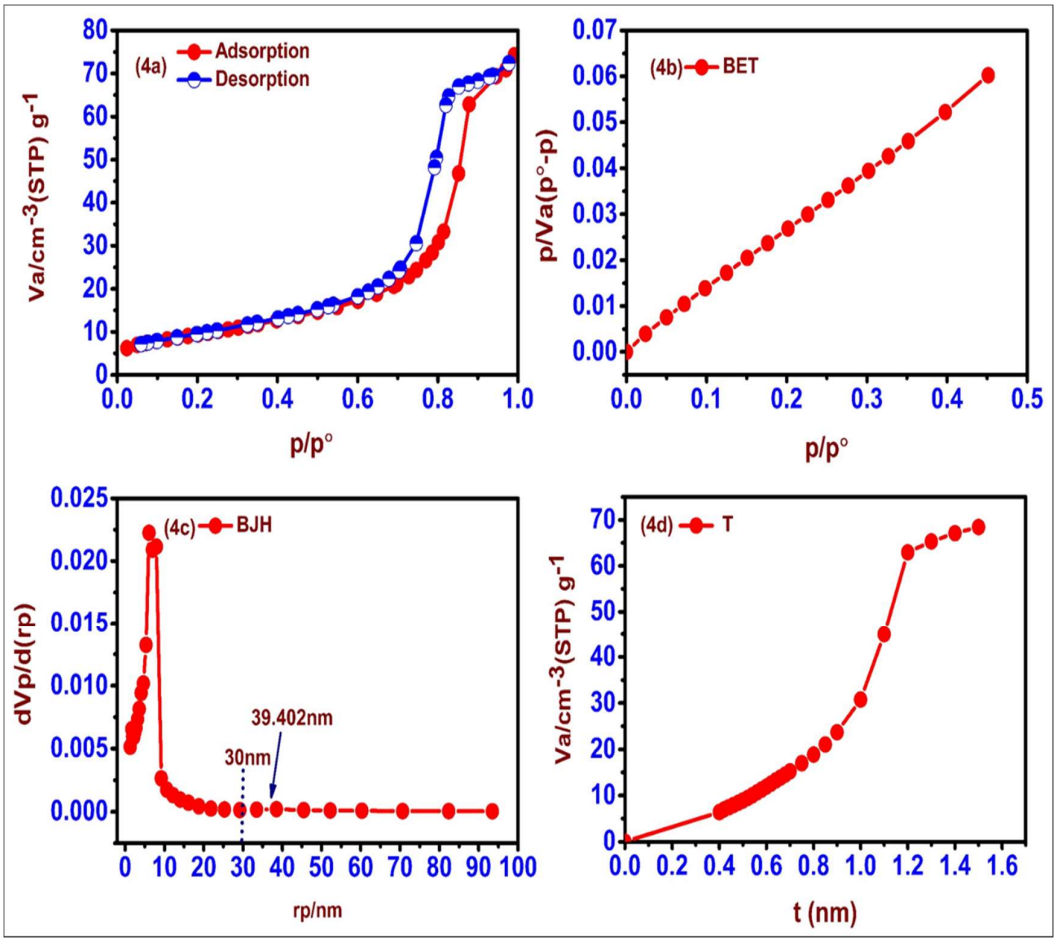

Figure 4. (4a).N_2 adsorption-desorption, (4b). BET, (4c). BJH and (4d). T graph of FA

3.1.5 X-ray diffraction analysis

The pXRD technique was used to investigate the crystalline phase and orientation of FA before and after adsorption (Figure 5). The crystalline structure of FA was confirmed by its spectra. There were four sharp diffraction peaks premised on 2θ (degree) values of 14.150, 17.050, 18.660, and 21.400, suggesting that the Accurell MP 1001 skeleton structure was identical [74]. Because of the functionalization (FA), there is a sharp peak between 23.210 and 42.320. There was a significant difference in the diffraction pattern after CMC adsorption onto FA, suggesting CMC adsorption. Furthermore, the shift in the peaks illustrated the unit cell's contraction. The loss of crystallinity of the polymeric surface of FA was also evidenced by the disappearance and shift in peaks. The difference in the material's diffraction pattern, on the other hand, could suggest adsorbate adsorption. Although the peak change reflects the contraction of the unit cell, both peak strength reduction and peak disappearance contribute to the material's loss of crystallinity under investigation [75].

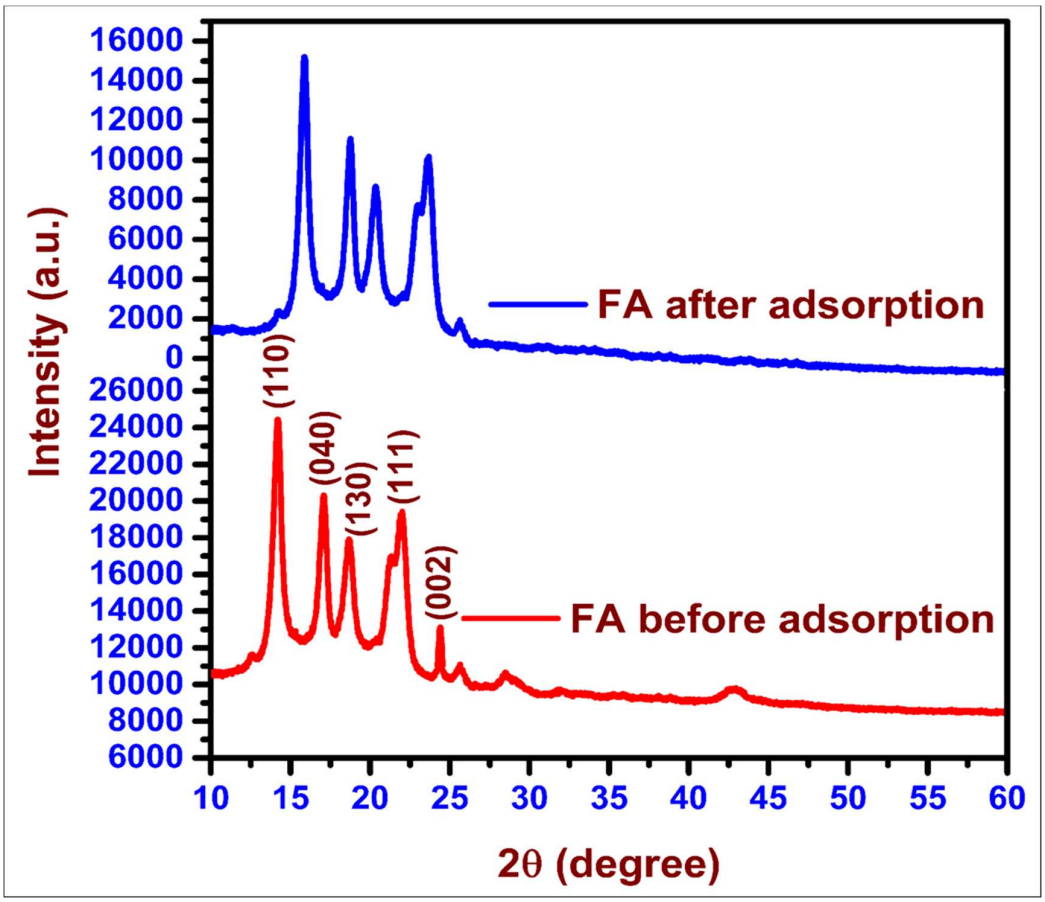

Figure 5. Typical pXRD of FA before and after adsorption of CMC

3.1.6 Electrokinetics studies

The solid addition technique [76] was performed to determine the zero point charge (pH_{ZPC}) of FA. In this method, 20 mL of cetrimide solutions (0.002 mol/L) and 20 ml of HCl (0.1mol/L) was taken in a series of stoppered conical flask (100 ml). The desired initial pH values (pH_i) of the solution were adjusted between 2, 4, 6, 8, 10, 12 and 14 (±0.1pH units) by adding either HCl (0.1mol/L) or 0.1 N NaOH (0.1mol/L). The total volume of the solution in each flask was adjusted exactly 50.0 ml by adding the KCl (0.1mol/L) and cetrimide solution (0.002 mol/L). The initial pH of the solution was then accurately recorded (±0.1pH units). 0.1 gram of FA was added to each flask. The suspension was shaken and allowed to equilibrate for two days with intermittent shaking after the centrifugation, the final pH value (pH_f) of the supernatant liquid was recorded (±0.1pH units). The difference between the initial and final pH values (ΔpH) was plotted against the initial value. The point of intersection of the resulting curve at which change in pH is zero gives the pH $_{PZC}$. The pH_{ZPC} of FA was found 7.21 (Figure. 6). Since, at any pH below pH_{ZPC}, the surface of the adsorbent is positively charged and at pH above pH_{ZPC}, the surface is negatively charged. However, at the pH_{ZPC} point, the surface of FA has no charge at all. These aspects of pH_{ZPC} were applied during the adsorption of CMC and the batch adsorption experiments were conducted in acidic medium preferably at pH (3.0) than the basic medium.

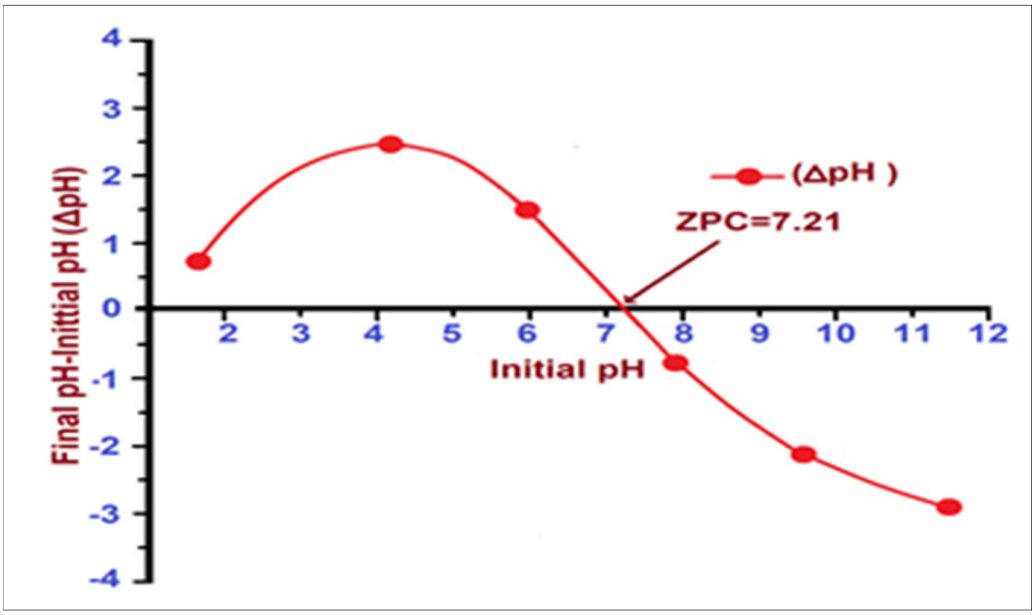

Figure 6. pH_{ZPC} analysis of FA by solid addition method

3.1.7 X-ray photoelectron spectroscopy (XPS) measurements

Non-destructive surface analysis technique (XPS analysis) was used to determine the surface structure and chemical composition of FA before and after adsorption. At optimum condition, XPS survey scans and high-resolution C1s XPS spectra of FA were scanned (Figure 7). Previously, XPS measurements were used to determine both the elemental and chemical composition of a material's surface and near-surface area [77-82]. The surface interface binding energy peaks corresponding to C–C, C–O, and C=O bonding appeared at 284.81, 286.2, and 289.1 eV, respectively, in the FA spectra before the adsorption of CMC. C–C, C–O, and C=O peaks were observed at 285.15, 286.9, and 289.5 eV, respectively, after CMC adsorption; the shifts in these peaks are associated with CMC adsorption facilitated by the carboxyl groups in CMC adsorption. After CMC adsorption, changes in the C–C, C–O, and C=O peaks were observed at 285.15, 286.9, and 289.5 eV, respectively, these shifts are significantly associated with CMC adsorption facilitated by the carboxyl groups in CMC adsorption.

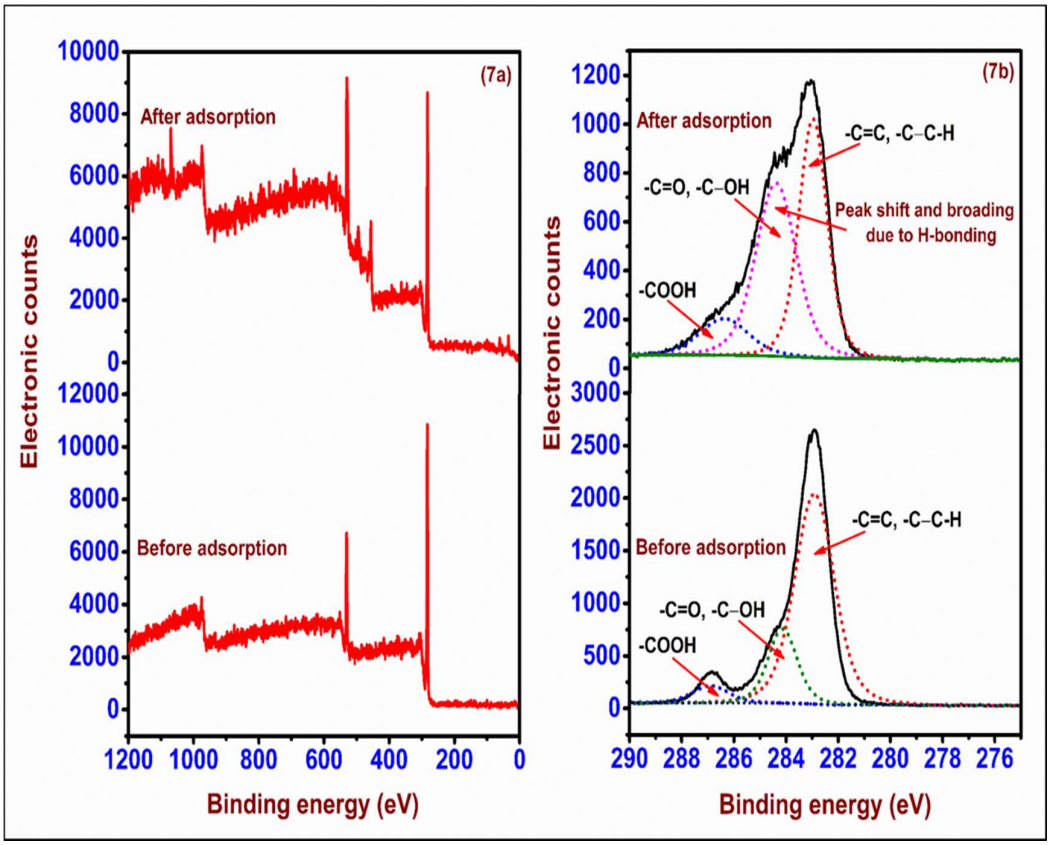

Figure. 7. (7a) XPS survey AlK α PES before and after adsorption, (7b). High-resolution C1s XPS spectra before and after

3.2. Effect of various parameters on CMC adsorption

3.2.1 Concentration

The effect of adsorbate (CMC) concentration onto adsorption was conducted at pH 3.0 in concentration range in 100-700mg/L of CMC. To ensure adsorption, each 50ml CMC solution was shaken for 3-4h after the addition of 1.0 g of FA at room temperature. Initially, adsorption occurs gradually, but after adsorbing high CMC concentrations, it becomes constant (Figure 8a). This is because the active sites on the surface of FA are free at low concentrations and gradually fill and with an amount of CMC, increasing the adsorption capacity. As the concentration of CMC increases, the active sites of FA become limited, and the adsorption of CMC becomes constant.

3.2.2 pH

Changing the pH of the solution has a significant impact on the adsorption capacity of CMC. Using 0.1 mol/L NaOH or 0.1 mol/L HCl, the pH was adjusted to a range of 2.0 to 12.0. According to the basic requirements of pHzpc of FA, the adsorption capability changed considerably at pH 3.0. Figure 8b demonstrates the relation between pH and adsorption capacity, suggesting that CMC has a high adsorption capacity at pH 3.0. At a lower pH than ZPC, the carboxyl groups on the surface of the FA are readily ionised, which was a favorable condition for adsorption.

3.2.3 Ionic strength

Adsorption tests were carried out with solutions of different ionic strengths (Figure 8c). Because of the screening effect of KCl (0.1mol/L), the amount of adsorption increases as the ionic strength increases. Since the FA surface was negatively charged when pH (9.0) is greater than ZPC (7.21), there would be more repulsion between the carboxylate ion of CMC and FA. The addition of salt (KCl, 0.1mol/L) decreases the repulsion between them, resulting in a higher density of CMC adsorption (Fig. 8c).

3.2.4 Urea

A urea test was performed to confirm the involvement of hydrogen bonding during the adsorption of CMC onto FA. It is well known fact that urea is a hydrogen breaker [83]. The batch adsorption was carried out by dissolving urea (0.1mol/L) in 700mol/L CMC solution. The obtained results showed that amount of adsorption decreased significantly

in the presence of urea which provides strong evidence that hydrogen bonding is responsible for the adsorption of CMC onto FA (Figure 8d).

3.2.5 Contact time

At a concentration of 700mg/L of CMC, the influence of contact time was observed at times ranging from 20 to 120 minutes. For each reading, 0.1 mg of FA was added to 50 mL of CMC solution (700 mg/L). Figure 8e shows that the amount of CMC adsorption increased steadily between 20 and 80 minutes, with no further changes observed as time passed. Based on the adsorption behaviour of CMC, we decided that 70-80 minutes was the optimal contact time for use in future experiments.

3.2.6 FA dose

The optimization of FA dose (1.0-7.0g) was conducted in a CMC concentration (700mg/L) at 3.0 pH at room temperature. The adsorption capacity decreases with increase FA dose. Therefore, 1.0 g was chosen as the adsorbent dose for further experiments (Figure 8f).

3.2.7 Temperature

The effect of temperature during the adsorption process was observed by adding 50ml CMC solution (700 mg/L) in 100 ml conical flasks with 1.0 g FA. The conical flasks containing CMC and FA were treated at 20-90^{0}C. The figure 8g illustrates that the adsorption capacity gradually with decreases with increasing temperature. This observation concluded that the hydrogen bonding between CMC and FA become weaker due to break of hydrogen bonds as temperature increases. Therefore, the higher temperatures were unfavourable for adsorption of CMC, and the adsorption is exothermic in nature (Figure 8g).

3.2.8 Sonication

The effect of power ultrasound (sonic - 20 kHz) during the adsorption process was examined to establish the role of hydrogen bonding. The adsorption test was conducted under optimized conditions in the presence and absence of ultrasound. The results indicates that, in the presence of ultrasound, the amounts of adsorption were also lower because the cavitation effect is higher at a smaller frequency (20 kHz) (due to larger bubbles) and leads to higher temperature and decrease in the amount of adsorption (Figure 8h).

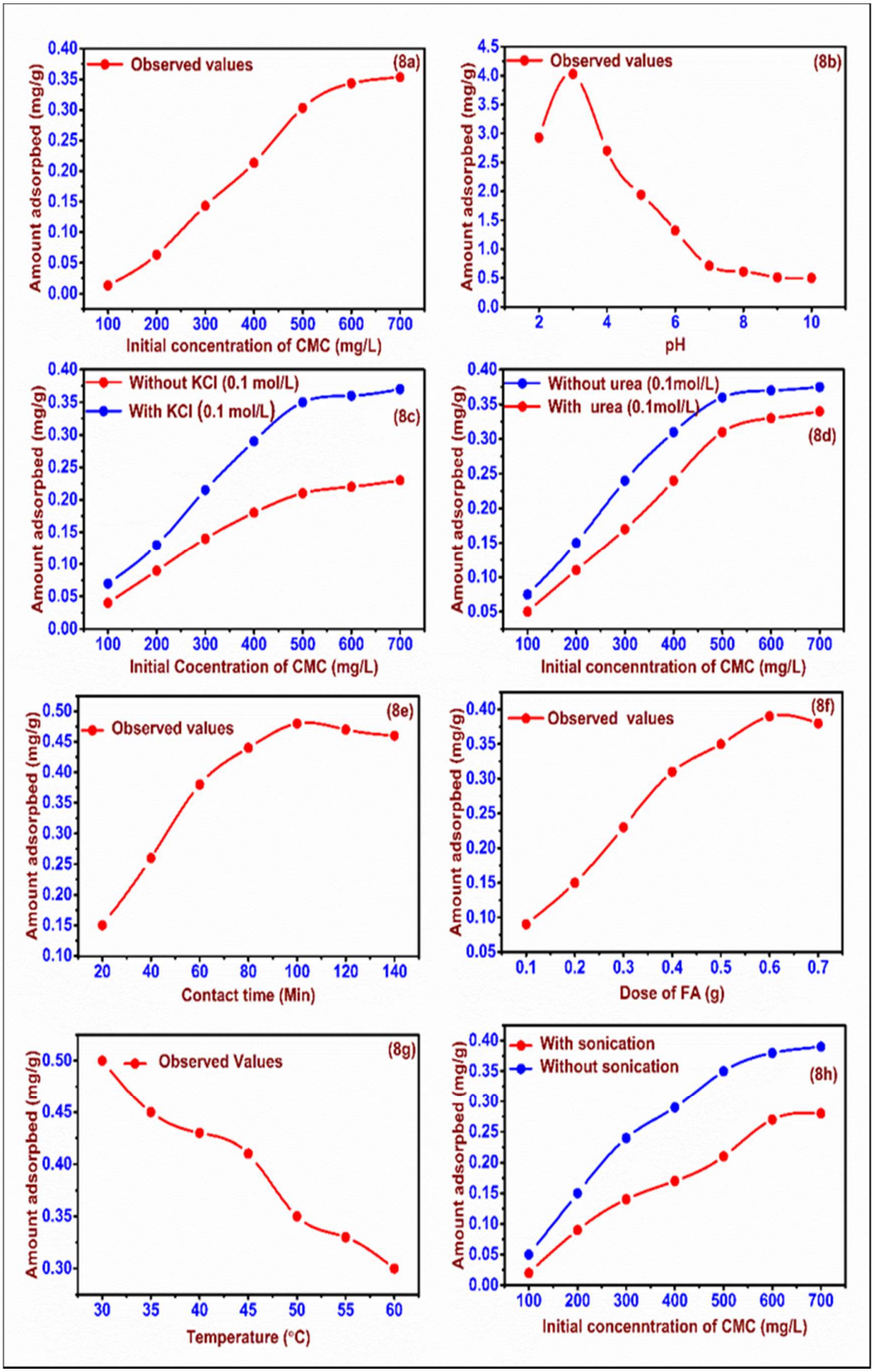

Figure 8. Effect of (8a). Concentration (mg/L), (8b). pH (3.0), (8c). Ionic strength (0.1mol/L), (8d). Urea (0.1mol/L), (8e). Contact time (Min), (8f). The dose of FA (g), (8g). Temperature (°C), (8h). Sonication (20 kHz)

3.3. Adsorption isotherms studies

To describe adsorption properties with their equilibrium parameters and explain the comprehensive understanding of the nature of the interaction between CMC and FA two most common used isotherms namely Freundlich and Langmuir while other two models namely Jovanovic and Temkin were studied [85,86] (Figure 9) and different parameters were tabulated in Table 4.

3.3.1 Freundlich adsorption isotherm

Freundlich isotherm demonstrated the variability in the amount of CMC adsorbed by FA unit mass with the variation in CMC-FA system concentration at optimized temperature. A linear form of the Freundlich equation, represented below, was used in order to calculate the adsorption behaviour of CMC to the FA surface [86].:-

$$\log Qe = \log K_L + \frac{1}{n}\log Ce \qquad (2)$$

Where Q_e = The amount of CMC adsorbed (mg/g); Ce = The equilibrium concentration of CMC in solution (mg/L); K_F and 1/n = Constants incorporating the factors affecting the adsorption capacity and intensity of adsorption. The values of K_F, 1/n and R^2 was obtained from linear plots of $\log Q_e$ *vs* $\log C_e$ (Figure 9a) and tabulated in Table 4.

3.3.2 Langmuir adsorption isotherm

The Langmuir isotherm was used to measure linear adsorption with low densities of adsorption, and overall surface coverage with higher CMC amounts. Monolayer adsorption of an adsorbed CMC species to a homogeneous surface has been calculated and the data evaluated in linear form (Eqn. 3)[85].

$$\frac{Ce}{Qe} = \frac{1}{q_{\max} K_F} + \frac{Ce}{q_{\max}} \qquad (3)$$

Where *Ce* = The equilibrium concentration (mg/L); *Qe* = The amount adsorbed at equilibrium (mg g^{-1}); Q_{max} and K_L = Langmuir constants associated with adsorption efficiency and energy of adsorption.

The linear plots of Ce/Qe ***vs*** Ce support the applicability of the Langmuir isotherms and it was found best fitted among studied models in the present study (Figure 9b). The values of Langmuir parameters were determined from slope and intercepts and

tabulated in Table 4. It was assumed that the monolayer adsorption took place onto FA surface with a finite number of similar homogeneous active sites as defined by the equation. [87] The values of n>1 indicate that the adsorption process is favourable in given conditions. The values of linear determination coefficient (R^2 = 0.9796) was high for Freundlich isotherm in comparison to Langmuir isotherm (R^2=0.9569) which confirms that Frendulich isotherm is more favourable adsorption of CMC onto FA.

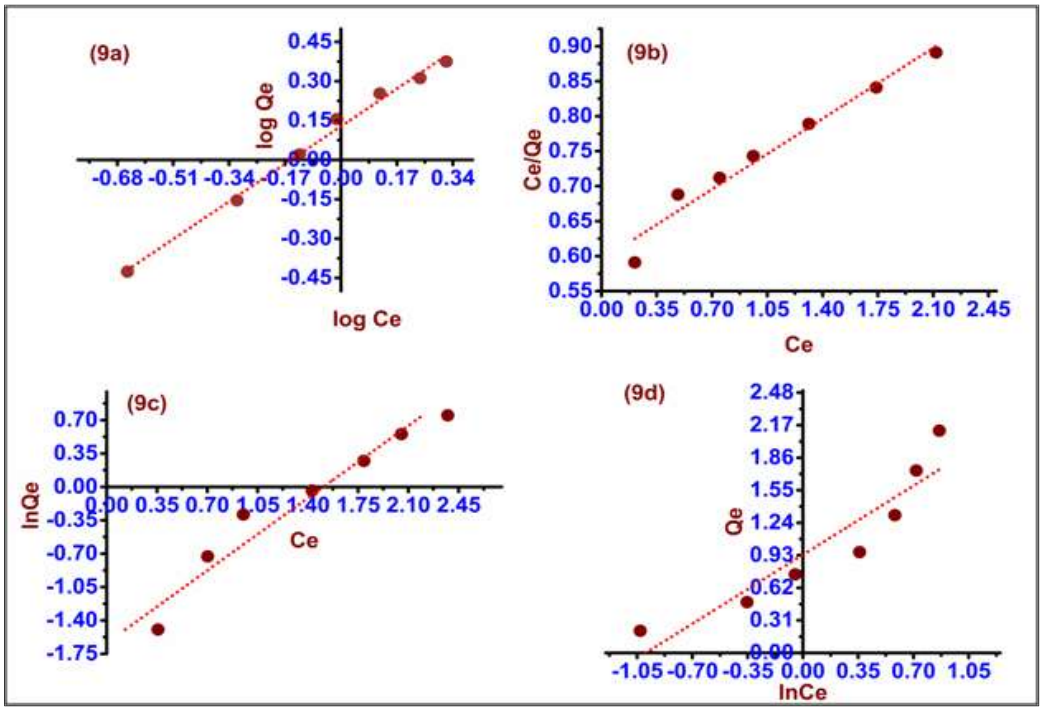

Figure 9. Plots illustrating various adsorption models (9a). Freundlich, (9b). Langmuir, (9c). Jovanovic and (9d) Temkin isotherm

3.3.3 Jovanovic isotherm

This adsorption isotherm was employed on the assumptions contained in the Langmuir model, additionally the possibility of some mechanical contacts between the CMC and FA. The linearized form of this isotherm is given as follows [88]:

$$\ln Qe = \ln q_{\max} - K_J Ce \qquad (4)$$

Where, Qe is the amount of CMC in the FA at equilibrium (mg/g), $q_{\max}$ is maximum uptake of CMC obtained from the plot of ln Qe *vs* Ce (Figure 9c) and K_J is Jovanovich constant (Table 4) the plot axis were interconverted.

Table 4 Isotherm parameters obtained from the fit of various models presented in figure 9

Isotherm models	Parameters		Determination coefficient (R^2)
Langmuir	q_{max} = 6.94±0.01 mg/g	K_L= 1.80±0.00 L/mg	0.9933
Freundlich	n = 1.20±0.009	K_F =1.34±0.01 (mg/g) $(L/mg)^{1/n}$	0.9830
Jovanovic	q_{max} = 4.52±0.0.11 mg/g	K_J = 0.93±0.15 L/mg	0.9428
Temkin	K_T = 2.71±0.12mg/L	B =0.94±0.02L/g b=2.65±0.03 KJ/mol	0.8667

3.3.4 Temkin isotherm

Temkin isotherm model was applied to explain the effects of indirect CMC/FA interactions within an intermediate range of concentrations of CMC on the adsorption process. The linear form of the Temkin equation is given below [89]:

$$Qe = B\ln K_T + B\ln Ce \quad (5)$$

Where q_e is the amount of CMC adsorbed at equilibrium (mg/g); Ce is the concentration of CMC in solution at equilibrium (mg/L). B is a constant related to the heat of adsorption and it is defined by the expression B = RT/b, b is the Temkin constant (J/mol), T is the absolute temperature (K), R is the gas constant (8.314 J/mol.K), and K_T is the Temkin isotherm constant (L/g). From the plot of Qe *vs* lnCe (Figure 9d) B and K_T can be calculated from the slope (B) and intercept (Bln K_T), respectively. The estimated values of K_T, B and b (Table 4) were an indication of a physical adsorption process (Table 3, 4).

3.4. Theoretical aspects

The QCCs have been carried out using Gaussian 09 electronic structure calculations package installed at Linux workstation with the deployment of Becke's three-parameter hybrid exchange and Lee-Yang-Parr correlation functionals (B3LYP)[90-92] and Pople's 6-31+G (d, p) basis set. Notably, no imaginary frequencies were found for all the

minima in the potential energy surface at all the theoretical levels investigated in this work for all the optimized adsorbate, adsorbent, and the corresponding dimer constructing the adsorbate-adsorbent complex (AAC). A very famous Bader's QTAIM was used to achieve more insights into the kind, nature, and strength of NCIs involved in the AAC[93].

According to the findings based on the QCCs, the adsorbate [dimer unit (α-D glucose) of the carboxymethyl cellulose (CMC)] was agglomerated at the solid surface FA derived from PP (*i.e.* OH, CO, CHO, and COOH functionalized coronene) which is stabilized by the intermolecular NCIs.

Assembling a three-dimensional adsorbent-adsorbate (FA/CMC) interfacial composition, the FA accumulation theoretical model has been put forwarded in this report. To get more facets about the chemisorptions of the CMC on the FA surface (*i.e.* CMC coverage and CMC adsorption energy with the FA surface), this molecular modelling approach provides subtle information *via* formation of conventional and nonconventional NCIs between the adsorbate (CMC) and adsorbent (FA) interface. A detailed report on the geometry, stability, and electronic features of the adsorbent (FA), adsorbate (CMC) and their associated dimer complex (FA-CMC) (*i.e.* AAC) has been carried out here in the present work is shown.

3.4.1 Structural features and energetic study

Let us start the discussion by looking into Figure. 10 (optimized structures of the adsorbate CMC (Figure 10a) and adsorbent FA (Figure 10b) monomer units, respectively) and Figure 11 (optimized structure of the FA-CMC complex) with proper atomic labelling. In the adsorbent FA model system, the central benzene fragment contains one CHO, one OH, and one COOH group and the outer benzene rings contain scattered OH, CHO, CO, and COOH functional groups. To look into the conventional and nonconventional NCIs (*i.e.* a range of weak to medium inter- and intramolecular interactions) involved in the AAC system, we adopt here as an approximation based on the theory that the CMC (adsorbate) is located over the FA (adsorbent). A few selected and important structural parameters of the covalent associated H-bonded fragments (D-H---A, where D is a proton donor and A is proton acceptor) including NCIs of the equilibrium structure (gas phase) of the FA-CMC model interface can be seen in Table 5. To maximize the number of NCIs (*i.e.* H-bonding between adsorbate and adsorbent) involved in the dimer complex AAC, fine-tuning was done in the original geometries of the AAC. Furthermore, computational modelling has been deployed from only a

single side of the adsorbent surface approach in attaining the preferable binding interactions engaged in the AAC system. It should be noted that the theoretical study on only the intermolecular NCIs have been focused herein as such type of interactions is dominantly engaged to stabilize the AAC complex.

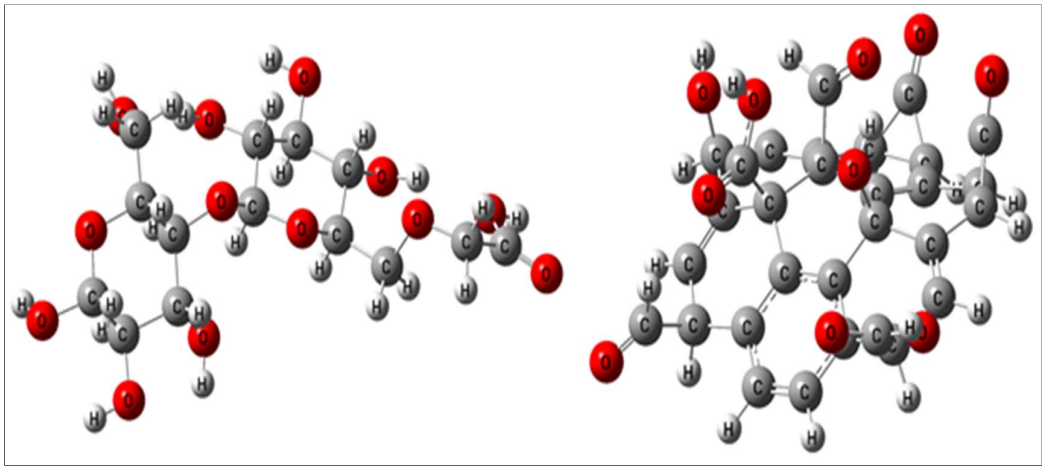

Figure 10. Optimized (equilibrium) structures of the (10a) CMC (Adsorbate, left side) and (10b) FA (Adsorbent, right side) models at M06-2X/6-31+G (d, p) level of theory

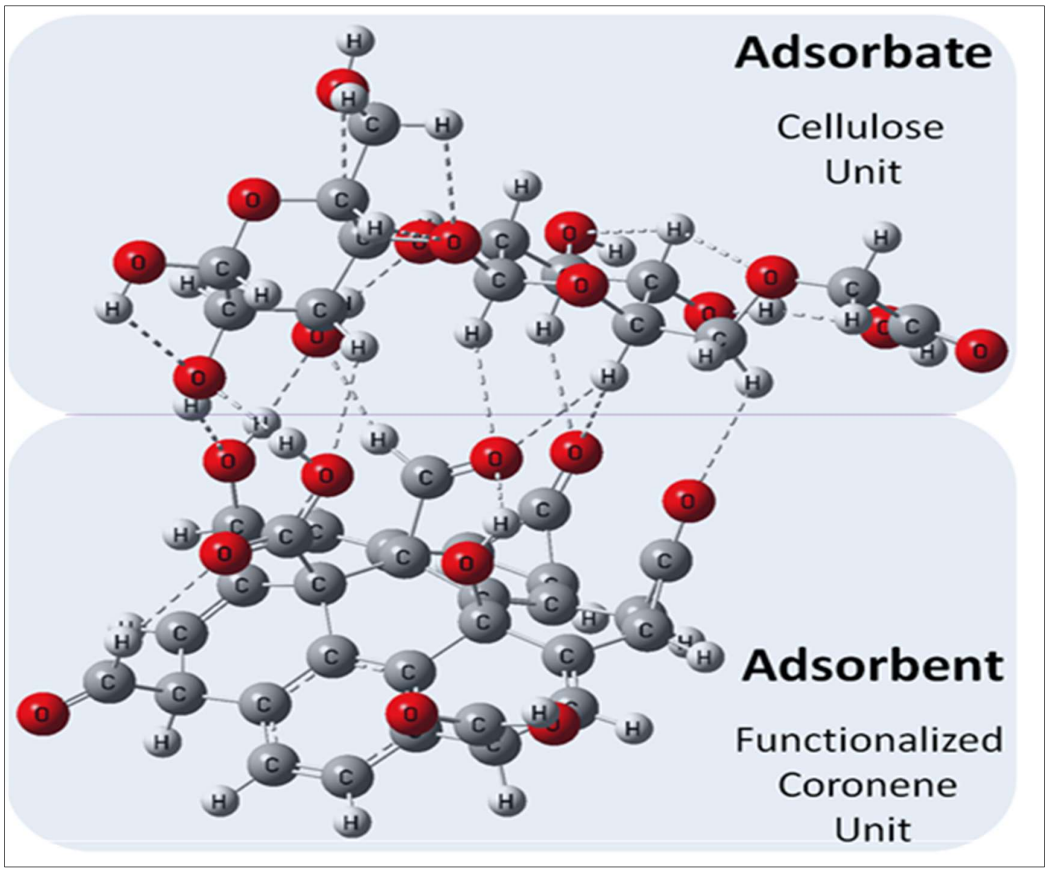

Figure 11. Optimized (equilibrium) structure of the FA-CMC model at M06-2X/6-31+G (d, p) level of theory

Table 5 Some selected covalent bonds associated with the NCIs of monomers CMC (adsorbate) and FA (adsrobent) and dimer complex FA-CMC at the B3LYP and M06-2X levels of theories using 6-31+G (d, p) basis set

System	Intermolecular H-bonds and NCIs (B3LYP/6-31+G (d, p), M06-2X/6-31+G (d, p))
Adsorbate (CMC)	O27-H44 (0.968, 0.966), C32-H23 (1.101, 1.102), C2-H10 (1.099, 1.101), C16-H7 (1.103, 1.104), C4-H12 (1.103, 1.104), C13-H42 (1.098, 1.099)
Adsorbent (FA)	O87-H88 (0.968, 0.965), O102-H103 (0.973, 0.970), C89-H91 (1.098, 1.098)
Adsorbent - Adsorbate complex (FA-CMC)	Adsorbate (CMC) O27-H44 (0.974, 0.974), C32-H23 (1.098, 1.102), C2-H10 (1.102, 1.104), C16-H7 (1.101, 1.101), C4-H12 (1.101, 1.101), C13-H42 (1.098, 1.099)
	Adsorbent (FA) O87-H88 (0.977, 0.973), O102-H103 (0.979, 0.980), C89-H91 (1.095, 1.096)

Here our main objective is to focus on the intermolecular NCIs involved in the AAC. The QTAIM picture of Figure 12 clearly shows that the C32, C2, C16, C4, and C13 atoms of the adsorbate (CMC) act as a proton donor and connected to O102, two O atoms (O24 and O90), O95, two O atoms (O90 and O95), and O209 of the adsorbent (FA) working as proton acceptor *via* the bridging hydrogen atoms H23, H10, H7, H12, and H42, respectively and are responsible for constructing the NCIs. On the other hand, the C89 atom of the adsorbent (FA) works to play a role as a proton donor linked to the O24 atom of the adsorbate (CMC) *through* H91 and forms NCIs. Moreover, it is very interesting to note that the O atoms (O27 of the adsorbate and O87 and O102 of the adsorbent) act as proton donor as well as proton acceptor and the HBs constructed by these O atoms form conventional *medium* (O–H--O) HBs which connect both monomer units FA and CMC as displayed in Figure 12. Such three *medium* O-H---O HBs (O27-H44---O87, O87-H88---O24, and O102-H103---O27) and seven *weak* C-H---O HBs (see in Table 6) have the major role for stabilizing the AAC structure which is formed between the HB donor and acceptor positions of the adsorbate to the supplementary sites of the adsorbents. The outcomes of the energetic features have been given in Table 6. The BEs using two different computational approaches (B3LYP and M06-2X in the gas phase) have also been calculated to get a clear insight into the stability pattern. The DFT based BE is found to be -6.3 kcal/mol whereas using the DFT-D approach the BE has been calculated as -64.6 kcal/mol. The DFT-D based BE is much higher (the

difference between the DFT-D and DFT based BE: -58.3 kcal/mol) is due to the presence of the dispersion correction term.

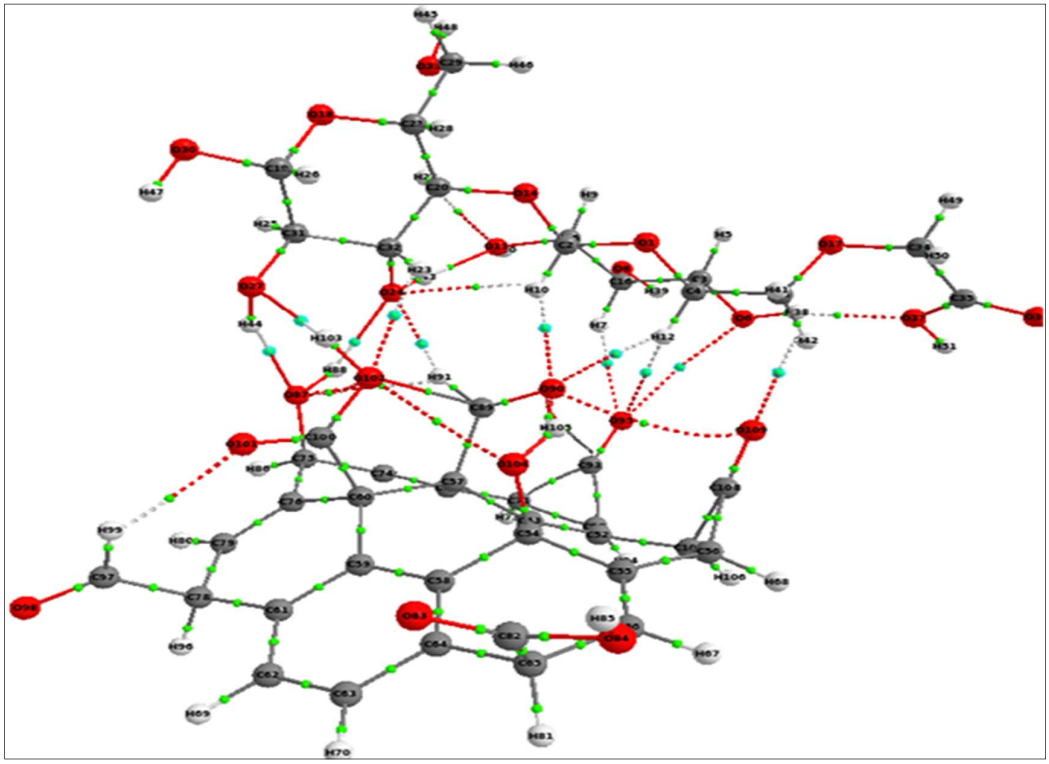

Figure 12. QTAIM molecular graph showing the different BCPs of the AAC (FA-CMC) calculated at M06-2X/6-31+G(d,p) level of study

Table 6 Some selected and important QTAIM based parameters (for intermolecular NCIs only) of the AAC at M06-2X/6-31+G (d, p) level of theory

	BL(Å)	**BPL(Å)**	***ρ* (au)**	**$\nabla^2\rho$ (au)**	***V(r)* (kcal/mol)**	**DI (au)**
Conventional H-bond						
O27-H44···O87	1.930	1.973	0.0230	+0.0800	-6.2	0.0573
O87-H88···O24	1.949	1.989	0.0251	+0.0831	-6.8	0.0545
O102-H103···O27	1.997	2.047	0.0245	+0.0764	-6.5	0.0513
C89-H91···O24	2.206	2.229	0.0174	+0.0505	-4.4	0.0541
C16-H7···O95	2.401	2.424	0.0104	+0.0359	-2.3	0.0391
C4-H12···O95	2.418	2.443	0.0096	+0.0345	-2.2	0.0330
C2-H10···O90	2.501	2.523	0.0097	+0.0316	-2.2	0.0326
C32-H23···O102	2.541	2.580	0.0083	+0.0309	-1.8	0.0258
C4-H12···O90	2.605	2.638	0.0070	+0.0253	-1.5	0.0222
C13-H42···O109	2.709	2.832	0.0064	+0.0259	-1.3	0.0199
Nonconventional bond path						
O6···O95	3.364	3.379	0.0036	+0.0159	-1.6	0.0167

Table 7. The electronic parameters HOMO (in eV), LUMO (in eV), HOMO-LUMO gap (in eV), and binding energy (BE) (kcal/mol) at B3LYP and M06-2X levels of theories using 6-31+G (d, p) basis set

Parameter	**Adsorbent (Coronene)**	**Adsorbate (Sucrose)**	**Adsorbent-adsorbate (FA-CMC) complex**
HOMO	-6.508, -7.843	-6.732, -8.441	-6.582, -8.021
LUMO	-2.140, -1.004	-0.710, -0.103	-2.272, -1.192
HLEG	4.368, 6.839	6.022, 8.338	4.310, 6.829
Binding energy (BE)	—	—	-6.3, -64.6

3.4.2. QTAIM analyses

To get a clear insight into the structure, reactivity, and interaction(s) any polyatomic chemical species, Bader's QTAIM [93] tool is extensively used. Among all four types of the critical points (see reference 138 for more details) given by Bader [94], the bond critical point (BCP) is incredibly useful regarding the atomic interaction studies. To understand better the molecular structure in terms of binding features, of course, the BCP describes (a necessary and sufficient condition) the binding interaction and NCIs by holding a BP between two atoms and well known as a bond path (BP). The QTAIM picture of the CMC-FA can be seen in Figure 12. Several selected and useful QTAIM based topological parameters related to the NCIs like bond path length (BPL), electron density (ED) $\rho(r)$, Laplacian of ED $[\nabla^2\rho(r)]$, potential energy density V(r), and the delocalization index DI can be seen from Table spectroscopy. A detailed study on such kinds of NCIs can be seen in the literature [95, 96].

The BCPs are denoted as light green points (tiny solid sphere). The BCPs having medium size light greenish-blue solid spheres as indicated in the region between the adsorbent and adsorbate play the main role in stabilizing the AAC *via* the formation of intermolecular NCIs (see Figure 12). Ten NCIs (three *medium* O-H---O and seven *weak* C-H---O) can be seen from the given below QTAIM molecular graph in which interestingly, the C4-H12 proton donor covalent bond forms two bifurcated HBs as C4-H12---O90 and C4-H12---O95 and stabilizes the AAC.

The energy of intermolecular/stabilizing primary (covalent) interactions or secondary (*i.e.* NCIs) (formula given below) can be calculated by using the QTAIM approach [97]:-

$$E = 1/2V(r) \sim E = 313.754\ V(r) \quad (6)$$

Where E is the energy of intra-/intermolecular (stabilizing) primary or NCIs (in au or kcal/mol) and V(r) is potential energy density.

The possibility of the accumulation of charge at a point surface directly renders the sign of the Laplacian operator at a BCP, $\nabla^2\rho(r)$. In the case of covalent (primary) interaction, the values of topological parameters $\nabla^2\rho(r)$ and $\rho(r)$ are less than zero and greater than 0.1 au, correspondingly. Such values for the aforementioned parameters are always greater than zero for closed-shell interaction(s) like HBs and NCIs. The $\rho(r)$ values are generally small magnitude *i.e.* in the order of 0.01 for the HB and ~0.001 au for van der Waals' type NCI. The values of some given parameters at the BCP primarily fix on the chemical interaction features by using the QTAIM technique. All topological parameters given in Table 7, are measured in au despite the intermolecular interaction energy (in kcal/mol).

In general, the $\rho(r)$, $\nabla^2\rho(r)$, V(r) (magnitude), and DI values become lower as there is an enhancement in the BL and BPL parameters which are very helpful to investigate more crucial insights into the structural feature analyses of any species. The bond order directly interprets the delocalization index (DI). For example, here the connection between the BL as well as BPL and the DIs falls reciprocally. The order of BL and BPL is O27-H44---O87 (BL: 1.930 Å, BPL: 1.973 Å) < O87-H88---O24 (BL: 1.949 Å, BPL: 1.989 Å) < O102-H102---O27 (BL: 1.997 Å, BPL: 2.047 Å) while the DI values (in au) are coming in the reverse order: O27-H44---O87 (0.0573) > O87-H88---O24 (0.0545) > O102-H102---O27 (0.0513). However correspondingly, a mixed effect has been observed, in which the previously mentioned relationship is different: O27-H44---O87 [$\rho(r)$: 0.0230 au, $\nabla^2\rho(r)$:+0.0800 au, V(r):-6.2 kcal/mol] < O87-H88---O24 [$\rho(r)$: 0.0251 au, $\nabla^2\rho(r)$:+0.0831 au, V(r):-6.8 kcal/mol] > O102-H102---O27 [$\rho(r)$: 0.0245 au, $\nabla^2\rho(r)$:+0.0764 au, V(r):-6.5 kcal/mol]. Similarly except a few one, there is expected order of the BL, BPL, $\nabla^2\rho(r)$, V(r) (magnitude), and DI values in the case of C-H---O type interactions linked *via* the BP as mentioned the connection between the geometrical and topological parameters (see Table 7). Despite these NCIs, another nonconventional intermolecular bond path (*i.e.* BCP) between the O6 atom of the CMC adsorbate and O95 atom of the FA adsorbent monomer units, has been detected in the QTAIM analyses for which the topological parameters are: [BL: 3.364 Å, BPL: 3.379 Å, $\rho(r)$: 0.0036 au, $\nabla^2\rho(r)$:+0.0159 au, V(r):-1.6 kcal/mol, and DI: 0.0167 au) [98].

3.4.3. Chemical reactivity

A huge application of the frontier molecular orbital (FMO) approach, for instance, the highest occupied molecular orbital (HOMO), lowest unoccupied molecular orbital (LUMO) is routinely used in the field of quantum chemical calculations.[99] The HOMOs, LUMOs, their energy difference (HLED) and their other associated parameters are mostly used in studying the electrical transport features of conjugated π-electron species as well as in measuring the capability of a species to interact with the other system [100-102] The molecular activity and the tendency of a system to absorb the light can also be obtained by the deployment of the HLED parameter. The larger FMO (HOMO-LUMO) gap between the HOMO and LUMO allows the reduced tunnelling of photo/thermally excited electrons and since establishes the electronic transport features. In any molecular system, there is a vital role of HOMOs and LUMOs in the chemical reaction where the ground state of the species is indicated by the HOMO and the first excited state is exposed by the LUMO. Therefore, the charge transfer from one site to another site with the same molecular species can be obtained directly in terms of the electronic transition occurring from the HOMO to LUMO.

A molecular system having a large HLED value reveals to show less polarizable nature demonstrating its low chemical reactivity (*i.e.* high kinetic stability) [103]. Using two distinct computational B3LYP and M06-2X approaches, the HLED values for the optimized H-bonded AAC have been calculated as 4.310 eV and 6.829 eV, respectively. By looking into the HLED values (see Table **7**) of the adsorbate (CMC), adsorbent (FA), and the FA-CMC complex, it seems that the AAC is chemically the most reactive (lowest HLED values).

The HOMO and LUMO FMOs surface plots of the AAC system have been displayed in figure 13 which were drawn by the DFT-D method. From the above figure 13, it can be seen that the HOMOs are primarily spread over the C cyclic framework of the five benzene rings of the functionalized coronene (adsorbent - FA) monomer unit. A small contribution of HOMOs are located over the C ring framework of the sixth outer benzene ring of the coronene (adsorbent) and no HOMOs were seen at the central benzene ring of FA monomer. Furthermore, the LUMOs are positioned over the same side of the adsorbent-adsorbate system consisting of the HOMOs and are spread over *via* one of the outer C benzene ring frameworks of the FA monomer along with the adjacent C atoms attached to the aforementioned ring framework.

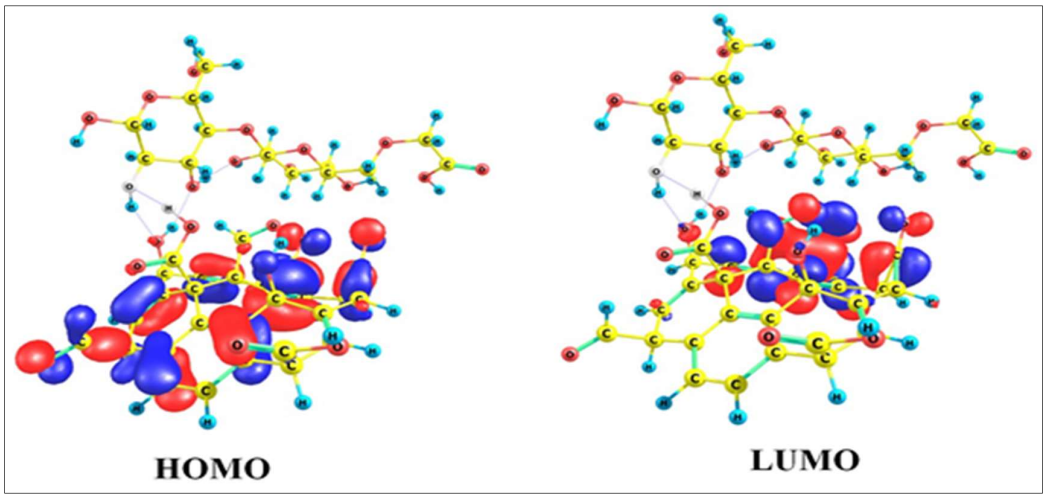

Figure 13. The HOMO and LUMO surfaces of the optimized (equilibrium) structures of the AAC at M06-2X/6-31+G (d, p) level of theory

An effective contribution has also been seen on the carbonyl group of the FA fragment. Since from the figure 13, it reveals that the electronic transition takes part from the HOMO to the LUMO *via* an exchange of the ED from some outer benzene rings of the adsorbent to the other benzene ring consisting of the CO and CHO functional group in the same molecular species.

3.4.4. Molecular electrostatic potential (MESP) surface

The molecular size, shape, and charge distribution can be simultaneously exhibited by the MESP. The MESP well linked with the ED is widely used to understand the relative polarity, the electrophilic and nucleophilic attack [104], NCIs, and the analyzing route based on 'recognition' of one molecular system by another [105]. The MESP map of the adsorbent-adsorbate pair can be seen in Figure 14. With the help of three-dimensional MESP surface plot, the reactivity nature of the species can be presumed. In the Figure 14, the electron-rich region (reactive site) is considered in the red colour scheme showing the absolute negative charge distribution and since there may be a high probability of electrophilic attack. Negative regions are positioned over the O atom of the OH group and all the C-O-C linkage of the monomer CMC. A small negative region is filled on the O atom of the OH group of the other monomer FA. The blue colour scheme is the diagnostic of nucleophilic attack depicting the strong positive region. The positive potential lies around the H atom of the COOH functional group of the CMC (dimer unit of glucose) as well as the FA monomer. As a potential halfway between the

two extremes blue and red region is demonstrated by the green colour scheme and this colour is indicative of a neutral region.

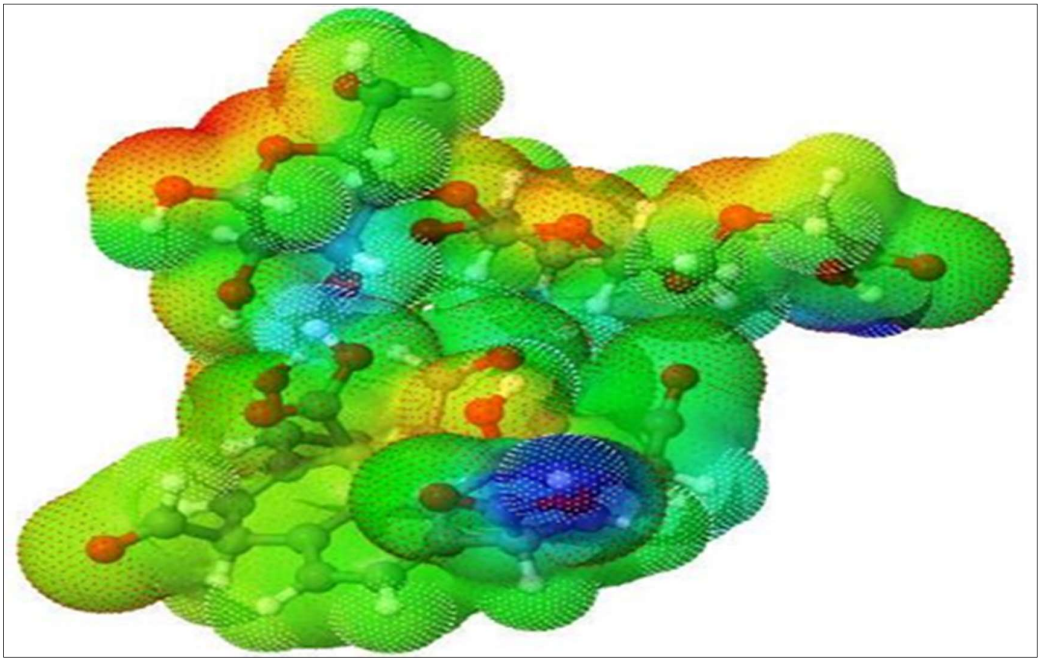

Figure 14. MESP plot of the CMC-FA system

3.4.5. Natural charge analyses (NPA)

For any molecular system, the natural population analysis (NPA) obtained from QCCs, is a very renowned and largely used tool to analyze the electron population of each atom as defined in the basic function and is used to obtain the charge distribution on the nuclei, bond orders, and other connected noteworthy information. It is very interesting to note that the H-bonded O24 atom of the OH group of one monomer (*i.e.* adsorbate CMC) contains the most electronegative natural charge (-0.85104) whereas the most positive natural charge (+0.85653) is found for the C82 atom of the other monomer (*i.e.* adsorbent FA) using the DFT-D (M06-2X) level of study. Moreover, the DFT (B3LYP) approach gives a similar pattern showing the most electronegative (-0.83859) and electropositive (+0.83136) natural charges on the same as previously mentioned O and C atoms. Now if we look into total natural charges on the respective monomer units adsorbent (FA) and adsorbate (CMC), the charges based on (DFT-D, DFT) methods, are negative (-0.0104, -0.03143) and positive (0.03158, 0.02309), correspondingly which fairly illustrates that the FA monomer unit behaves like an electron acceptor because of having a total negative natural charge. More importantly, it appears that the formation of the intermolecular NCIs could be due to the survival of a net positive charge on the H atom and negative charges on the carbon and oxygen atoms.

4. Conclusions

The physiochemical parameters of functionalized accurel such as specific surface area (S_{BET}) =34.472 m^2/g, pore volume (Vp) =0.07-0.121 cm^3/g, total pore volume (Vtp) = 0.115 cm^3/g, mean pore diameter = 13.692nm and pore diameter =39.402nm was determined by BET method. The particle size and pXRD studies confirmed that FA possessed mesoporous and crystalline nature respectively. It was found that the adsorption of CMC on FA affected by the change of various factors like the initial concentration of CMC, FA dose, pH, ionic strength (0.1mol/L), temperature (℃), sonication (20 kHz) and the presence of urea (0.1mol/L). These observed results concluded that the non-covenant force played a significant role in the binding of CMC at FA/water interfaces. The results obtained from the FTIR analysis provided useful information on spectral changes which are attributed to hydrogen bonding between CMC and FA. The adsorption was observed as evidenced by changes in the IR frequencies of some main functional groups -OH, -C=O, -C-O, -C-H, and –COOH in which the -C–O stretch coupled to the -C–C stretch and -O–H deformation, were significant and thus support strong hydrogen bonding of CMC on FA surface. The presence of urea and sonication were found to reduce significantly which suggested that the role of hydrogen bonding is a predominant force rather than hydrophobic force. The batch shaking adsorption experiments with various parameters were tested and the equilibrium isotherm data were fitted with Freundlich, Langmuir, Temkin and Jovanovic models of adsorption and compared by linear regression coefficient (R^2) which obeyed the order as Langmuir (R^2=0.9933)> Freundlich (R^2=0.9830)>, Temkin (R^2=0.9428)> Jovanovic (R^2=0.8667). The adsorption free energy of CMC is close to that of physical adsorption suggesting H-bonding to be a dominant force for CMC (L2 type) adsorption. XPS analysis illustrated the binding of -OH groups available onto FA surface with carboxylate ions of the CMC confirmed the hydrogen bonding during adsorption. Thus, the present study provides substantial evidence to prove beyond doubt that adsorption of CMC onto FA surface governs by hydrogen bonding and other weak non-covalent interactions. Moreover, the theory-based quantum mechanical calculations provide a better understanding of the adsorbate – adsorbent binding features and to understand better such molecular agglomeration systems, this model could overlay a new insight in the area of food, pharmaceutical, and industrial chemistry.

References

1. Khalil, H.; Tye, Y.; Saurabh, C.; Leh, C.; Lai, T.; Chong, E.; et al. Biodegradable polymer films from seaweed polysaccharides: a review on cellulose as a reinforcement material. *Express Polym. Lett.* **2017**, 11, 244-265.
2. Arancibia, C.; Navarro-Lisboa, R.; Zúñiga, R.; Matiacevich, S. Application of CMC as thickener on nanoemulsions based on olive oil: physical properties and stability. *Int. J. Polymer Sci.* **2016**, 20, 1-11.
3. Vicent, M.; Greco F.; Nicholson, R.; Duncan, R. Polymer-drug conjugates as a novel combination therapy for the treatment of hormone-dependent cancers. *Angew. Chem. Int. Ed*. **2005**, 44, 2-6.
4. Hollabaugh, C.; Burt, L.H.; Walsh, AP. Carboxymethylcellulose. uses and applications. *Ind. Eng. Chem.* **1945**, 37, 943-7.
5. Kroschwitz, J. I. Concise encyclopedia of polymer science and engineering, John Wiley & Sons: New York, 1990; 1st Ed. 1st Ed, pp. xxiv + 1341.
6. Laskowski, JS.; Ralston J. Colloid chemistry in mineral processing, Elsevier Science; Amsterdam, **2015**; pp. 1-428.
7. Boruvkova, K.; Wiener J. Water absorption in carboxymethyl cellulose. *AUTEX Res. J*. **2011**, 11, 110-3.
8. Hamad, AM.; Ates, S.; Durmaz E. Evaluation of the possibilities for cellulose derivatives in food products. *Cellulose*. **2016**, 45, 42-2.
9. Priya, B.; Gupta, V. K.; Pathania, D.; Singha, A. S. Synthesis, characterization and antibacterial activity of biodegradable starch/PVA composite films reinforced with cellulosic fibre. *Carbohydr. Polym*. **2014**, 109, 171-179.
10. Gupta, V.; Carrott, P.; Singh, R.; Chaudhary, M.; Kushwaha, S. Cellulose: a review as natural, modified and activated carbon adsorbent. *Bioresour. Technol*. **2016**, 216, 1066-1076.
11. Ahmaruzzaman, M.; Gupta, V. K., Rice husk and its ash as low-cost adsorbents in water and wastewater treatment. Ind. Eng. Chem. Res. **2011**, 50, 13589-13613.
12. Ali, I.; Alharbi, O. M.; Alothman, Z. A.; Alwarthan, A., Facile and eco-friendly synthesis of functionalized iron nanoparticles for cyanazine removal in water. *Colloid Surface B*. **2018**, 171, 606-613.
13. Prasad, M.S. Reagents in the mineral industry-recent trends and applications. *Miner. Eng.* **1992**, 5, 279-294.

14. Raju, GB.; Holmgren, A.; Forsling, W. Complexation mechanism of dextrin with metal hydroxides. *J. Colloid Interface Sci*. **1998**, 200, 1-6.
15. Liu, Q.; Laskowski, J. The role of metal hydroxides at mineral surfaces in dextrin adsorption, ii. chalcopyrite-galena separations in the presence of dextrin. *Int. J. Miner. Process*. **1989**, 27, 147-55.
16. Liu, Q.; Laskowski J. The role of metal hydroxides at mineral surfaces in dextrin adsorption, i. studies on modified quartz samples. *Int. J. Miner. Process*. **1989**, 26, 297-316.
17. Mackenzie, M.; Malhotra, I.; Riggs, D. Chemical reagents in the mineral processing industry. *Soc. Min.Eng.*. **1986**, 1, 139-45.
18. Pugh, R. Macromolecular organic depressants in sulphide flotation—a review, 1. principles, types and applications. *Int. J. Miner. Process*. **1989**, 25, 101-30.
19. Pugh R. Macromolecular organic depressants in sulphide flotation—a review, 2. theoretical analysis of the forces involved in the depressant action. *Int. J. Miner. Process*. **1989**, 25, 131-46.
20. Healy T. Principles of adsorption of organics at solid-solution interfaces. *J. Macrom. Sci. Chem*. **1974**, 8, 603-19.
21. Rath, RK.; Subramanian, S.; Laskowski J. Adsorption of dextrin and guar gum onto talc. a comparative study. *Langmuir*. **1997**, 13, 6260-6.
22. Steenberg E. The depression of the natural floatability of talc: the mechanism involved in the adsorption of organic reagents of high molecular mass, PhD Thesis, **1982**.
23. Peter, J.; Steenberg E. Adsorption of carboxymethylcellulose, guar gum, and starch onto talc, sulphides, oxides, and salt-type minerals. *S. Afr. J. Chem*. **1984**, 37, 85-90.
24. Jenkins, P.; Ralston, J. The adsorption of a polysaccharide at the talc–aqueous solution interface. *Colloids Surf. A Physicochem. Eng. Asp.*. **1998**, 139, 27-40.
25. Laskowski, J.. Processing of Hydrophobic Minerals and Fine Coal: Canadian Institute of Mining, Metallurgy and Petroleum; **1995**.
26. Jucker, B.; Harms, H.; Hug, S.; Zehnder A. Adsorption of bacterial surface polysaccharides on mineral oxides is mediated by hydrogen bonds. *Colloids and Surfaces B: Biointerfaces*. **1997**, 9, 331-43.
27. Wang, J.; Somasundaran P. Adsorption and conformation of carboxymethyl cellulose at solid-liquid interfaces using spectroscopic, AFM and allied techniques. *J. Colloid Interface Sci*. **2005**, 291, 75-83.

28. Cuba-Chiem LT, Huynh L, Ralston J, Beattie DA. In situ particle film ATR-FTIR spectroscopy of carboxymethyl cellulose adsorption on talc: Binding mechanism, pH effects, and adsorption kinetics. *Langmuir*. **2008**, 24, 8036-44.
29. Fujimoto, J.; Petri, D. Adsorption behaviour of carboxymethylcellulose on amino-terminated surfaces. *Langmuir*. **2001**, 17, 56-60.
30. Beaussart, A.; Mierczynska, V.A.; Beattie, DA. Evolution of carboxymethyl cellulose layer morphology on hydrophobic mineral surfaces: variation of polymer concentration and ionic strength. *J. Colloid Interface Sci*. **2010**, 346, 303-10.
31. Stuart, MC.; Fokkink, R.; Van der Horst, P.; Lichtenbelt, JT. The adsorption of hydrophobically modified carboxymethylcellulose on a hydrophobic solid: effects of pH and ionic strength. *Colloid Polym. Sci*. **1998**, 276, 335-41.
32. Hoogendam, C.; De Keizer, A.; Cohen Stuart, M.; Bijsterbosch, B.; Batelaan, J.; Van der Horst, P. Adsorption mechanisms of carboxymethyl cellulose on mineral surfaces. *Langmuir*. **1998**, 14, 3825-39.
33. Bacchin, P.; Bonino, J-P.; Martin, F.; Combacau, M.; Barthes, P.; Petit, S.; et al. Surface pre-coating of talc particles by carboxyl methylcellulose adsorption: Study of adsorption and consequences on surface properties and settling rate. *Colloids Surf. A Physicochem. Eng. Asp.*. **2006**, 272, 211-9.
34. Phenrat, T.; Saleh, N.; Sirk, K.; Kim, H-J.; Tilton, RD.; Lowry, GV. Stabilization of aqueous nanoscale zerovalent iron dispersions by anionic polyelectrolytes: adsorbed anionic polyelectrolyte layer properties and their effect on aggregation and sedimentation. *J. Nanopart Res*. **2008**, 10, 795-814.
35. Sedeva, IG.; Fornasiero, D.; Ralston, J.; Beattie, DA. Reduction of surface hydrophobicity using a stimulus-responsive polysaccharide. *Langmuir*. **2010**, 26, 15865-74.
36. Duker, E.; Lindström, T. On the mechanisms behind the ability of CMC to enhance paper strength. *Nordic Pulp Paper Res. J.*. **2008**, 23, 57-64.
37. Rakkolainen, M.; Kontturi, E.; Isogai, A.; Enomae, T.; Blomstedt, M.; Vuorinen, T.; Carboxymethyl cellulose treatment as a method to inhibit vessel picking tendency in printing of eucalyptus pulp sheets. *Ind. Eng. Chem. Res*. **2009**, 48, 1887-92.
38. Zemljič, LF.; Stenius, P.; Laine, J.; Stana-Kleinschek, K. Topochemical modification of cotton fibres with carboxymethyl cellulose. *Cellulose*. **2008**, 15, 315-21.

39. Orelma, H.; Filpponen, I.; Johansson, L-S.; Laine, J.; Rojas, OJ. Modification of cellulose films by adsorption of CMC and chitosan for controlled attachment of biomolecules. *Biomacromolecules*. **2011**, 12, 4311-8.
40. Filpponen, I.; Kontturi, E.; Nummelin, S.; Rosilo, H.; Kolehmainen, E.; Ikkala, O.; et al. Generic Method for modular surface modification of cellulosic materials in aqueous medium by sequential "click" reaction and adsorption. *Biomacromolecules*. **2012**, 13, 736-42.
41. Orelma, H.; Teerinen, T.; Johansson, L-S.; Holappa, S.; Laine, J. CMC-modified cellulose biointerface for antibody conjugation. *Biomacromolecules*. **2012**, 13, 1051-8.
42. Mohan, T.; Kargl, R.; Köstler, S.; Doliška, A.; Findenig, G.; Ribitsch, V, et al. Functional polysaccharide conjugates for the preparation of microarrays. *ACS Appl. Mater. Inter*. **2012**, 4, 2743-51.
43. Kulterer MR, Reichel VE, Kargl R, Köstler S, Sarbova V, Heinze T, et al. Functional polysaccharide composite nanoparticles from cellulose acetate and potential applications. *Adv. Funct. Mater*. **2012**, 22, 1749-58.
44. Gilli, E.; Horvath, A.; Horvath, A.; Hirn, U.; Schennach, R. Analysis of CMC attachment onto cellulosic fibres by infrared spectroscopy. *Cellulose*. **2009**, 16, 825-32.
45. Laine, J.; Lindström, T. Studies on topochemical modification of cellulosic fibres. *Nordic Pulp Paper Res. J.*. **2000**, 15, 520-6.
46. Laine, J.; Lindström, T.; Nordmark, GG.; Risinger, G. Studies on topochemical modification of cellulosic fibres. *Nordic Pulp Paper Res. J.*. **2002**, 17, 50-6.
47. Mohan, T.; Kargl, R.; Doliška, A.; Vesel, A.; Köstler, S.; Ribitsch, V.; et al. Wettability and surface composition of partly and fully regenerated cellulose thin films from trimethylsilyl cellulose. *J. Colloid Interface Sci*. **2011**, 358, 604-10.
48. Mohan, T.; Kargl, R.; Doliška, A.; Ehmann, HM.; Ribitsch, V.; Stana-Kleinschek K. Enzymatic Digestion of Partially and fully regenerated cellulose model films from trimethylsilyl cellulose. *Carbohydr. Polym*. **2013**, 93, 191-8.
49. Liu, Z.; Choi, H.; Gatenholm, P.; Esker, AR. Quartz crystal microbalance with dissipation monitoring and surface plasmon resonance studies of carboxymethyl cellulose adsorption onto regenerated cellulose surfaces. *Langmuir*. **2011**, 27, 8718-28.
50. Amim, J.; Kosaka, PM.; Petri, DFS. Characteristics of thin cellulose ester films spin-coated from acetone and ethyl acetate solutions. *Cellulose*. **2008**, 15, 527-35.

51. Kargl, R.; Mohan, T.; Bračič, M.; Kulterer, M.; Doliška, A.; Stana-Kleinschek K, et al. Adsorption of carboxymethyl cellulose on polymer surfaces: evidence of a specific interaction with cellulose. *Langmuir*. **2012**, 28, 11440-7.
52. Kondo, T.; Sawatari, C.; Manley, RSJ.; Gray, DG. Characterization of hydrogen bonding in cellulose-synthetic polymer blend systems with regioselectively substituted methylcellulose. *Macromolecules*. **1994**, 27, 210-5.
53. Ozaki, K.; Sumitomo, N.; Ito, S. Molecular cloning and nucleotide sequence of the gene encoding an endo-1, 4-β-glucanase from Bacillus sp. KSM-330. *Microbiology*. **1991**, 137, 2299-305.
54. Li, H-G.; Wu, G.; Chen, H-Z.; Wang, M. Solution-processed organic UV photodetectors based on polyfluorene and naphthalene diimide. *Curr. Appl. Phys*. **2011**, 11, 750-4.
55. Singh, K.; Bharose, R.; Singh, VK.; Verma, SK. Sugar decolourization through selective adsorption onto functionalized accurel hydrophobic polymeric support. *Ind. Eng. Chem. Res.* **2011**, 50, 10074-82.
56. Singh, K.; Singh, V.K.; Verma, S.K.; Bhaarose, R.; Suman, A. Characterization of modified polypropylene powder(Accurel) and it's use for adsorption of phenols from aqueous solution. *Indian J.Chem.Technol*. **2013**, 20,385-39.
57. Guoliang Tao, Aijun Gong, Jianjun Lu, Hung-June Sune, David E. Bergbreither, Surface functionalized polypropylene: Synthesis, characterisation and adhesion properties, Macromolecules, **2001**, 34,7672-7679.
58. DuBios, M.; Gilles, K.A.; Hamilton, JK.; Rebers, PA.; Smith, F. Colorimetric method for determination of sugars and related substances. *Anal. Chem*. **1956**, 28, 350-356.
59. Anderson, M. J.; Whitcomb, P. J.; Simplified: RSM. Optimizing Processes Using Response Surface Methods for Design of Experiments, Productivity Press, New York, NY, **2005**.
60. Sabbani, S.; Hedenstrom, E.; Nordin, O. The Enantioselectivity of Candida Rugosa Lipase Influenced by the Particle Size of the Immobilizing Support Material. *J. Mol. Catal. B: Enzym*. **2006**, 42, 1.
61. Salis, A.; Sanjust, E.; Solinas, V.; Monduzzi, M. Characterization of accurel MP 1004 polypropylene powder and its use as a support for lipase immobilization. *J. Mol. Catal. B: Enzym*. **2003**, 2425, 75.

62. Sher, P.; Ingavle, G.; Ponrathnam, S.; Pawar, A. M. Low density porous carrier based conceptual drug delivery system. *Microporous Mesoporous Mater*. **2007**, 102, 290.
63. Singh, K.; Kumar, A.; Awasthi, S.; Pandey, SK.; Mishra, P. Adsorption mechanism of carboxymethyl cellulose onto mesoporous mustard carbon: Experimental and theoretical aspects. *Colloids and Surfaces A: Phys. Eng. Asp*. **2019**, 581, 123786.
64. Singh; K. Kumar, A. Adsorption and conformation of carboxymethyl cellulose at TiO_2 modified mesoporous carbon derived from mustard cake. *GCGHGSPCT-2k19*, **2019**, pp131-150.
65. Goldstein, J. I.; Newbury, D. E.; Joy, D. C.; Lyman, C.; E.; Echlin, P.; Lifshin E.; Sawyer, L.; Michael, J.. Scanning electron microscopy and X-ray microanalysis. 3rd ed. New York: Springer. **2003.**
66. Chowdhury, F.; Neale, S. Acid behaviour of carboxylic derivatives of cellulose. part i. carboxymethylcellulose. *J. Polym. Sci. A1*.. **1963**, 1, 2881-91.
67. Chowdhury, F.; Neale, S. Acid behaviour of carboxylic derivatives of cellulose. part ii. oxycellulose. *J. Polym. Sci. A1*. **1963**, 1, 2893-904.
68. Brunauer S.; Emmett, P.H.; Teller E. Adsorption of gases in multimolecular layers. *J. Am. Chem. Soc.* **1938**, 60, 309-19.
69. Barrett, E. P.; Joyner, L. G.; Halenda, P. P. The Determination of pore volume and area distributions in porous substances. i. computations from nitrogen isotherms. *J. Am. Chem. Soc.* **1951**, 73, 373-80.
70. Joyner, L. G.; Barrett, E. P.; Skold, R. The Determination of pore volume and area distributions in porous substances. ii. comparison between nitrogen isotherm and mercury porosimeter methods. *J. Am. Chem. Soc.* **1951**, 73, 3155-8.
71. Lippens, B.C.; de Boer, J.H.; Studies on pore systems in catalysts v. the t method, *J. Catalysis*. **1965,** 4, 319.
72. Dąbrowski, A. Adsorption—from theory to practice. Adv. Colloid Interface Sci. **2001**, 93, 135-224.
73. McCusker L, Liebau F, Engelhardt G. Nomenclature of structural and compositional characteristics of ordered microporous and mesoporous materials with inorganic hosts (IUPAC recommendations 2001). *Pure Appl. Chem*. **2001**, 73, 381-94.
74. McCusker, L.; Liebau, F.; Engelhardt, G. Nomenclature of structural and compositional characteristics of ordered microporous and mesoporous materials

with inorganic hosts:(IUPAC recommendations 2001). *Microporous Mesoporous Mater*. **2003**, 58, 3-13.

75. Rao, B. S.; Maramu, N.; Rao, E. V.; Rao, N. S.; Prasad, K. R., Deconvolution of X-ray diffraction spectrum of polypropylene. *Res. Rev. J. Physics*. **2018**, 2, 1-4.
76. Shin, E.W.; Han, J. Phosphate adsorption on aluminum-impregnated mesoporous silicates: surface structure and behavior of adsorbents. *Environ. Sci. Technol*. **2004**, 38, 912–917.
77. Lataye, H. D.; Indra, M.M.; Indra, D. M. Removal of pyridine from aqueous solution by adsorption on bagasse fly ash. Ind. Eng. Chem. Res. **2006** 45, 3934-3943.
78. Rabek, J.; Lucki, J.; Rånby, B.; Watanabe, Y.; Qu B. Photoozonization of polypropylene: oxidative reactions caused by ozone and atomic oxygen on polymer surfaces. *ACS Pub.*; **1988**.
79. Gongjian, B.; Yunxuan, W.; Xingzhou, H. Surface modification of polyolefine by uv light/ozone treatment. *J. Appl. Polym. Sci.* **1996**, 60, 2397-402.
80. Occhiello, E.; Morra, M.; Morini, G; Garbassi, F.; Humphrey P. Oxygen-plasma-treated polypropylene interfaces with air, water, and epoxy resins: part i. air and water. *J. Appl. Polym. Sci.* **1991**, 42, 551-9.
81. Briggs, D.; Beamson, G. Primary and secondary oxygen-induced C1s binding energy shifts in x-ray photoelectron spectroscopy of polymers. *Anal. Chem*. **1992**, 64, 1729-36.
82. Kill, G.; Hunter, D.; McIntyre, N. Reactions of polyethylene surfaces with the downstream products of an air plasma: gas phase and surface spectroscopic studies. *J. Polym. Sci, Part A: Polym. Chem*. **1996**, 34, 2299-310.
83. Singh, K.; Bharose, R.; Verma, S. K., Isolation of sugarcane amino acids from aqueous solution by arha. *Mat. Today Pro*. **2020**. 26, 1037-1045
84. Langmuir I. The Adsorption of gases on plane surfaces of glass, mica and platinum. *J. Am. Chem. Soc.* **1918**, 40, 1361-403.
85. Haghdoost, G.; Aghaie , H.; Monajjemi, M. Investigation of Langmuir and Freundlich adsorption isotherm of Co^{2+} ion by micro powder of cedar leaf. *Orient. J. Chem.* **2017**, 33, 1569-1574.
86. Zhou, X.; Zhou, X. The unit problem in the thermodynamic calculation of adsorption using the langmuir equation. *Chem. Eng. Commun*. **2014**, 201, 1459-67.

87. Salvestrini, S.; Leone, V.; Iovino, P.; Canzano, S.; Capasso, S. Considerations about the correct evaluation of sorption thermodynamic parameters from equilibrium isotherms. *J. Chem. Thermodyn*. **2014**, 68, 310-6.
88. Gubernak, M.; Zapała, W.; Kaczmarski, K. Analysis of amylbenzene adsorption equilibria on an rp-18e chromatographic column. *Acta Chromatographica*. **2003**, 13, 38-59.
89. Temkin, M. I.; Pyzhev, V. Kinetics of ammonia synthesis on promoted iron catalyst. *Acta Physiochem. U.S.S.R.* **1940**,12, 327–356.
90. Frisch, M. J.; Trucks, G. W.; Schlegel, H. B.; Scuseria, G. E.; Robb, M. A.; Cheeseman, J. R.; Scalmani, G.; Barone, V.; Petersson, G. A.; Nakatsuji, H.; Li, X.; Caricato, M.; Marenich, AV; Bloino, J.; Janesko, BG.; Gomperts, R.; Mennucci, B.; Hratchian, HP.; Ortiz, JV.; Izmaylov, AF.; Sonnenberg, JL.; Williams-Young, D.; Ding, F.; Lipparini, F.; Egidi, F.; Goings, J.; Peng, BA.; Petrone, T.; Henderson, D.; Ranasinghe, VG.; Zakrzewski, J.; Gao, N.; Rega, G.; Zheng, W.; Liang, M.; Hada, M.; Ehara, K.; Toyota, R.; Fukuda, J.; Hasegawa, M.; Ishida, T.; Nakajima, Y.; Honda, O.; Kitao, H.; Nakai, T.; Vreven, K.; Throssell, JA.; Montgomery J E Jr. .; Peralta, F.; Ogliaro, MJ.; Bearpark, JJ.; Heyd, EN.; Brothers, KN.; Kudin, VN.; Staroverov, TA.; Keith, R.; Kobayashi, J.; Normand, K.; Raghavachari, AP.; Rendell, JC.; Burant, SS.; Iyengar, J.; Tomasi, M.; Cossi, JM.; Millam, M.; Klene, C.; Adamo, R.; Cammi, JW.; Ochterski, RL.; Martin, K.; Morokuma, O.; Farkas, JB.; Foresman, DJ.; Fox, Gaussian 16, Revision B.01, *Gaussian*, Inc., Wallingford CT, **2016**.
91. Lee, C.; Yang, W.; Parr, RG. development of the Colle-Salvetti correlation-energy formula into a functional of the electron density. *Phy. Rev. B*. **1988**, 37, 785.
92. Miehlich, B.; Savin, A.; Stoll, H.; Preuss H. Results obtained with the correlation energy density functionals. *Chem. Phys. Lett*. **1989**;157:200-6.
93. Dennington, R.; Keith, T.; Millam, J. GaussView, Version 5.0. 8, R. Dennington, Semichem Inc., Shawnee Mission, KS; **2009**.
94. Becke, A. The quantum theory of atoms in molecules: from solid state to DNA and drug design: John Wiley & Sons; **2007**.
95. Pandey, S. K.; Khan, M. F.; Awasthi, S.; Sangwan, R.; Jain, S. A quantum theory of atoms-in-molecules perspective and dft study of two natural products: trans-communic acid and imbricatolic acid. *Aust. J. Chem.* **2017**, 70, 328.
96. Mehdi, S H.; Ghalib, R M.; Awasthi, S.; Alshahateet, SF.; Hashim, R.; Sulaiman, O.; Pandey, S K . Synthesis, characterization, crystal structure, and stability of 2-

(5, 5-dimethyl-3-oxocyclohex-1-en-1-yl) hydrazinecarbothioamide: a combined experimental and theoretical study. *ChemistrySelect*. **2017**, 2, 6699–6709.

97. Singh, R.; Singh, K.; Pandey, S. K. Computational scrutiny on the stability, structure, and electronic features of alkanesulfonate based zincate salts with varying countercations. *ChemistrySelect*. **2018,** 3, 13048-56.
98. Singh, R.; Kociok-Köhn, G.; Singh, K.; Pandey, S. K.; Singh, L. influence of ligand coordination, solvent, and non-covalent interaction on the structural outcomes in coordination polymers with direct cd (ii)-alkanesulfonate bonds: a combined experimental and computational study. *J. Solid State Chem*. **2019**, 280, 120992.
99. Espinosa, E.; Molins, E.; Lecomte, C., Hydrogen bond strengths revealed by topological analyses of experimentally observed electron densities. *Chem. Phys. Lett.* **1998,** 285, 170-173.
100. Ermolaev, V.; Miluykov, V.; Rizvanov, I.; Krivolapov, D.; Zvereva, E.; Katsyuba, S.; et al. Phosphonium ionic liquids based on bulky phosphines: synthesis, structure and properties. *Dalton transactions*. **2010**, 39, 5564-71.
101. Parr, R. G.; Yang, W., Density functional approach to the frontier-electron theory of chemical reactivity. *J. Am. Chem. Soc.* **1984,** 106, 4049-4050.
102. Fukrd, K.; Yomezawa T.; Skrlnga, H. A molecular orbital theory of reactivity in aromatic hydrocarbons. 1. *Chem. Phys*. **1952**, 20, 722-5.
103. Sinha, L.; Prasad, O.; Narayan, V.; Shukla, S. R. Raman, FT-IR spectroscopic analysis and first-order hyperpolarizability of 3-benzoyl-5-chlorouracil by first principles. *Mol. Simul.* **2011**, 37, 153-63.
104. Scrocco, E.; Tomasi, J. Electrostatic molecular potential analysis of electron density distribution in (clalme2) 2 and (alcl3) 2. *Adv. Quantum Chem*. **1978**, 11, 115-21.
105. Dubois, J. E.; Yue, S.; Doucet J. P. Grid stage modelling functions and molecular vector graphics. *Visual Computer*. **1986**, 2, 367-78.

Chapter 5

Physiochemical aspects for the adsorption behaviour of sodium carboxymethylcellulose onto mesoporous granular fine quartz surface from its aqueous solutions

Abstract

The present study focused onto adsorptive properties and nature of the interaction between sodium carboxymethylcellulose (NaCMC) and mesoporous granular fine quartz (MGFQ) employing various in-depth characterization techniques. The obtained data were tested with various adsorption isotherm models and effect of various operational variables such as pH, ionic strength, temperature, the concentration of adsorbents, amounts of adsorbents, etc. on adsorption were investigated.. The physiochemical parameters of MGFQ such as specific surface area (S_{BET}) =11.34 m^2/g, pore volume (Vp) =0.09 cm^3/g, total pore volume (Vtp) = 0.09 cm^3/g, mean pore diameter =32.52 nm were determined. The thermal result revealed that NaCMC could be used at specific temperature (251°C), which was suitable for its application. The equilibrium isotherm data were fitted with Langmuir, Freundlich, Temkin and Jovanovic models of adsorption and compared by linear determination coefficient (R^2) and obeyed the order as Freundlich (R^2=0.9984)> Langmuir (R^2=0.9194)>Temkin (R^2 =0.8899)>Jovanovic (R^2= 0.8709). The infra-red spectral changes in the region 1104 cm^{-1} and 1076 cm^{-1} suggested that NaCMC accumulation onto MGFQ was stabilized by H-bonding and some other weak noncovalent interactions depending on the solution conditions.

1. Introduction

Sodium carboxymethylcellulose (NaCMC) is a water-soluble, hydrophilic, and macromolecular anionic polymer and produced as polyelectrolyte salt at industrial scale without any refinement for several applications in various sectors [1]. The most promising area of application of NaCMC as strong depressants that could replace the highly toxic inorganic modifiers in the differential flotation process such as flotation of sulfide minerals [2]. The applicability of this polymer was associated with adsorption behaviour onto solid surfaces and makes it suitable for a wide range of applications in the mineral processing, food, pharmaceutical, and cosmetics industries. The polymeric unit of NaCMC (Figure 1) illustrated that each unit contains three hydroxyl groups and carboxylate ions responsible for hydrogen bonding [3, 4]. Several studies were conducted in the past but the mechanism of adsorption of polysaccharides on solid surfaces is not yet well understood. Several researchers proposed that the mechanisms governing the adsorption of polymers (polysaccharides) onto mineral surfaces include hydrophobic interaction, hydrogen bonding, chemical, and electrostatic interactions [5-19]. However, the reasons for the selectivity of the adsorption of depressants on minerals have not been accounted, Therefore, physiochemical aspect for the adsorption behaviour of NaCMC onto oxide mineral/ mesoporous granular fine quart (MGFQ) surface from its aqueous solutions was the topic of research interest. The crystalline mineral oxide and other allied materials was studied extensively for various applications [19-25]. Quartz crystals have piezoelectric on the influence of the -COOH and -COONa groups will also alter the application of this polysaccharide [26-27].

The prime objective of this research was to establish an understanding of the binding behaviour of NaCMC onto mineral surfaces (MGFQ) and to determine the most desirable conditions to increase the applicability of NaCMC in various fields. The MGFQ was evaluated with various physicochemical parameters such as point of zero charges, iodine test, and molasses test, specific surface area, pore diameter, pore-volume, particle size distribution, mesoporous nature employing various depth characterizations. For the validation of the adsorption data various adsorption isotherm models were considered. Based on the results, it was suggested that the physicochemical binding aspects of NaCMC onto MGFQ was stabilized by H-bonding and other weak noncovalent interactions and such alteration could play a noteworthy role in the field of food, pharmaceutical, and industrial applications.

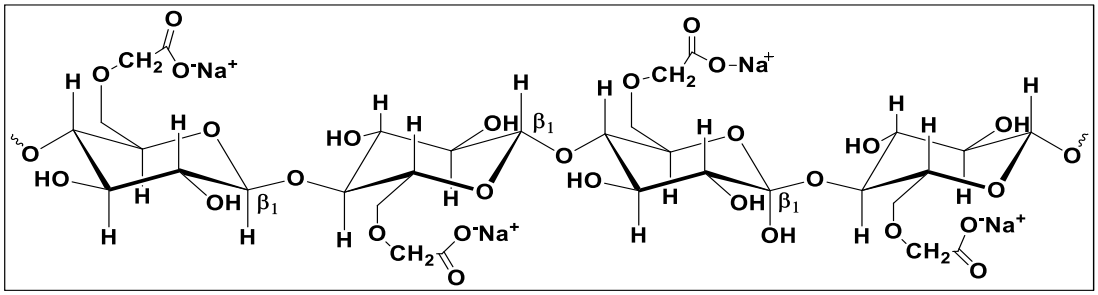

Figure 1. Structure of sodium carboxymethyl cellulose (Repeating unit of glucose) shows the d-glucose units are linked through β-1, 4 bonds. O~ represents the continuation of the polymeric chain

2. Experimental

2.1 Materials

All the reagents used for synthesis and experimental studies were of analytical and laboratory grade. Granular fine quartz (99.9%), extra pure sodium carboxymethylcellulose (99.5%), sodium hydroxide (98%), hydrochloric acid (35.5%), potassium chloride (99.5%), sulphuric acid (98%), sodium sulphate (99.9%) cetrimide (96%), methanol and isopropyl alcohol (99.9%) were used and supplied by Loba Chemie Pvt. (Maharashtra, India). Reference activated carbon 20-40 mesh (99.97%) purchased from Sigma Aldrich Chemie Gmb H. (Steinheim, Germany) was used for iodine and molasses test. Iodine resublimed (99.8%) was purchased by Sisco Research Laboratories Pvt. Ltd. (Maharashtra, India). Organic sugar, brown (100%) was supplied by M/s Pro Nature Organic Foods Pvt. Ltd. (Karnataka, India). The double distilled water was used for processing of adsorbent and batch adsorption experiments.

2.2 Preparation of mesoporous granular fine quartz (MGFQ) as an effective adsorbent

The supplied granular fine quartz was washed using double distilled water and dried in an oven at optimized [28, 29] temperature (120°±2C) for 2-3 hr to remove all the volatile impurities and undesired impurities adsorbed on the surface. After drying, the sample was sieved to obtain the uniform size and kept in a desiccator for further characterization and experimental use. After depth characterization of this material results confirms its mesoporous nature, henceforth it was termed as mesoporous granular fine quartz (MGFQ).

2.3 Characterizations

2.3.1 Point of zero charge (ZPC)

The pH_{ZPC} of MGFQ was determined by the salts addition method [30-34] using 0.1M $NaNO_3$ solution at room temperature (25±0.02^{0}C. In this process, the 40 ml of 0.1M $NaNO_3$ solution were taken in seven different stoppered bottles (50ml) namely 1, 2, 3, 4, 5, 6, 7, 8 and then an initial pH value of 2- 12 were adjusted respectively by adding either 0.1 M HNO_3 or 0.1 M NaOH solutions. The pHs were recorded using digital pH meter (CL54+, Toshcon Industries Pvt Ltd, Haridwar, India) with an accuracy 0.01pH±1digit. The MGFQ (0.1 g) was added to each bottle and stirred at 500rpm on a magnetic stirrer (MS-M-S10, DLAB Scientific Pvt Ltd. Hyderabad, India) for a day. After stirring the samples these were kept for equilibrium, and then was filtered using Millipore filter paper (0.45µm), the final pH of each bottle (filtrate) was recorded very carefully. The difference between the final and initial pH (ΔpH) values were calculated and then plotted against the initial pH values.

2.3.2 Iodine test

The physio-chemical and adsorption characteristic of MGFQ was determined by the earlier reported method [34] using percentage iodine removal (PIR) analysis. The following formula was applied to calculate the PIR value for MGFQ.

$$PIR_{\mathrm{MGFQ}} = \frac{ml\ thiosulphate\ used\ for\ blank - ml\ thiosulphate\ used\ for\ sample}{ml\ thiosulphate\ used\ for\ blank} \times 100 \qquad (1)$$

2.3.3 Molasses test

The adsorptive characteristic of MGFQ was determined by per cent molasses colour removed (PMCR) analysis. The $PMCR_{MGFQ}$ was determined using the following formula [34]:

$$\mathrm{PMCR_{MGFQ}} = \frac{\text{Absranace of blank} - \text{Absrobance of MGFQ treated samples}}{\text{Absranace of blank}} \times 100 \qquad (2)$$

2.3.4 Brunauer-Emmett-Tiller (BET) surface area measurements

BET analysis of MGFQ was performed by surface area analyzer (BELSORP-Mini II, Japan). Before further analysis, the sample (MGFQ) was pre-treated in the presence of

N_2 at 500-600^{0}C for 2-3 h to remove the undesired species present on the surfaces of samples. After pre-treatment, the sample was cooled at room temperature in the inert atmosphere. A definite amount of the sample (1.0g) was scanned using nitrogen (as adsorbate) and helium (as carrier) gas and all observation were continuously under examine at BELSORP data analysis program (BDAP). After complete scanning of the sample, the results (data) were analysed by Version info. of the analysis software (VAS) [35].

2.3.5 Scanning electron microscopy (SEM) analysis

The particle morphologies of the MGFQ were investigated employing SEM of JEOL (Nicole-6700, TFS, USA). The samples were sputter-coated with gold-palladium using an ion sputter coater (auto fine coater) (JFC1600, JEOL Ltd, Japan) before SEM analysis [36].

2.3.6 Energy-dispersive X-ray spectroscopy (EDS) analysis

The elemental composition was done by the energy-dispersive X-ray spectroscopy (EDS) with EDS 133, EV dry detector (INCAx-act, Oxford, UK) coupled with SEM [37].

2.3.7. *Fourier transformation infrared (FTIR) analysis*

Vibrational spectroscopy in the infrared region was is used for the characterization of the molecular structure of the adsorbent from the vibrational modes related to functional groups present in the adsorbent. For the functional group analysis, the MGFQ was mixed with the required amount of potassium bromide and then pelletized under high pressure in a vacuum atmosphere and then pelletized MGFQ was scanned in transmittance mode with wave region ranging from 4000 to 500 cm^{-1} by Fourier transform infrared (FTIR) spectrometer (Nicole-6700, TFS, USA) [38].

2.3.8 Powder x-ray diffraction (pXRD) analysis

Crystallographic parameters of the MGFQ were obtained from pXRD study. The $_P$XRD spectra patterns were recorded on a Rigaku Miniflex II desktop X-ray diffractometer at 30kV and using CuK radiation. in 2-theta(degree) angle range 5°-80° at 45kV using CuK radiation with 148.92 times per step [39].

2.3.9 Thermogravimetric analysis (TGA)

The mass loss of a sample as it was heated, cooled or held at a constant temperature in a defined atmosphere was performed using TGA Perkin Elmer (Switzer Land) with accuracy ±1°C. The thermal degradation of NaCMC was investigated by means of TGA in nitrogen atmosphere with the flow rate 100 mL/min at the heating rate of 10-30 °C/min until the furnace wall temperature reached 800 °C. The change in the mass-loss like evaporation, decomposition was recorded [40].

2.6 Adsorption experiments

The stock solution of desired concentration was prepared in accordance with the earlier reported method, briefly, an appropriate amount of NaCMC was dissolved and the prepared solution was then refrigerated over 24hr. After attaining the room temperature this was further used for batch adsorption experiments. For the adsorption tests, the desired concentration was taken in Erlenmeyer flasks and 1.0 g MGFQ was then added into each flask. This suspension was then agitated for half an hour using orbital shaking incubator at 25±0.5 °C. After equilibration, pH of the solution was again recorded. The solution was then centrifuged for 10 min at 500 rpm by centrifugation process. The supernatant liquid was used to analyze the adsorption concentration determination employing earlier reported method [41] and monitored spectrophotometrically, λmax=375nm, (Spectronic, $20D^{+}$, TEC, US) by measuring the absorbance at temperature (22 ± 2°C). The cuvette was cleaned with acetone after few absorbances run to remove the deposited concentration. Each adsorption test was done in duplicate and triplicate when necessary and the results was averaged.

The amount of NaCMC adsorbed on MGFQ, Γ (mg/L), was evaluated using the following equation [42]:

$$\Gamma = \frac{(C_0 - C_e)}{M} . V \qquad (3)$$

Where, C_0 and Ce (mg/1) referred to the initial and the equilibrium concentration of NaCMC respectively; V (L) is the volume of the NaCMC solution, and M (g) is the mass of the GFQ.

2.7. Influence of various factors onto adsorption of NaCMC onto MGFQ surface

2.7.1 Effect of NaCMC concentration

The effect concentration of NaCMC onto adsorption was conducted by varying the concentration in the ranges 10 -100 mg/L of NaCMC. Meanwhile, other influencing factors like dose, pH, ionic strength, temperature and the presence of alcohols, etc. were kept constant during the adsorption.

2.7.6 Effect of MGFQ dose

The amount of adsorbent (MGFQ) was an important factor to affect the adsorption behaviour of NaCMC. The desired amount (1.0g) was taken during the batch adsorption experiments keeping all factors constant.

2.7.2 Effect of pH

The pH of the solution was introduced as another factor affecting the adsorption amount of the NaCMC onto MGFQ surface. The adsorption of NaCMC onto MGFQ were studied by varying pHs with ranges 2.0-12.0.

2.7.4 Effect of ionic strength

The binding mechanism of NaCMC onto MGFQ was explained as a function of ionic strength. Sodium sulphate (0.2mg/L) was used to conduct. During the batch adsorption experiments, Na_2SO_4 solution (0.2mg/L) was added in the selected concentration of NaCMC.

2.7.5 Effect of alcohols

The presence of various alcohols during the adsorption process of NaCMC was investigated. Methanol (CH_3OH) and isopropyl alcohol ($C_3H_8O_3$) were selected as different alcohols. A definite volume ratio (v/v) of alcohols were added during the adsorption of NaCMC onto MGFQ.

2.7.3. Effect of temperature

The adsorption amount was determined at different temperatures (20, 30, 40, 50 and 60 ^{0}C). For this study, all desired samples (solutions of NaCMC) were placed in a water bath at aforesaid different temperatures to conduct the batch adsorption experiments.

2.7.7 Effect of sonication

Non-chemical factor (sonication) was introduced for the adsorption of NaCMC onto MGFQ. During the adsorption experiment, sonication (20kHz) was applied for 30 min. For this study, this ultrasonicator (Sonics Vibra-cell VCX750, USA) a high-intensity liquid processor was used for sonication to examine the effect of power ultrasound on adsorption of NaCMC onto MGFQ. The ultrasonicator used in the present case was an amplifier power (automated). It is a "high intensity ultrasonic having probe (Coupler solid, Part No.630- 0421) with stepped tip 1/8″-630-0422 [49].

2.7.8 Effect of contact time

The effect of contact time on the adsorption of NaCMC was investigated. The adsorption experiment was conducted at selected optimized conditions while keeping all factors constant.

2.8. Adsorption isotherm and their statistical physics based model studies

The equilibrium adsorption isotherm is an important parameter to consider when designing an adsorption system. An equilibrium isotherm describes the mode of interactions between the solute and adsorbent. Moreover, the shape of an isotherm provides information about the affinity of adsorbate information about the affinity of an adsorbate toward the adsorbent [51]. Therefore, for isotherms investigation, the adsorption equilibrium data was originated at NaCMC solution within optimum conditions. The equilibrium behaviour of NaCMC onto MGFQ was explained by two most common adsorption isotherm models namely Freundlich [52] and Langmuir [53]. Furthermore, two other models [54, 55] were also applied in this study. Adsorption data were fitted employing these different methods and a comparison was made.

Adsorption isotherms were described in various mathematical forms, some of which were based on a simplified physical model of adsorption and desorption, while others are purely empirical and are intended to correlate the experimental data. However, a

simple Hill model [55] obtained by statistical physics treatment was applied to define the parameter which represents the number of molecules adsorbed per site. Further, a basic statistical physics assumption of the Langmuir theory was also considered.

2.9. Regeneration study

Regeneration study was conducted for recycling use of MGFQ employing different eluents. After the equilibrium adsorption batch experiments, the MGFQ was regenerated using desoption process. The desorption experiments were carried out with double distilled water and different concentration of HCl solution (0.5M to 0.15M). First, 5.0 g of MGFQ loaded with NaCMC after adsorption was dried in the oven. After drying, the MGFQ was added into 40 mL of HCl solution and shaken at 30 °C for 24 h. Now, the solution was centrifuged at 6000 rpm for 5 min. The separation process reveled that on the action of centrifugal force to separate MGFQ particles in a solid-liquid mixture into two distinct phases consisting of the sediment and supernatant. From the supernatant, the adsorbed/residual amount of NaCMC was determined. The MGFQ precipitant (sediment) was collected from the bottom of centrifuge tube. Moreover, the sediment was again used for the adsorption of NaCMC with 50 mL of NaCMC solution for investigation of the reusability. The regeneration tests were repeated 4 times.

3. Results and discussion

3.1 Characterization of the adsorbent and adsorbate

3.1.1 Point of zero charge (pH_{ZPC})

The adsorption of NaCMC was directly related to the surface charge characteristics of the MGFQ as determined by the pH_{ZPC} relationship. An efficiency of adsorption of NaCMC can also be due to a low pHzpc of the MGFQ particles. The zero point of charge was found [46-59] to be 3.35±021. Above pH_{zpc} = 3.35±021 the surface of the MGFQ particles is negatively charged and upon increasing the pH value the adsorption was also decreased and *vice versa*. The carboxylate ions of NaCMC was completely adsorbed under pH conditions where the solution has a positive surface charge, i.e. when the pH is below the pH_{zpc}. However, adsorption also occurred when the pH was above the pH_{zpc} suggesting that adsorption also occurs *via* van der Waals forces. However, greater adsorption occurs when the pH is below the pH_{zpc}. Maximum

hydrogen bonding is believed to occur when the interaction of carboxylate ions of NaCMC and the positive surface of MGFQ when the pH is below the pH_{zpc}.

3.1.2 Iodine test

The PIR $_{MGFQ}$ was found to be 71.73% for MGFQ suggests that it follow a similar trend as reference activated carbon (RAC) (Table1). This experimental study supports that MGFQ has sufficient adsorptive potential for present work. This is because of the availability of the active sites of MGFQ. When the concentration increases, the iodine dissociated also increases. The availability of active sites for binding onto MGFQ surface for iodine are limited for the higher concentration [26].

3.1.3 Molasses test

The PMCR $_{MGFQ}$ was found to be 67.96% was similar trend indicator with RAC (Table1). The obtained data suggest that MGFQ has potential adsorption application for interpretation of the adsorption behaviour of polysaccharides. The finding was based on the concept that the adsorption amount decrease with increases in temperature [26].

3.1.4 BET analysis

The textural properties of MGFQ like specific surface area, surface nature, particle size distribution and total pore volume were measured using BET analysis (Figure 2b-2d). The BET analysis [60] reveals that MGFQ had a typical specific surface area (S_{BET} =34.74m2g^{-1}). The N_2 adsorption isotherm was measured which represents type IV isotherm (Giles' classification) [60]. The capillary condensation phenomenon in IV isotherm was the characteristic properties of mesoporous material, therefore, it was interpreted that MGFQ was mesoporous material. For the determination of pore size distribution, the Barrett-Joyner-Halenda (BJH) model [61, 62] was applied and results were found in the mesoprous domain (32.52nm) which confirmed that MGFQ possesses mesoporous nature as per defined by IUPAC nomenclature [63-67]. These physicochemical properties of MGFQ make it suitable and potential adsorbent for the adsorption of CMC (Table 1).

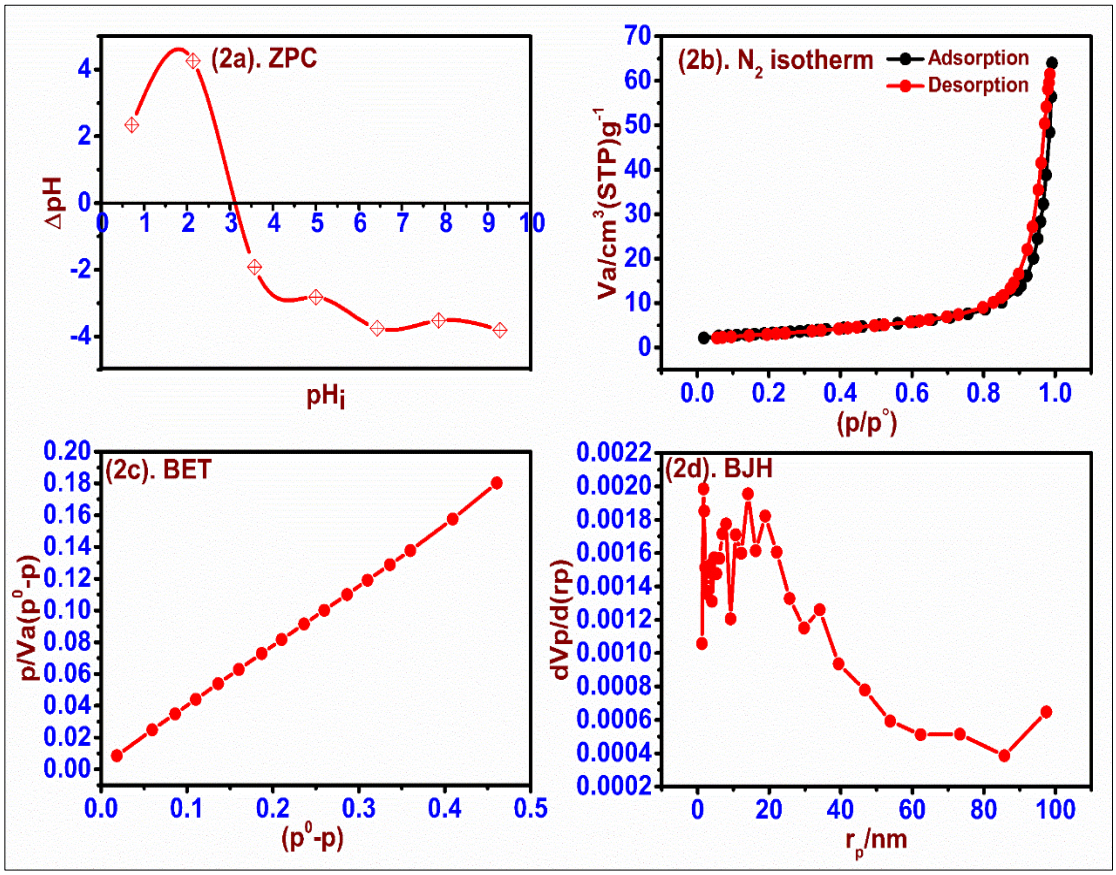

Figure 2. Physiochemical analysis of MGFQ (2a). pH_{ZPC} analysis, (2b). N_2 adsorption-desorption isotherm, (2c). BET graph and (2d). BJH graph

Table 1 Physio-chemical parameters of MGFQ presented in figure 2

ZPC analysis (pH_{ZPC})				
Initial pH range(pHi)		The difference in pH range (ΔpH)		pH_{ZPC}
2-10		2.34 to -3.814		3.35±021
Iodine test				
Thiosulphate used for blank (ml)	RAC		MGFQ	
	Thiosulphate used (ml)	PIR_{RAC}	Thiosulphate used (ml)	PIR_{MGFQ}
12.53	0.66	94.77	3.85	69.20
12.50	0.65		3.84	
12.50	0.65		3.85	
Molasses test				
Sugar solution (15%)	RAC		MGFQ	
Absorbance (λmax=420nm)	Absorbance	$PMCR_{RAC}$	Absorbance	$PMCR_{MGFQ}$
0.85	0.024	97.52	0.27	70.23
0.84	0.021		0.25	
0.84	0.021		0.25	
Surface analysis				
Methods	Surface parameters of MGFQ			

N_2 isotherm	Saturated vapour pressure (kPa)	Sample weight (g)	Ratio of rate constant (adsorption / desorption)	
	96.67	0.1	0.371	
BET plot	Specific surface area (S_{BET}) (m^2g^{-1})	Monolayer volume V_{mono} ($cm^3\ g^{-1}$)	Total pore volume (Vp)	Mean pore diameter (nm)
	11.34	2.31	0.09	32.52
BJH plot	Pore volume (Vp) ($cm^3\ g^{-1}$)	Pore specific surface area (a_p) (m^2g^{-1})	Micropore radius (cylindrical shape (r_p) (nm)	
	0.09	12.25	1.66	

3.1.4. *Functional group analysis*

The FTIR spectra of MGFQ with NaCMC before and after adsorption are shown in Figure 3. The bands at 1082 and 791 cm^{-1} attributed to the asymmetric and symmetric stretching vibration of Si–O, the intense absorption peak at 3433.79 cm^{-1} was observed due to presence of both free and hydrogen-bonded -OH groups on the MGFQ. The absorption peaks at 2918.53 cm^{-1}, 1629.99 cm^{-1}, 1431.02 cm^{-1}, 1162.2 cm^{-1} and 876.05 cm−1 may be due to -CH_2, -C-C, -C-H, and -C=O stretching, respectively [68] (Figure 3a). The stretching band at 2920.8 cm^{-1} were due to –CH_2 groups of the NaCMC. The ring stretching of the glucose unit appeared at 1610.32 cm^{-1}. Additionally, the bands at 1350–1450 cm^{-1} were due to symmetrical deformations of --CH_2 and –C-OH groups, respectively. The bands due to primary alcoholic –CH_2OH stretching mode and -CH_2 twisting vibrations appear at 1060 and 1010 cm^{-1} respectively. The mid-frequency bands at 714-610.70 cm^{-1} were due to ring stretching and ring deformation of α-D-(1–4) and α-D-(1–6) linkages[69] (Figure 3b). After the adsorption of NaCMC onto MGFQ, the characteristic peaks at 1780 cm^{-1} and 1383 cm^{-1} due to carbonyl stretching of carboxylic acid groups and unsaturated groups have successfully confirmed MGFQ and associated with the interactions of NaCMC with MGFQ, as shown in Figure 3c [70,71].

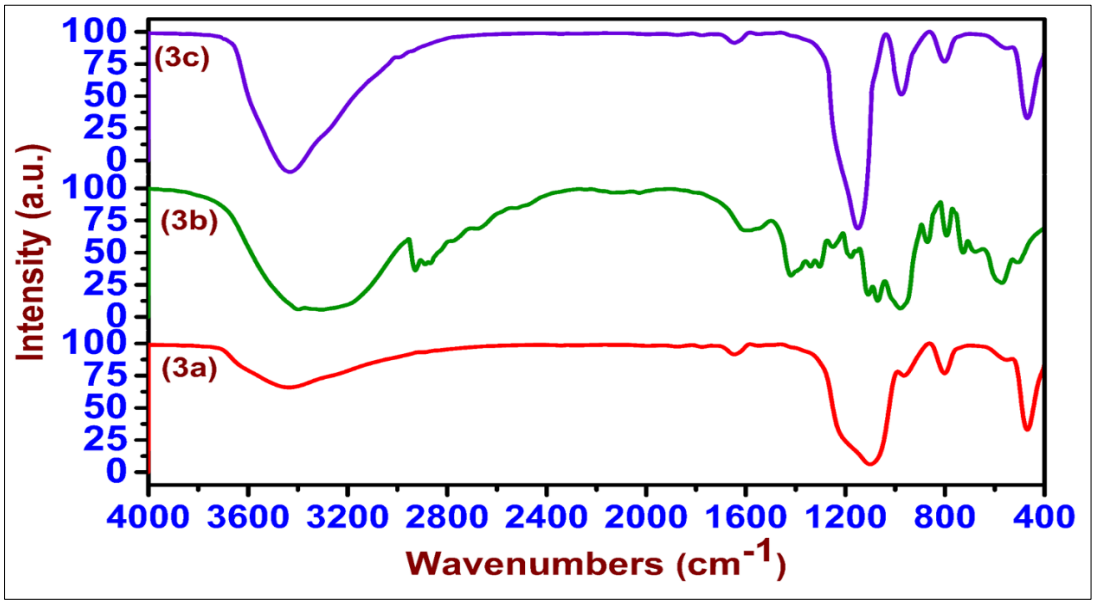

Figure 3. FTIR spectra (3a). MGFQ before adsorption, (3b). NaCMC and (3c). MGFQ After adsorption

3.1.5. Surface morphology analysis

The textural/morphological characteristics of the MGFQ were evaluated by SEM studies (Figure 4). SEM photographs of the unloaded MGFQ show the rough, uneven surfaces porosity with small openings and holes responsible for intra pore diffusion during the adsorption process. Therefore, these surface properties should be a considerable factor for NaCMC adsorption. After NaCMC adsorption, a significant change was observed in the structure of the MGFQ (Figure 4a). The NaCMC adsorbed surface appeared to have a rough surface and pores containing new shiny particles after adsorption (Figure 4b) [72-75].

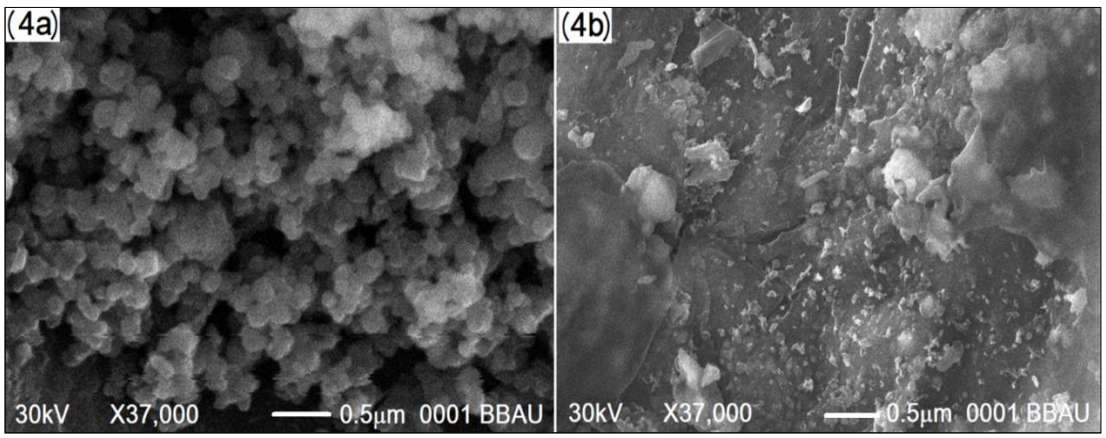

Figure 4. Shows the MGFQ morphology (4a). Before adsorption and (4b). After adsorption

3.1.6. Elemental microanalysis

The purpose of elemental analysis is to determine the quantity of a particular element within a molecule or material for point of view of qualitative and quantitative aspects. SEM-EDX elemental analysis before and after shown in Figure 5 Before adsorption MGFQ confirmed the presence of Si and O (Figure 5a) whereas NaCMC adsorbed MGFQ revealed the presence of O, Na, Si, and K surface (Figure 5b). The source of Na is in carboxymethyl cellulose salt, used in the adsorption process [76, 77]. The changes in the SEM-EDS was associated NaCMC adsorption onto MGFQ.

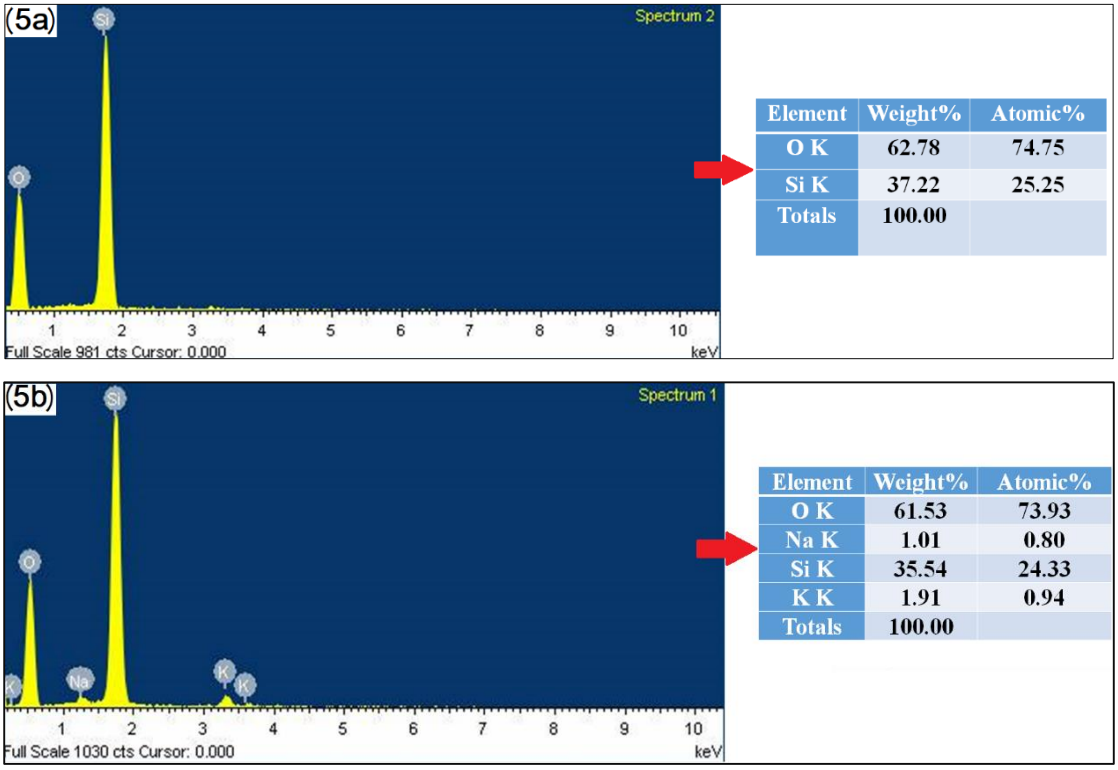

Figure 5. EDS and percentage composition of MGFQ (5a). Before adsorption and (5b). After adsorption

3.1.7 Crystalline structure analysis

The XRD spectra of MGFQ were scanned before and adsorption of NaCMC presented in Figure 6. There were observable differences in the XRD spectra of MGFQ before and after the adsorption of NaCMC. A series of small and sharp characteristic peaks of MGFQ before adsorption were at 2θ = 22, 26, 37, 41,43, 46, 50, 57, and 60 corresponding to (100), (101), (110), (102), (201), (112), (202) and (211) Bragg reflection (Figure 6a), respectively[78-80]. This confirmed crystalline nature and the presence of silica oxide particles in the prepared MGFQ (Figure 6a). After adsorption,

the shifting in peaks namely (101) supported the hydroxylation behaviours of quartz (101) surface and suggested that hydroxyl of NaCMC interaction with MGFQ surfaces and associated with the contraction of the unit cell. The disappearance in peaks suggested there was a slight loss of crystallinity of MGFQ surface (Figure 6b).

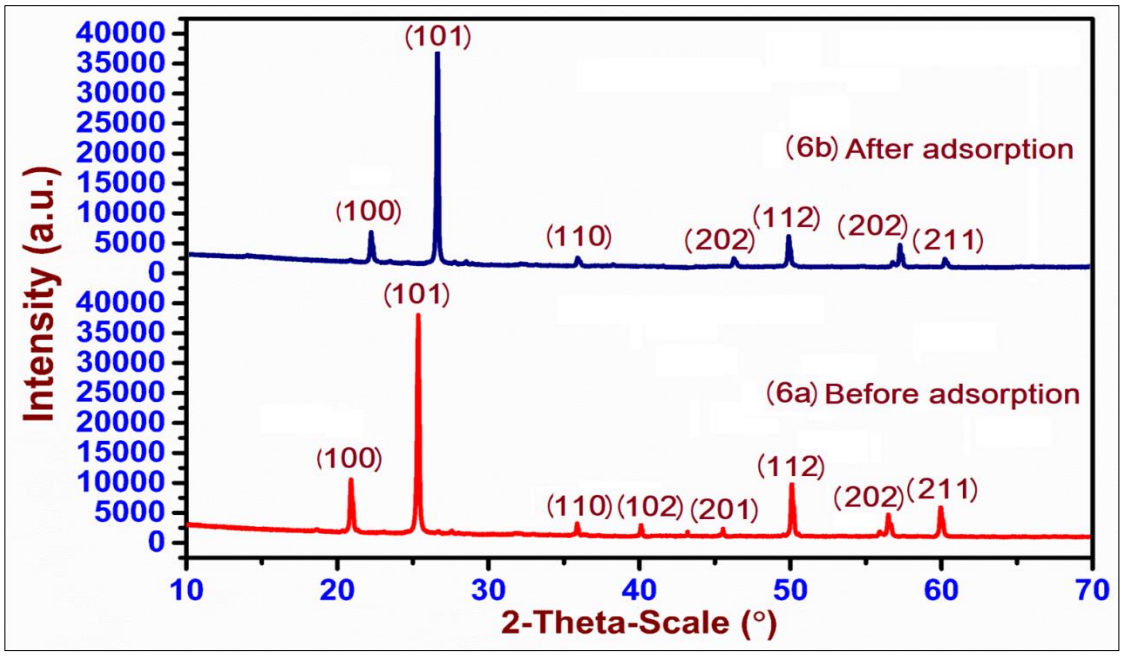

Figure 6. XRD spectra of MGFQ (6a). Before adsorption and (6b). After adsorption

3.1.8 Thermal measurement

The thermal characterization behaviour of polysaccharides (NaCMC) was analysed and results have been shown in Figure 7, which illustrated that the TGA curve consists of four stages [40]. The first initial weight loss (Δm=8.964%) was observed in the temperature range of 49.36 to 148.79 °C. The initial weight loss was due to the presence of moisture in the sample (NaCMC) and suggested that this was the due to evaporation of moisture. This (evaporation) was because of NaCMC tends to absorb moisture from its surroundings. The second weight loss (Δm=20.106) in the temperature range of 149.52 to 252.57 °C was due to volatilization of the volatile matter from the sample. The third stage illustrated the maximum weight losses (Δm=28.342%) as a result of the pyrolysis process with loss of -COO^- from the NaCMC. In this stage, the thermal degradation started at the temperature range 253.00 to 352.00°C with weight loss (Δm=28.342%). The final stage represented the conversion of the remaining material to carbon residues which ends at 749.43°C with weight loss of (Δm=10.682%). The obtained result revealed that the NaCMC could be used at moderate temperatures (251 °C), which was suitable for its application.

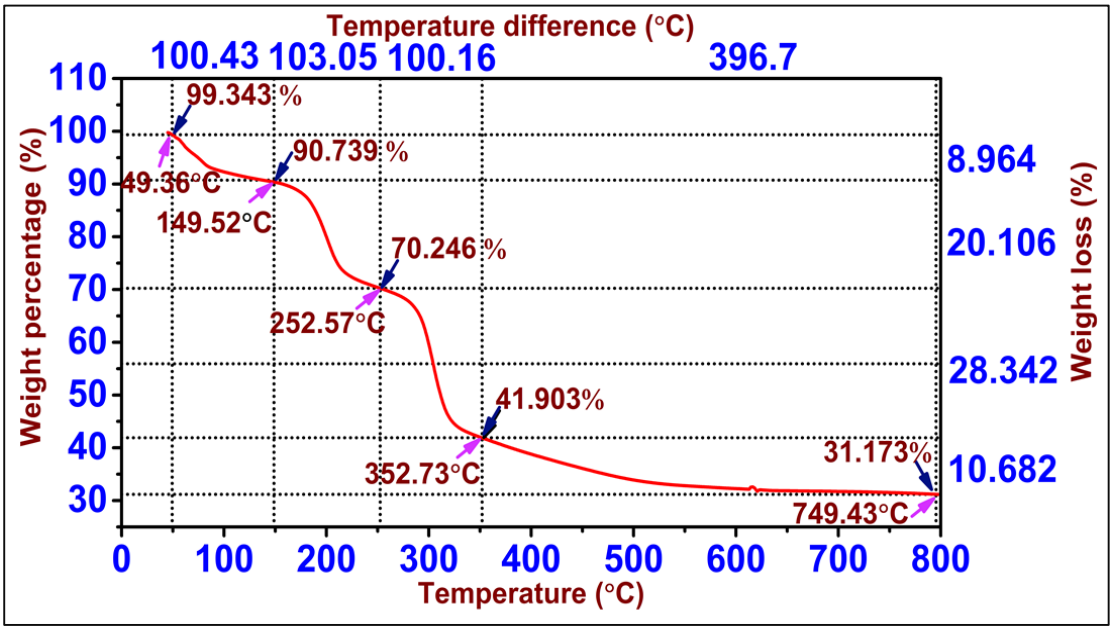

Figure 7. Thermal characterization behaviour of NaCMC

3.3. Effect of various factors onto NaCMC adsorption

3.3.1 Concentration

The adsorption of NaCMC onto MGFQ was studied as a function of concentration to determine where the equilibrium exists. By measuring the NaCMC concentration the adsorption amount (mg/g) were determined. It is shown in Figure 8a that the NaCMC adsorption rate was low at the beginning of the adsorption process because the active sites on the surface of the MGFQ were initially abundant and the NaCMC chain could be adsorbed in a flatty manner. As the concentration of NaCMC increases, there was a gradual increase in the adsorption. After 80mg/L concentration of NaCMC, the adsorption capacity no longer changed, suggesting that the adsorption had reached equilibrium. This was partly due to the unavailability of vacant active sites with increasing concentration [83, 84]. Therefore, 80mg/L concentration was selected as the adsorption equilibrium concentration.

3.3.6 MGFQ dose

To explore the role of surface active sites during the adsorption process were explained [85] by performing the effect of dose of MGFQ onto adsorption. The optimization of MGFQ dose (1.0-7.0g) was taken in a NaCMC concentration at 3.0 pH and room temperature. The adsorption capacity was decreased with increase MGFQ amount (Figure 8b). Therefore, 1.0 was chosen as the adsorbent dose for further experiments.

3.3.2 pH

The pH of the solution has been reported [86-97] as a significant variable to affect the adsorption of polysaccharides onto various solid surfaces. Therefore, the effect of pH was carried out at room temperature (25±0.2^{o}C) keeping all variables constant. The adsorption of NaCMC onto MGFQ was studied in the pH range of 2.0-12.0. The point of zero charge (PZC) of MGFQ was found to be near pH 3.5. With the pH value ranging from 2 to 12, the surface of the quartz was negatively charged. The effect of pH on adsorption is shown in Figure 8c. With the increase of pH values, the adsorption amount of NaCMC on MGFQ decreased gradually. Since, NaCMC is a type of anionic polymer, the negatively charged MGFQ surface and NaCMC, therefore, repel each other, and thus adsorption decreases (Figure 8c). Also, the competitive adsorption between NaCMC and hydroxyl ions at higher pH values can result in a decrease in the adsorption amount.

3.3.4 Ionic strength

The adsorption behaviour of NaCMC onto MGFQ was illustrated in the presence of inorganic salt (Na_2SO_4). The adsorption amount was found almost unchanged with the addition of NaCl and KCl during the adsorption experiments. The adsorption amount increased with the increasing concentration of Na_2SO_4 in the solution of the desired concentration. With the addition of SO_4^{2-} ions, there was an interaction between the water molecules and SO_4^{2-} ions due to the formation of hydrogen bonds [98, 99]. Meanwhile, the hydroxyl groups present in NaCMC have also formed hydrogen bonds to SO_4^{2-} ions resulting in the aggregation of NaCMC. Furthermore, SO_4^{2-} has salt effects on NaCMC, and this gives rise to the aggregation of NaCMC (Figure 8d). Furthermore, NaCMC has more opportunities to interact with the active sites on the surface of the MGFQ. As a result, the adsorption amount increased when SO_4^{2-} exist in the solution [88]. In conclusion, the presence of divalent anion could increase the adsorption amount of NaCMC onto the mineral surface (MGFQ) [100-102].

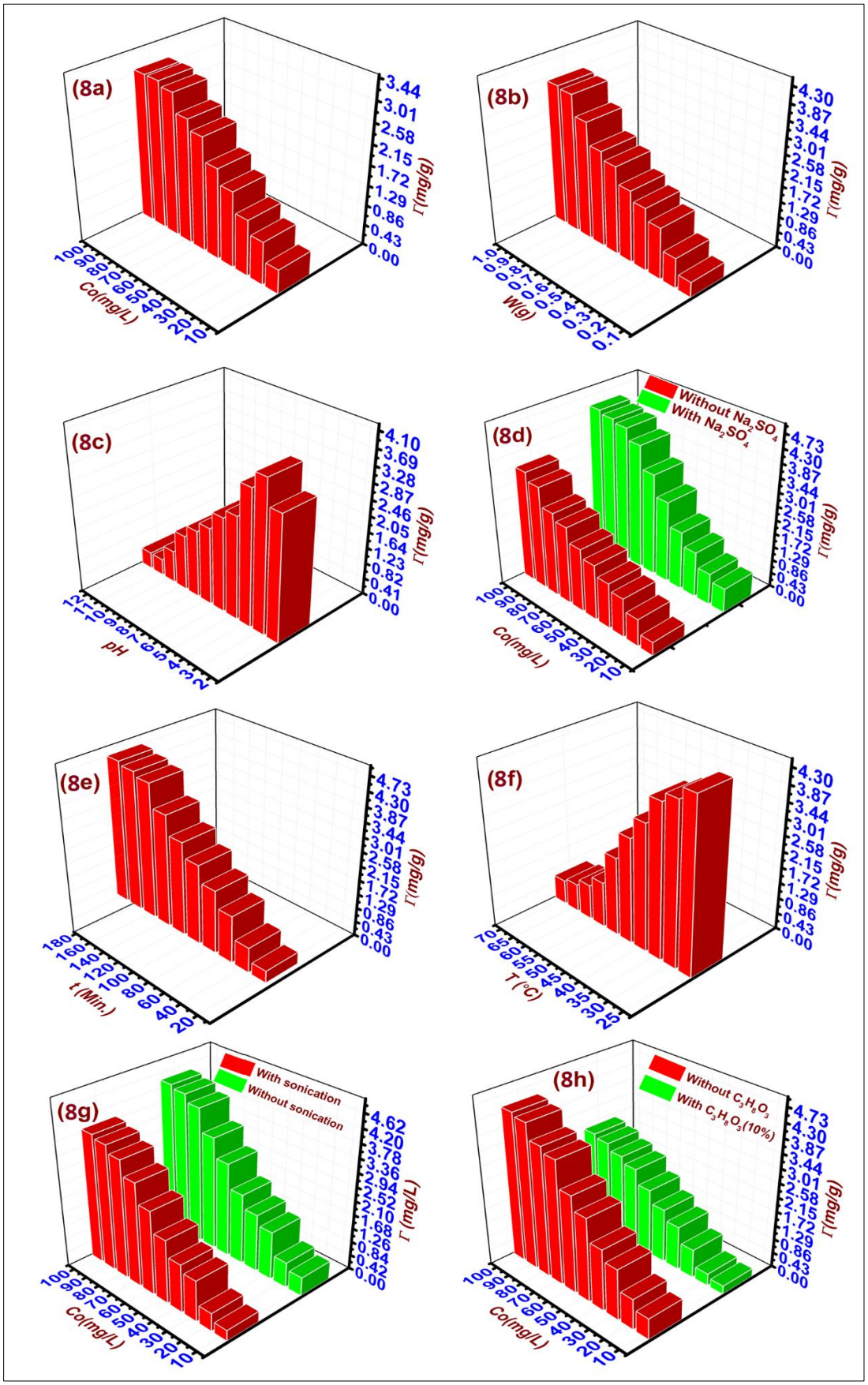

Figure 8. Effect of various factors onto NaCMC adsorption (8a). Concentration, (8b). Dose of MGFQ, (8c). pH, (8d). Ionic strength, (8e). Contact time, (8f). Temperature, (8g). Sonication and (8h). Alcohol

3.3.8 Contact time

To determine the equilibrium condition, the adsorption of NaCMC onto MGFQ was performed as a function of contact time [103]. The adsorption amount was determined by measuring the concentration of NaCMC at different time intervals (Figure 8e). It was observed that initially the adsorption amount increases due to the availability of actives sites on the surface of MGFQ and the NaCMC macromolecules could be adsorbed easily. The adsorption amount of NaCMC onto MGFQ was found a maximum within 360min. After 360 min, the adsorption amount remained unchanged, suggesting that this was the equilibrium state. The equilibrium state was achieved due to a reduced number of available vacant active sites with increasing contact time (Figure 8e). Therefore, 6h was adopted as the adsorption equilibrium time for the NaCMC adsorption onto MGFQ surface.

3.3.3 Temperature

The adsorption behaviour of NaCMC was studied as a function of temperature and the results between amount adsorbed and temperature (20, 30, 40, 50 and 60 C, $\pm 0.5^0$C unit temperature) is shown in Figure 8f. The absorption amount of NaCMC onto MGFQ decreased as the temperature increased, suggesting that the adsorption process was physical and exothermic in nature. Furthermore, the van der Waals and other non-covalent forces decreased with an increase in temperature [104]. This means that the interactions between MGFQ and NaCMC are weak, leading a decrease in adsorption amount. The physisorption of NaCMC on MGFQ occurred mainly through dispersive interactions between the adsorbate-adsorbent systems. Hence, the adsorption amount of NaCMC found to decrease with increasing temperature as mentioned in the literature [105].

3.3.7 Sonication

To find out the role of interaction between NaCMC and MGFQ, the effect of power ultrasound (sonication-20 kHz) was examined during the adsorption process. The adsorption experiment was conducted in the presence and absence of ultrasound. Results indicated that the adsorption amount in the presence of ultrasound is lower than that of in the absence of ultrasound because at a lower frequency (20 kHz) the cavitation effect is more (due to larger propagating bubble) and which caused to a weakened

interactive force between the MGFQ and NaCMC resulting decrease in the adsorption amount (Figure 8g) [49].

3.3.5 Presence of alcohols (hydrogen bond breakers)

To explain the role of interaction of the hydrogen bonding effect of alcohols [methanol (CH_3OH), and ethylene glycol [$(CH_2OH)_2$] were studied during the adsorption process. It was found that there was no change in the adsorption amount of NaCMC was examined upon addition of CH_3OH during the adsorption experiments. However, the adsorption amount was found decrease with the addition of $(CH_2OH)_2$ because $(CH_2OH)_2$ has more hydroxyl groups[106] (Figure 8h). The existence of more hydroxyl groups in $(CH_2OH)_2$ and NaCMC was responsible in the formation of a hydrogen bond between the MGFQ and NaCMC [107]. As a result, there was less interaction between NaCMC and MGFQ and decreases the adsorption [108-110].

3.4 Adsorption isotherm studies

3.4.1 Frendulich isotherm

The non-uniform distribution of adsorption that the surface of MGFQ was heterogeneous and described by an empirical Freundlich isotherm model. The following Freundlich equation was applied [111]:-

$$logQe = logK_F + \frac{1}{n} logCe \quad (4)$$

Where Γ was the amount of NaCMC adsorbed (mg/g), Ce is the equilibrium concentration of the NaCMC in solution (mg/L) and K_F and n are Freundlich constants. The values of n and K_F are calculated from the slopes and intercepts of the linear plots between log Qe *vs* log Ce (Figure 9a) were recorded in Table 2. The values of n> 1, attributed the favourable adsorption conditions. Freundlich plots are shown in Figure 9a and linearity supported that data fitted well with regression coefficient value for the adsorption system under the studied concentration range.

3.4.2 Langmuir isotherm

The maximum adsorption amount and energy of adsorption was associated with a saturated monolayer of NaCMC macromolecules onto MGFQ surface. The Langmuir isotherm model was expressed by the following formula [112]:

$$\frac{Ce}{Qe} = \frac{1}{q_{max}K_L} + \frac{C_e}{q_{max}} \quad (5)$$

Where, K_L is the Langmuir constant (L/ mg) related to the affinity of binding sites and the free energy of adsorption; Qe is the NaCMC concentration at equilibrium onto the MGFQ (mg/g); Ce is the NaCMC concentration at equilibrium in solution (mg/L); q_{max} is the NaCMC concentration when monolayer forms on the MGFQ (mg/ g). K_L and q_{max} can be determined from the slope and intercept of plot Ce/Qe *vs* Ce (Figure 9b) and are given in Table 2. The Langmuir parameters suggested that this model was highly favourable for the adsorption of NaCMC in present conditions.

3.4.3 Temkin isotherm model

To determine the indirect NaCMC/MGFQ interaction in the intermediate range of ion concentration, Temkin isotherm model was applied [113]. The linear form of Temkin isotherm model is given by the following [114-116]:

$$Qe = B_T lnA_T + B_T lnCe \quad (6)$$

Where $B_T=RT/b_T$

Qe= The amount of adsorbate adsorbed at equilibrium (mg/g), Ce= Concentration of adsorbate in solution at equilibrium (mg/L), A_T =Temkin isotherm equilibrium binding constant corresponding to maximum binding energy (L/g), b_T=Temkin isotherm constant (J/mol/.g/L), R=Universal gas constant (8.314 J/mol/K) and T= Temperature at 298 K. B_T= A constant related to the heat of adsorption (J/mol) and it is defined by the expression $B_T=RT/b_T$. if B_T has a positive value that means adsorption is exothermic and if B_T is negative value then adsorption is Endothermic. From the plot of Qe *vs* lnCe (Figure 9c), B_T and A_T can be calculated from the slopes (B_T) and intercepts B_T lnA_T respectively and given in Table 2.

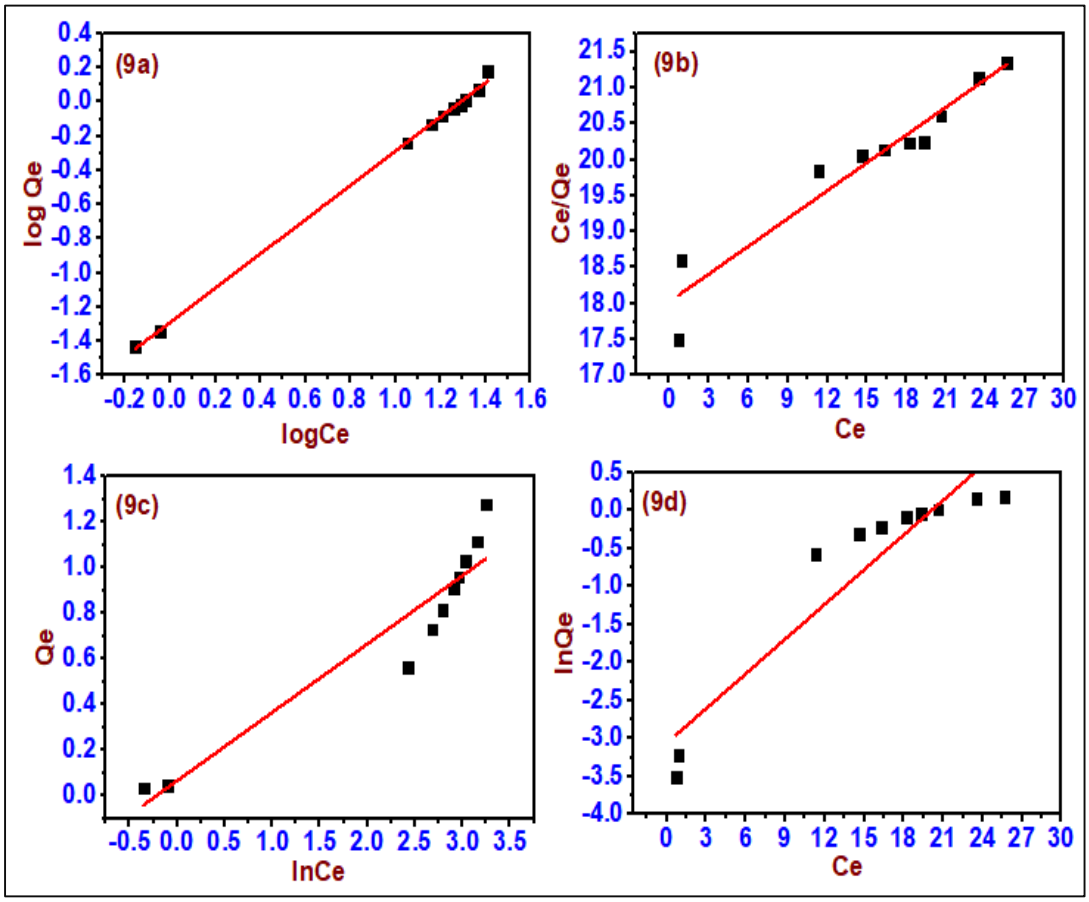

Figure 9. Adsorption isotherms models (9a). Frendulich, (9b). Langmuir, (9c). Temkin and (9d). Jovanovic

Table 2 Isotherm parameters obtained from the fit of various equations presented in figure 9

Isotherm models	**Parameters**		**Determination coefficient (R^2)**
Freundlich	n =0.99 ±0.012	K_F =0.052±0.01L/g	0.9984
Langmuir	q_{max} = 7.78±0.013 mg/g	K_L= 0.025±0.00 L/mg	0.9194
Temkin	A_T =1.255 ±0.09.mg/L	B_T = 0.299±0.00.013L/g b_T=±826.62±0.03J/mol/.g/L	0.8899
Jovanovic	q_{max} = 0.047±0.03 mg/g	K_J = ±0.15±0.01 L/mg	0.8709
Hill	n^H=0.971±0.02 K_D= -1.382×10^2	Q_H=1.306×10^2	0.9981

3.4.4 Jovanovic isotherm

The Jovanovic model was applied to find out some mechanical contacts between NaCMC and MGFQ into the aqueous system[117]. The linearized form of the Jovanovic isotherm is expressed as follows [118]:

$$\ln Qe = \ln q_{max} - K_J Ce \quad (7)$$

Where, qe is the amount of NaCMC in the MGFQ at equilibrium (mg/g), q_{max} is maximum uptake of NaCMC obtained from the plot of lnQe *vs* Ce (Figure 9d), and K_J is Jovanovic constant and summarised in Table 2. Furthermore, the obtained results of adsorption capacity of the polysaccharides were also compared with other reported work [119-124] (Table 3).

Table 3 Adsorption capacities of NaCMC onto various adsorbents compared with previous literature based on the maximum adsorption capacity

Adsorbents	Adsorbates	Amount adsorbed, Qmax (mgm^{-2})	References
Biotite Mica	Guar gum	Not reported	[119]
Amino-terminated surfaces	CMC	2.2	[120]
		1.7	
		1.2	
Talc	CMC	0.53	[121]
		0.002	
Pyrite	Guar gum, CMCs	N.A.	[122]
Talc	Dextrin and Guar gum	N.A.	
Talc	Guar gum	0.97-4.52	
Leached Talc	Guar gum	0.93-4.03	
Calcined Talc	Guar gum	0.83-3.68	
Leached Calcined Talc	Guar gum	0.76-3.45	
Talc	CMC	N.A.	[123]
Polymeric surfaces	CMC	N.A.	[124]
Mesoporous mustard carbon	CMC	0.53	[4]
MGFQ	NaCMC	Table 2	Present work

N.A. Data not available

3.4.5 Statistical physics based isotherm model treatment

A simple Hill's model obtained by statistical physics treatment was applied to define the parameter which represents the number of molecules adsorbed per site. The

assumption in this model was considered that adsorption could be a cooperative phenomenon, with the NaCMC having the ability to bind at one site on the adsorbent, which could be influencing other binding sites on the same adsorbent. Originally, the equation of this adsorption isotherm model was derived from the non-ideal competitive adsorption isotherm. The non-linear forms of this isotherm model are expressed as follows [125-127]:

$$Q_e = \frac{Q_H C_e^{n^H}}{K_D + C_e^{n^H}} \quad (8)$$

Where, Q_H=Hill isotherm maximum uptake saturation (mg/L), K_D=Hill constant, n^H=Hill cooperativity coefficient of the binding interaction. These parameters be determined non-linear fitting of experimental data (Figure 10). Furthermore, in this model if n^H =1 means that binding is hyperbolic or non-cooperative, if n^H>1, binding has positive cooperativity, while negative cooperativity occurs when nH<1. The calculated results were summarized in Table 2. The value of Hill cooperativity coefficient of the binding interaction revelled that negative cooperativity and the adsorption mechanism of NaCMC onto MGFQ accompanied by hydrogen bonding [128-131].

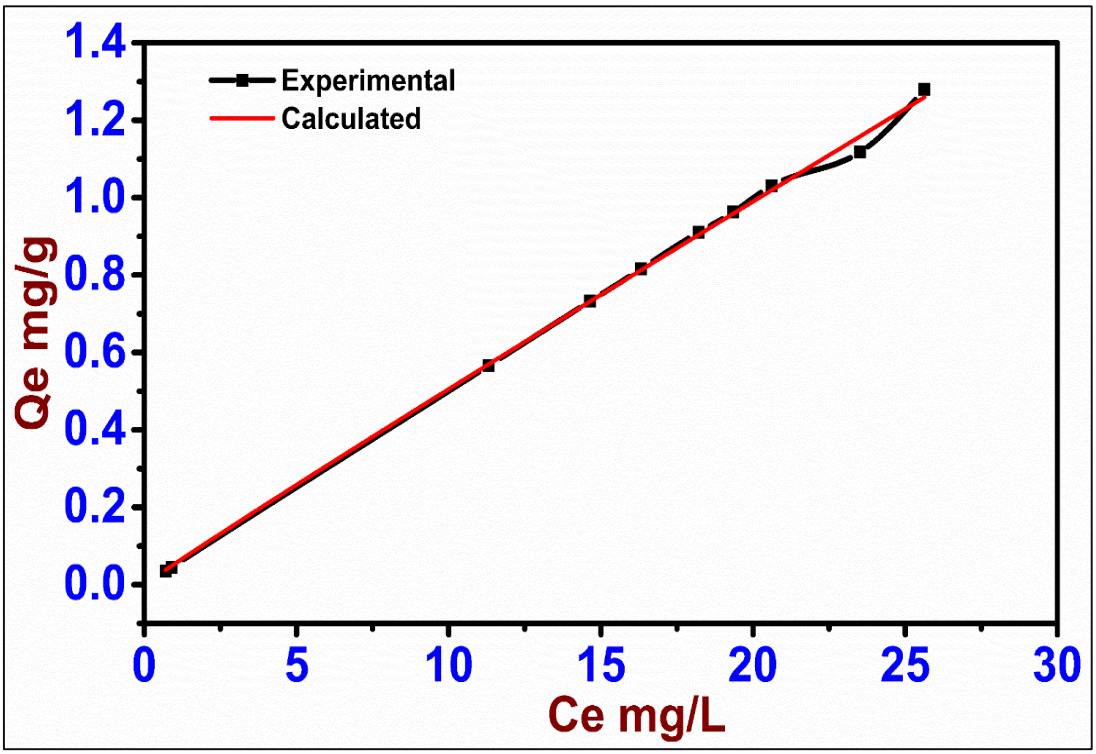

Figure 10. Hill models illustrating experimental and calculated

4. Regeneration measurement

The opposite process of adsorption was known as desorption and had a great impact on reusability of the adsorbent. Since, recent industrial trend for regeneration and reuse of adsorbents, desorption illustrated an important role for the selection (as adsorbent) of a material. So, a material, which can easily desorb, considered valuable. Therefore, the experiments for desorption of NaCMC from MGFQ was done by hydrochloric acid and double-distilled water (DDW) and the results are summarized in Table 4.

Table 4 Effect of different concentration of desorbing agent on the desorption NaCMC from MGFQ

MGFQ - NaCMC system	**Amount loaded (g)**	**% Adsorption**	**% Desorption**	**Amount recovered**	**Desorbing agents used**
	5.0	94.80	15.43	0.56	DW
		98.55	43.52	1.21	0.02M HCl
		97.84	56.66	2.32	0.05M HCl
		84.50	58.23	3.42	0.10M HCl

The adsorption efficiency decreased with re-generation cycles for H_2O and HCl. The used MGFQ regenerated by HCl possessed better efficiency. Adsorption efficiency, indicating that HCl was a suitable reagent for the regeneration process. After three cycles, the adsorption efficiency of treated MGFQ decreased from 98.55% to 84.50%. On the contrary, the adsorption efficiency decreased with regeneration cycles for H_2O which suggested that the interaction between MGFQ and NaCMC was relatively stronger, therefore, desorption of NaCMC was not easy when H_2O was used as a regeneration reagent (Table 4).

5. Conclusions

This study demonstrated that mesoporous granular fine quartz (MGFQ) was successfully prepared from supplied granular fine quartz only by one physical step and utilized further adsorption of NaCMC. The physiochemical characterizations (Table 1) and experiments confirm that MGFQ has very efficient potential adsorptive properties (Table 2). It was observed that the adsorption of NaCMC on MGFQ remarkably affected by the change in adsorptive optimized conditions such as pH, ionic strength,

sonication and presence of alcohols as hydrogen bond breaker. These observed results concluded that hydrogen bonding plays a significant role during the adsorption. The FTIR spectral changes appeared nearby 1104 cm^{-1} and 1076 cm^{-1} provided sufficient evidence to confirm the participation of strong hydrogen bonding during adsorption. The chemical structure of NaCMC was relatively open and has low steric effect for interaction with the functional groups present on MGFQ. The adsorption mechanism was associated with hydrogen bonding between active chemical functions of MGFQ (Si-O-H) and carboxylates ions of NaCMC. These Si-O-H localized active sites intract with carboxylate ion of NaCMC to form hydrogen bonding. In the aqueous system, carboxylic functions of NaCMC developed affinities with most of Si-O-H of the NaCMC. The adsorption of NaCMC on adsorbent was as a result of interaction of Si-O-H and carboxylate ion of adsobate (NaCMC). However, adsorbent being porous assist to enhance the surface area which provide the more active sites on the adsorbent (MGFQ). More active sites on the MGFQ, there could be more interaction between Si-O-H of the adsorbent and –COOH groups of NaCMC. Experimental data of the present work were excellently fitted to the Freundlich equation since the regression analysis gave high correlation coefficients R^2>0.99, as shown in Table 2. The adsorption tests resulted in the extent of interaction, various parameters, and correlation coefficient (Table 2). Therefore, it was confirmed that the adsorption was an exothermic and physical which obeyed the order as Freundlich (R^2=0.9830)> Langmuir (R^2=0.9933)>Temkin (R^2 =0.8663)>Jovanovic (R^2= 0.9428). Thus, these physicochemical adsorption aspects of NaCMC onto MGFQ provided substantial evidence to prove beyond doubt that adsorption mainly occurs *via* hydrogen bonding followed by some electronic interactions and such alteration could play a noteworthy role in the field of food, pharmaceutical, and industrial applications without damage of the environment. The results of the study presented here suggest several possibilities for future research.

References

1. Kukrety, A.; Singh, R. K.; Singh, P; Ray, S. S. Comprehension on the Synthesis of Carboxymethylcellulose (CMC) Utilizing Various Cellulose Rich Waste Biomass Resources. *Waste Biomass Valori*. **2017**, *9*, 1587–1595.

2. Hollabaug, C.B.; Burt, L.H.; Walsh, A.P. Carboxymethylcellulose. Uses and Applications. *Ind. Eng. Chem.* **1945**, *37*, 943-947.

3. Mackenzie, M.; Malhotra, D.; Riggs, W. F. Chemical Reagents in the Mineral Processing Industry. *Soc. Min. Eng*.**1986**, *1*, 312.

4. Singh, K.; Kumar, A.; Awasthi, S.; Pandey, S.K.; Mishra, P. Adsorption Mechanism Of Carboxymethyl Cellulose onto Mesoporous Mustard Carbon: Experimental and Theoretical Aspects. *Colloids Surfaces A: Physicochem. Eng. Asp*. **2019**, 581, 123786.

5. Pugh, R.J. Macromolecular Organic Depressants in Sulphides Flotation-A Review, 1. Principles, Types and Applications. *Int. J. Miner. Process*. **1989**, 25, 101-130.

6. Pugh, R.J. Macromolecular organic depressants in sulphide flotation-a review: 2. theoretical analysis of the forces involved in the depressant action. *Int. J. Miner. Process*. **1989**, 25, 131-146. 131.

7. Healy, T. W. Principals of adsorption of organics at solid –solution interfaces. *J. Macromol*. *Sci. Chem*. *A*. **1974,** *8*, 603-19.

8. Rath, R.K.; Subramanian, S. Studies on the Adsorption of Guar Gum onto Biotite and Mica. *Miner. Eng*. **1997**, *10*, 1405–1420.

9. Rath, R.K.; Subramanian, S. Adsorption, electrokinetic and differential flotation studies on sphalerite and galena using dextrin. *Int. J. Miner. Process*. **1999**, *57*, 265–283.

10. Rath, R.K.; Subramanian, S.; Laskowski, J. In: Laskowaki, J. S.; Poling, G.W. (Eds.), Processing of hydrophobic minerals and fine coal. canadian institute of mining, metallurgy and petroleum, *Montreal, Que., Canada*, **1995,** p.546**.**

11. Rath, R. K.; Subramanian, S.; Laskowski J.S. Adsorption of dextrin and guar gum onto talc. a comparative study. *Langmuir*. **1997**, *13*, 6260-6266.

12. Shortridge, P. G.; Harris, P. J.; Bradshaw, D. J.; Koopal, L. K. The effect of chemical composition and molecular weight of polysaccharide depressants on the flotation of Talc. *Int. J. Miner. Process.* **2000**, *59*, 215–224.

13. Liu, Q.; Laskowski, J. S. The role of metal hydroxides at mineral surfaces in dextrin adsorption, i. studies on modified quartz samples. *Int. J. Miner. Process*. **1989**, 26, 297–316.

14. Liu, Q.; Laskowski, J.S. The interactions between dextrin and metal hydroxides in aqueous solutions. J. *Colloid Interface Sci*. **1989**, 130, 101–111.

15. Liu, Q.; Laskowski, J.S. The role of metal hydroxides at mineral surfaces in dextrin adsorption. ii: chalcopyrite–galena separations in the presence of dextrin. *Int. J. Miner. Process*. **1989**, 27, 147–155.

16. Khraisheh, M.; Holland, C.; Creany, C.; Harris, P.; Parolis, L. Effect of molecular weight and concentration on the adsorption of CMC onto talc at different ionic strengths. *Int. J. Miner. Process*. **2005**, 75, 197–206.

17. Wang, J.; Somasundaran, P.; Nagaraj, D.R. Adsorption mechanism of guar gum at solid–liquid. *Interfaces. Miner. Eng*. **2005**, *18*, 77–81.

18. Steenberg, E.; Harris, P.J. Adsorption of carboxymethyl cellulose, guar gum and starch onto talc, sulphides, oxides and salt-type minerals. *S. Afr. J. Chem*. **1984**, *37*, 85–90.

19. O'sullivan, C. K.; Guilbault, G. G. Commercial quartz crystal microbalances–theory and applications. **1999**

20. Kalantary, R. R.; Jafari, A. J.; Kkavandi, B.; Nasseri, S.; Ameri, A.; Azari, A. Adsorption and magnetic separation of lead from synthetic wastewater using carbon/iron oxide nanoparticles composite. *J. Mazandaran Univ Med. Sci*. **2014**, 24, 172-183.

21. Nabizadeh, S.; Shariatifar, N.; Shokoohi, E.; Shoeibi, S.; Gavahian, M.; Fakhri, Y.; Khaneghah, M. A. Prevalence and probabilistic health risk assessment of aflatoxins

B1, B2, G1, and G2 in Iranian edible oils. *Env.Sci. Poll. Res*. **2018**, 25, 35562–35570.

22. Karamia, A.; Karimyan, K.; Davoodia, R.; Karimaeic, M.; Sharafiee, K.; Rahimif, S.; Khosravia, T.; Mirig, M.; Sharafia, H.; Azaria, A. Application of response surface methodology for statistical analysis, modeling, and optimization of malachite green removal from aqueous solutions by manganese-modified pumice adsorbent. *Desal. Water Treat*. **2017**, 89, 150–161.

23. Azari1, A.; Salari, M.; MDehghani, M.H.; Alimohammadi, M.; Ghaffari , H.; Sharafi1, K.; Shariatifar, N.; Baziar, M. Efficiency of magnitized graphene oxide nanoparticles in removal of 2, 4-dichlorophenol from aqueous solution. *J. Mazandaran Univ. Med. Sci.* **2016**, 26, 265-281.

24. Badi1, M. Y.; Esrafili, A.; Kalantary, R. R.; Azari, A.; Ahmadi, E.; Gholami, M. Removal of diethyl phthalate from aqueous solution using persulfate-based (UV / Na2S2O8 / Fe^{2+}) advanced oxidation process. *J. Mazandaran Univ. Med. Sci*. **2015**, 25, 122-135.

25. Badi1, M.Y.; Azari, A.; Esrafili, A.; Ahmadi, E.; Mitra Gholami, M. Performance evaluation of magnetized multiwall carbon nanotubes by iron oxide nanoparticles in removing fluoride from aqueous solution. *J. Mazandaran Univ. Med. Sci*. **2015**, 25, 128-142.

26. Wu, J.; Lin, J.; Li, G.; Wei, C. Influence of the COOH and COONa groups and crosslink density of poly (acrylic acid)/montmorillonite superabsorbent composite on water absorbency. *Poly. Int.* **2001**, *50*, 1050–1053.

27. Anderson, Robert S.; Anderson Suzanne P. Geomorphology: the mechanics and chemistry of landscapes. *University Press, Cambridge*. **2010** pp.187.

28. Moazzen, M.; Khaneghah, A.M.; Shariatifar, N.; Ahmadloo, M.; Baghani, I. Eş, A.N.; Yousefinejad, S.; Alimohammadi, M.; Azari, A.; Dobaradaran, S.; Rastkari, N.; Nazmara, S.; Delikhoon, M.; Khaniki, J. G. Multi-walled carbon nanotubes modified with iron oxide and silver nanoparticles (MWCNT-Fe3O4/Ag) as a novel adsorbent for determining paes in carbonated soft drinks using magnetic SPE-GC/MS method. *Arabian J. Chem*. **2018**, 2-41.

29. Azari, A.; Babaei A.A.; Rezaei-Kalantary, R.; Esrafili, A.; Moazzen, M.; Kakavandi, B. Nitrate removal from aqueous solution using carbon nanotubes magnetized by nano zero-valent iron. *J. Mazand Univ Med. Sci*. **2014**, 23, 15-27.

30. Singh, K.; Gautam, M. Development of inexpensive biosorbents from de-oiled mustard cake for effective removal of As(V) And Pb(II) ions from their aqueous solutions. *J. Sci. Ind. Res*. **2016**, *75*, 444.

31. Mahmood, T.; Saddique, M. T.; Naeem, A.; Westerhoff, P., Mustafa, S.; Alum, A. Comparison of different methods for the point of zero charge determination of NiO. *Ind. Eng. Chem. Res*. **2011**, *50*, 10017–10023.

32. Fiol, N.; Villaescusa, I. Determination of sorbent point zero charge: usefulness in sorption studies. *Environ. Chem. Lett*. **2008,** *7*, 79–84.

33. Malekbala, M. R.; Hosseini, S.; Kazemi Yazdi, S.; Masoudi Soltani, S.; Malekbala, M. R. The study of the potential capability of sugar beet pulp on the removal efficiency of two cationic dyes. *Chem. Eng. Res. Des*. **2012**, *90*, 704–712.

34. Singh, K.; Chandra, B. Synthesis, Characterization of new adsorbent material from agriculture waste and its use for removal of phenols. *Frontiers Env. Res*. **2014,** 1, 11-21.

35. Singh, K.; Kumar, A. Adsorption and conformation of carboxymethyl cellulose at Tio_2- modified mesoporous carbon derived from mustard cake. *Proceeding of GCGHGSPCT–2K19*. **2019.** 1, pp.131-150.

36. Singh, K.; Gautam, M.; Chandra, B.; Kumar, A. Removal of Pb(II) from its aqueous solution by activated carbon derived from Balam Khira (Kigelia Africana). *Desal. Water Treat*. **2016**, *57*, 1-11.

37. Scimeca, M.; Bischetti, S.; Lamsira, H. K.; Bonfiglio, R.; Bonanno, E. Energy dispersive X-ray (EDX) microanalysis: A powerful tool in biomedical research and diagnosis. *Eur. J. Histochem*. **2018**, 62, 2841.

38. Awang1, M.; , Zuki, A. A. A.; Mahmud, A. A., Jaafar, J. J.; Zain, M. H. Application of microwave-treated casuarina equisetifolia seeds in adsorption of dyes. *J. Fundam. Appl. Sci*. **2017**, 9, 458-471.

39. Moore, D. M.; Reynolds, J.R. C. X-Ray Diffraction and the identification and analysis of clay minerals. 2nd Ed. *Oxford University Press, New York*. **1997,** pp.819-842**.**

40. Ahmad, N.; Rizwan Wahab, R.; Omar, S.Y.A. Thermal decomposition kinetics of sodium carboxymethyl cellulose: model-free methods. *European J. Chem*. **2014**, 5, 247-251.

41. Dubois, M.; Gilles, K. A.; Hamilton, J. K.; Rebers, P. A. Smith, F. Colorimetric method for determination of sugars and related substances. *Anal. Chem.* **1956**, 28, 350.

42. Mirji, S. A. Octadecyltrichlorosilane adsorption kinetics on Si(100)/SiO_2 surface: contact angle, AFM, FTIR and XPS analysis. *Surf. Interface Anal.* **2016**, 38, 158–165.

43. Yang, X.H.; Zhu, W.L.; Viscosity Properties of Sodium carboxymethyl cellulose solutions. *Cellulose*. **2007**, 14, 409–417.

44. Iftekhar, S.; Ramasamy, D. L.; Srivastava, V.; Asif, M. B.; Sillanpaa, M. Understanding the factors affecting the adsorption of lanthanum using different adsorbents: A critical review. *Chemosphere*. **2018**, 204, 413–430.

45. Rani, S.; Sud, D. Effect of temperature on adsorption-desorption behaviour of triazophos in indian soils. *Plant Soil Environ*. **2015**, 61, 36–42.

46. Chytil, M.; Lišková, K.; Janeček, J. The influence of counterions of different valency on carboxymethylcellulose viscoelastic behavior. *Book Chapter*. **2014**.

47. Davis, J.A.; Leckie, J.O. Surface ionization and complexation at the oxide/water interface. 3. adsorption of anions. *J. Colloid Interface Sci*. **1980**, 74, 32-43.

48. Panda, H.; Tiadi, N.; Mohanty, M.; Mohanty, C. R. Studies on adsorption behavior of an industrial waste for removal of chromium from aqueous solution. *South Afr. J. Chem. Eng*. **2017**, 23, 132–138.

49. Singh, K.; Gupta, S. P.; Kumar, A.; Kumar, A. (2018). The effect of high intensity ultrasound (HIU) on the kinetics of crystallization of sucrose: Elimination of Latent Period. *Ultrason. Sonochem*. **2019**, 52, 19-24.

50. Anwar, J.; Shafique, U.; Waheed-uz-Zaman, M. S.; Dar, A.; Anwar, S. Removal of Pb (II) and Cd(II) from water by adsorption on peels of Banana, *Bioresour. Technol*. **2010**, 101, 1752–1755.

51. Piccin, J. S.; Dotto, G. L.; Pinto, L. A. A. Adsorption isotherms and thermochemical data of FD&C Red N 40 binding by chitosan. *Braz. J. Chem. Eng*. **2011**, 28, 295-304.

52. Freundlich H. Über die adsorption in Lösungen. *Z Fã¼r PhysChemie/international J. Res. Phys. Chem. Chem. Phys*. **1907**, 57U, 385–470.

53. Langmuir I. The adsorption of gases on plane surfaces of glass, mica and platinum. *J. Am. Chem. Soc*. **1918**, 40, 1361–403.

54. Amin, M.T.; Alazba, A.A.; Shafiq, M. Adsorptive removal of reactive black 5 from wastewater using bentonite clay: isotherms, kinetics and thermodynamics. *Sustainability*. **2015**, 7, 15302–15318.

55. Temkin M.I.; Pyzhev V. Kinetics of ammonia synthesis on promoted iron catalyst. *Acta Physiochem. U.S.S.R*. **1940**, 12, 327–356.

56. Hernandez, B.; Ibanez, J. G.; Ramirez J. J. G.; Calvo, F.A. Microscale environmental chemistry: Part 7. Estimation of the point of zero charge (PZC) for simple metal oxides by a simplified potentiometric mass titration method. *Chem. Educator*. **2006**, 11, 267.

57. Ibanez, J. G.; Esparza, M. H.; C. Serrano, C. D.; Infante, A. F.; Singh, M. M. Environmental chemistry fundamentals. *Env. Chem. Fund. Springer*, New York. **2007**.

58. Kriaa, A.; Hamdi, N.; Srasra, A. Proton adsorption and acid-base properties of tunisian illites in aqueous solution. *J. Struct. Chem.* **2009**, 50, 273-287.

59. Mahmood, T.; Saddique, M.T.; Naeem, A.; Westerhoff, P.; Mustafa, S.; Alum, A. Comparison of different methods for the point of zero charge determination of NiO. *Ind. Eng. Chem. Res*. **2011**, 50, 10017-10023.

60. Brunauer, S; Emmett, PH; Teller, E. Adsorption of gases in multimolecular layers. *J. Am. Chem. Soc.* **1938**, 60, 309-19.

61. Barrett, E. P.; Joyner, L. G.; Halenda, P. P. The determination of pore volume and area distributions in porous substances. i. computations from nitrogen isotherms. *J. Am. Chem. Soc.* **1951**, 73, 373-80.

62. Joyner, L. G.; Barrett, E. P.; Skold, R. The determination of pore volume and area distributions in porous substances. ii. comparison between nitrogen isotherm and mercury porosimeter methods. *J. Am. Chem. Soc*. **1951**, 73, 3155-8.

63. Lippens, B.C.; de Boer, J. H. Studies on pore systems in catalysts v. the T method. *J. Catalysis*. **1965**, 4, 319.

64. Dąbrowski, A. Adsorption—from theory to practice. *Adv. Colloid Interface Sci*. **2001**, 93, 135-224.

65. McCusker, L.; Liebau, F.; Engelhardt, G. Nomenclature of structural and compositional characteristics of ordered microporous and mesoporous materials with inorganic hosts (IUPAC recommendations 2001). *Pure Appl. Chem*. **2001**, 73, 381-94.

66. McCusker, L.; Liebau, F.; Engelhardt, G. Nomenclature of structural and compositional characteristics of ordered microporous and mesoporous materials with inorganic hosts:(IUPAC recommendations 2001). *Microporous Mesoporous Mater*. **2003**, 58, 3-13.

67. Guo, M.; Wang, H.; Huang, D.; Han, Z.; Li, Q, Wang, X.; et al. Amperometric catechol biosensor based on laccase immobilized on nitrogen-doped ordered mesoporous carbon (N-OMC)/PVA matrix. *Sci. Technol. Adv. Mat*. **2014**, 15, 035005.

68. Yang, X. H.; Zhu, W.L. Viscosity properties of sodium carboxymethylcellulose solutions. *Cellulose*. **2007**, 14, 409–417.

69. Veis, A. E.; Palazoglu, T. K.; Sandeep, K. P.; Daubert, C. H. R. Rheological characterization of carboxymethylcellulose solution under aseptic processing conditions. *J. Food Process Eng*. **2002**, 25, 41–61.

70. Heinze, T.; Koschella, A. Carboxymethyl ethers of cellulose and starch-a review. *Macromol. Symp*. **2005**, 223, 13–39.

71. Du, B.; Li, J.; Zhang, H.; Huang, L.; Chen, P.; Zhou, J. Influence of molecular weight and degree of substitution of carboxyethylcellulose on the stability of acidified milk drinks. *Food Hydrocolloids*. **2009**, 23, 1420-1426.

72. O'sullivan, C. K.; Guilbault, G. G. Commercial quartz crystal microbalances–theory and applications. *Biosensors and Bioelectronics*. **1999**, 14, 663-670.

73. Grant, F. S. Aeromagnetics, geology and ore environments, i. magnetite in igneous, sedimentary and metamorphic rocks: An overview. *Geoexploration*. **1985**, 23, 303-333.

74. Vos, K.; Vandenberghe, N.; Elsen, J. Surface textural analysis of quartz grains by scanning electron microscopy (SEM): From sample preparation to environmental interpretation. *Earth Sci. Rev*. **2014**, 128, 93–104.

75. Krinsley, D. H.; Doornkamp, J. C. Atlas of quartz sand surface textures. *Cambridge. University Press, Cambridge*. **1973**, pp.91.

76. Charalampides, A. G.; Liana, A.; Vatalis, K.; Benetis, N. P. Elemental and phase characterization of quartz samples from meliti (Florina, Greece). *MATEC Web. of Conf.* **2017,** 112, 10013.

77. Rottier, B.; Rezeau, H.; Casanova, V.; et al. Trace element diffusion and incorporation in quartz during heating experiments. *Contrib. Mineral Petr.* **2017,** 172, 1-23.

78. Kammler, H. K.; Beaucage, G.; Mueller, R.; Pratsinis, S. E. Structure of flame-made silica nanoparticles by ultra-small-angle X-ray scattering. *Langmuir***. 2004**, 20, 1915-1921.

79. Kammler, H. K.; Beaucage, G.; Kohls, D. J.; Agashe, N.; Ilavsky, J. Monitoring simultaneously the growth of nanoparticles and aggregates by in situ ultra-smallangle X-ray scattering. *J. Appl. Physics*. **2005**, 97, 054309-11.

80. Hyeon-Lee, J.; Beaucage, G.; Pratsinis, S. E.; Vemury, S. Fractal analysis of flame synthesized nanostructured silica and titania powders using small-angle X-ray scattering. *Langmuir*. **1998**, 14. 5751-5756.

81. Gallagher, P. K. Thermogravimetry and thermomagnetometry, in handbook of thermal analysis and calorimetry, Ed. Brown, *M. E. Elsevier Science B. V., Amsterdam*, **1998**, 1, pp. 225-278.

82. Gongwer, P. E.; Arisawa, H.; Brill, T. B. Kinetics and products from flash pyrolysis of cellulose acetate butyrate (CAB) at 460–600°C. *Combust Flame*. **1997**, 109, 370–381.

83. Qin, Qu.; Sharom, F. J. FRET Analysis indicates that the two atpase active sites of the p-glycoprotein multidrug transporter are closely associated. *Biochemistry*. **2001**, 40, 1413-1422.

84. Kurtz, M.; Dipl. C. J. S.; Hinrichsen, O.; Muhler, M.; Fink, K.; Meyer, B.; Wöll, C. Active sites on oxide surfaces: ZnO-catalyzed synthesis of methanol from CO and H_2. **2005**, 44, 2790-2794.

85. Zhang, L.; Zhang, B.; Wu, T.; Sun D.; Li, Y. Adsorption behavior and mechanism of chlorophenols onto organoclays in aqueous solution. *Colloids Surf. A*, **2015**, 484, 118–129.

86. Kondor, A.; Quellet C.; Dallos, A. Surface characterization of standard cotton fibres and determination of adsorption isotherms of fragrances by IGC. *Surf. Interface Anal*. **2015**, 47, 1040–1050.

87. Ma X.; Pawlik, M. Effect of alkali metal cations on adsorption of guar gum onto quartz. *J. Colloid Interface Sci*. **2005**, 289, 48–55.

88. Liu, Q.; Zhang, Y.; Laskowski, J.S. The adsorption of polysaccharides onto mineral surfaces: an acid/base interaction. *Int. J. Miner. Process*. **2000**, 60, 229–245.

89. Ma, X.; Pawlik, M. Adsorption of guar gum onto quartz from dilute mixed electrolyte solutions. *J. Colloid Interface Sci.* **2006**, 298, 609–614.

90. Suresh, S. J.; Kapoor, K.; Talwar, S. *J. Mol. Liq.* **2012**, 174, 135–142.

91. Ma X. Pawlik, M. Internal structure of water around cations. *J. Colloid Interface Sci*. **2007**, 313, 440–448.

92. Wang, J.; Somasundaran, P.; Nagaraj, D.R. The importance of rheology in mineral flotation: A Review. *Miner. Eng.* **2005**, 18, 71–81.

93. Grza˛dka, E. Wis´niewska, M. Diabetic ketoacidosis and acute mountain sickness: case report and review of treatment options in type 1 diabetes mellitus. *J. Surfactants Deterg*. **2015**, 18, 445–453.

94. K.; Lin, Wu, C.; Jochems, A. P. The Constitution and fundamental properties of solids and liquids. part i. solids. *J. Mol. Liq.* **2017**, 232, 269–276.

95. Saien J.; Kharazi, M. A comparative study on the interface behavior of different counter anion long chain imidazolium ionic liquids. *J. Mol. Liq.* **2016**, 220, 136–141.

96. Leone, V. O.; Pereira, M.C.; Aquino, S.F.; Oliveira, L.C.A.; Correa, S.; Ramalho, T.C.; Gurgel, L.V.A.; Silva, A.C. Adsorption of Diclofenac on A magnetic adsorbent based on maghemite: experimental and theoretical studies. *New J. Chem.* **2018**, 42, 437–449.

97. Liu, W.; Yang, L.; Xu, S.; Chen, Y.; Liu, B.; Li, Z.; Jiang, C. Efficient removal of hexavalent chromium from water by an adsorption–reduction mechanism with sandwiched nanocomposites. *RSC Adv.* **2018**, 8, 15087–15093.

98. Gupta, S.S.; Bhattacharyya, K.G. Adsorption of metal ions by clays and inorganic solids. *RSC Adv.* **2014**, 4, 28537–28586.

99. Zhang, Z.; Fenter, P.; Cheng, L.; Sturchio, N.C.; Bedzyk, M.J. Ion adsorption at the rutile−water interface: linking molecular and macroscopic properties. *Langmuir.* **2016**, 20, 4954–4969.

100. Ona-Nguema, G.; Morin, G.; Juillot, F.; Calas, G.; Brown, G. EXAFS analysis of arsenite adsorption onto two-line ferrihydrite, hematite, goethite, and lepidocrocite. *Environ. Sci. Technol*. **2005**, 39, 9147–9155.

101. Zhang, Y.; Cremer, P. Molecular mechanisms of ion-specific effects on proteins. *Curr. Opin. Chem. Biol*. **2006**, 6, 658–663.

102. Be´nard, P.; Chahine, R. Modeling of high-pressure adsorption isotherms above the critical temperature on microporous adsorbents: application to methane. *Langmuir*. **1997**, 13, 808–813.

103. Nolan, M. Molecular adsorption on the doped (110) ceria surface. *J. Phys. Chem. C*. **2016**, 113, 2425–2432.

104. Milligan M.S.; Altwicker, E.R. Chlorophenol reactions on fly ash. 2. Equilibrium surface coverage and global kinetics. *Environ. Sci. Technol*. **1996**, 30, 230–236.

105. Davis J. A.; Leckie, J. O. Surface ionization and complexation at the oxide/water interface. 3. adsorption of anions. *J. Colloid Interface Sci*. **1980**, 74, 32–43.

106. Baghenejad, M.; Javaheri, F.; Moosavi, A. A. Adsorption isotherms of some heavy metals under conditions of their competitive adsorption onto highly calcareous soils of southern iran. *Arch. Agron. Soil Sci*. **2016**, 62, 1462–1473.

107. Kinniburgh, D.G. General purpose adsorption isotherms. *Environ. Sci. Technol.* **1986**, 20, 895–904.

108. Foo, K. Y.; Hameed, B. H. Insights into the modeling of adsorption isotherm Systems. *Chem. Eng. J.* **2010**, 156, 2–10.

109. Vasilev, A. M.; Beattie, D. A. Adsorption of tailored carboxymethyl cellulose polymers on talc and chalcopyrite: correlation between coverage, wettability, and flotation. *Min. Eng.* **2010**, 23, 985–993.

110. Hoogendam, C. W.; de Keizer, A.; Cohen Stuart, M. A.; Bijsterbosch, B. H.; Batelaan, J. G.; van der Horst, P. M. *Langmuir*, **1998**, 14.

111. Boparai, H. K.; Joseph, M.; O'Carroll, D. M. Kinetics and thermodynamics of cadmium ion removal by adsorption onto nano zerovalent iron particles. *J. Hazardous Materials*. **2011**, *186*, 458–465.

112. G¨unay, E.; Arslankaya, I. T. Lead removal from aqueous solution by natural and pretreated clinoptilolite: adsorption equilibrium and kinetics. *J. Hazardous Materials*. **2007**, 146, 362–371.

113. Ringot, D.; Lerzy, B.; Chaplain, K.; Bonhoure, J.-P.; Auclair, E.; Larondelle, Y. In vitro biosorption of ochratoxin a on the yeast industry by-products: comparison of isotherm models. *Bio. Tech.* **2007**, 98, 1812–1821.

114. Vijayaraghavan, K.; Padmesh, T.V.N.; Palanivelu, K.; Velan, M. Biosorption of nickel(II) ions onto sargassum wightii: application of two-parameter and three-parameter isotherm models. *J. Hazardous Materials*. **2006**, 133, 304–308.

115. Samarghandi, M.R.; Hadi, M.; Moayedi, S.; Askari, F.B. Two-parameter isotherms of methyl orange sorption by pinecone derived activated carbon. *Iranian J. Env. Health Sci. Eng*. **2009**, 6, 285–294.

116. Aharoni, C.; Ungarish, M. Kinetics of activated chemisorption. part 2. theoretical models. *J Chem. Soc. Faraday Trans.1*. **1977**, 73, 456–464.

117. V. C. Kiseler. Vapour. Adsorption in the formation of adsorbate mollecule complexes on the surface. *Kolloid Zhur*. **1958**, 20, 338–348.

118. Gubernak, M.; Zapała, W.; Tyrpien, K. Kaczmarski, K. Analysis of amylbenzene adsorption equilibria on different RP-HPLC. *Acta Chromatographica*. **2004**, 42, 9, 457–463.

119. Rath, R. K.; Subramanian, S. Studies on adsorption of guar gum onto biotite mica. *Miner. Eng*. **1997**, 10, 1405–1420.

120. Fujimoto, J.; Petri, D. F. S. Adsorption behavior of carboxymethylcellulose on amino-terminated surfaces. *Langmuir*. **2001**, 17, 56–60.

121. Wang, J.; Somasundaran, P. Adsorption and conformation of carboxymethyl cellulose at solid-liquid interfaces using spectroscopic, AFM and allied techniques. *J. Colloid Interface Sci*. **2005**, 291, 75-83.

122. Bicak, O.; Ekmekci, Z.; Bradshaw, D. J.; Harris, P. J. Adsorption of guar gum and CMC on pyrite. *Miner. Eng.* **2007**, 20, 996–1002.

123. Linh, T.; Chiem, C.; Huynh, L.; Ralston, J.; Beattie, D. A. In situ particle film atr ftir spectroscopy of carboxymethyl cellulose adsorption on talc: binding mechanism, ph effects, and adsorption kinetics. *Langmuir*. **2008**, 24, 15, 8036–8044.

124. Rupert, K.; Tamilselvan, M.; Matej, B.; Martin, K.; Aleš, D.; Karin, S.K.; Volker, R. Adsorption of carboxymethyl cellulose on polymer surfaces: evidence of a specific interaction with cellulose. *Langmuir*. **2012**, 28, 11440-11447.

125. Dotto, G. L.; Pinto, L. A. A.; Hachicha, M. A.; Knani, S. New physicochemical interpretations for the adsorption of food dyes on chitosan films using statistical physics treatment. *Food Chem*. **2015**, 171, 1–7.

126. Bergaoui, M.; Nakhli, A.; Benguerba, Y.; Khalfaoui, M.; Erto, A.; Soetaredjo, F. E.; Ernst, B. Novel insights into the adsorption mechanism of methylene blue onto organo-bentonite: adsorption isotherms modeling and molecular simulation. *J. Mol. Liq*. **2018**, 697-707.

127. Sellaoui, L.; Guedidi, H.; Knani, S.; Reinert, L.; Duclaux, L.; Lamine, B. A. Application of statistical physics formalism to the modeling of adsorption isotherms of ibuprofen on activated carbon. *Fluid Phase Equil*. **2015**, 387, 103–110.

128. Al-Qodah Z.; Shawaqfeh A.T.; Lafi W.K. Two-resistance mass transfer model for the adsorption of the pesticide deltamethrin using acid treated oil shale ash. *Adsorption*. 2007, 13, 73-82.

129. Al-Qodah Z. Adsorption of methylene blue with diatomite. *J. Eng. Technol*. **1998**, 17, 128-37.

130. Al-Qodah, Z.; Lafi, W.K.; Al-Anber, Z.; Al-Shannag, M.; Harahsheh, A. Adsorption of methylene blue by acid and heattreated diatomaceous silica. *Desalination.* **2007,** 217, 212-224.

131. Al-Qodah, Z.; Shawaqfeh, A.T; Lafi, W.K. Adsorption of pesticides from aqueous solutions using oil shale ash. *Desalination.* **2007**, 208, 294-305.

Chapter 6

Interpretation of adsorption behaviour of cellulose, sodium carboxymethylcellulose and hydroxyethylcellulose onto activated kaolin

Abstract

This chapter reports systematic investigation of the adsorption behaviour of polysaccharides such as cellulose (CL), sodium carboxymethylcellulose (Na-CMC) and hydroxyethylcellulose (HEC) onto activated kaolin (AK). The specific surface area of activated kaolin was S_{BET}=18.57 m^2/g. The AK exhibited pore distribution with a maximum peak centered at 10.534 nm and pore diameter=2.113nm which indicating mesoporous nature. The zeta potential of AK was found to be 92.44(mV) suggested that it has strong stability and positive surface in aqueous medium. The effect of various factors (concentration, adsorbent dose, pH, contact time and temperature) on adsorption of aforesaid polysaccharides onto activated kaolin was investigated. The shifting has occurred in Si-O-H stretching at bands 1114^{-1} and 694 cm^{-1} that may be attributed to the formation of hydrogen bonds between Si-O-H of activated kaolin and carboxylate ion of Na-CMA, hydroxyl ion of CL and HEC. Experimental data were best fitted to the Langmuir model since the adjusted R^2 gave high correlation coefficients R^2>0.99, for Na-CMC than HEC and CL. Therefore, it was confirmed that the adsorption is exothermic and physical in nature. These finding confirmed that adsorption of selected polymers onto activated kaolin occurs via hydrogen bonding followed by some electronic interactions.

Chapter 7

Conclusions and prospectus

1. Introduction

The importance of organic polymers, cellulose and its derivatives, have been generally recognized for a broad range of applications throughout the world because of its simple availability, characteristics properties and low-cost [1]. Cellulose is the most abundant and widely used organic polymers. On a dry basis, wood contains about 40 to 50% cellulose. Due the presence of numerous hydroxyl groups in polymeric chain of cellulose, it is also known as polyhydroxyl alcohol. These hydroxyl groups allow several chemical modifications. Most of the chemically modified cellulose polymers are accounted for by cellulose esters and cellulose ethers (sometimes referred to as "classical cellulose derivatives") [2]. Cellulose and its derivatives (polysaccharides) are condensation polymers of high molecular weights based on simple monosaccharide sugar units. Many different types of polysaccharides exist in nature but only a small number of them have been used in mining and mineral processing industries and their allied industries, especially in flotation and mineral processing [3-4]. These include cellulose and its derivatives namely cellulose (CL), sodium carboxymethylcellulose (NaCMC) and hydroxyethylcellulose (HEC) and they were mainly used as flotation depressants. The most common representatives of the group of cellulose ethers are methylcellulose/CL, Na-CMC and HEC. The selected polymers exhibit the characteristics properties such as a water-soluble, hydrophilic, and macromolecular anionic polymer without any refinement in various sectors. Methylcellulose is employed, amongst others, as coating agent, as thickeners. HEC is prepared by treating alkali cellulose with ethylene oxide. HEC usually has polyethylene oxide side chains. Since HEC is a water-soluble polymer it is applied as a thickener and pigment-protective colloid in water-based paints. Further it has also applications in cement, in pharmaceutical emulsions, as a binder in tablets, and in cosmetic products. The Na-CMC is an anionic cellulose ether which is prepared by the reaction of sodium monochloroacetic acid and alkali cellulose [5]. Though most applications concern the sodium salt of CMC, it is generally referred to Na-CMC. As Na-CMC has such abilities as thickening water, suspending solids, thickener coating agents, etc. [6]. The applicability of polymers were associated with adsorption behaviour onto solid surfaces and makes them suitable for a wide range of applications in various sectors especially in mineral processing [7]. The adsorption behaviour of selected polymer could vary due to functional groups present on them (Scheme 1). Several studies were presented for

the adsorption of natural polysaccharides (dextrin, starch) on mineral surfaces through chemical interaction with superficial metal hydroxides and it was suggested that a their adsorption mechanism on mineral surfaces as chemical complex formations [8-12]. Even the chemical interaction was proposed as the main mechanism of polysaccharide adsorption on mineral surfaces the totally different mechanisms were observed by different researchers for the same mineral-polysaccharide system [13]. However, for the flotation system, it is crucial to understand how the adsorption of each reagent takes place on the minerals surfaces and what is the adsorption capacity of each one to have more information about the rate of over coating of the minerals and which adsorption processes are involved [14]. The adsorption behaviour of cellulose and derivatives polysaccharides various solid surfaces have been reported including kaolinite surface and other oxide minerals at different pH, background electrolyte, and ionic strength. The polymer adsorbed onto the mineral surface through various interaction were reported by several researchers [15]. The reported studies raveled that polymers have a natural affinity towards these mineral surfaces. The majority of these works were carried out to understand application of polymers as a depressant in flotation, mineral processing and selective flocculation system. However, not many reports were available regarding the polymers for adsorption behaviour mechanism. Therefore, the adsorption behaviour of polymers (CL, Na-CMC, and HEC) onto activated kaolin (AK) was studied. Several studies were conducted in the past but the mechanism of adsorption of polysaccharides on solid surfaces is not yet well understood. Several researchers proposed that the mechanisms governing the adsorption of polymers (polysaccharides) onto mineral surfaces include hydrophobic interaction, hydrogen bonding, chemical, and electrostatic interactions [16-26]. However, the reasons for the selectivity of the adsorption of depressants on minerals have not been accounted. The present study has shown polymers adsorption to be more complex than this and has highlighted the need for a more comprehensive model of the adsorption mechanism. Therefore, physiochemical aspect for the adsorption behavior of CL, Na-CMC and HEC onto AK from its aqueous solutions was the topic of research interest and gave CL, Na-CMC and HEC's selective adsorption behaviour onto AK.

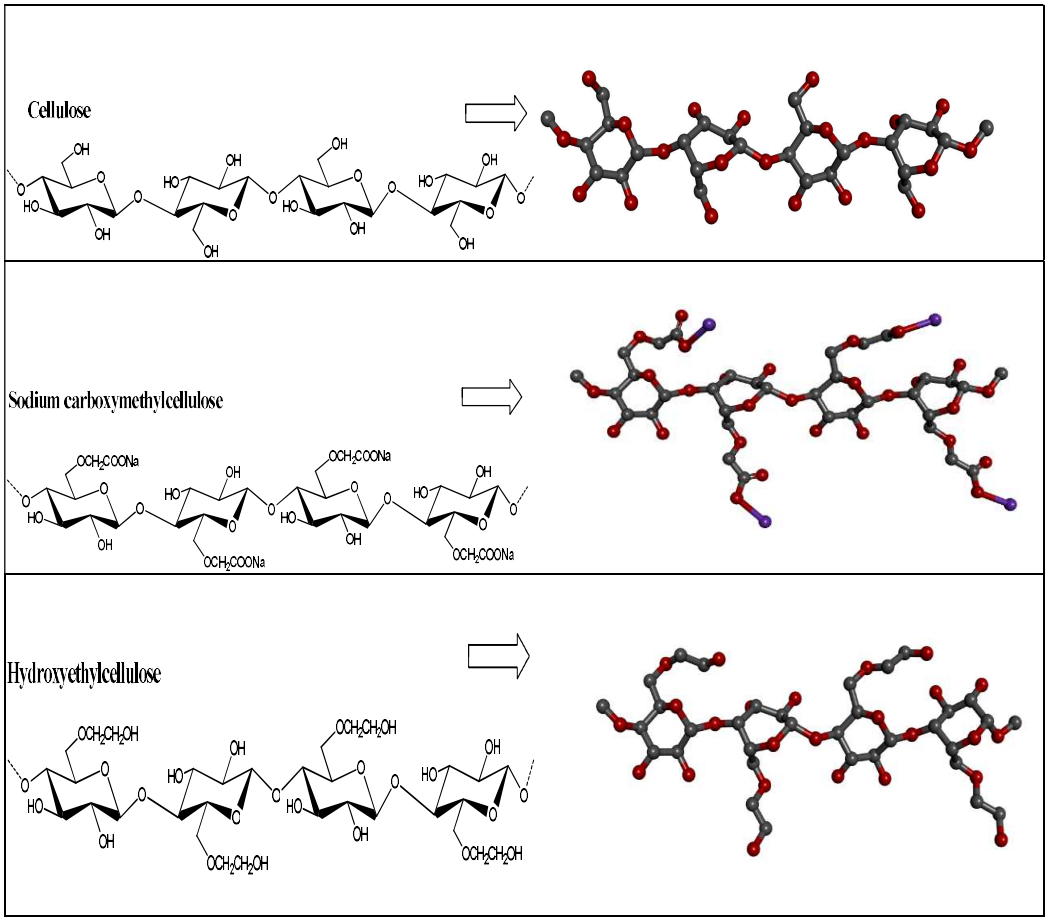

Scheme 1: Structuer of cellulose and its derivaatives (Repeating unit of glucose) shows the d-glucose units are linked through β-1, 4 bonds. ----O represents the continuation of the polymeric chain (2D chain) and Black, red, and pruple colure represnts carbon, oxygen and sodium atoms (3D chain) respectively [3, 4]

The experimental data were treated and modelled according to adsorption theories because adsorption has been an effective separation process for a wide variety of applications and comparison of linear regression of Frendulich, Langmuir, Elovich and Halsey models have been applied to the experiment data.

The prime objective of this research was to establish an understanding of the binding behaviour of CL, Na-CMC and HEC onto AK and to determine the most desirable conditions to increase the applicability of selected polymers in various fields. The AK was evaluated with various physicochemical parameters such as zeta potential, specific surface area, pore diameter, pore-volume, particle size distribution, mesoporous nature employing various depth characterizations. For the validation of the adsorption data, Frendulich, Langmuir, Elovich and Halsey models were computed and compared with

adjusted R^2. Based on the results, it was suggested that the physicochemical binding aspects of selected polymers onto AK was stabilized by H-bonding and other weak noncovalent interactions and such alteration could play a noteworthy role in the field of food, pharmaceutical, and industrial applications particularly in mineral processing.

2. Experimental

2.1 Materials

All the reagents used for synthesis and experimental studies were of analytical and laboratory grade. High-purity grade of nitrogen gas (99.999%) and helium gas (99.9999%) were used for physiochemical characterization of the sample supplied by Krishna Gas Agencies (Lucknow, India). The extra pure cellulose (99.99%), carboxymethylcellulose extra pure of IP specification, hydroxyethylcellulose with low viscosity (145mPas), sodium hydroxide (98%), hydrochloric acid (35.5%), potassium bromide (99.5%), sulphuric acid (98%), and dimethyl sulfoxide (99%) and Kaoline material were purchased form Loba Chemie Pvt. (Maharashtra, India). The double distilled water (DDW) was prepared using double distillation unit (GLDD15AQ, Glassco Laboratory Equipment Pvt. Ltd, Ambala Cantt., India) and used for the preparation of modified adsorbent, batch adsorption experiments and other required purpose throughout the study.

2.2 Preparation of activated kaolin

The supplied kaolin (a mineral consisting alumina (aluminum-oxygen octahedral) and silica (silicon-oxygen tetrahedral) sheets and contains more than 90% of mineral kaolinite ($Al_2O_3 \cdot 2SiO_2 \cdot 2H_2O$) [27] which was washed with DDW in order to avoid possible interference during the determination of physicochemical and absorbance properties. It was then sun dried and grounded using pestle mortar. After proper crushing the material was kept in a hot air oven (JSGW/1210D/6, Jain Scientific Glass Works, Ambala Cantt., India) equipped with microprocessor based PID electric digital temperature controller at 110±1°C for 3-4 h. After cooling the sample at room temperature, it was sieved using standard test sieves (BSS240, Continental Scientific Emporium, Lucknow, India) to remove all the debris and was stored in desired sample tubes. These tubes containing AK were kept in a desiccator (159PC/PP, Kasablanka

Corporation, Mumbai, India) and further identities of the activated kaolin were confirmed using stored samples by depth characterization techniques/ experiments.

2.3 Characterizations

2.3.1 Fourier transform infra-red spectrometer (FTIR)

FTIR measurements before and after adsorption onto AK surface, in the range 4000-400 cm^{-1}, with 4.0 cm^{-1} of spectral resolution, were recorded using a FTIR spectrometer (Thermo Nicolet 6700, USA). A mixture of 1.0 mg of the each samples and 200.0 mg of KBr was prepared and pressed by a hydraulic press at a pressure (8 metric tons=cm^2) to obtain approximately 13.0 mm diameter pellets. The pellets were then heated overnight at 110°C to remove adsorbed water and then were cooled under vacuum before recording the spectra. The thermo scientific system with full integration with the OMNIC software (Thermo Scientific) was used to monitor, control the scanning samples and focus for interpretation scanned data [28].

2.3.2 Scanning electron microscope (SEM)

The surface morphology, chemical composition and elemental mapping of activated kaolin before and after adsorption were carried out using a scanning electron microscope (CARL ZEISS EVO 50Tungsten SEM, Germany) at different analytical working distance. The accelerating potential 20 kV and the beam current 20mA was applied during the scanning the samples. Quantitative analyses was done by microanalysis system equipped with high sanative detector (SE in HV -Everhart-Thornley). Before scanning, the samples were prepared by dispersing dry powder on double-sided conductive adhesive tape and coated with gold by arc-discharged method employing a compact design sputter coater (EMITECH SC 7620, United Kingdom) for SEM/EDAX /mapping. Prior to the SEM-EDS measurements, all samples were dried using the oven at 110^o C for 4h [29].

2.3.3 Zeta potential analyzer (ZPA)

The determination of surface charge and stability of AK in colloidal solution was determined by zeta potential analyzer (ZPA). The zeta potential (f) of AK suspension was measured by using a zeta potential analyzer particulate system (NanoPlus 3 Common, Japan). An electric field of 80±1V was employed during the zeta potential

measurements. Prior zeta potential measurement, the AK was well dried in oven (at 100°C for 30 Min followed by cooling at room temperature and AK powder was added to double deionized water to prepare a dilute suspension. The suspension was then passed through an ultrasonicaction using advanced high intensity ultrasonicator (Sonics Vibra-cell VCX750,) to be well disaggregated and then kept constantly under stir-ring. The detail zeta potential measurement procedure has been discussed in earlier work [30, 31].

2.3.4 BET method

The N_2 adsorption and desorption isotherms of activated kaolin were measured using high precision gas/vapor adsorption apparatus (BELSORP-miniII, Japan,) at constant operated power (Single phase: AC100 - 120V) and 450VA for vacuum pump. Before running BET measurement of AK, the flow heating process was applied to remove any undesired moiety onto the surface of the AK. The AK was pretreated at 200 °C under the inert atmosphere at a continuous flow of N_2 using a programmed temperature control pretreatment unit operated at a constant power supply (AC100V/400 W) equipped with BELSORP-miniII which enabled high accuracy and reproducible data analysis. The Window based software's namely BELSORP-mini(S/N-0000, V2.5.3) for monitoring of running sample and data analysis/measurement after complete run of the sample were used. All observations for running sample was collectively examine continuously at BELSORP data analysis program (BDAP) [32].

2.3.5 X-ray diffractmeter

The X-ray powder diffraction measurement (XRPD) of activated kaolin before and after adsorption was carried out by an X-ray diffractmeter (Bruker ecoD8 Advance Eco, Germany) using Cu Kα radiation. For scanning the samples two sets of 2θ angle ranges were used. The range (10 to 80º) 2θ (degree) was used for the raw sample to determine mineral composition. For more precise determination of present clay mineral, oriented samples of fraction < 2 μm were used and X-ray data was collected in the range mentioned range by detector (SSD1602) equipped with instrument. The monitoring of the diffractogram and phase analysis by making interpretation of scanned samples was done on window based software (Bruker DIFFRAC.EVA V5.1, Germany). Phase identification and quantitation was analyzed and correlated using international center

for diffraction data of the powder diffraction file (ICDD PDF-4 Axiom 2020, USA) employing evaluation software (DIFFRAC.TOPAS, USA) [33].

2.4 Batch mode adsorption experiments

The stock solution of desired concentration (50 mgL^{-1}) was prepared. An appropriate amount of polymers was dissolved and the prepared solution was then refrigerated over 24hr. After attending the room temperature this was further used for batch adsorption experiments. For the adsorption tests, the desired concentration was taken in Erlenmeyer flasks and 1.0 g AK was then added into each flask. This suspension was then agitated for half an hour at 25±0.5 °C. The solution was then centrifuged for 10 min by centrifugation process. The supernatant liquid was used to analyze the adsorbed concentration determination employing earlier reported method [34] and monitored spectrophotometrically (Spectronic, $20D^{+}$, TEC, USA) by measuring the absorbance at temperature (22±2°C). The cuvette was cleaned with acetone after few absorbance's run to remove the deposited concentration. Each adsorption test was done in duplicate and triplicate when necessary and the results averaged. The amount of aforesaid polymers adsorbed onto activated kaolin, Γ (ppm), was evaluated using the following equation [35-36]:-

$$\Gamma = \frac{(C_0 - C_e)}{M}.V \qquad (1)$$

Where, C_0 and Ce (ppm) referred to the initial and the equilibrium concentration of adsorbate respectively; V (L) is the volume of the adsorbate solution, and M (g) is the mass of the activated kaolin.

2.5. Influence of various factors onto adsorption of aforesaid polymers onto activated kaolin surface

The effect of various factors (concentration, adsorbent dose, pH, contact time and temperature) on adsorption of HEC, CL and Na-CMC onto activated kaolin was investigated. The effect of concentration on adsorption of selected polymers onto activated kaolin was studied at different concentration (2.0-20.0ppm). Meanwhile, other influencing factors were kept constant. The amount of adsorbent (AK) was an important factor to affect the adsorption amount of selected polymers. A definite amount (1.0g) was taken during the batch adsorption experiments. The adsorption experiments were also was studied at different pHs (2.0 to 11.0) and temperature range 22 to 37 ±0.5°C.

3. Results and discussion

3.1. Functional group analysis

The FTIR spectra of AK with CL, Na-CMC and HEC before and after adsorption is shown in Figure 1. FTIR spectrum of AK reveled main characteristic bands and tabulated in Table 1(Figure 1a). The bands at 3694 and 3619 cm^{-1} (-OH stretching vibrations), 1114 and 694 cm^{-1} (Si-O stretching), 1031 cm^{-1} (Si-O-Si), 1008 and 540 cm^{-1} (Si-O-Al) and, 912 cm^{-1} (Al-OH) were typical of kaolinite mineral. Similar results were also reported by other researchers [46-48]. Bands located at 789, 753 and 468 cm^{-1} can be attributed to the presence of quartz [48-50]. Vibration at 399.5 cm^{-1} can be related to the deformation mode of Si-O or Al-O bonds [49-52]. After the adsorption of selected polymers, the remarkable changes were observed in the spectrum of activated kaolin (Figure 1b, 1c and 1d). The shifting has occurred in Si-O stretching at bands 1114 and 694 cm^{-1} that may be attributed to the formation of new hydrogen bonds between Si-O of activated kaolin and carboxylate ion of Na-CMA, hydroxyl ion of CL and HEC. Such interactions of other polymers like corn starch, dextrin from maize starch, humic acid, sodium salt and sodiumcarboxymethyl cellulose onto solid surface (hematite and magnetite) have also been reported by others researchers [53-60]. A light change in the position of peaks between the ranges 500 to 400cm^{-1} were observed which lessens the frequency and energy of functional groups.

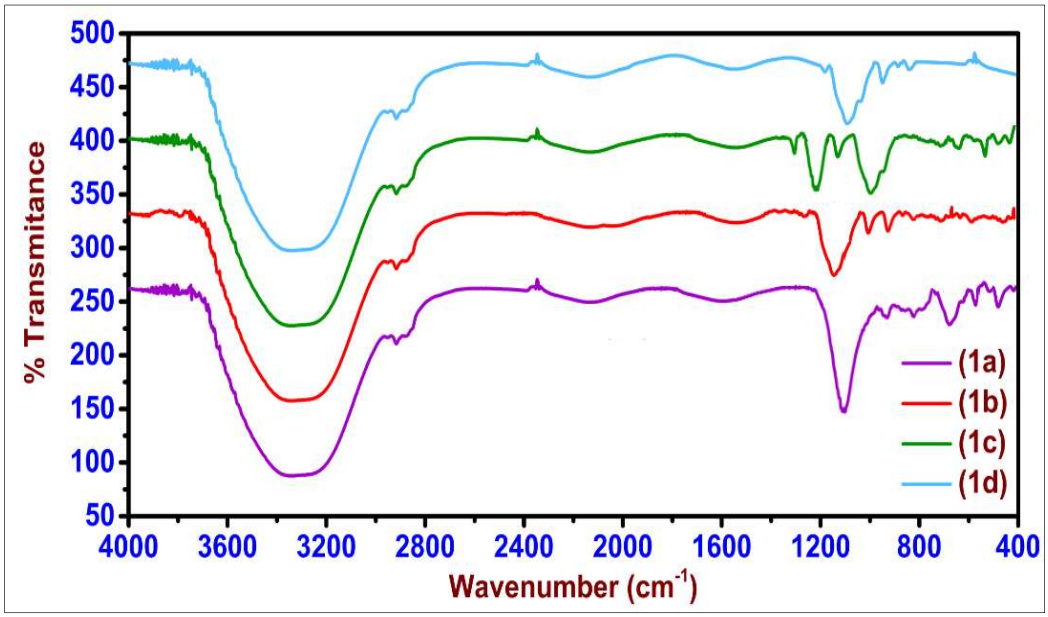

Figure 1. FT-IR spectra (1a). AK before adsorption, (1b). CL adsorbed AK and (1c). Na-CMC adsorbed AK and (1d). HEC adsorbed AK

3.2. Surface morphology, elemental and microstructural analysis

The textural/morphological characteristics of the AK were evaluated by SEM, EDS and elemental mapping studies (Figure 4*)*. The SEM photographs of the unloaded AK show the sheet silicate structure, rough, uneven surfaces porosity with small openings and holes responsible for intra pore diffusion during the adsorption process. Therefore, these surface properties should be a considerable factor for polymer adsorption. After polymer adsorption, a significant change was observed in the structure of the AK (Figure 2b-2d). The polymers adsorbed surface appeared to have a rough surface and pores containing new shiny particles after adsorption (Figure 4b) [61-62]. Furthermore, specific analytical method namely scanning electron microscopy coupled with energy dispersive X-ray spectrometry (SEM-EDX) was carried out to observe such morphological and chemical changes before and after adsorption.

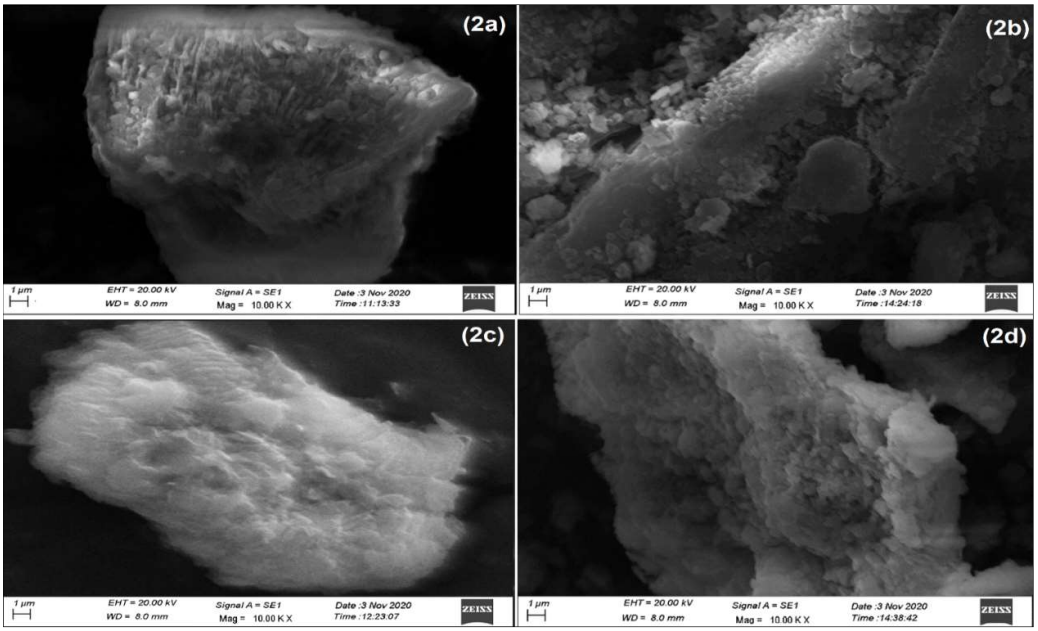

Figure 2. SEM micrograph of (2a). AK (Blank), (2b).CL adsorbed AK (2c). *Na-CMC* adsorbed AK and (2d).HEC adsorbed AK

The energy dispersive spectroscopy (EDS), more commonly known as electron probe X-ray microanalysis (EDX) is a technique of elemental analysis associated to electron microscopy based on the generation of characteristic X-rays that revealed the presence of elements present in the sample. Therefore, the purpose of elemental analysis is to determine the quantity of a particular element within a material for qualitative and quantitative point of view [63-64]. The SEM-EDX elemental analysis before and after

adsorption of CL, Na-CMC and HEC onto activated kaolin is shown in Figure 3. Before adsorption the activated kaolin confirmed the presence of C, Si, Al and O (Figure 3a) while Na-CMC adsorbed AK revealed the presence of C, Si, Al, Na and O surface (Figure 3b). The source of Na is in carboxymethyl cellulose salt, used in the adsorption process [63, 64]. The changes in the SEM-EDS was associated to adsorption of aforesaid polymers onto AK.

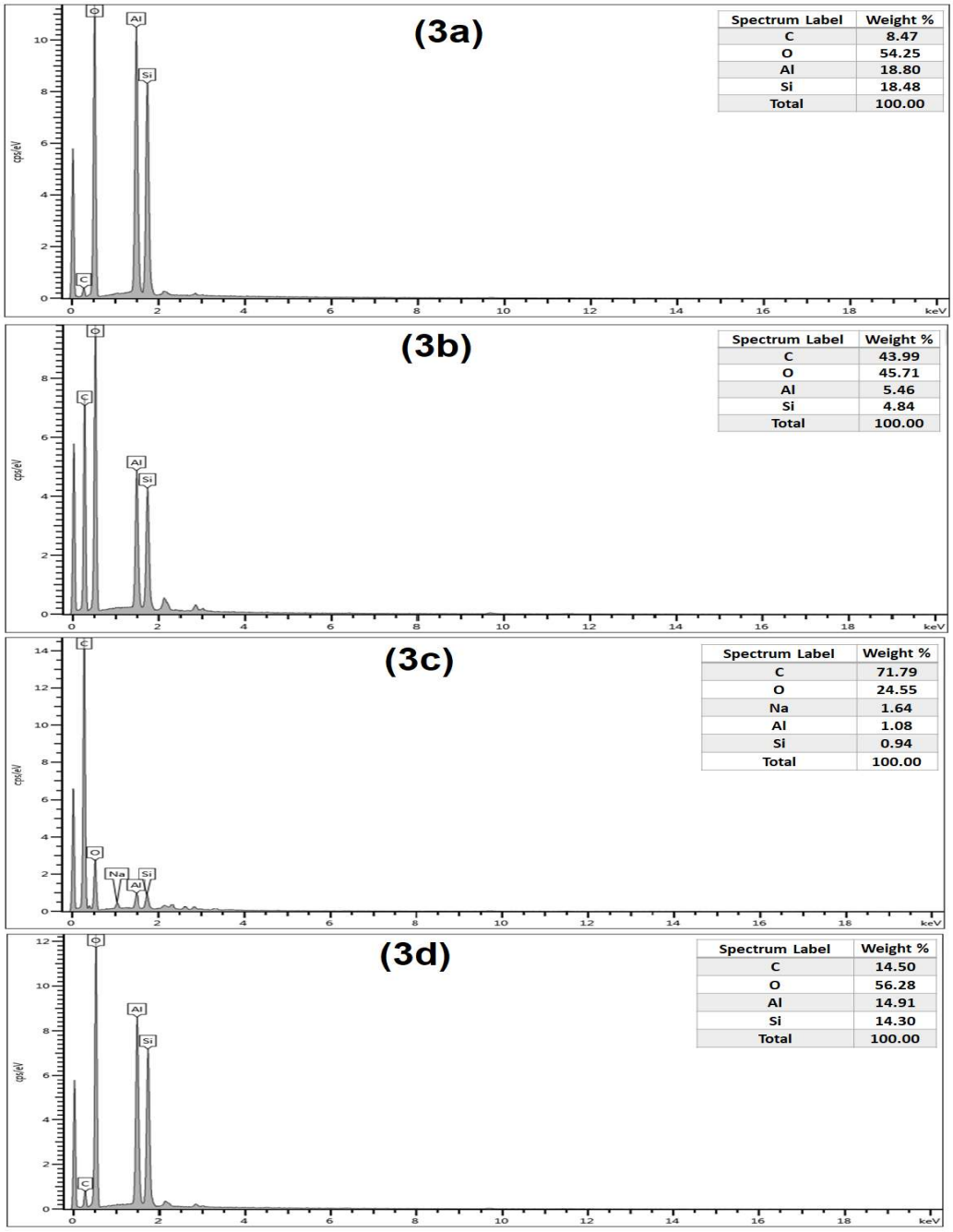

Figure 3. EDS spectra and elemental composition of (3a). AK before adsorption (3b). After adsorption of CL, (3c). NaCMC and (3d). HEC onto AK

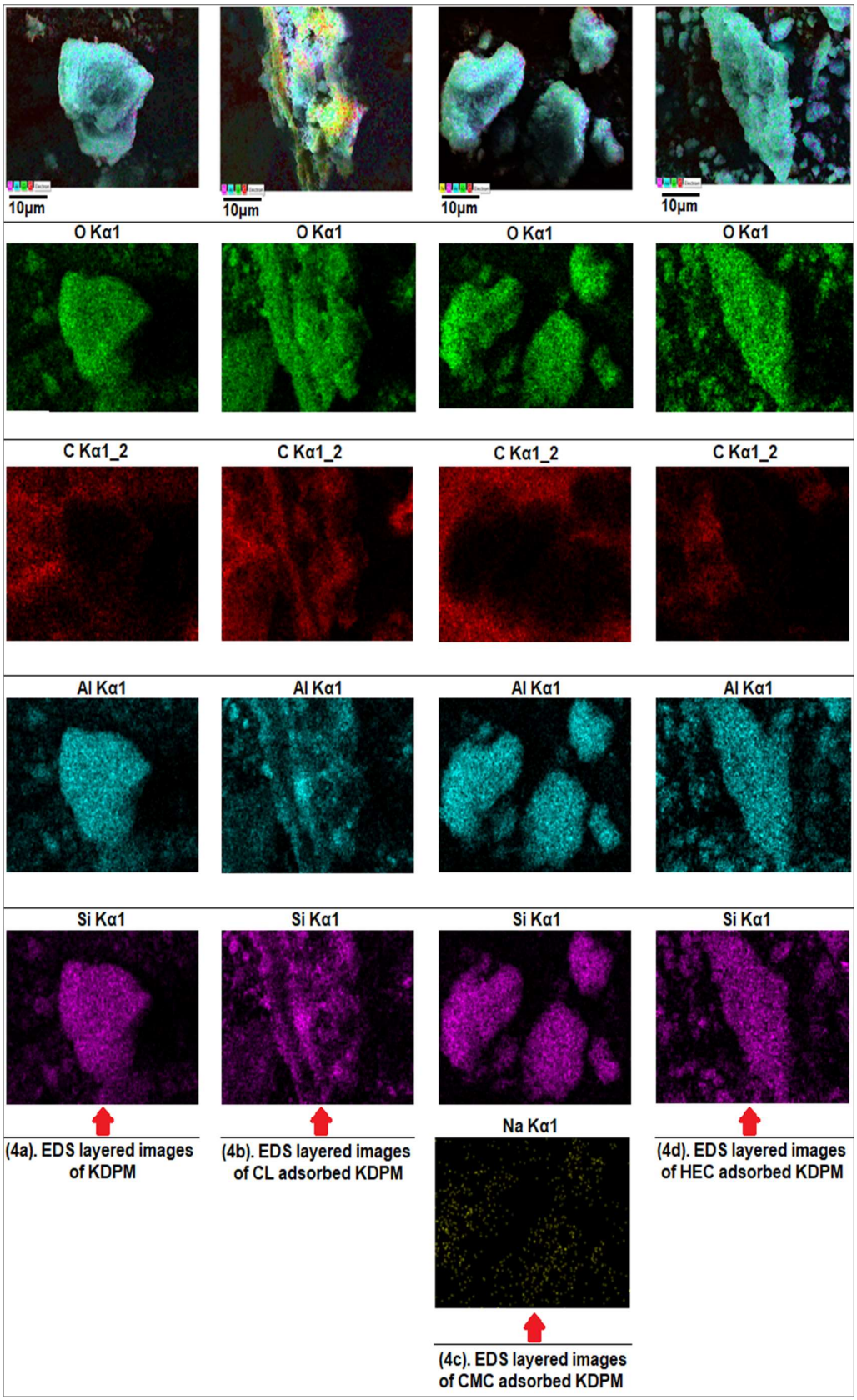

Figure 4. Elemental mapping analysis /EDS layered images of (4a). AK before adsorption (4b). After adsorption of CL, (4c). Na-CMC and (4d). HEC onto AK

As seen in Figure 2, the surface of AK before adsorption is not uniform; it consists of sheet like structures as well as fibrous strands. However, upon adsorption of polymers, the surface morphology changes and becomes smoother. After adsorption with CL, Na-CMC, it can be seen from figure 3 (3b-3c) that the amount of C present on the surface increases significantly i.e. from 44% and 72%, respectively while in case of HEC there was decrease in the amount of carbon. The presence of sodium (Na=1.64%) Figure 4c supported that this was due to adsorption of Na-CMC onto AK. These changes in the amount of elemental composition suggested that it could be due to interaction of polymers onto AK where functional groups of polymers were attached on the surface's functional groups of AK. Furthermore, these chemical elemental changes *were* investigated by elemental mapping analysis and the results are shown in Figure 4. The elemental mapping images showing the spatial distribution of chemical elements [65] before and after adsorption of polymers onto AK (Figure 4a-4d) and elemental mapping also emphasized the existence of increase in chemical composition in the structure after the adsorption process (Figure. 4b-4d) [66].

3.3. Zeta potential measurements

Zeta potential, based on dynamic light scattering (DLS), is the essential characterization method to determine the charge and stability of the solid particle in aqueous system. Therefore, the zeta potential of activated kaoline in aqueous medium was mesured prior to adsorption of CL, Na-CMC and HEC (Figure 5). The result suggests that the colloidal AK particulates were highly positively charged and stable in aqueous system. Similar studies were also reported Peng and Di, Massaro et al. and Yan et al., for activated kaolin activated by chemical method [67-69]. The zeta potential of AK was found to be 92.44(mV) which suggested that it has strong stability and positive surface in aqueous medium. The obtained zeta potential results with their operational conditions for activated kaolin were summarized in Table 1.

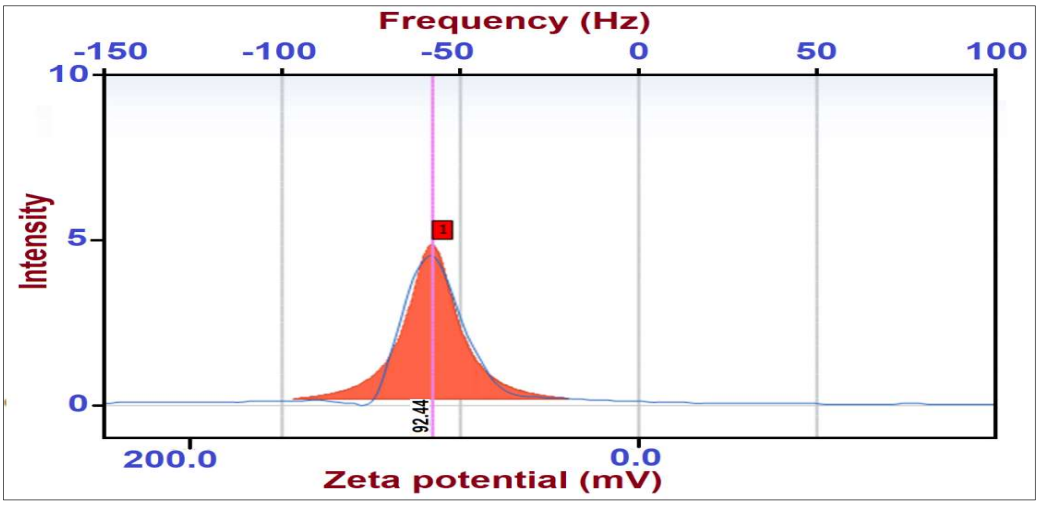

Figure 5. Electrokinetics measurement for AK

Table 1 Optimized parameters and data obtained from electrokinetics measurement for AK

Measurement results				
Zeta Potential	92.44(mV)		Doppler shift	-58.02 Base(Hz)
Mobility	7.209e-004 (cm²/Vs)		Frequency	123.6(Hz)
Conductivity	0.020 (mS/cm)		Conversion Equation:	Smoluchowski
Zeta potential of cell			**Diluent properties**	
Upper Surface Lower Surface Cell Condition Cell Type Avg. Electric Field Avg. Current	-229.48(mV) 179.14(mV) Disposable -16.72(V/cm) -0.07(mA)		Diluent Name Temperature Refractive Index Viscosity Dielectric Constant	Water 25.0 (°C) 1.3328 0.8878 (cP) 78.3
Peak data table of distribution graph				
PeakFrequency (Hz)	Intensity	Half Width (Hz)	Zeta Potential (mV)	Mobility (cm²/Vs)
-58.0	4.89	7.78	92.44	7.209e-004

3.4. BET analysis

The physicochemical parameters of activated kaolin were measured using BET method (Figure 6a-6d) and obtained results were summarized in Table 2. Figure 1a illustrates that the N_2 adsorbed/desorbed from the activated kaolin in relation to the relative pressure (p/p°) and used to identify nature of the AK and falls in the type IV category of Giles classification [70] which was indicative of predominantly mesoporous material due to capillary condensation phenomenon. Figure 6b show The BET plot which revealed that typical specific surface area of AK was S_{BET} =25.431 m^2/g. The

pore size distribution and pore diameter were determined employing Barrett-Joyner-Halenda (BJH) model [71, 72] and T-method [73], respectively. The AK exhibited a narrow pore distribution with a maximum peak centered at 10.534 nm and pore diameter=2.113 nm indicating mesoporous characteristics as defined by IUPAC nomenclature of porous materials [74-76]. These physicochemical parameters of activated kaolin make it suitable and potential adsorbent for the adsorption of polymers. The results for the BET surface area of AK are presented in Table 2.

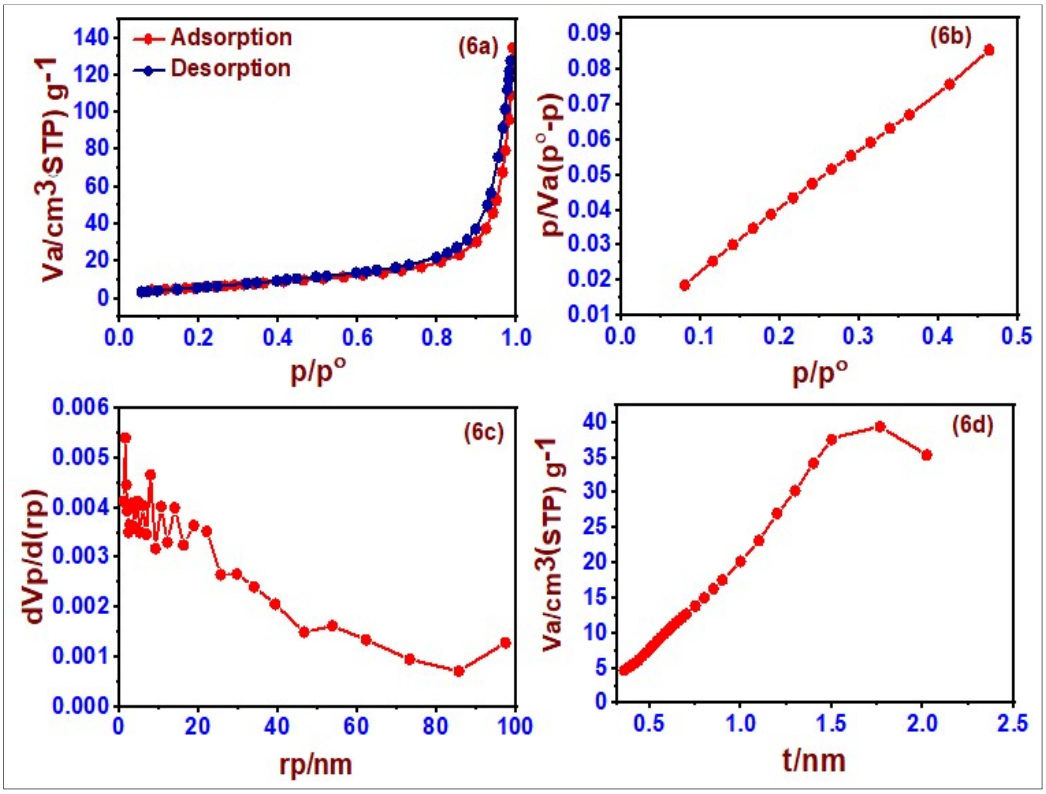

Figure 6. Physiochemical analysis of AK (6a). N_2 adsorption-desorption isotherm, (6b). BET graph, (6c). BJH and (6d). T- Graph

3.5. Crystalline structure analysis

The XRD spectra of all scanned samples before and after absorption were shown in Figure 7. The diffractogram of AK suggested that it has very strong peaks of kaolin and a low intensity of the peaks of quartz (Figure 7a). These intense and sharp peak were assigned at 26.68˚, 29.55 ˚ and 39.65 ˚ showing an ordered structure also matched with the JCPDS database file (PDF-01-089-6538) and similar results were also reported by Paricio [77].

Table 2 Specific conditions and physiochemical parameters of AK using BET analysis

Methods	**Surface parameters of activated kaolin**			
N_2 Adsorption-desorption	Sample weight (g)	Saturated pressure (kPa)	Degassing Time (hr)	
BET	0.04	94.898	6.19	
	Specific surface area (S_{BET}) (m^2 /g)	Monolayer volume (V_{mono}) (cm^3 /g)	Total pore volume (Vp) (cm^3/g)	Mean pore diameter (nm)
	25.431	5.873	0.115	31.158
BJH	Pore volume (Vp) (cm^3 /g)	Pore specific surface area (a_p) (m^2/g)	Micropore radius (cylindrical shape (r_p) (nm)	
	0.199	30.554	2.663	
T	Total specific surface area (a_1) (m^2/g)	External surface area (a_2) (m^2/g)	Pore volume (V_1 &V_2) (cm^3/g)	Pore diameter (2t) (nm)
	31.177	56.229	0.026	2.113

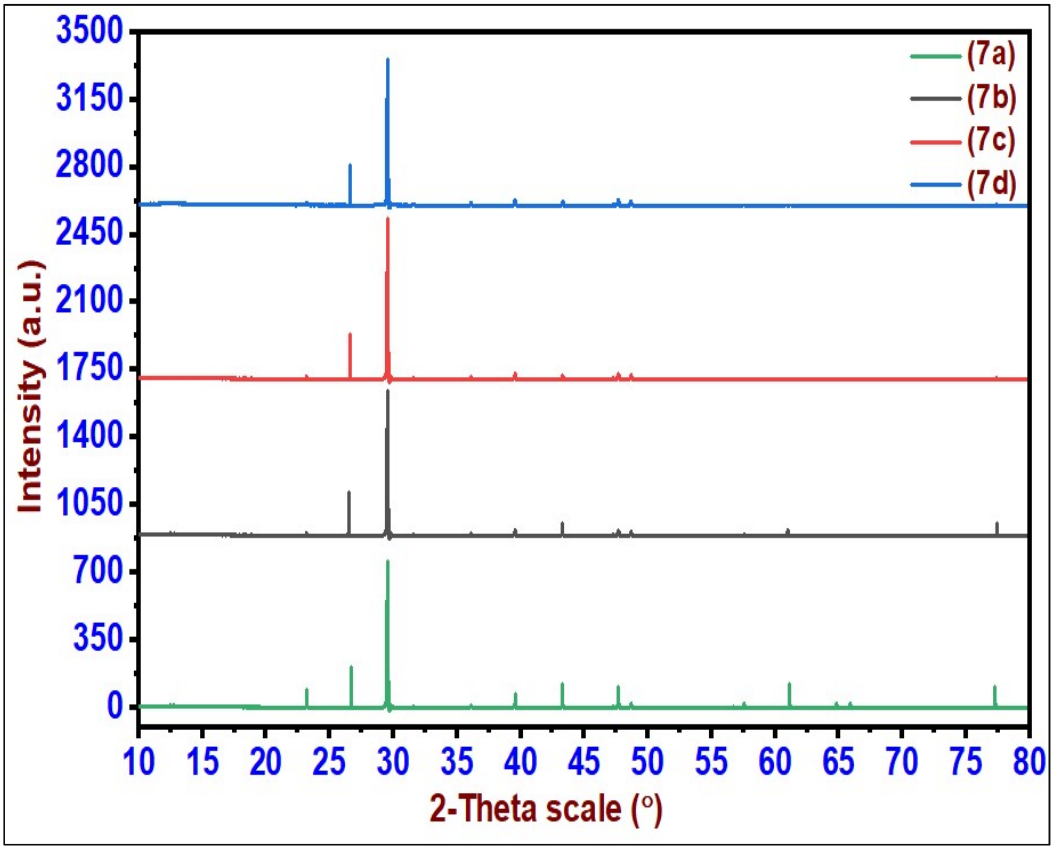

Figure 7. Comparing diffractogram before adsorption (7a). AK and after adsorption of (7b). CL, (7c). NaCMC and (7d). HEC onto AK

The AK diffraction pattern show intense peak at 2 θ angle of 26.68˚ assigned to quartz (Si_3O_6) and another instance peak at 29.55 assigned to kaoline (AK) ($Al_2Si_2O_5(OH)_4$). A small peak at 39.65 was associated to Al_2O_3. These obtained results confirmed crystalline phase and presence of SiO_2 and Al_2O_3 in AK (Figure 7a) [78]. After adsorption, the shifting in peaks supported the hydroxylation behaviours of AK surface and suggested that hydroxyl of selected polymers interaction with AK surfaces and associated with slight contraction of the unit cell which suggested there was no loss of crystallinity of AK (Figure 7b-7d). The slight difference in the diffraction pattern of the activated kaolin after adsorption of polymers could be the indication of adsorption as reported by Shin [79].

3.8. Effect of various factors onto polymers adsorption

3.8.*1 Concentration*

The adsorption of HEC, CL and Na-CMC onto AK was studied as a function of concentration to determine where the equilibrium condition was achieved. By measuring the HEC, CL and Na-CMC concentration, the adsorption amount (mg/g) were determined. It is shown in Figure 8a that the HEC, CL and Na-CMC adsorption rate was low at the beginning of the adsorption process because the active sites on the surface of the AK were initially abundant and the polymeric chain could be adsorbed in a flatty manner. As the concentration of polymers increases, there was a gradual increase in the adsorption. After certain concentration of polymers, the adsorption amount no longer changed, suggesting that the adsorption had achieved equilibrium. This was partly due to the unavailability of vacant active sites with increasing concentration.

3.8.2 Dose of AK

To explore the role of surface active sites during the adsorption process were explained by performing the effect of dose of AK onto adsorption. The optimization of AK dose (0.1-1.0g) was taken in polymers (HEC, CL and Na-CMC) concentration keeping other parameter constant. The adsorption capacity was decreased with increase AK amount (Figure 8b). Therefore, the selected amount chosen as the adsorbent dose for further experiments.

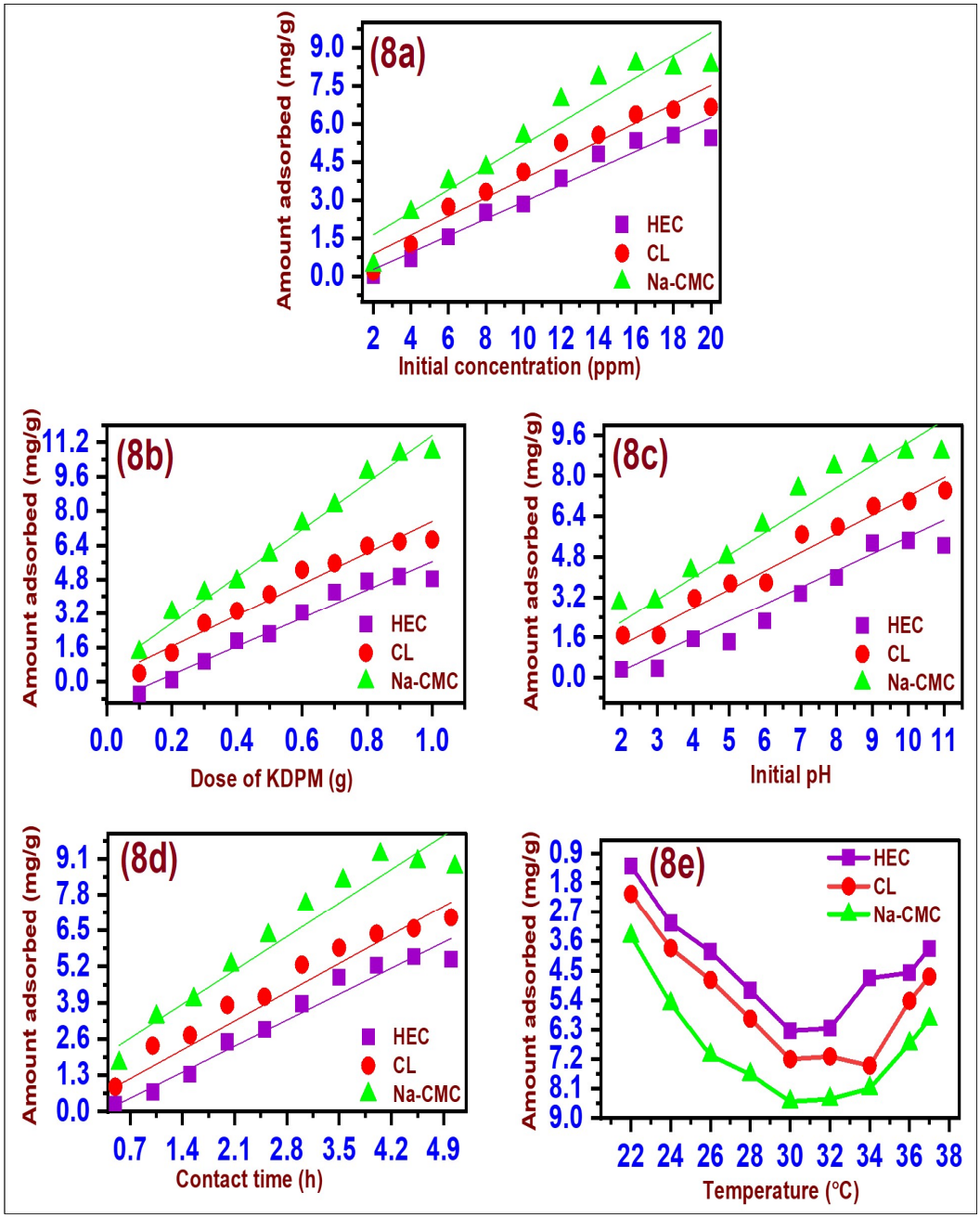

Figure 8. Effect of various factors onto adsorption (8a). Concentration, (8b). Dose of activated kaolin, (8c). pH, (8d). Contact time, (8e). Temperature

3.8.3 pH

The pH of the solution has been reported as a significant variable to affect the adsorption of polysaccharides onto various solid surfaces, therefore, the effect of pH was carried out at room temperature (25±0.2°C) keeping all variables constant. The adsorption of polymers (HEC, CL and Na-CMC) onto AK was studied in the pH range of 2.0-11.0.

The effect of pH on adsorption is shown in Figure 8c. With the increase of pH values, the adsorption amount of NaCMC on AK increases gradually. After certatin interval of pH, adsorption decreases (Figure 8c). Also, the competitive adsorption between polymers and hydroxyl ions at higher pH values can result in a decrease in the adsorption amount.

3.8.5 Contact time

To determine the equilibrium condition, the adsorption of polymers (HEC, CL and Na-CMC) onto AK was performed as a function of contact time. The adsorption amount was determined by measuring the concentration of polymers at different time's intervals (0.5 to 5 h) (Figure 8d). It was observed that initially the adsorption amount increases due to the availability of actives sites on the surface of AK and the macromolecules could be adsorbed easily. The adsorption amount of NaCMC onto the quartz AK was found a maximum within 3.7h. After 3.7h, the adsorption amount remained unchanged, suggesting that this was the equilibrium state. The equilibrium state was achieved due to a reduced number of available vacant active sites with increasing contact time (Figure 8d). Therefore, 3.7h was adopted as the adsorption equilibrium time for the polymer adsorption onto AK surface.

3.8.6 Temperature

The adsorption behaviour of polymers (HEC, CL and Na-CMC) was performed as a function of temperature and the results between amount adsorbed and temperature (22, 24, 26, 28, 30, 32, 34, 36 and 37 $\pm 0.5^0$C unit temperature) shown in Figure 8e. The absorption amount of polymers onto AK decreased as the temperature increased, suggesting that the adsorption process as exothermic. Furthermore, the van der Waals and other non-covalent forces decreased with an increase in temperature. This means that the interactions between AK and polymers are weak, leading a decrease in adsorption amount. The physisorption of polymers on AK occurred mainly through dispersive interactions between the adsorbate-adsorbent systems. Hence, the adsorption amount of polymers was found to decrease with increasing temperature.

3.4 Adsorption isotherm and thermodynamic studies

3.4.1 Frendulich isotherm

The non-uniform distribution of adsorption that the surface of AK was heterogeneous and described by an empirical Freundlich isotherm model. The following Freundlich equation was applied: [80]

$$logQe = logK_F + \frac{1}{n} logCe \quad (2)$$

Where Q_e was the amount of NaCMC adsorbed (mg/g), C_e is the equilibrium concentration of the polymers (HEC, CL and Na-CMC) in solution (ppm) and K_F and n are Freundlich constants. The values of n and K_F are calculated from the slopes and intercepts of the linear plots between $\log Q_e$ *vs* $\log C_e$ (Figure 9a) were recorded in Table 3 for selected polymers. Freundlich plots are shown in Figure 9a and linearity supported that data fit was well with adjusted R^2 value for the adsorption system under the studied concentration range for all polymers. However for Na-CMC it was best described (Table 3).

3.4.2 Langmuir isotherm

The maximum adsorption amount and energy of adsorption was associated with a saturated monolayer of titled polymers onto AK surface. The Langmuir isotherm model was expressed by the formula: [74]

$$\frac{Ce}{Qe} = \frac{1}{\Gamma_{max} K_L} + \frac{C_e}{\Gamma_{max}} \quad (3)$$

Where, K_L is the Langmuir constant (L/ mg) related to the affinity of binding sites and the free energy of adsorption; Qe is the NaCMC concentration at equilibrium onto the AK (mg/g); Ce is the NaCMC concentration at equilibrium in solution (mg/L); Γ_{max} is the NaCMC concentration when monolayer forms on the AK (mg/ g). K_L and Γ_{max} can be determined from the slope and intercept of plot Ce/Qe *vs* Ce (Figure 9b) and are given in Table 3. The Langmuir parameters suggested that this model was highly favorable for the adsorption of Na-CMC in present optimized conditions.

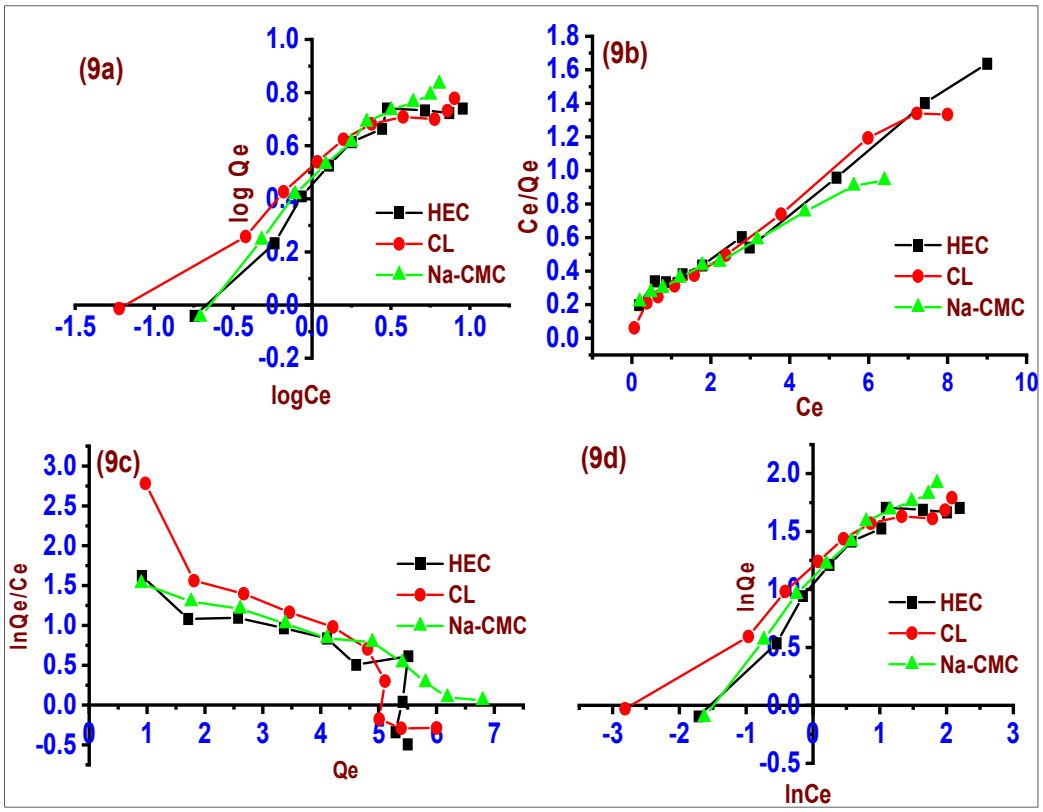

Figure 9. Adsorption isotherms models (9a). Frendulich, (9b). Langmuir, (.9c). Elovich and (9d). Halsey

Table 3 Adsorption parameters for different isotherm models for selected polymers adsorption onto activated kaolin

Isotherm models	Parameters	HEC	CL	Na-CMC
Frundlich	n	6.27±0.06	2.71±0.02	1.79±0.01
	K_F	1.45±0.01 mg/g $(L/mg)^{1/n}$	2.97±0.03 mg/g $(L/mg)^{1/n}$	0.70±0.04 mg/g $(L/mg)^{1/n}$
	Adj. R^2	0.92605	0.94616	0.96151
Langmuir	Γ_{max}	6.23± 0.03 mg/g	6.10± 0.03mg/g	8.34±0.01mg/g
	K_L	0.96±0.01 L/mg	1.36±0.01L/mg	0.58±0.01L/mg
	Adj. R^2	0.98807	0.98653	0.99440
Elovich	Γ_{max}	2.91±0.30 mg/g	1.79±0.27 mg/g	3.95±0.09 mg/g
	K_E	1.95±0.07 L/mg	5.43±0.06 L/mg	1.59±0.02 L/mg
	Adj. R^2	0.71040	0.89285	0.95295
Halsey	n_H	2.13±0.07	2.71±0.045	1.79±0.04
	K_H	7.26±0.06mg/L	19.20±0.03 mg/L	5.90±0.04 mg/L
	Adj. R^2	0.88419	0.94616	0.96151

3.4.3. Elovich isotherm

This model is based on the kinetic hypothesis considering that the adsorption sites rise dramatically with adsorption; this means that adsorption is multilayered. The linearized form of this model is given below [81].

$$ln\frac{Q_e}{C_e} = lnK_E\Gamma_{max} - \frac{Q_e}{\Gamma_{max}} \quad (4)$$

Elovich maximum adsorption capacity (Γ_{max}) and Elovich constant (K_E) can be calculated from the slope and intercept of the plot of $\ln(Qe/Ce)$ *vs* Qe (Figure 9c). Their investigation showed that the value of the adjusted R^2 for the Elovich model was 0.96151 which is higher for Na-CMC than other polymers (Table 3) *i.e.* CL and HEC; therefore the adsorption of Na-CMC onto AK was best described by the Elovich isotherm.

3.4.4. Halsey isotherm

The Halsey isotherm is used for measurement of multi-layer surface adsorption in a reasonably wide range. The following linear form of this equation was applied to interpretate the Halsey's parameters-[82]

$$lnQ_e = \frac{1}{n_H}lnK_H - \frac{1}{n_H}lnC_e \quad (5)$$

Where K_H and n_H are Halsey isotherm constants which can be obtained from the slope and intercept of the plot of $\ln Q_e$ *vs* $\ln C_e$ (Figure 9d). The fitting of their experimental data to the Halsey isotherm model assists to the heteroporous nature of the activated kaolin. The Halsey isotherm fits the experimental data well due to high adjusted R^2 (Table 3), which may be attributed to the heterogeneous distribution of activate sites and multilayer adsorption of Na-CMC, CL and HEC onto AK, respectively [16]. The adsorption study revealed that Na-CMC was best described by each model at optimized model because the pKa values of CL, Na-CMC and HEC were reported 11.97, 4.84 and 13.95 respectively. Since, solubility of the polymers depends on the pKa values therefore, the theoretical solubility order will be Na-CMC, CL, and HEC. This aspect is directly associated for the adsorption behaviour of selected polymers onto activated kaolin.

5. Conclusions

This study demonstrated that activated kaolin was successfully prepared from supplied material only by one physical step and utilized to adsorption for HEC, CL and Na-CMC. The physiochemical characterizations and experiments confirm that AK has very efficient potential adsorptive properties. It was observed that the adsorption of polymers on AK remarkably affected by the change in adsorptive conditions such as concentration, dose, pH, contact time and temperature. The adsorption of polymers show some remarkable shifting in Si-O stretching at bands 1114 and 694 cm^{-1} that may be attributed to the formation of new hydrogen bonds between Si-O of AK and carboxylate ion of Na-CMA, hydroxyl ion of CL and HEC resulting hydrogen bonding exhibit significant role during the adsorption. The chemical structure of Na-CMC was relatively open and has low steric effect for interaction with the functional groups present on AK rather than HEC and CL. The adsorption mechanism was associated with hydrogen bonding between active chemical functions of AK (Si-O-H) and carboxylates ions of Na-CMC. These Si-O-H localized active sites binds with carboxylate ion of Na-CMC to form hydrogen bonding. In the aqueous system, carboxylic functions of Na-CMC developed affinities with most of Si-O-H of the Na-CMC. The adsorption of Na-CMC on AK was as a result of interaction of Si-O-H and carboxylate ion of adsobate. However, adsorbent being porous assists to enhance the surface area which provide the more active sites on the adsorbent. More active sites on the adsorbent, there could be more interaction between Si-O-H of the adsorbent and –COOH groups of Na-CMC. However, for HEC and CL such interactions were not observed significantly. Experimental data of the present work were excellently fitted to the Langmuir equation since the adjusted R^2 gave high correlation coefficients $R^2>0.99$, as shown in Table 3 than HEC and CL. The adsorption tests resulted in the extent of interaction, various parameters and correlation coefficient (Table 3). Therefore, it was confirmed that the adsorption was an exothermic and physical in nature. Thus, these exploration of adsorption behaviour of titled polymers onto activated kaolin provides substantial evidence to prove beyond doubt that adsorption mainly occurs via hydrogen bonding followed by some electronic interactions and such alteration could play a noteworthy role in the field of food, pharmaceutical, and industrial applications without damage of the environment. The results of the study presented here suggest several possibilities for future research.

References

1. Kukrety, A.; Singh, R. K.; Singh, P; Ray, S. S. Comprehension on the synthesis of carboxymethylcellulose (cmc) utilizing various cellulose rich waste biomass resources. *Waste Biomass Valori*. **2017**, *9*, 1587–1595.
2. Eggleston G.: Finley J.W.; deMan J.M. (2018) Carbohydrates. in: principles of food chemistry. Food Science Text Series. Springer, Cham.
3. Hollabaug, C.B.; Burt, L.H.; Walsh, A.P. Carboxymethylcellulose. uses and applications. Ind. Eng. Chem. **1945**, *37*, 943-947.
4. Mackenzie, M.; Malhotra, D.; Riggs, W. F. Chemical reagents in the mineral processing industry. *Soc. Min. Eng*.**1986**, *1*, 312.
5. Pugh, R. J. Macromolecular organic depressants in sulphides flotation-a review, 1. principles, types and applications. *Int. J. Miner. Process*. **1989**, *25*, 101-130.
6. Pugh, R. J. Macromolecular organic depressants in sulphide flotation-a review: 2. theoretical analysis of the forces involved in the depressant action. *Int. J. Miner. Process*. **1989**, *25*, 131-146. 131.
7. Healy, T. W. Principals of adsorption of organics at solid –solution interfaces. *J. Macromol*. *Sci. Chem*. *A*. **1974,** *8*, 603-19.
8. Rath, R.nK.; Subramanian, S. Studies on the adsorption of guar gum onto biotite and mica. *Miner. Eng*. **1997**, *10*, 1405–1420.
9. Rath, R. K.; Subramanian, S. adsorption, electrokinetic and differential flotation studies on sphalerite and galena using dextrin. *Int. J. Miner. Process*. **1999**, *57*, 265–283.
10. Rath, R. K.; Subramanian, S.; Laskowski, J. In: Laskowaki, J.S.; Poling, G.W. (Eds.), processing of hydrophobic minerals and fine coal. Canadian institute of mining, metallurgy and petroleum, Montreal, Que., Canada, **1995,** p.546**.**
11. Rath, R. K.; Subramanian, S.; Laskowski J.S. Adsorption of dextrin and guar gum onto talc. a comparative study. *Langmuir*. **1997**, *13*, 6260-6266.
12. Shortridge, P.G.; Harris, P.J.; Bradshaw, D.J.; Koopal, L.K. The effect of chemical composition and molecular weight of polysaccharide depressants on the flotation of talc. *Int. J. Miner. Process.* **2000**, *59*, 215–224.
13. Liu, Q.; Laskowski, J.S. The role of metal hydroxides at mineral surfaces in dextrin adsorption, i. studies on modified quartz samples. *Int. J. Miner. Process*. **1989**, *26*, 297–316.

14. Liu, Q.; Laskowski, J.S. The interactions between dextrin and metal hydroxides in aqueous solutions. J. *Colloid Interface Sci*. **1989**, *130*, 101–111.
15. Liu, Q.; Laskowski, J.S. The role of metal hydroxides at mineral surfaces in dextrin adsorption. ii: chalcopyrite–galena separations in the presence of dextrin. *Int. J. Miner. Process*. **1989**, *27*, 147–155.
16. Khraisheh, M.; Holland, C.; Creany, C.; Harris, P.; Parolis, L. Effect of molecular weight and concentration on the adsorption of cmc onto talc at different ionic strengths. *Int. J. Miner. Process*. **2005**, *75,* 197–206.
17. Wang, J.; Somasundaran, P.; Nagaraj, D.R. Adsorption mechanism of guar gum at solid–liquid interfaces. *Miner. Eng*. **2005**, *18,* 77–81.
18. Steenberg, E.; Harris, P.J. Adsorption of carboxymethyl cellulose, guar gum and starch onto talc, sulphides, oxides and salt-type minerals. *S. Afr. J. Chem*. **1984**, *37*, 85–90.
19. O'sullivan, C. K., & Guilbault, G. G. (1999). Commercial quartz crystal microbalances– theory and applications.
20. Kalantary, R.R; Jafari, A. J.; Kkavandi, B.; Nasseri, S.; Ameri, A.; Azari, A. Adsorption and magnetic separation of lead from synthetic wastewater using carbon/iron oxide nanoparticles composite. *J. Mazandaran Univ Med. Sci*. **2014**, 24, 172-183.
21. Malmsten, M. Adsorption of polymers at the solid/liquid interface. Ph.D. thesis, University of Lund, Sweden, 1992.
22. Malmsten, M.; Lindman, B. Ellipsometry studies of the adsorption of cellulose ethers. *Langmuir,* **1990**, 6, 357-364.
23. Malmsten, M.; Claesson, P. M.; Pezron, E.; Pezron, I. Temperature-dependent forces between hydrophobic surfaces coated with ethyl hydroxyethyl cellulose. *Langmuir*, **1990,** 6, 10, 1572–1578.
24. Malmsten, M.; Claesson, P. Temperature-dependent adsorption and surface forces in aqueous ethyl(hydroxyethyl)cellulose solutions. *Langmuir*, **1991**, 7, 5, 988–994.
25. Kapsabelis,C.; Clive A. Prestidge, Adsorption of Ethyl(hydroxyethyl)cellulose onto Silica Particles: The Role of Surface Chemistry and Temperature, *J. Colloid and Interface Sci*. **2000**, 228, 297-305.
26. Claesson, P. M.; Malmsten, M.; Lindman, B. Forces between hydrophobic surfaces coated with ethyl(hydroxyethyl)cellulose in the presence of an ionic surfactant. *Langmuir*, **1991**, 7, 1441–1446.

27. Tosoni, S.; Doll, K.; Ugliengo, P. Hydrogen bond in layered materials: structural and vibrational properties of kaolinite by a periodic B3LYP approach, *Chem. Mater*. **2006**, 18, 2135–2143.
28. Singh, K.; Kumar, A. Adsorption and conformation of carboxymethyl cellulose at TiO_2- modified mesoporous carbon derived from mustard cake. *Proceeding of GCGHGSPCT*, 131-150, 1, 2019.
29. Singh, K.; Kumar, A. Physiochemical aspects for the adsorption behavior of sodium carboxymethyl cellulose onto mesoporous granular fine quart surface from its aqueous solutions. *Sep. Sci. Tech*. **2020**.
30. Dash, M.; Dwari, R.K.; Biswal, S.K; Reddy P.S.R.; Chattopadhyay, P., Mishra, B.K. Studies on the effect of flocculant adsorption on the dewatering of iron ore tailings. *Chem Eng J.* **2011**; 173, 318–25.
31. Addai-Mensah J, Ralston J. Interfacial chemistry and particle interactions and their impact upon the dewatering behavior of iron oxide dispersions. *Hydromet* 2004, *74*, 221–31.
32. Singh, K.; Kumar. Physicochemical aspects for the binding mechanism of sodium carboxymethyl cellulose onto mesoporous tea waste carbon from its aqueous solutions. *J. .Dispern Sci. Tech.*
33. Singh, K.; Kumar, A,; Awasthi, S.; Pandey, S.K.; Gupta, S.P.; Mishra, P. Interpretation of adsorption behaviour of carboxymethyl cellulose onto functionalized accurel polymeric surface. *Ind. Eng. Chem. Res*. **2020**, *59*, 43, 19102–19116.
34. Dubois, M.; Gilles, K. A.; Hamilton, J. K.; Rebers, P. A. Smith, F. Colorimetric method for determination of sugars and related substances. *Anal. Chem.* **1956**, *28,* 350.
35. Mirji, S. A. octadecyltrichlorosilane adsorption kinetics on si(100)/sio_2 surface: contact angle, AFM, FTIR and XPS analysis. *Surf. Interface Anal.* **2016**, *38*, 158–165.
36. Yang, X.H.; Zhu, W.L. Viscosity properties of sodium carboxymethyl cellulose solutions. *Cellulose*. **2007**, *14*, 409–417.
37. Iftekhar, S.; Ramasamy, D. L.; Srivastava, V.; Asif, M. B.; Sillanpaa, M. Understanding the factors affecting the adsorption of lanthanum using different adsorbents: A critical review. *Chemosphere*. **2018**, *204*, 413–430.

38. Panda, H.; Tiadi, N.; Mohanty, M.; Mohanty, C. R. Studies on adsorption behavior of an industrial waste for removal of chromium from aqueous solution. *South Afr. J. Chem. Eng*. **2017**, *23*, 132–138.
39. Chytil, M.; Lišková K.; Janeček, J. The influence of counterions of different valency on carboxymethylcellulose viscoelastic behavior. Rheology: theory, properties and practical applications. 1st ed. Hauppauge (NY): Nova Science Publishers. **2014**.
40. Davis, J.A.; Leckie, J.O. Surface ionization and complexation at the oxide/water interface. 3. Adsorption of Anions. *J. Colloid Interface Sci*. **1980**, *74*, 32-43.
41. Rani, S.; Sud, D. Effect of temperature on adsorption-desorption behaviour of triazophos in indian soils. *Plant Soil Environ*. **2015**, *61*, 36–42.
42. Singh, K.; Gupta, S. P.; Kumar, A.; Kumar, A. (2018). The effect of high intensity ultrasound (hiu) on the kinetics of crystallization of sucrose: Elimination of latent period. *Ultrason. Sonochem*. **2019**, *52*, 19-24.
43. J. Anwar, U. Shafique, M.S. Waheed-uz-Zaman, A. Dar, S. Anwar, Removal of Pb (II) and Cd(II) from water by adsorption on peels of banana. *Bioresour. Technol*. **2010**, *101*, 1752–1755.
44. Freundlich H. Über die adsorption in Lösungen. *J. Res. Phys. Chem. Chem. Phys*. **1907**, *57U*, 385–470.
45. Langmuir I. the adsorption of gases on plane surfaces of glass, mica and platinum. *J. Am. Chem. Soc*. **1918**, *40*, 1361–403.
46. Nallis, K.; Katsumata, K.; Isobe, T.; Okada, K.; Bone, P.; Othman, R. Preparation and uv-shielding property of Zr0.7Ce0.3O2-kaolinite nanocomposites. *App. Clay Sci.* **2013**, *80*, 147-153.
47. Volzone, C.; Ortiga, J. Removal of gases by thermal-acid leached kaolinitic clays: Influence of mineralogical composition. App. Clay Sci. **2006**, *32*, 87-93.
48. Bikiaris, D.; Daniilia S.; Sotiropoulou, S.; Katsimbiri, O.; Pavlidou, E.; Moutsatsou ,A.P.; Chryssoulakis, Y. Ochre-differentiation through micro-Raman and micro-FTIR spectroscopies: application on wall paintings at Meteora and Mount Athos, Greece. *Spectrochimica Acta Part A: Molecul. Biomol.Spectro.* **2000**, 56, 3-18.
49. Foletto, E.L.; Volzone, C.; Morgado, A.F.; Porto, L.M. Obtenção e caracterização de materiais argilosos quimicamente ativados para utilização no descoramento de óleo vegetal. *Mat. Res.* **2001**, 4, 211-215.

50. Foletto, E.L.; Volzone, C.; Porto, L.M. Performance of an Argentinian acid-activated bentonite in the bleaching of soybean oil. *Brazilian J. Chem. Eng*. **2003**, *20*, 139-145.
51. Hildebrando, E.A.; Andrade, C.G.B.; Rocha Junior, C.A.F.; Angélica, R.S.; Valenzuela-Diaz, F.R.;, Neves, R.F. Synthesis and characterization of zeolite NaP using kaolin waste as a source of silicon and aluminum. *Mat. Res*. **2014**; *17*, 174-179.
52. Zvezdova, D. Synthesis and characterization of chitosan from marine sources in Black Sea, Annu. Proceedings," Angel Kanchev" Univ. Ruse, 2010, *49*, 65-69.
53. Tironi, M.A.; Trezza, E.F.; Irassar, A.N. Scian, Thermal treatment of kaolin: effect on the pozzolanic activity. *Procedia Mater. Sci*. **2012,** *1*, 343-350.
54. G.-I. E. Ekosse, Fourier transform infrared spectrophotometry and X-ray powder diffractometry as complementary techniques in characterizing clay size fraction of kaolin. *J. App. Sci. Environ. Manag.* **2005**, *23*, 43-48.
55. Zhao, A.; Yang, S; Wang, B.; Tian, X.; Zhang, Y. Effects of ZnSO4 and Zn-EDTA broadcast or banded to soil on Zn bioavailability in wheat (Triticum aestivum L.) and Zn fractions in soil. *Chemosphe*re. **2018**, *205*, 350-360.
56. Esrafili, L.; Safarifard, V.; Tahmasebi, E.; Esrafili, M.; Morsali, A. Functional group effect of isoreticular metal–organic frameworks on heavy metal ion adsorption. *New J. Chem*. **2018**, *42*, 8864–8873.
57. Tironia, A.; Trezza, M. A.; Irassara, E.F., Scian, A. N. Thermal treatment of kaolin: effect on the pozzolanic activity. *Procedia Mat. Sci***. 2012**, *1*, 343 – 350.
58. Wilson, M.J., A Handbook of determinative methods in clay mineralogy, Editor. Chapman and Hall Publ., , **2003**.
59. Madejová, J. FTIR techniques in clay mineral studies: review., Vib. Spectro. **2003**, *31*, 1-10.
60. Bich, Ch. Contribution à l'étude de l'activation thermique du kaolin: évolution de la structure cristallographique et activité pouzzolanique, Ph. D. Thesis, Institut National des Sciences Appliqués de Lyon, France. **2005**.
61. Voinov, M.A.; Sosa Pagán J.O.; Morrison, E.; Smirnova, T.I.; Smirnov, AI. Surface-mediated production of hydroxyl radicals as a mechanism of iron oxide nanoparticle biotoxicity. *J. Am. Chem. Soc.* **2011**, *133*, 35-41.

62. Turci, F.; Colonna, M.; Tomatis, M.;, Mantegna, S.;, Cravotto, G.; Gulino, G.; et al. Surface reactivity and cell responses to chrysotile asbestos nanofibers. *Chem. Res. Toxicol*. **2012**, *25*, 884-94.
63. Scimeca, M.; Bischetti, S.; Lamsira, H..K.; Bonfiglio, R.; Bonanno, E. Energy Dispersive X-ray (EDX) microanalysis: A powerful tool in biomedical research and diagnosis. *Eur. J. Histochem*. 2018, 62, 2841.
64. Fernandez-Segura E, Warley, A. Electron probe X-ray microanalysis for the study of cell physiology. *Methods Cell Bio*l. **2008**, *88*, 19-43.
65. Priyantha, N.; Lim, L. Khairud, M.; Dahri, M.K.; Tennakoon, D.T.B.. Dragon fruit skin as a potential low-cost biosorbent for the removal of manganese(ii) ions. *J .App. Sci. Env. Sanitat*. **2013**, 8, 179-188.
66. Shayegan, H.; Gomaa, A. M. Ali, Vahid safarifard. Amide-functionalized metal–organic framework for high efciency and fast removal of pb(ii) from aqueous solution. *J..Inorg. .Organo Poly. Mater*.**2020**. 30:3170–3178.
67. Felicia F, Peng P. Di Effect of multivalent salts—calcium and aluminum on the flocculation of kaolin suspension with anionic polyacrylamide. *J Colloid Interface Sci* **1994**, 164, 229–37.
68. Braggs B, Fornasiero D, Ralston J, St Smart R. The effect of surface modification by an organosilane on the electrochemical properties of kaolinite. *Clays Clay Miner.* **1994**, 42,123–36.
69. Qin WQ, Qiu G-Z, Hu Y-H. Flotation of kaolinites and its iteraction with hexadecyl ammonium bromide. *Trans. Nonferrous Met. Soc. China..* **2003**, 13, 901--910
70. Brunauer, S.; Emmett, P.H.; Teller E. Adsorption of gases in multimolecular layers. *J. Am. Chem. Soc.* **1938**, 60, 309-19.
71. Barrett, E.P.; Joyner, L.G.; Halenda, P.P. The Determination of pore volume and area distributions in porous substances. i. computations from nitrogen isotherms. *J. Am. Chem. Soc.* **1951**, 73, 373-80.
72. Joyner, L.G.; Barrett, E.P.; Skold, R. The Determination of pore volume and area distributions in porous substances. ii. comparison between nitrogen isotherm and mercury porosimeter methods. *J. Am. Chem. Soc.* 1**951**, 73, 3155-8.
73. Lippens, B.C.; de Boer, J.H.; Studies on pore systems in catalysts v. the t method, *J. Catalysis*. **1965,** 4, 319.
74. Dąbrowski, A. Adsorption—from theory to practice. *Adv. Colloid Interface Sci*. **2001**, 93, 135-224.

75. McCusker, L.; Liebau, F.; Engelhardt, G. Nomenclature of structural and compositional characteristics of ordered microporous and mesoporous materials with inorganic hosts (IUPAC recommendations 2001). *Pure Appl. Chem*. **2001**, *73*, 381-94.
76. McCusker, L.; Liebau, F.; Engelhardt, G. Nomenclature of structural and compositional characteristics of ordered microporous and mesoporous materials with inorganic hosts:(IUPAC recommendations 2001). *Microporous Mesoporous Mater*. **2003**, 58, 3-13.
77. Paricio, P.; Galán, E. mineralogical interference on kaolinite crystallinity index measurements. clays clay miner.**1999**, 47, 12–27.
78. Hashemian, S.; Parsaei, Y.; Adsorption of 2-picoline and 3-Amino-2-picoline onto kaolin and organo-modified kaolin. *Orient. J. Chem.* **2015**, 31. 912–917.
79. Shin, E.W.; Han, J. Phosphate adsorption on aluminum-impregnated mesoporous silicates: surface structure and behavior of adsorbents. *Environ. Sci. Technol*. 2004, 38, 912–917.
80. Boparai, H K.; Joseph, M.; O'Carroll, D. M. Kinetics and thermodynamics of cadmium ion removal by adsorption onto nano zerovalent iron particles. *J. Hazard. Mater.* **2011**, 186, 458–465.
81. Peers, A.M. Elovich adsorption kinetics and the heterogeneous surface, *J. Catalysis*, **1965**, 4, 499-503.
82. Halsey, G. Physical Adsorption on Non-uniform Surfaces. *J. Chem. Phy*. **1948**, 16, 9317937.

Chapter 7

Conclusion and prospectus

Chapter 7

Conclusions and prospectus

Conclusions and prospectus

Cellulose and its derivatives (CDs) have been extensively used in various fields due to their valuable and remarkable chemical and physical properties. The CDs have characteristics properties like improve stability of the drug, good lubrication, good binding properties, rapid disintegration, good flowing properties, reduced friability & weight loss, excellent compression & hardness, good depressants. CDs have also been introduced, specifically in an industrial area and many other applications such as textile, paper, rubber, plastic and pharmaceutical industries, etc. The importance of polymers (CDs) is widely recognized due to their broad range of applications. Adsorption of polysaccharides onto solid-liquid interface has been a topic of long-standing debate. However, there was a lack of understanding of the interaction mechanism between the polysaccharides (CDs) and solid surfaces which has hindered their possible applications. Therefore, the adsorption behaviour of CDs was studied using various solid surfaces as adsorbents (mesoporous mustard carbon, functionalized accurel, mesoporous granular fine quartz and activated kaolin) and cellulose, carboxymethylcellulose, sodium carboxymethylcellulose and hydroxyethylcellulose as adsorbates and as representative selection of the polysaccharides. The prime objective of the work was to explore the adsorption mechanism of CDs onto various modified adsorbents in the aqueous medium to enhance the existing knowledge of binding mechanism and the possible application of CDs in industrial areas. Several modified adsorbents were prepared from agricultural wastes and mineral containing raw materials. These model surfaces were further utilized to study the interactions of the CDs with solid surfaces in aqueous system. Various characterization techniques such as Fourier-transform infrared spectroscopy (FTIR), attenuated total reflection-Fourier transform infrared (ATR-FTIR) spectroscopy, scanning electron microscopy (SEM), energy dispersive X-Ray analysis (EDX), elemental mapping analysis (EMA), powder X-ray diffraction (PXRD), Brunauer–Emmett–Teller (BET) surface area analyzer, X-ray photoelectron spectroscopy (XPS), zeta potential analyzer (ZPA) thermogravimetric analyzer (TGA), advanced high-intensity ultrasonicator (AHIU) and ultraviolet-visible (UV-Vis) spectrophotometery were used to identify the synthesized adsorbents/adsorbates and their interaction. Adsorption isotherm equations *viz* Langmuir, Freundlich, etc. have been tested for their applicability to represent the

experimental data. The kinetic study was explored using various kinetic models (first-order, pseudo-first-order, second-order, pseudo-second-order Temkin, etc.) on studied adsorbed-adsorbent systems. The thermodynamic study was also undertaken to establish the endothermic/exothermic nature of the adsorption process of CDs onto various solid surface. Moreover, for better understanding, the adsorption mechanism at the molecular level, density functional theory (DFT) was also employed for some selected CDs. The conclusion and prospectus may be understood as follow:-

To understand the binding mechanism of carboxymethylcellulose (CMC) onto a solid surface, mesoporous mustard carbon (MMC) was chosen as a solid surface. The MMC was derived from the mustard cake by chemical activation method which was utilized for the adsorption of CMC from the aqueous solution. The BET study revealed that the specific surface area of MMC was S_{BET}= 16.576 m^2 g^{-1}. The average pore diameter and total pore volume of MMC were found to be 12.432 nm and 0.051 cm^3g^{-1}, respectively which confirm the mesoporous nature of the MMC as per the IUPAC classification of porous materials. The adsorption of CMC onto MMC was found to be affected by changes in various process parameters. The findings of the ATR-FTIR study helped to detect spectral changes associated with hydrogen bonding between CMC and MMC. The differences in the ATR FTIR bands in the 1000–1080 cm^{-1} region were important, owing to the -C–O stretching coupled to the -C–C stretch and -O–H disability, confirming strong bond formation due to hydrogen bonding of CMC onto the MMC/water interface. Since urea functions as a hydrogen bond breaker, the presence of urea during adsorption significantly reduced the adsorption amount of CMC. This finding further favoured that hydrogen bonding was responsible for the occurrence of adsorption of CMC rather than a hydrophobic one as suggested by other groups of researchers. Since the adsorption free energy (-22.561kJmol^{-1}) of CMC is similar to that of hydrogen bond formation, Langmuir adsorption isotherm studies endorse hydrogen bonding as the dominant force for CMC adsorption. AFM study was also used for the distribution of CMC at a particular pH in which it was found that CMC was more distributed at acidic medium rather than the basic medium in its aqueous solution.

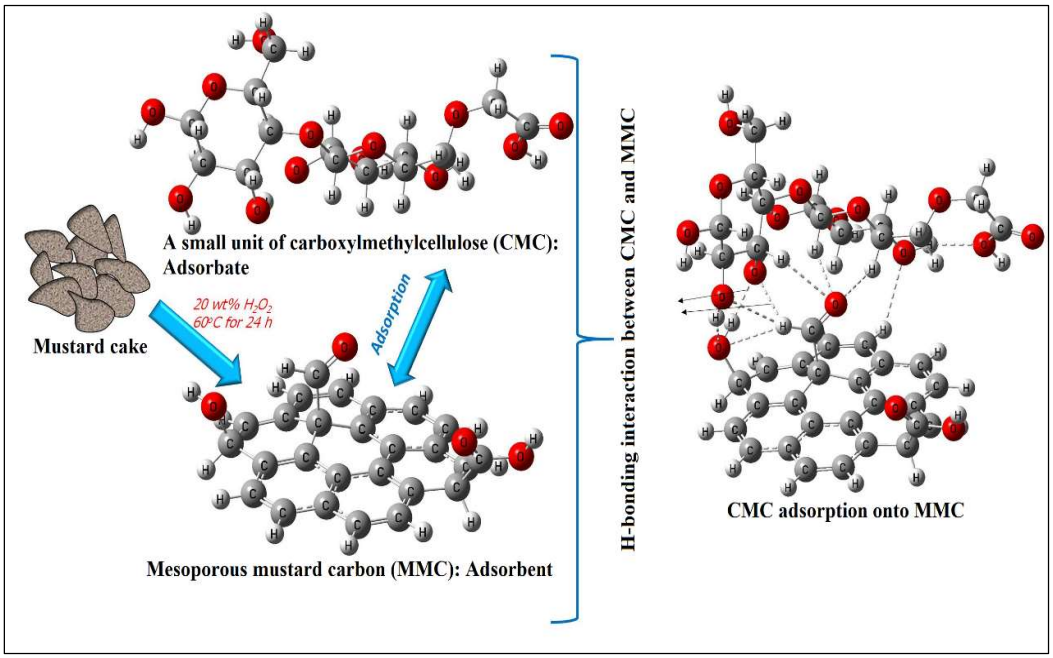

Figure 1. Schematic graphical representation of an overall summary of the adsorption mechanism of CMC on MMC.

Table 1 Covalent bonds associated with the intra- and intermolecular H-bonds and some selected covalent bonds of functionalized coronene at B3LYP and M06-2X level of theories with 6-31+G (d, p) Basis Set.

System	B3LYP/6-31+G (d, p)	M06-2X/6-31+G (d, p)
Sucrose (CMC)	O27-H44 (0.969) Intramolecular H-bond Case: O24-H43 (0.975), O6-H38 (0.970)	O27-H44 (0.968) Intramolecular H-bond Case: O24-H43 (0.972), O6-H38 (0.969)
Coronene (MMC)	O92-H93 (0.968) C-H (1.108) of CHO, C=O (1.204) of CHO	O92-H93 (0.965) C-H (1.110) of CHO, C=O (1.198) of CHO
Complex (MMC-CMC)	Intermolecular H-bonds Case: O27-H44 (0.978), O92-H93 (0.980)	Intermolecular H-bonds Case: O27-H44 (0.972), O92-H93 (0.978)
	Intramolecular H-bonds in Sucrose: O24-H43 (0.977), O6-H38 (0.970)	Intramolecular H-bonds in Sucrose: O24-H43 (0.974), O6-H38 (0.969)
	Coronene: C-H (1.108) of CHO, C=O (1.206) of CHO	Coronene: C-H (1.108) of CHO, C=O (1.202) of CHO

The survey scan and high resolution of C1S XPS spectra confirmed that the -OH groups on the MMC surface interact with the carboxylate ion of CMC. Thus, the present research provided sufficient evidence that adsorption of CMC onto the MMC was

governed by hydrogen bonding and electrostatic interaction and may be influenced by experimental conditions. This adsorbent-adsorbate model (Figure 1) was supposed to pave a new path towards a deeper understanding of molecular aggregation mechanisms in food and industrial applications, based on theoretical investigations (Table 1).

The polypropylene (PP), its trade name is accurel, is an inactive material was used for the functionalized accurel (FA), by the chemical activation method. The physiochemical parameters of FA such as specific surface area (S_{BET}) =34.472 m^2/g, pore volume (Vp) =0.07-0.121 cm^3/g, total pore volume (Vtp) = 0.115 cm^3/g, mean pore diameter = 13.692nm and pore diameter =39.402nm were determined by BET method. The particle size and pXRD studies confirmed that FA possessed mesoporous and crystalline nature, respectively. The batch shaking adsorption experiments with various parameters were tested and the equilibrium isotherm data were fitted with Freundlich, Langmuir, Temkin and Jovanovic models of adsorption and compared by linear regression coefficient (R^2) which obeyed the order as Langmuir (R^2=0.9933)> Freundlich (R^2=0.9830)>, Temkin (R^2=0.9428)> Jovanovic (R^2=0.8667) (Table 2). It was found that the adsorption of CMC on FA affected by the change of various factors like the initial concentration of CMC, FA dose, pH, ionic strength (0.1mol/L), temperature (°C), sonication (20 kHz) and the presence of urea (0.1mol/L). The results obtained from the FTIR analysis provided useful information on spectral changes which were assigned with hydrogen bonding between CMC and FA. To the changes in the IR frequencies of some main functional groups -OH, -C=O, -C-O, -C-H, and –COOH in which the -C–O stretch coupled to the -C–C- stretch and -O–H deformation, were significant and thus supports strong hydrogen bonding of CMC on FA surface. A urea test was performed to confirm the involvement of hydrogen bonding during the adsorption of CMC onto FA. The batch adsorption was carried out by dissolving urea (0.1mol/L) in 700mol/L CMC solution. Since urea is a hydrogen bond breaker, the obtained results showed that the amount of adsorption decreased significantly in the presence of urea. It provides strong evidence that hydrogen bonding is responsible for the adsorption of CMC onto FA. The adsorption experiment was conducted in the presence and absence of ultrasound at optimized conditions. Results indicated that the adsorption amount in the presence of ultrasound is lower than that in the absence of ultrasound because at a lower frequency (20 kHz) the cavitation effect is more (due to larger propagating bubble) and which caused a weakened interactive force between the CMC and FA resulting decrease in the adsorption amount. Thus, the effect of urea and

sonication confirmed that hydrogen bonding was a predominant force rather than a hydrophobic force. XPS analysis illustrated the binding of -OH groups available onto the FA surface interacts with carboxylate ions of the CMC and thus confirmed the role of hydrogen bonding during the adsorption process. Moreover, the theory-based quantum mechanical calculations (Table 3**)** provide a better understanding of the adsorbate – adsorbent binding features and to understand such molecular agglomeration systems (Figure 2).

Table 2 Isotherm parameters obtained from various adsorption models

Isotherm models	**Parameters**		**Determination coefficient (R^2)**
Langmuir	q_{max} = 6.94±0.01 mg/g	K_L= 1.80±0.00 L/mg	0.9933
Freundlich	n = 1.20±0.009	K_F =1.34±0.01 (mg/g) $(L/mg)^{1/n}$	0.9830
Jovanovic	q_{max} = 4.52±0.0.11 mg/g	K_J= 0.93±0.15 L/mg	0.9428
Temkin	K_T = 2.71±0.12mg/L	B =0.94±0.02L/g b=2.65±0.03 KJ/mol	0.8667

Table 3 The electronic parameters HOMO (in eV), LUMO (in eV), HOMO-LUMO gap (in eV), and binding energy (BE) (kcal/mol) at B3LYP and M06-2X levels of theories using 6-31+G (d, p) basis set

Parameter	**Adsorbent (Coronene)**	**Adsorbate (Sucrose)**	**Adsorbent-adsorbate (FA-CMC) complex**
HOMO	-6.508, -7.843	-6.732, -8.441	-6.582, -8.021
LUMO	-2.140, -1.004	-0.710, -0.103	-2.272, -1.192
HLEG	4.368, 6.839	6.022, 8.338	4.310, 6.829
Binding energy (BE)	—	—	-6.3, -64.6

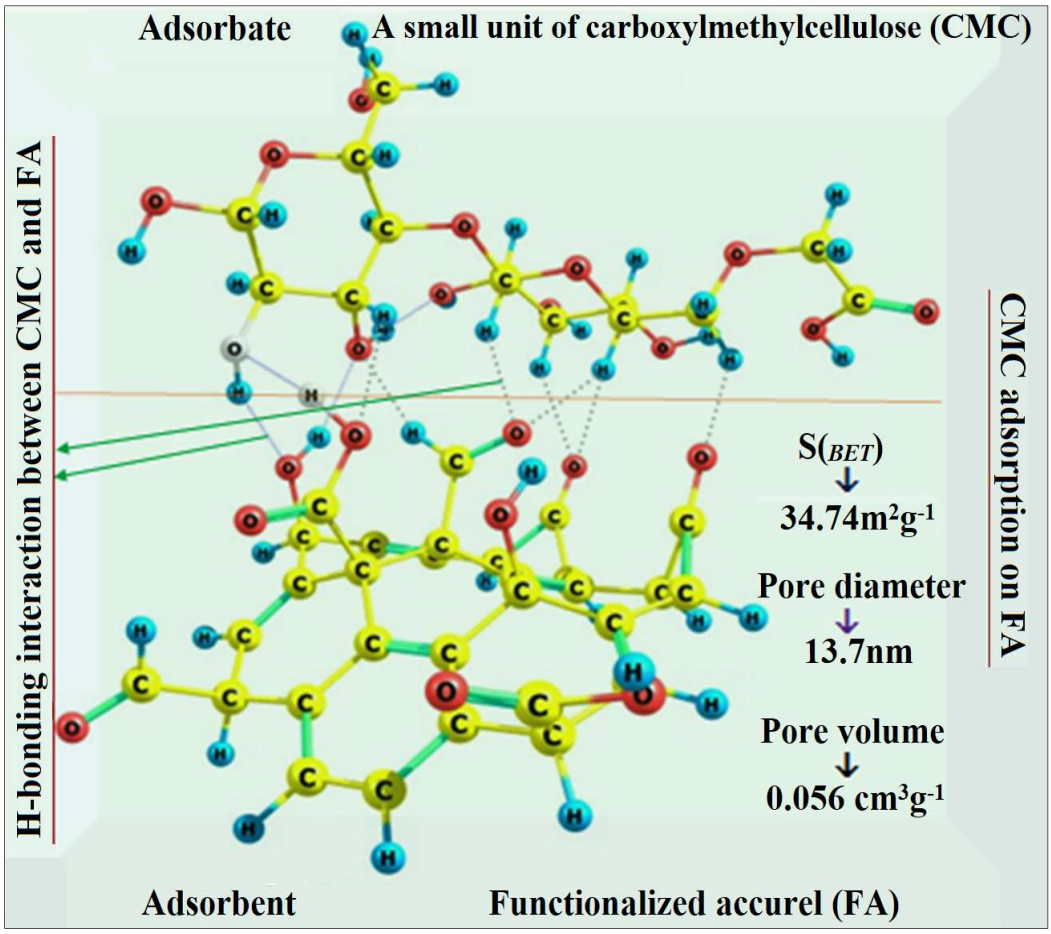

Figure 2. Theoretical graphical interaction between CMC and FA

The mesoporous granular fine quartz surface was obtained from quartz by the physical activation method. The physiochemical characterizations and experiments confirm that MGFQ has very efficient potential adsorptive properties. It was observed that the adsorption of NaCMC on MGFQ remarkably affected by the change in adsorptive optimized conditions such as pH, ionic strength, and sonication and the presence of alcohols. These observed results concluded that hydrogen bonding shows a significant role during the adsorption. The FTIR spectral changes appeared nearby 1104 cm^{-1} and 1076 cm^{-1} which provided sufficient evidence to confirm the participation of strong hydrogen bonding in adsorption. The adsorption mechanism was associated with hydrogen bonding between active -Si-O-H of MGFQ and carboxylates ions of NaCMC. Experimental data were excellently fitted to the Freundlich equation since the regression analysis gave high correlation coefficients R^2>0.99 and obey to order as Freundlich (R^2=0.9830)> Langmuir (R^2=0.9933)>Temkin (R^2 =0.8663)>Jovanovic (R^2= 0.9428) (Table 4).

Table 4 Isotherm parameters obtained from various equations

Isotherm models	**Parameters**		**Correlation coefficient (R^2)**
Freundlich	n =0.99 ±0.012	K_F =0.052±0.01L/g	0.9984
Langmuir	q_{max} = 7.78±0.013 mg/g	K_L= 0.025±0.00 L/mg	0.9194
Temkin	A_T =1.255 ±0.09.mg/L	B_T = 0.299±0.00.013L/g b_T=±826.62±0.03J/mol/.g/L	0.8899
Jovanovic	q_{max} = 0.047±0.03 mg/g	K_J= ±0.15±0.01 L/mg	0.8709
Hill	n^H=0.971±0.02 K_D= -1.382×10^2	Q_H=1.306×10^2	0.9981

The adsorption behaviour of three polymers namely cellulose (CL), sodium carboxymethylcellulose (Na-CMC) and hydroxyethylcellulose (HEC) onto activated kaolin was conducted. The activated kaolin was derived from supplied kaolin by physical activation method and characterized by various characterization techniques. The specific surface area (S_{BET}) of activated kaolin (AK) was S_{BET} =18.57 m^2/g. The electrophoresis measurements at pH 7.0 revealed that activated kaolin possesses a positive surface. Moreover, the experimental data were computed employing several isotherm models such as Freundlich, Langmuir, Elvoich and Halsey for the adsorption of CL, Na-CMC and HEC onto activated kaolin from aqueous solutions. The adjusted R^2 values suggested the results were in favour of the data collected from the adsorption experiment. The equilibrium data of CL, Na-CMC and HEC onto activated kaolin was found to best fit the Langmuir equation since the adjusted R^2 gave high correlation coefficients R^2>0.99 than HEC and CL (Table 5).

These studies confirmed that the mechanism of adsorption of aforesaid polysaccharides/cellulose derivatives (CDs) onto various solid surfaces was attributed to the hydrogen bonding followed by some weak interactions. The FTIR spectra of studied adsorbents/adsorbates before and after adsorption illustrated that there were remarkable changes during adsorption.

Table 5 Parameters determined for various adsorption models based on experimental observations for adsorption of selected polymers onto AK

Isotherm models	Parameters	HEC	CL	Na-CMC
Frundlich	n	6.27±0.06	2.71±0.02	1.79±0.01
	K_F	1.45±0.01 mg/g $(L/mg)^{1/n}$	2.97±0.03 mg/g $(L/mg)^{1/n}$	0.70±0.04 mg/g $(L/mg)^{1/n}$
	Adj. R^2	0.92605	0.94616	0.96151
Langmuir	Γ_{max}	6.23± 0.03 mg/g	6.10± 0.03mg/g	8.34±0.01mg/g
	K_L	0.96±0.01 L/mg	1.36±0.01L/mg	0.58±0.01L/mg
	Adj. R^2	0.98807	0.98653	0.99440
Elovich	Γ_{max}	2.91±0.30 mg/g	1.79±0.27 mg/g	3.95±0.09 mg/g
	K_E	1.95±0.07 L/mg	5.43±0.06 L/mg	1.59±0.02 L/mg
	Adj. R^2	0.71040	0.89285	0.95295
Halsey	n_H	2.13±0.07	2.71±0.045	1.79±0.04
	K_H	7.26±0.06mg/L	19.20±0.03 mg/L	5.90±0.04 mg/L
	Adj. R^2	0.88419	0.94616	0.96151

The shifting in IR bands has occurred in –OH/ Si-O-H and –COOH/Si-COOH stretching of adsorbents due to interactions with carboxylate and hydroxyl groups of adsorbates which confirmed the formation of new hydrogen bonds between adsorbents and carboxylate/hydroxyl ion of polysaccharides. The changes in the infrared bands in the region of 1000–1080 cm^{-1} associated with the -C–O stretch coupled to the -C–C stretch and -O–H deformation, were significant and thus support strong hydrogen bonding of CDs on solid/water interface. However, some small change in the position of peaks were also observed which suggests non-covalent interactions.

To provide experimental proof to show that hydrogen bonding plays a vital role in the adsorption process in the present case, batch adsorption experiments were conducted by adding specific amount of hydrogen bond breakers (urea, DMSO and alcohols) in the adsorbate solution. In the presence of these hydrogen bond breakers, the amount of adsorption decreases significantly. These results consistent with this statement clearly illustrate that in the presence of hydrogen bond breakers, the amount of adsorption decreased significantly. Therefore, it is beyond doubt that hydrogen bonding plays an important role during the adsorption of polysaccharides.

The effect of power ultrasound (sonication-20 kHz) during the adsorption process was examined to establish the role of hydrogen bonding during the adsorption process. The adsorption experiment was conducted in the presence and absence of ultrasound. The obtained results suggested that the adsorption amount in the presence of ultrasound is lower than that of in the absence of ultrasound because at a lower frequency the cavitation effect is more (due to larger propagating bubble) and which caused to a weakened hydrogen bonding between the selected adsorbents and CDs resulting decrease in the adsorption amount.

Additionally, the adsorption free energy (-22.561 $kJmol^{-1}$) of CDs was in close agreement with the hydrogen bond formation. After the adsorption of CDs onto adsorbents, both XPS survey scan and high-resolution CIs XPS spectra were scanned in which binding energy is different because the chemical shifts are related to electron density changes. This is due to available hydroxyl groups on adsorbents interacts with carboxylate ion of CDs resulting in an increase in carbon-oxygen functional groups (C-O and C=O) of MPP) which also confirmed the role of hydrogen bonding. Furthermore, to the best of our knowledge, the reliability of the theoretical approach in producing the structural, stability, and electronic feature analyses of the adsorbate-adsorbent complex has also been evaluated for some selected CDs. Obtained results reveal that the energetic compounds considered in the present investigation form a favourable and stable complex. The adsorbate-adsorbent complex is strongly stabilized by the presence of two strong intermolecular hydrogen bonds (HBs) formed between HB accepting and donating sites of adsorbates to the complementary sites of the adsorbents. Some weak conventional (C-H···O) and nonconventional (C-H···C and C-H···H) HBs joins the molecules and thus appears to be responsible for the formation of the stabilizing adsorbate- adsorbent system. Thus, the binding mechanism of aforesaid CDs onto various solid surfaces was mainly attributed to the hydrogen bonding followed by some other non-covalent interactions.

Present study concludes that the binding mechanism of polysaccharides/CDs onto various solid surfaces depends on solution conditions mainly pH. Under acidic condition, the binding mechanism of polysaccharides onto various solid surfaces is attributed to hydrogen bonding which has been proved beyond doubt. However, under basic condition the role of hydrophobic interaction and formation of complex between polysaccharides and solid surfaces (mainly metal containing surfaces) can not be ruled out. Thus, the binding mechanism of polysaccharides onto various solid surfaces is a

complex interplay of electrostatic (hydrogen bonding, van der Waals forces, etc.), hydrophobic and complex formation between polysaccharides and various solid surfaces containing mainly metal ions, depending on solution conditions.

Herein, the alternate adsorbents have been used for explaining a systematic understanding of the binding mechanism of cellulose and its derivatives. The result of the present study could be extended to systems of significant importance. It will not only be beneficial for the industries but also the surrounding environment from the potential toxicity caused by inorganic dispersant and depressants (used in mineral processing). Thus, the use of studied adsorbents may contribute towards the sustainability of the environment also. Undoubtedly, adsorbents used in this study for the adsorption of cellulose and its derivatives could offer a lot of probable benefits for the future prospectus.

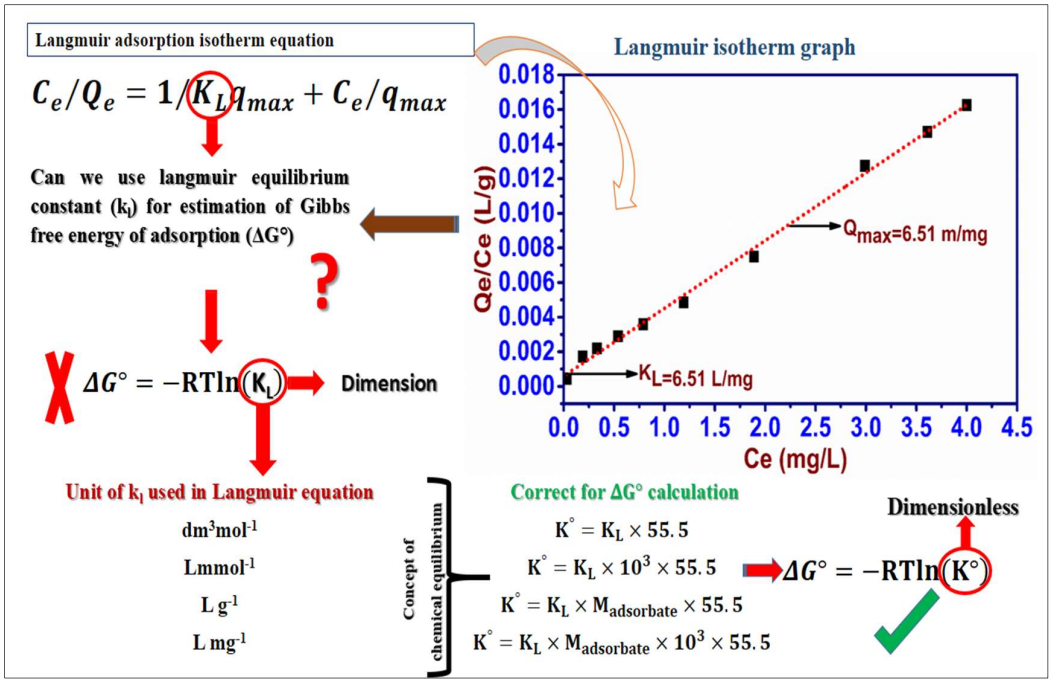

Figure 3. Graphical representation of correct calculation of Gibbs free energy of adsorption (ΔG^o) employing Langmuir equilibrium constant (K_L)

Furthermore, Langmuir isotherm equations has been used extensively for interpreting several adsorption processes. However, this equations has its limitations and flaws while determining thermodynamic parameters, especially in the calculation of the change in the free energy of adsorption using Langmuir equilibrium constant (K_L). Several authors employed K_L for the calculation of Gibbs free energy of adsorption (ΔG^o) without its qualification (expressed instead of dimensionless in some

concentration units (for example L mol^{-1}, L g^{-1}, ml mg^{-1}, etc.). Thus, there is semantic confusion and it has become customary to evaluate ΔG^o. The equilibrium constant (K_L) in the Langmuir isotherm is usually used to calculate the standard Gibbs free energy of adsorption (ΔG^o). But in the context of theory, this calculation method is not accurate.

This is so because the K_L in the Langmuir isotherm has a dimension. However, as per the provisions of the International Union of Pure and Applied Chemistry (IUPAC), the standard equilibrium constant (K_L) for calculating ΔG^o must be a dimensionless parameter. We examined the data carefully and found that the estimation of ΔG^o reported in various published papers was seemingly incorrect. Based on the fact that this miscalculation is now has become customary in the adsorption literature and it seems impossible to address this semantic confusion, we herein, however, attempted to correct the related literature and gives a detailed comment and solution of this problem. The standard free energy of adsorption (ΔG°) related to the Langmuir adsorption equilibrium constant, K_L, can be calculated using the flowing expression:-

$$\Delta G^\circ = -TRlnK_L$$

Where R is the general gas constant (8.314J/(mol K) and T is the absolute temperature.

Herein, it was suggested that before the calculation of ΔG° it is required first to express the value of K_L dimensionless (Figure.3).

Plagiarism report

URKUND

Urkund Analysis Result

Analysed Document:	Ph.D. Thesis Ashok Kumar.pdf (D100703453)
Submitted:	4/6/2021 7:31:00 AM
Submitted By:	gbl.bbau@gmail.com
Significance:	5 %

Sources included in the report:

JCIS Manscript.docx (D40289118)
Manuscript RSC.docx (D39423710)
Manuscript.docx (D40289117)
b1191e1d-9816-41ec-9414-3737ae087f09
195a1343-cc33-45e3-ba78-4eae8efc5a83
c0b1895d-1cf9-4e3f-b379-e70801f907b9
http://edepot.wur.nl/201590
https://www.researchgate.net/publication/223310932_Effect_of_calcium_ions_on_the_adsorption_of_CMC_onto_the_basal_planes_of_New_York_talc_-_A_ToF-SIMS_study
https://pubs.rsc.org/en/content/articlehtml/2021/ra/d0ra09292d
https://pubmed.ncbi.nlm.nih.gov/15907862/
https://www.sciencedirect.com/science/article/abs/pii/S0927775719307745
https://www.ncbi.nlm.nih.gov/pmc/articles/PMC6470896/
https://www.researchgate.net/publication/335108271_Adsorption_mechanism_of_carboxymethyl_cellulose_onto_mesoporous_mustard_carbon_Experimental_and_theoretical_aspects
https://espace.library.uq.edu.au/view/UQ:409120/s42968520_final_thesis.pdf
https://www.researchgate.net/publication/311619375_Adsorption_laboratory_experiment_for_undergraduate_chemical_engineering_Introducing_kinetic_equilibrium_and_thermodynamic_concepts
https://www.intechopen.com/online-first/experimental-study-of-adsorption-on-activated-carbon-for-co-sub-2-sub-capture
https://www.jmaterenvironsci.com/Document/vol11/vol11_N8/JMES-2020-11111-Ndaye.pdf
https://www.researchgate.net/publication/312648607_Carboxymethyl_Cellulose_Silver_Nanoparticles_Composite_Synthesis_Characterization_and_Application_as_a_Benign_Corrosion_Inhibitor_for_St37_Steel_in_15_H2SO4_Medium
https://www.researchgate.net/figure/Repeat-unit-of-CMC_fig1_312648607
https://revues.imist.ma/index.php/JACEP/article/download/11285/6393
https://www.science.gov/topicpages/a/adsorption+isotherm+adsorption.html
https://www.science.gov/topicpages/n/n2%2Badsorption%2Bisotherm

Kumar

URKUND

https://www.science.gov/topicpages/h/h2+adsorption+capacity
https://docplayer.net/50315181-Adsorption-of-phenol-on-natural-clay.html
https://www.science.gov/topicpages/n/n2+adsorption+isotherm
https://www.science.gov/topicpages/a/adsorption+isotherm+study.html
https://www.scirp.org/xml/41392.xml
https://docplayer.net/163034759-Removing-pb-ii-ions-from-aqueous-solution-by-a-promising-absorbent-of-tannin-immobilized-cellulose-microspheres.html
https://www.researchgate.net/publication/312665535_Adsorption_Properties_of_Nano-MnO2-Biochar_Composites_for_Copper_in_Aqueous_Solution
https://core.ac.uk/download/pdf/48655671.pdf
http://www.socphyschemserb.org/media/publications/pc2016.pdf
https://www.science.gov/topicpages/a/adsorption+capacity+state.html
https://worldwidescience.org/topicpages/z/znii+cdii+hgii.html
https://www.science.gov/topicpages/p/physical+adsorption+chemisorption
https://www.researchgate.net/publication/7989723_Effect_of_OH_and_Silanol_groups_in_the_removal_of_dyes_from_aqueous_solution_using_diatomite

Instances where selected sources appear:

134

Kumar 16/04/2021

16/04/2021